Journal of Advanced Transportation

Partially Connected and Automated Traffic Operations in Road Transportation

Lead Guest Editor: Md. A. S. Kamal

Guest Editors: Mohsen Ramezani, Guoyuan Wu, Claudio Roncoli, Jackeline Rios-Torres, and Olivier Orfila

Partially Connected and Automated Traffic Operations in Road Transportation

Journal of Advanced Transportation

Partially Connected and Automated Traffic Operations in Road Transportation

Lead Guest Editor: Md. A. S. Kamal
Guest Editors: Mohsen Ramezani, Guoyuan Wu, Claudio Roncoli, Jackeline Rios-Torres, and Olivier Orfila

Editorial Board

Contents

Partially Connected and Automated Traffic Operations in Road Transportation
Md Abdus Samad Kamal, Mohsen Ramezani, Guoyuan Wu, Claudio Roncoli, Jackeline Rios-Torres, and Olivier Orfila
Editorial (3 pages), Article ID 9490586, Volume 2020 (2020)

Modeling and Prediction of Ride-Sharing Utilization Dynamics
Tal Altshuler, Yaniv Altshuler, Rachel Katoshevski, and Yoram Shiftan
Research Article (18 pages), Article ID 6125798, Volume 2019 (2019)

Simulation-Based Connected and Automated Vehicle Models on Highway Sections: A Literature Review
Wooseok Do, Omid M. Rouhani, and Luis Miranda-Moreno
Review Article (14 pages), Article ID 9343705, Volume 2019 (2019)

Modified Traffic Flow Model with Connected Vehicle Microscopic Data for Proactive Variable Speed Limit Control
Jie Fang, Huixuan Ye, and Said M. Easa
Research Article (11 pages), Article ID 8151582, Volume 2019 (2019)

Context-Aware Intelligent Traffic Light Control through Secure Messaging
Mükremin Özkul, Ilir Capuni, and Elton Domnori
Research Article (10 pages), Article ID 4251701, Volume 2018 (2018)

Modeling Microscopic Car-Following Strategy of Mixed Traffic to Identify Optimal Platoon Configurations for Multiobjective Decision-Making
Mudasser Seraj, Jiangchen Li, and Zhijun Qiu
Research Article (15 pages), Article ID 7835010, Volume 2018 (2018)

Potentialities of Autonomous Vehicles for Online Monitoring of Motorway Traffic Volume
Hyun-ho Chang and Byoung-jo Yoon
Research Article (12 pages), Article ID 4276593, Volume 2018 (2018)

A Separation Strategy for Connected and Automated Vehicles: Utilizing Traffic Light Information for Reducing Idling at Red Lights and Improving Fuel Economy
Lin-heng Li, Jing Gan, and Wen-quan Li
Research Article (10 pages), Article ID 5679064, Volume 2018 (2018)

Hindawi
Journal of Advanced Transportation
Volume 2020, Article ID 9490586, 3 pages
https://doi.org/10.1155/2020/9490586

Editorial

Partially Connected and Automated Traffic Operations in Road Transportation

Md Abdus Samad Kamal,[1] **Mohsen Ramezani**,[2] **Guoyuan Wu**,[3] **Claudio Roncoli**,[4] **Jackeline Rios-Torres**,[5] **and Olivier Orfila**[6]

[1]*Graduate School of Science and Technology, Gunma University, 1-5-1 Tenjincho, Kiryu 376-8515, Japan*
[2]*The University of Sydney, School of Civil Engineering, Sydney, NSW, Australia*
[3]*Department of Electrical and Computer Engineering, and Center for Environmental Research and Technology, UC Riverside, Riverside, CA, USA*
[4]*School of Engineering, Aalto University, Espoo 02150, Finland*
[5]*Energy and Transportation Science Division, Oak Ridge National Laboratory, Oak Ridge, TN 37831, USA*
[6]*IFSTTAR, 25 allée des Marronniers, 78000 Versailles, France*

Correspondence should be addressed to Md Abdus Samad Kamal; maskamal@ieee.org

Received 28 October 2019; Accepted 29 October 2019; Published 15 January 2020

Transportation is a key driver of development, enabling people to have access to jobs, education, health, and goods. Still, the unintended consequences of transportation constitute a big risk, threatening the global sustainable development. About 64% of global oil consumption and 23% of the worldwide CO_2 emissions are attributed to transportation [1]. Moreover, every year, congestion accounts for billions of dollars due to wasted time and fuel consumption, and the World Health Organization (WHO) [2] estimated that 1.3 million people died on roads in 2015. Connected and Automated Vehicles (CAVs) hold the potential to improve the current operational safety and efficiency of the transportation system by relieving drivers from some or all the driving tasks and enabling the cooperation among vehicles, between vehicles, and roadway infrastructure or other road users.

A variety of CAV applications have been devised, modeled, simulated, and deployed to substantialize their performance recently. They mostly target various traffic scenarios and contexts including traffic coordination at intersections and merging, dynamic speed control on the highway, traffic forecasting, and anticipative vehicle control. These research efforts have revealed the benefits of CAVs, including the potential to improve safety [3], alleviate traffic congestion [4] and reduce fuel consumption and emissions [5, 6].

With the full penetration of CAVs, the traffic can be operated in a fully automated manner achieving undoubtedly improved traffic performances. However, many challenges remain before a massive deployment of CAVs can be witnessed. It is then expected that CAVs will gradually appear in the market, increasing the complexity of the current transportation system as vehicles with different levels of connectivity and automation will start interacting with manually driven vehicles. There have been some early efforts to explore the implications of these complex interactions [7–10]. Overall, these early attempts seem to show a consensus on the benefits of higher market penetrations of vehicles enabled with connectivity and/or automation, but there is still a large level of uncertainty regarding the effects of lower market penetrations. Furthermore, a priori prediction of interaction between human and CAVs, now relying on simulation methodologies needs new numerical developments in order to be more representative of the reality. The design of prospective scenarios is also a challenge while trying to predict the impact of a system that will not be widespread in the market before several decades.

The ongoing and future research will probably provide more insights and innovative frameworks for analysis. This special issue includes research and review articles focusing on the connectivity in vehicular traffic with the presence of autonomous vehicles for potential improvement in traffic performances. It covers seven novel research articles including one review describing the modeling of traffic with CAVs, and use of CAVs for traffic light control and monitoring the traffic network, which are summarized as follows:

1. Modeling Traffic with CAVs

Review Article: Simulation-Based Connected and Automated Vehicle Models on Highway Sections: A Literature Review.

In this paper, Wooseok et al. conducted a detailed review on modeling methods of vehicle motion that are used in recent simulation-based studies of the intelligent vehicles (CAVs with various levels of autonomy), and provided new insights for future intelligent vehicle analyses, potential scopes, and research gaps. The connectivity of vehicles is essential to improve the roadway capacity by the automated vehicles (AVs). However, the improvements in the roadway capacity and energy consumption in traffic directly depend on the market-penetration rate of intelligent vehicles. The necessity of experimental calibration of models recently developed for AVs is highlighted, and the comprehensive study of the socio-economic impact of such vehicles has not been conducted. With respect to the car-following and lane-changing characteristics of intelligent vehicles, empirical data are needed for the model calibration.

Article: Modeling Microscopic Car-Following Strategy of Mixed Traffic to Identify Optimal Platoon Configurations for Multiobjective Decision-Making.

In this paper, a naïve strategy for microscopic car-following in a mixed traffic scenario has been proposed. Depending on the driving system of consecutive vehicles, a vehicle with an automated driving system (ADS) may decide either to use adaptive cruise control (ACC) or a cooperative adaptive cruise control (CACC) scheme for driving. Specifically, this study explores the influences of ADS market-penetration and platoon properties on the overall performance of the mixed traffic stream. It is confirmed from the simulation that the grouping of ADS vehicles using a CACC system provides maximum mobility benefits and environmental improvements at the cost of reduced safety. It is proposed that, for a comprehensive balance in mobility, safety, and environmental advantages the platoon configuration should be adjusted dynamically considering the ADS market penetrations in the mixed traffic.

Article: Modified Traffic Flow Model with Connected Vehicle Microscopic Data for Proactive Variable Speed Limit Control.

The variable speed limit (VSL) technique using model predictive control (MPC) framework has the potential to improve the traffic flows on the freeways. However, the MPC framework directly relies on the traffic state prediction model in deciding the optimal speed of the traffic. This paper extends a VSL technique based on an MPC framework by incorporating microscopic online data for better prediction of the traffic flows using METANET macroscopic model. Simulations conducted on the VISSIM platform confirm that the proposed method improves the speed prediction accuracy, and hence improves mobility performance.

Article: Modeling and Prediction of Ride-Sharing Utilization Dynamics.

An efficient ride-sharing scheme may significantly reduce traffic congestion and facilitate better transportation services to realize smart cities. This paper analyzes a dataset of over 14 million taxi trips taken in New York City and proposes a network-centric approach for modeling and forecasting the potential ride-sharing utilization over time. Despite significant volatility of ride-sharing utilization, using the proposed approach the potential utilization can be forecasted reliably a few hours ahead of time.

2. Traffic Light Control Considering CAVs

Article: Context-Aware Intelligent Traffic Light Control through Secure Messaging.

This paper presents a secure messaging method for vehicle-to-infrastructure (V2I) communication, and based on it a traffic light control scheme has been developed. Using computationally lightweight protocol, the privacy of individual vehicles is maintained among themselves, while the identity of emergency vehicles and public transportation is securely received by the trusted controller of traffic lights. Compared to the existing traffic light control schemes, the proposed traffic responsive signal control scheme—adaptive Webster's method—significantly reduces the waiting time of vehicles in both light and heavy traffic conditions.

Article: A Separation Strategy for Connected and Automated Vehicles: Utilizing Traffic Light Information for Reducing Idling at Red Lights and Improving Fuel Economy.

Efficient flows of CAVs at a signalized intersection can be realized by forming platoons of suitable size. Within a platoon, all vehicles run through the intersection at the same speed and hence their trajectories are parallel to each other. However, for passing through successive intersections, the same platoon may not be able to pass through the next intersection fully in the given green signal. In this paper, a scheme for both velocity control and separation strategy of CAVs has been proposed that takes into account the traffic efficiency and fuel-saving simultaneously. Simulation results show that the proposed scheme improves both the travel time and fuel economy significantly on a typical urban road with successive signalized intersections.

3. Traffic Monitoring Using CAVs

Article: Potentialities of Autonomous Vehicles for Online Monitoring of Motorway Traffic.

Connectivity in vehicular traffic opens a new reliable way to collect traffic information online over a road-network, which may provide essential information for an effective control measure. Particularly, CAVs can be used as virtual sensors in estimating the traffic volumes on the road-ways. In this paper, based on the hypothesis that CAV traffic volume is a direct portion of total traffic volume, a new method of monitoring real-time traffic volume has been proposed. Furthermore, the capabilities of the proposed method are demonstrated using an experimental study based on vehicle navigation data available from smartphones. The developed method is found to be effective when the probe volume data are available at least with the penetration rate of 0.05 or higher.

Conflicts of Interest

The editors declare that there are no conflicts of interest in publishing this editorial.

Md Abdus Samad Kamal
Mohsen Ramezani
Guoyuan Wu
Claudio Roncoli
Jackeline Rios-Torres
Olivier Orfila

References

[1] The World Bank, "Understanding poverty: transport," https://www.worldbank.org/en/topic/transport.

[2] WHO, "Global status report on road safety," 2018, https://www.who.int/violence_injury_prevention/road_safety_status/2018/en/.

[3] O. Orfila, D. Gruyer, K. Hamdi, and S. Glaser, "Safe and ecological speed profile planning algorithm for autonomous vehicles using a parametric multiobjective optimization procedure," *International Journal ofAutomotive Engineering*, vol. 10, no. 1, pp. 26–33, 2019.

[4] M. Ramezani and E. Ye, "Lane density optimisation of automated vehicles for highway congestion control," *Transportmetrica B: Transport Dynamics*, vol. 7, no. 1, pp. 1096–1116, 2019.

[5] J. Rios-Torres and A. A. Malikopoulos, "A survey on the coordination of connected and automated vehicles at intersections and merging at highway on-ramps," *IEEE Transactions on Intelligent Transportation Systems*, vol. 18, no. 5, pp. 1066–1077, 2017.

[6] D. Tian, G. Wu, K. Boriboonsomsin, and M. J. Barth, "Performance measurement evaluation framework and co-benefit tradeoff analysis for connected and automated vehicles (CAV) applications: a survey," *IEEE Intelligent Transportation Systems Magazine*, vol. 10, no. 3, pp. 110–122, 2018.

[7] J. Rios-Torres and A. A. Malikopoulos, "Impact of partial penetrations of connected and automated vehicles on fuel consumption and traffic flow," *IEEE Transactions on Intelligent Vehicles*, vol. 3, no. 4, pp. 453–462, 2018.

[8] M. A. S. Kamal, T. Hayakawa, and J.-I. Imura, "Road-speed profile for enhanced perception of traffic conditions in a partially connected vehicle environment," *IEEE Transactions on Vehicular Technology*, vol. 67, no. 8, pp. 6824–6837, 2018.

[9] G. Perraki, C. Roncoli, I. Papamichail, and M Papageorgiou, "Evaluation of a model predictive control framework for motorway traffic involving conventional and automated vehicles," *Transportation Research Part C: Emerging Technologies*, vol. 92, pp. 456–471, 2018.

[10] Y. Ito, M. A. S. Kamal, T. Yoshimura, and S. Azuma, "Coordination of connected vehicles on merging roads using pseudo-perturbation-based broadcast control," *IEEE Transactions on Intelligent Transportation Systems*, vol. 20, no. 9, pp. 3496–3512, 2019.

Hindawi
Journal of Advanced Transportation
Volume 2019, Article ID 6125798, 18 pages
https://doi.org/10.1155/2019/6125798

Research Article

Modeling and Prediction of Ride-Sharing Utilization Dynamics

Tal Altshuler,[1] Yaniv Altshuler ,[2] Rachel Katoshevski,[1] and Yoram Shiftan [1]

[1]*Department of Civil and Environmental Engineering, Israel Institute of Technology, Israel*
[2]*MIT Media Lab, USA*

Correspondence should be addressed to Yaniv Altshuler; yanival@mit.edu

Received 22 February 2019; Accepted 29 May 2019; Published 28 November 2019

Guest Editor: Olivier Orfila

The potential of an efficient ride-sharing scheme to significantly reduce traffic congestion, lower emission level, and drivers' stress, as well as facilitating the introduction of *smart cities* has been widely demonstrated in recent years. Furthermore, ride sharing can be implemented within a sound economic regime through the involvement of commercial services that creates a win-win for all parties (e.g., *Uber*, *Lyft* or *Sidecar*). This positive thrust however is faced with several delaying factors, one of which is the volatility and unpredictability of the potential benefit (or utilization) of ride-sharing at different times, and in different places. Better understanding of ride-sharing dynamics can help policy makers and urban planners in increase the city's "ride-sharing friendliness" either by designing new ride-sharing oriented systems, as well as by providing ride-sharing service operators better tools to optimize their services. In this work the following research questions are posed: (a) Is ride-sharing utilization stable over time or does it undergo significant changes? (b) If ride-sharing utilization is dynamic can it be correlated with some traceable features of the traffic? and (c) If ride-sharing utilization is dynamic can it be predicted ahead of time? We analyze a dataset of over 14 million taxi trips taken in New York City. We propose a dynamic travel network approach for modeling and forecasting the potential ride-sharing utilization over time, showing it to be highly volatile. In order to model the utilization's dynamics, we propose a network-centric approach, projecting the aggregated traffic taken from continuous time periods into a feature space comprised of topological features of the network implied by this traffic. This feature space is then used to model the dynamics of ride-sharing utilization over time. The results of our analysis demonstrate the significant volatility of ride-sharing utilization over time, indicating that any policy, design, or plan that would disregard this aspect and chose a static paradigm would undoubtably be either highly inefficient or provide insufficient resources. We show that using our suggested approach it is possible to model the potential utilization of ride sharing based on the topological properties of the rides network. We also show that using this method the potential utilization can be forecasting a few hours ahead of time. One anecdotal derivation of the latter is that perfectly guessing the destination of a New York taxi rider becomes nearly three times easier than rolling a "Snake Eyes" at a casino.

1. Introduction

The increasing availability of portable technologies gives new fuel to studies on metropolitan transportation optimization, pushing urban design one step closer towards the long sought concept of "smart cities" [1, 2]. Mobile devices and ubiquitous connectivity make it easier than ever to collect data on the way people live in cities and big-data analytic methods facilitate the extraction of actionable insights from it. City administrators and policy makers can in turn act upon such results to enhance city management, channeling current advancements in data analysis for the immediate improvement of urban quality of life.

Many of the fundamental problems in big cities nowadays relate to cars. The high number of vehicles congests the streets, vehicles standing in traffic jams increase air pollution while also increasing traveling times, significantly increasing passengers' stress levels. Availability of large-scale datasets accompanied with recent advancements in the analysis of big-data and the development of novel models of human mobility give rise to new possibilities to study urban mobility.

Such new models include for example the work of [3] in which large-scale mobile phone data were analyzed in order to characterize individual mobility, show that human travel patterns are far from random, and are efficiently describable by a single spatial probability distribution. Similarly, [4] show that mobile phone data can be used as a proxy to examine urban mobility and [5] analyzes social network data of different cities to find that mobility highly correlates with the

distribution of urban points of interest. Mobile technologies are also the enablers of many successful consumer applications, such as Waze [6], that provide traffic-aware city navigation by using data provided by the community. Alternative ways of moving in the city, such as autonomous mobility-on-demand and short-term car rental have been identified among the possible solutions to the ever-growing transport challenge [7].

Ride sharing has the potential of improving traffic conditions by reducing the number of vehicles on the roads, reducing the emission of CO_2 and the fuel consumption per person, and giving the riders the opportunity to socialize with people (that otherwise would have been fierce "road competitors"). A recent study [8] shows that traffic in the city of Madrid can be reduced by 59% if people are willing to share their home-work commute ride with neighbors. Even if they are not willing to ride with strangers, but only with friends of friends (for safety issues), the potential reduction is still up to 31%. Another recent study [9] had shown that on-demand route-free public transportation based on mobile phones outperforms standard fix-route assignment methods when comparing traveling times. These results encourage the deployment and policies supporting ride sharing in urban settings.

However, despite such evidence and others, ride-sharing adoption rate in cities worldwide is slower than what can be expected given the clear benefits of ride-sharing [10, 11]. One important reason, as suggested by [12–14] and others is the uneven, and often unstable, potential benefits associated with ride-sharing. When the value that can be extracted from using a service such as *Lyft* [15], *Uber* [16], or *Sidecar* [17] is high at one part of the city, but significantly lower at another neighborhood, or worse—suddenly decreases for a period of two days—potential users of the service are much likely to opt for a private car usage [18].

In this work we propose a data-driven framework to dynamically predict the impact, or *potential utilization*, of ride sharing in a city, at different times, and in different regions. Specifically, the technique we propose provides both policy makers as well as ride-sharing operators tools for assessing the future benefit of ride-sharing, encapsulated through the percent of rides saveable through merging of nearby departures and destinations. Simply put, a shared taxi service can use this proposed technique in order to know ahead of time what the ride-sharing demand is going to be (at various places in the city), whereas municipal services can dynamically change tolls and service fees in order to incentivize the use of ride-sharing in "low hours" that are predicted in advance.

Our method is based on analyzing the network features of the dynamic O–D matrix as represented by data collected by various sources, such as mobile phone call records, or sensors mounted on the taxis themselves. In our research, we show a clear correlation between such properties and the portion of "merge-able rides". We have analyzed the efficacy of our proposed network-oriented method using a dataset of over 14 million taxi trips taken in New York City during January 2013 [19].

This work is structured as follows: Section 2 presents an overview of the relevant related research in the field. In Section 3, we discuss the data and analytic methodologies that were used for this work: starting with the calculation of the average ride-sharing potential as a function of the maximum delay a taxi-user would be willing to sustain, we demonstrate that more than 70% of the rides can be shared when users are willing to undertake up to 5 minute delay. We then demonstrate that urban ridesharing potential is not only highly dynamic, but that it can also be predicted using the analysis of the rides that took place in the city a few hour beforehand. We present a method for comprising a dynamically changing network using the taxi-rides, and analyzing the topological properties of this network (Section 4). We analyze the dynamics of these properties over time, and demonstrate our ability to accurately predict changes in the utilization of ride-sharing several hours in advance. Concluding remarks and suggestions for future works are contained in Section 5.

2. Related Work

Network features can signal and are often used to predict events or properties that are external to the network, but influence it. A network can often be built on easily available data and serve as an important source for predictions regarding various (seemingly unrelated) events and large-scale decision-making processes [20–22]. Features of a phone call network can signal the occurrence of an emergency situation or predict trust among individuals [23], and specific behaviors in a Twitter account can identify a spammer [24]. Such discoveries had sparked the interest of researchers in different research fields, who could benefit from this new ability to model large-scale human dynamics. One of the fields most influences by this evolving research thrust was the data-driven study of human mobility and its potential application for Intelligent Transportation Systems [11, 25–28].

It has been recently shown that in trying to detect semantic network events (such as an accident or a traffic jam) it is crucial to understand the underlying structure of the network these events are taking place at [29, 30], the role of the link weights [31], as well as the response of the network to node and link removal [32]. Past research [33] had pointed out the existence of powerful patterns in the placement of links, or that clusters of strongly tied together individuals tend to be connected by weak ties [31]. It was also shown that this finding provides insight into the robustness of the network to particular patterns of link and node removal, as well as into the spreading processes that take place in the network [34, 35]. In addition, recent work had demonstrated the trade-off between the number of individuals (the width of the data) and the amount of information available from each one (the depth of the data), with respect to the ability to accurately model crowds behavior [36–38]. An analytical approach to this problem discussing the (surprisingly large) amount of personal information that can be deduced by an "attacker" who has access to one's personal interactions' meta-data can be found in [39–41].

One of the first works that examined the statistical distribution of event appearance in mobility and communication networks have found that these follow a power law principle [42], and that such distribution is significantly affected by anomalous events that are external to the networks [43]. A

method for filtering mobile phones Call Data Records (CDRs) in space and time using an agglomerative clustering algorithm in order to reconstruct the origin-destination urban travel patterns was recently suggested in [44].

Recent works that have been analyzing data collected by the pervasive use of mobile phones have broadly supported the notion that most of human mobility patterns are affected by a relatively small number of factors, easily modeled, and very predictable [4, 45–47]. A comprehensive survey of ride-sharing literature can also be found in [48] and another recent relevant study that developed spatial, temporal, and hierarchical decomposition solution strategy for ride-sharing is presented in [49].

To-date, much of the research related to ride sharing has focused on understanding the characteristics of ride-sharing trips and users. In a recent survey of app-based, on-demand rideshare users in San Francisco, researchers found that 45% of ridesharers stated they would have used a taxi or driven their own car had ridesharing not been available, while 43% would have taken transit, walked, or cycled [50].

A recent work by Santi et al. [51] introduces a way of quantifying the benefits of sharing. The study applies to a GPS dataset of taxi rides in New York City and uses the notion of *shareability network* to quantify the impact and the feasibility of taxi-sharing. When passengers have a 5 minutes flexibility on the arrival time, and they are willing to wait up to 1 minutes after calling the cab, over 90% of the sharing opportunities can be exploited and 32% of travel time can be saved. The authors have also shown that the problem is computationally tractable when we look for sharing a taxi among two people with the option of in-route picking up. Furthermore, sharing solutions involving more people are not tractable, but do not provide a significant improvement with respect to solutions involving only two people. Similar results have been demonstrated using a theoretical model analyzing *Autonomous Mobility On Demand* system, demonstrating that a combined predictive positioning and ridesharing approach is capable of reducing customer service times by up to 29% [52].

An extensive simulation infrastructure for ride-sharing analysis is suggested in [53], allowing the initialization and tracking of a wide variety of realistic scenarios, monitoring the performance of the ride-sharing system from different angles, considering different stakeholders interests and constraints. The simulative infrastructure is claimed to use an optimization algorithm that is linear in the number of trips and makes use of an efficient and fully parallelized indexing scheme.

In another study by Cici et al. [8] mobile phone data and social network data were used to estimate the benefits of ride sharing on the daily home-work commute. Mobile phone data are easier to collect than GPS traces, and have a higher penetration, providing a good sample of a city mobility. Social network data are used to study the effect of friendship on the potential of ride sharing, showing that if people want to travel only with friends then expected ride-sharing benefits are negligible. On the other hand, when people are willing to ride with friends of friends the achieved efficiency resembles this of the variant that also allows riding with strangers (implying that safety issues may have significant effect on the actual success of a ride-sharing solution).

A similar study has been presented by [54] calculating shareability curves using millions of taxi trips in New York City, San Francisco, Singapore, and Vienna, showing that a natural rescaling collapses them onto a single, universal curve. The authors presented a model that predicts the potential for ride sharing in any city, using a few basic urban quantities and no adjustable parameters.

The issue of pricing policies in ride-sharing services have gained significant attention recently. with the booming expansion of commercial ride-sharing services such as *Uber*, *Lyft* and others. The work of [55] studies dynamic pricing policies for ride-sharing platforms. As such platforms are two-sided this requires economic models that capture the incentives of both drivers and passengers. In addition, such platforms support high temporal-resolution for data collection and pricing. The combination of the latter requires stochastic models that capture the dynamics of drivers and passengers in the system.

In [56] the authors highlight the impact of the demand pattern of the underlying network on the platforms optimal profits and aggregate consumer surplus. In particular, the authors establish that both profits and consumer surplus are maximized when the demand pattern is balanced across the networks locations. In addition, the authors show that profits and consumer surplus are monotonic with the "balancedness" of the demand pattern (as formalized by the patterns structural properties).

The work of [57] proposes a recommendation framework to predict and recommend whether and where should ride-sharing users wait in order to maximize their chances of getting a ride. In the framework, a large-scale GPS data set generated by over 7,000 taxis in a period of one month in Nanjing, China was utilized to model the arrival patterns of occupied taxis from different sources.

The recent work of Alexander and Gonzalez [11] uses smart-phone data in order to model the behavior of an urban population in Boston, in an attempt to assess the impact of efficient ride-sharing service on the urban traffic, and specifically on the expected levels of congestion. This data-centric approach leads to a highly accurate modeling of the mobility patterns in the city. However, much like most of the recent work on this subject, the researchers have followed an aggregative modeling, that tries to find the static long-term definitive mobility patterns, purposely omitting any dynamic fluctuations.

In another study, researchers from the Microsoft Research Center [58] analyzed the ride data of 12,000 taxis during 110 days in order to model the mobility patterns of potential passengers. Using this probabilistic model, the researchers were able to build a recommendation system for taxi drivers that would maximize their profits (yielding an overall 10% improvement in the overall profits) and a second recommendation system for passengers, advising them where to turn in order to maximize their chances of finding a vacant taxi (with 67% accuracy). A similar research can be found in [59].

A recent review of dynamic ridesharing systems [60] focused on the optimization problem of finding efficient

matches between passengers and drivers. This ride-matching optimization problem determines vehicle routes and the assignment of passengers to vehicles considering the conflicting objectives of maximizing the number of serviced passengers, minimizing the operating cost, and minimizing passenger inconvenience. Another study [61] presented an algorithm that increases the potential destination choice for ride-sharing schemes set by considering alternative destinations that are within given space-time budgets.

On a similar note, a recent study [62] analyzed the benefits of meeting points in ride-sharing systems, investigating the potential benefits of introducing meeting points in a ride-sharing system. With meeting points, riders can be picked up and dropped off either at their origin and destination or at a meeting point that is within a certain distance from their origin or destination. The increased flexibility results in additional feasible matches between drivers and riders, and allows a driver to be matched with multiple riders without increasing the number of stops the driver needs to make. A similar approach for the optimization of such meetings points was discussed in [63].

The challenge of rides-matching was also discussed in works such as [64, 65] or [66], which have demonstrated that 2,000 vehicles (15% of the taxi fleet in New York) of capacity 10 passengers (or 3,000 vehicles of capacity of 4 passengers) can serve 98% of the New York taxi demand within a mean waiting time of 2.8 minutes and mean trip delay of 3.5 min.

A *path merging* approach, which instead of merging rides to and from the same locations calculate new paths which go through the same locations of the original trips, at the same order, and thus improves the ability to merge rides, was discussed in [67].

In a recent theoretical study [68] where the combinatorial optimization of ridesharing matching problem was tackled using the proof of the equivalence between classical centroid clustering problems and a special case of set partitioning called metric k-set partitioning, in which an efficient expectation maximization algorithm was used to achieve a 69% reduction in total vehicle distance, as compared with no ridesharing.

A fully decentralized reputation-based approach is discussed in [69], using a peer-to-peer architecture to provide self-assembling ride-sharing infrastructure capable of functioning with no central authority or regulator.

3. Dataset and Methodology

Our analysis was performed using a dataset of 14,776,615 taxi rides collected in New York City over a period of one month (January 2013) [19]. Each ride record consists of the following fields: pick-up time, pick-up longitude, pick-up latitude, drop-off longitude, drop-off latitude, number of passengers per ride, average velocity, and overall trip duration. Times granularity is second-based and positional information has been collected via GPS technology by the data provider. From this raw data sample, we omit records containing missing or erroneous GPS coordinates, as well as records that represent rides that started or ended outside Manhattan, yielded a cleaned dataset containing 12,784,243 rides.

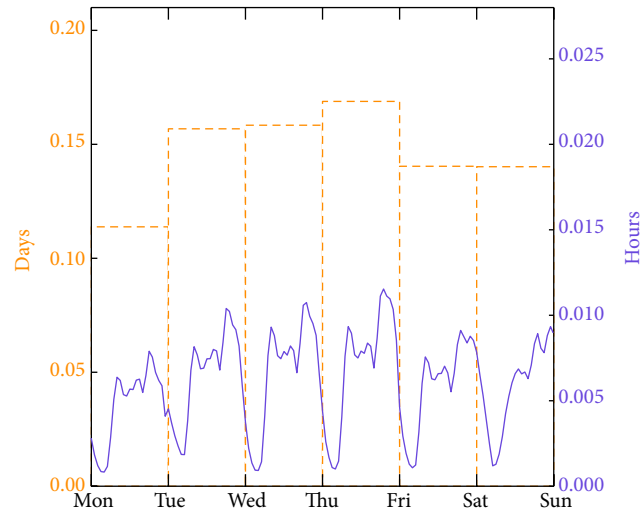

Figure 1: Probability Density Function (PDF) of the number of rides per day of week/hour of day. Afternoon peaks are centered on average around 7 pm.

As a first step in modeling the feasibility and efficiency of ride-sharing schemes using taxi rides in New York City, a comprehensive understanding of the data itself is required. How do the rides distribute over the various geographic locations? Are there patterns that emerge when observing the O'D matrix of the various rides? Can we use those in order to predict the destinations of passengers when they board a taxi at a certain location? The figures below attempt to answer some of the Power Low distribution) strongly implying on the potential of a network-centric approach as the method of choice with respect to the modeling of the dynamics of the data.

Some of the following illustrations analyzing the dataset's statistical properties were first presented in our previous publication [70]. These illustrations appear here to contribute to the reader's understanding of the nature of the data and the behavior dynamics it encapsulates.

Figure 1 reports the distribution of rides per day of the week and per hour of the day. As can be seen in the figure, the number of rides has a far-from-uniform time distribution. More specifically, the number of rides is higher in the middle of the week and is lower during the weekend. In addition, the daily rides distribution peaks, as expected, in the morning hours and around 6-7 pm.

We use the set of taxi ride records to construct a "rides network" G_{T_1,T_2}, comprising of $|V|$ nodes representing equally sized squared regions of New York City, and a set of $|E|$ edges, such that each edge $(u, v) \in E$ corresponds to a connection between two regions $u, v \in V$ if and only if there exists at least one ride from region u to region v in the time-frame referred to by the network. Such a connection exists if and only if a ride started at some time t departing at u and reaching v, or vice versa, such that $T_1 \leq t \leq T_2$ is contained in the time period defined for the network G_{T_1,T_2}.

As we create edges only based on rides that were created during a certain period of time the network may change (and quite significantly so) for various values selected for T_1 and T_2. As the time period defined by these values increases the

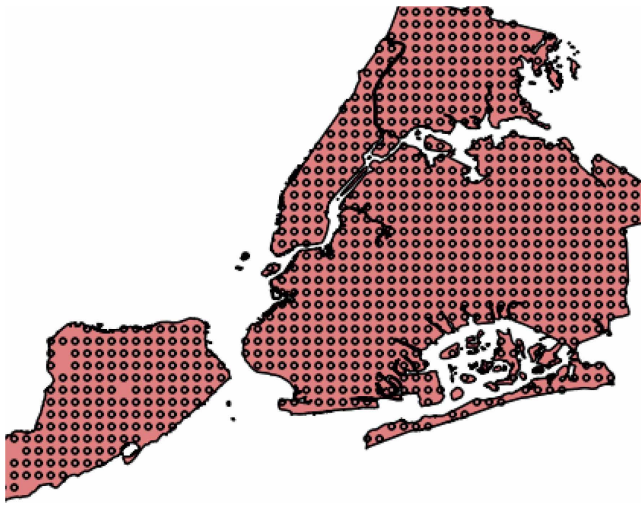

Figure 2: Illustration of the rides network G, portrayed on the map of NYC. It can be seen that the network has high density through the city, with a few empty spots in Staten Island.

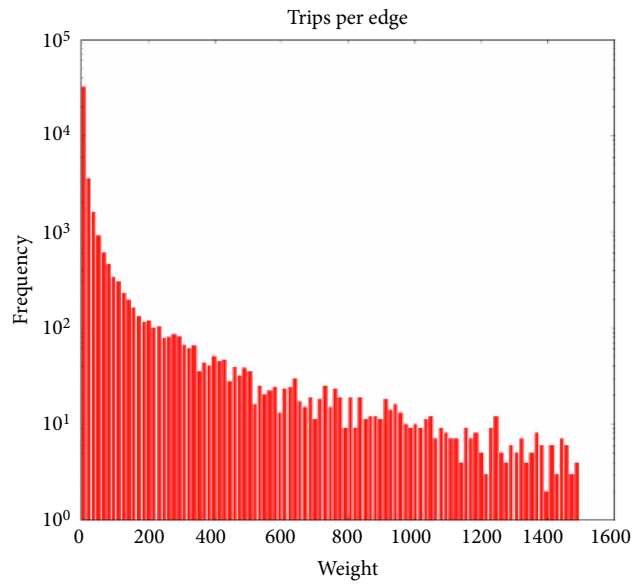

Figure 3: Edge weights of the taxi rides network G, denoting the number of trips per edge (namely, between every two nodes in the city). The X-axis denotes the number of trips per edge (representing a pair of origin-destination nodes), and the Y-axis (shown in a log-scale) represents the number of edges who have such number of trips.

network is expected to contain more edges, with the densest network received for $G = G_{-\infty,\infty}$ being the network that is based on the complete aggregation of all the rides. In order to encapsulate the traffic properties of a certain point in time T we would observe the time period circumventing T. Similarly, in order to analyze the network dynamics, that is – the way it changes over time, we would analyze the evolution of the network properties for networks created in nonidentical, yet partially-overlapping time periods. This methodology is extensively used in Section 4.

For different granularity of city partitioning (reflecting through the use of different sizes of the square regions) different ride networks would be produced. However, Network Theory implies that changing this parameter would not affect the existence of various mathematic invariants such as the network's "Scale Free-ness" or its expected small diameter [71], but rather – mainly change the sparsity of the network and its number of nodes. During this work we have examined several sizes of squared-regions, ranging from rectangular regions of 0.0156 square miles in size, to 1 square mile, obtaining similar results. The analysis below is based on square tiles of 0.39 square mile (i.e. 1 square kilometer). In such a case, when taking $G = G_{-\infty,\infty}$, the network that aggregates all the rides, it comprises 813 nodes and 58,014 edges. Figure 2 illustrates the geographical distribution of the nodes V_G on the map of New York.

Figure 3 illustrates the distribution of the number of trips on the various O-D routes in the taxi network. By *weight* we refer to the number of trips that took place through this edge and by *Frequency* we refer to the number of edges that have a specific weight. Note the small number of edges who have more than 500 rides (approximately 5,000 edges out of 58,000 edges). Similarly, over 47,000 edges have less than 50 rides passing through them. This observation coincides well with the fact that human mobility is known to follow a power low distribution [3].

As we analyze the network properties of graph implied by the taxi rides, it is interesting to observe the characteristics of the degrees of the nodes of the network G. A 'degree' of a node $v \in V$ is the number of nodes v is connected to through edges in E, where such nodes represent the actual destinations passengers who boarded a taxi at location v chose to go to. Namely, a degree of a node v represents, therefore, the number of possible destinations a passenger boarding a taxi on location v may chose to go to. An important observation is that the popularity of a node v as reflected both by its in-degree (i.e. the number of origins passengers depart from in order to get to v) as well as by its out-degree (i.e. the number of destinations passengers leaving v may go to) is independent of the geographic size or shape of node v – as all nodes refer to equally-sized square regions.

Interestingly, analyzing the distribution of this property reveals that whereas there are some nodes with a high degree (probably corresponding to main train stations or large administration facilities) the vast majority of the nodes have a very low degree. In other words – for the vast majority of the locations in New York, it is extremely easy to predict the destination of a passenger starting his ride there (as a low degree implies a low number of possible destinations, and a high chance of guessing the correct one). This observation is quite remarkable, as it implies that taxi users are *much more predictable* than may seem. Indeed, it seems that when one boards a taxi, one's destination can quite accurately be predicted.

Specifically, in 24% of the possible origins of a taxi ride in New York City, the number of possible destination of a passenger leaving these origins is on average 5, and in 43% of the origins it is 10. A quick arithmetics yields that if at some point in time we would pick a random person just boarding a taxi anywhere in New York, we would have more than 7.5% of

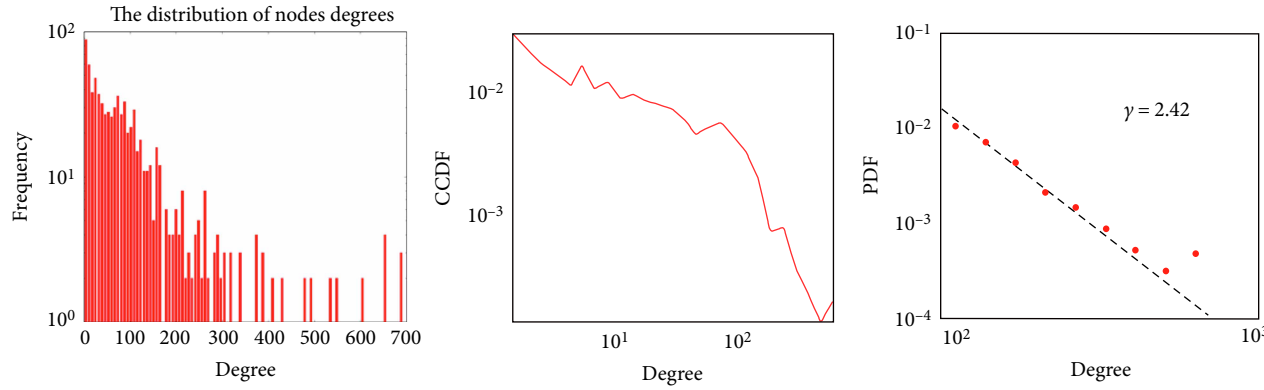

FIGURE 4: The distribution of nodes degrees in the taxi rides network, representing the number of possible destinations a passenger boarding a taxi at some location in the city may chose to go to. Note the surprisingly high number of origins with very low degrees – number of possible destinations. The nodes' degrees are unaffected by the size or shape of the actual geographic region they refer to as all nodes refer to equally-sized square patches of the city.

guessing precisely his or her destination. This probability is about three times *higher* than rolling a "Snake Eyes" (two 1's in a 6-sides dice). See Figure 4 for more details.

In this context, it is also important to note that in this work we are less interested in the specific characterization of nodes having high (or low) degrees, but rather – in the dynamics those values represent over time, as discussed in detail in the following sections.

In order to analyze the "sharability", or the ability to merge rides using the same vehicle at an overlapping times, we applied a simplified version of the methodology used by Santi et al. [51] to calculate the potential benefits of ride sharing: Let $T_i = \left(o_i, d_i, t_i^o, t_i^d\right), \quad i = 1 \cdots k$ be k trips where o_i denotes the origin of the trip, d_i the destination, and t_i^o, t_i^d the starting and ending times, respectively. We say that multiple trips T_i are shareable if there exists a route connecting all of their origins and destinations in any order where each o_i precedes the corresponding d_i.

Sharability, or 'ridesharing utilization' is expressed in terms of the number of rides that can be 'merged', as a function of the guaranteed quality of service, expressed through the number of latency minutes agreeable by the passengers – the maximum time delay in catching a ride and arriving at destination, representing the maximum discomfort that a passenger can experience using the service. In other words, given a predefined level of discomfort passengers are willing to undertake (expressed in a prolonged wait-time), the ride-sharing utilization depicts the portion of rides that are redundant and can be saved by merging with other rides to and from the same locations.

Our analysis aims at finding pairs of rides, which are represented in the network by the same edge (i.e., have the same origin and destination), that can be shared. For each edge, we examine its corresponding set of originating rides, and count the number of ride pairs that can be merged, taking into consideration the maximum time delay parameter.

The main difference between our approach and the one discussed in [51] is that we only merge rides that leave the same origin 'tile' and go to the same destination 'tile'. There are several advantages for this approach:

(1) The routing-agnostic scheme is significantly less sensitive to the temporary changes in the infrastructure, such as detours, traffic jams, accidents, and so on.

(2) Merging rides based only on their origin and destination makes our ride-sharing policy entirely agnostic to the routing decision of the driver. Alternatively, the approach that is based on allowing rides to be merged even if they do not leave from the same origin, but are rather partially overlapping, depends on the assumption that the route of the "containing ride" indeed passes through the origin of the second ride. This assumption in turn depends on either perfectly guessing the routing decisions of the driver, or – dictating those decisions to the driver by the ridesharing service.

(3) As a result, our routing-agnostic approach is also expected to be easier to implement in real-life scenario, as it requires less cooperation from the drivers.

(4) In addition, the increased simplicity of the routing-agnostic approach makes it easier to optimize from a computational point of view. The routing-aware approach discussed in [51] has a time complexity of $O\left(n^2 \log(n)\right)$ when merging pairs of rides [72], becomes much harder when triple rides merging is allowed [73], and eventually becomes computationally unfeasible for larger numbers of rides-to-be-merged [51].

(5) When comparing the merging efficiencies of our proposed routing-agnostic approach with the routing-aware one, it is shown that whereas the latter is slightly more efficient when long wait-times are allowed (increasing our proposed 73% sharability to 93% for 5 minutes maximal delay), the improvement for shorter wait times becomes significantly smaller (this is illustrated by comparing Figure 5 to Figure 3 in [51]).

Figure 6 shows the probability density function (pdf) of the number of rides per edge. As can be seen from the figure, the distribution is heavy tailed and seems to follow a

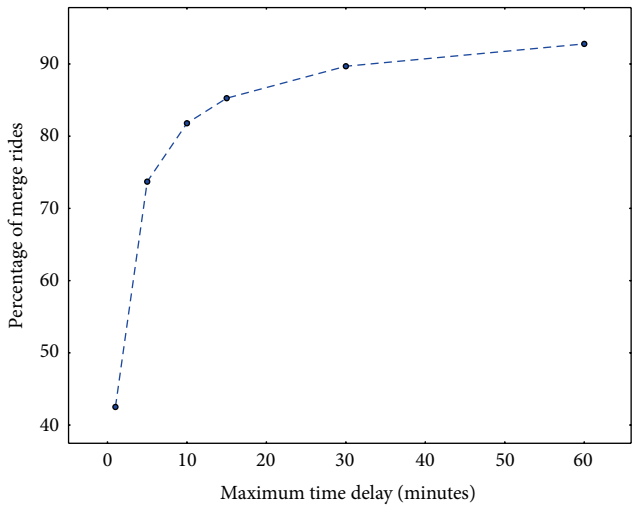

Figure 5: Percentage of merged rides (for the entire network).

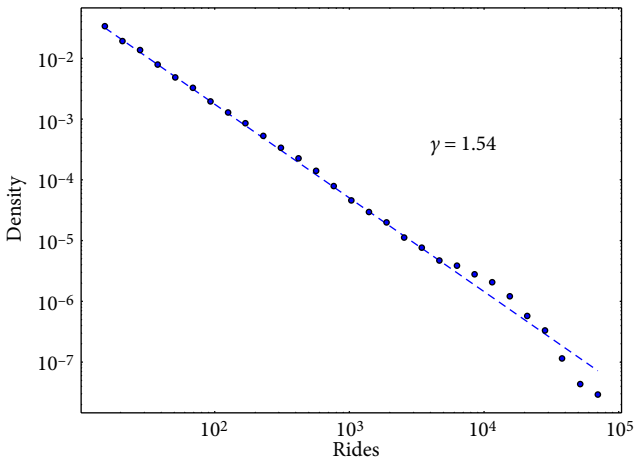

Figure 6: Probability Density Function of the number of rides per edge.

power-law. In other words, most of the edges (i.e., pairs of origin-destination) induce a small number of rides, while a small number of edges induce an extremely high number of rides.

Figure 5 presents the percentage of shareable rides as a function of the maximum time delay parameter. Results are encouraging: more than 70% of the rides can be shared when passengers can accept a delay of up to 5 minutes. As expected, the benefit of ride sharing increases when the passengers are willing to take a higher discomfort, and the percentage of shareable rides is more than 90% when passengers can wait 30 minutes or more.

It should be noted that the simplified analysis illustrated in Figure 5 assumes that two rides that took place at the same time can always be merged, regardless of the number of passengers in each ride. Since the average number of passengers per ride is 1.7 and most of the rides involve a single passenger, the number of saved rides could have been even higher by merging more than 2 rides at a time. On the other hand, in some cases, even the merging of two rides at a time might have resulted in overcrowding of the vehicle.

In order to assess the effect of these two potential phenomena over our analysis, we can observe the distribution of the number of passengers per trip in the data. While doing so, we artificially segregate trip made using private taxi caps (that can board up to 4 passengers) and trips made with larger vehicles (capable of boarding from 5 to 48 passengers):

(i) 49.22 percent of the trips have 1 passenger.
(ii) 24.22 percent of the trips have 2 passengers.
(iii) 15.72 percent of the trips have 3 passengers.
(iv) 10.84 percent of the trips have 4 passengers.

We examine two approaches for the assessment of the actual theoretical ride-sharing utilization.

Greedy merging, assuming an even distribution of number of passengers: in this approach, we analyze the merging process in a two-phase greedy approach. In the first phase, we assume that all the original trips that can be merged are indeed merged, and are done so under the assumption that the number of passengers is distributed approximately uniformly, with respect to the various geographic locations. Then, the resulting merged trips are merged again, if possible. This analysis approach should result in a lower bound for the actual ride-sharing utilization, as in real life our ride-matching algorithm would aspire for maximizing the number of merged rides, where possible.

Optimal merging: in this approach we assume that whenever two rides are merged, the number of passengers they have receives the value that would result in the most efficient merging scheme possible (confined to the overall distribution of the numbers of passengers for rides). This analysis approach should result in an upper bound for the actual ride-sharing utilization, as in real life there will be times where the only way to merge rides would be in a suboptimal way.

Following is a detailed analysis of both approaches:

Greedy merging: the expected distribution of the merged trips for the first phase would be:

(i) In 24.23 percent of the pairs, we would merge a trip that has 1 passenger with a trip that has 1 passenger. This results in a merged trip of 2 passengers.
(ii) In 23.84 percent of the pairs, we would merge a trip that has 1 passenger with a trip that has 2 passengers. This results in a merged trip of 3 passengers. These trips cannot be merged, assuming the greedy 2-step approach.
(iii) In 15.48 percent of the pairs, we would merge a trip that has 1 passenger with a trip that has 3 passengers. This results in a merged trip of 4 passengers, that cannot be further merged.
(iv) In 5.87 percent of the pairs, we would merge a trip that has 2 passengers with a trip that has 2 passengers. This results in a merged trip of 4 passengers, that cannot be further merged.
(v) In 30.58 percent of the pairs, we would not be able to merge the trips, has these would be pairs that either

(a) have one of the trips with 4 passengers, or (b) having a trip with 2 passengers and a trip with 3 passengers, or (c) having two trips having 3 passengers each.

The second phase will, therefore, be able to merge another $0.2423 \cdot 0.2423 \cdot 100 = 5.87$ percent of the original pairs, which reflects a $5.87 \cdot 2 = 11.74$ percent increase. Overall, this would sum up to $100 - 30.58 + 11.74 = 81.16$ percent of the naive potential utilization (namely, the utilization that is calculated under the assumption that all rides are merge-able, and that we do not merge more than two rides.

Optimal merging: assuming an optimal merging scheme we can calculate the merging of the relevant New York City data as follows:

(i) The 10.84 percent of the rides that have 4 passengers cannot be merged at all.

(ii) The 24.22 percent of the rides that have 2 passengers would be merged among themselves.

(iii) The 15.72 percent of the rides that have 3 passengers would be merged with a matching 15.72 percent of the rides that have 1 passenger.

(iv) This would leave another $(49.22 - 15.72 =)$ 33.5 percent of the rides, that have 1 passenger. These rides would be merged in a 4-to-1 ratio, virtually implying a $33.5 \cdot 1.5 = 50.25$ percent save.

Altogether, the actual optimal theoretical utilization would sum up to $24.22 + 15.72 + 15.72 + 50.25 = 105.91$ percent (namely, under the assumption of optimal merging the benefit from merging 4 rides of a single passenger more than compensates the loss due to rides with 4 passengers.

Therefore, the actual theoretical utilization for the New York City taxi dataset, denoted as U, would be bounded by:

$$0.8116 \cdot \alpha \leq U \leq 1.0591 \cdot \alpha \quad (1)$$

such that α is the potential utilization that is calculated throughout this work, using the method that was described above, ignoring the effect of multiple merges, as well as the effect of over-population of rides.

4. Analyzing the Dynamic Ride-Sharing Network

In the previous section we have described the taxi data that were used for this study, illustrated various mathematical properties of these, and discussed the way they can be analyzed for the purpose of assessing the potential ability of ride-sharing schemes to merge rides between similar locations (denoted as the *ride-sharing potential utilization*). In this section we demonstrate the inability of static analytic approaches to efficiently model this utilization and suggest an alternative approach, that is based on the construction of multiple network-snapshots, derived using a sliding-window based aggregation of the taxi rides. We show that this technique can serve as a valuable methodology for both (a) assessing the potential ride-sharing utilization of the current supply and demand scheme (as appears in Section 4.2), as well as (b) serve as a prediction method for estimating *changes* in this utilization, in the near future, up to a few hours (as shown in Section 4.3).

4.1. The Need for Dynamic Ridesharing Optimization and Prediction. Mainstream transportation analysis models (such as [74–78] and many more) approach the problem of transportation forecasting and analysis through the use of long-term data aggregation. Simply put, the dominating approach today sees the accurate approximation of the "steady state", or "average state", of the transportation system as the most efficient way to understand the behavior of the system, and to use this understanding in order to reach better decisions [79]. Such decisions are often concerned with the locations, type, or size of new infrastructures that should be built, large-scale budgets investment alternatives or long-term policy revisions [80].

When examining the rapidly expanding field of ridesharing this approach suffers an inherent limitation, as it is not well adequate for the nature of decisions ridesharing operators and regulators are required to make. As ridesharing uses existing roads and metropolitan infrastructure, does not require setting fixed-place stations of fixed-paths, and often uses existing vehicles, it is mostly located "outside" the realm of these analysis methodologies. Furthermore, ridesharing introduces a new set of factors that traditional methods usually cannot easily cope with, such as dynamic changes in fares, which may significantly influence network properties such as global congestion [81].

Analyzing ridesharing using the existing models would be inefficient at best. Taking the static approach using a long-term aggregation of the supply and demand would inevitably result in a model that would be optimized for the *average states* of the rides network, ignoring its inherent volatility (that is caused due to daily and weekly patterns as well as irregular spikes created by events such as street-parties, sports events, etc.).

Interestingly, as shown in Section 4.2, the dynamic rides network spends only an extremely *small portion* of the time in those average network states. Furthermore, our analysis demonstrates that overlooking the dynamic nature of the traffic scheme disregards the vast majority of the network states, as manifested in the O–D matrix, as well as the possible ridesharing utilization of it. Specifically, this phenomenon is demonstrated in Figure 7 that reveals that the system spends approximately 33% of the time in states that have a potential utilization of either 50% above the monthly average, or 50% below it.

Ignoring this dynamic nature of the urban rides system through the use of a static analysis model (which is the mainstream approach of today) will be inherently limited in its efficiency. The key to unlocking the development of effective next generation ridesharing systems, therefore, lays in an analysis that is rooted in the understanding of its dynamic nature, and the way to use it in order to develop proactive strategies that dynamically adapt their forecast using an ad-hoc analysis of the network's state.

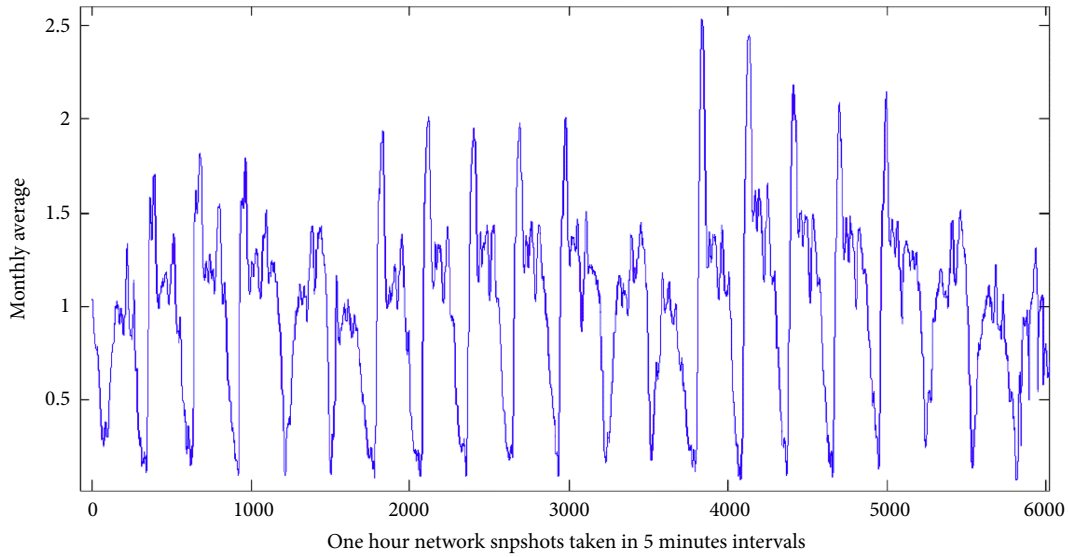

FIGURE 7: Dynamics of the potential ride-sharing utilization over time. X-axis denotes the time, given in 5-minute granularity. Y-axis denotes the change of the potential utilization compared to its monthly average.

A potential example for this approach can be found in [82], containing a computational study aimed at identifying environments in which the use of "dedicated drivers" are most useful. As urban supply and demand environments are constantly (and significantly) changing (as demonstrated in our analysis of the New York taxi data), it is therefore likely that a strategy that detects the *times* where the use of such drivers is most efficient and upon such detection – launches these drivers to supply the demand (this can be done using a dynamic change in the commission drivers are required to pay, giving such drivers a temporary priority in certain roads, or forbidding them from granting service on a regular basis expect from when their service is required) – would achieve a superior performance compared to a static strategy that does not react to such changes.

Another example can be the work of [83] in which the size of a carsharing fleet is optimized in order to maximize the monetary operational savings. Again, such an approach reaches the global optimization assuming a static approach, whereas the incorporation of the dynamic nature of the system could yield a significant. This could be done for example by allowing the fleet operators to dynamically use the services of a public service (such as Uber or Lyft), rented cars, or private drivers. Using such service when needed will allow to reduce the ongoing basic cost.

4.2. Dynamic Network Analysis. As discussed in previous sections, one of the main hurdles that prevents the wide adoption of ride-sharing might be the high volatility of its potential utilization, and the extreme unpredictability of it. In this section, we propose to mitigate this problem by using a dynamic network that represents the evolving travel patterns in the city. That is, a multitude of rides-networks, representing data of fixed-length periods of time, each of which starting at different points in time of equal distances. Such "sliding window" approach is useful for tracking changes in various properties of this dynamic network, which we show are not only highly correlated with the potential ride-sharing utilization at the corresponding points in time, but can also *predict* the utilization few hours ahead of time.

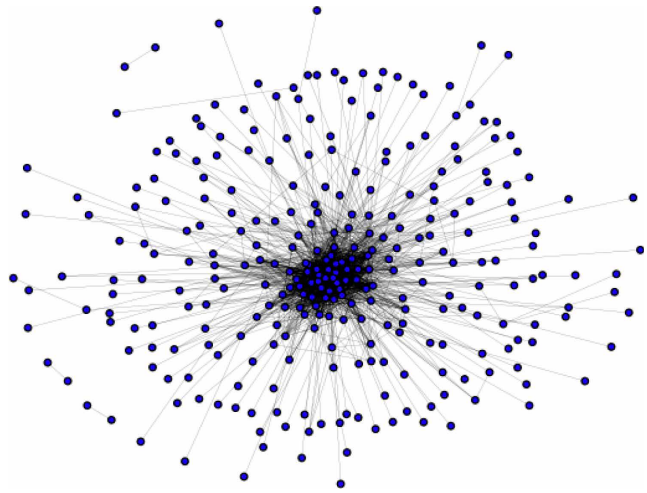

FIGURE 8: An illustration of the rides sub-network $G_{T_{144},T_{145}}$, denoting the structure that is implied by the aggregation of the rides between the 144-th and the 145-th hour of the month.

We divide the rides dataset into hourly aggregated snapshots, creating $31 \times 24 = 744$ sub-networks, each is denoted by $G_{T_n,T_{n+1}}$, such that T_n represents the n-th hour in the month. An illustration of one such sub-network is shown in Figure 8. Intuitively, we see that most of the nodes are highly connected, but a considerable number of nodes are connected to only one other node in the network.

Similarly to Figure 5 in which the potential benefit of ride-sharing over the entire data was shown, we have performed the same calculation for every hourly network separately. Figure 9 presents the average potential ride-sharing

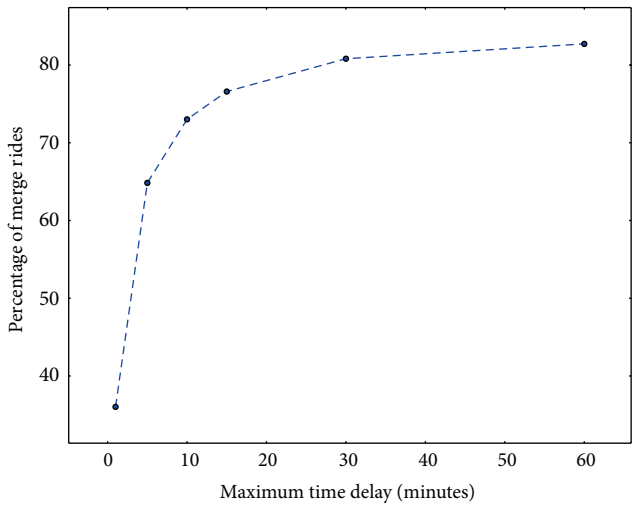

FIGURE 9: Potential of ride-sharing utilization, measured as the percentage of potentially merged rides (averaged over all sub-networks), as a function of maximal delay agreeable by the passengers. The figure is based on the result presented [70].

utilization taken on all hourly networks, as a function of the maximal delay allowed (notice that this is in fact a lower bound, since we artificially prevent passengers from being merged with rides "outside" their hourly network). It can be seen that this produces a lower utilization than the previous calculation using the overall aggregation (approximately 10% decrease), caused by the fact that each pair of nodes has a lower probability of being connected.

We now extract a set of six common network properties for each traffic-network G_{T_i,T_j}, to be used as the features values representing each network. These features encapsulate various topological aspects of the network and enable us to project each hourly-collection of traffic data (containing a large and apriorically unknown number of rides) into a single coordinate in a 6-dimensional feature-space.

(1) *Number of Nodes:* the number of nodes in the network G, denoted as $|V|$, representing the number of unique pick-up and drop-off locations of rides made during this time window. Note that although all the networks refer to the same dataset, and the same geographic environment, different networks may have different values of $|V|$, since at different time-segments different locations may be "active".

(2) *Number of Edges:* the number of edges in the network G, denoted as $|E|$, representing the number of unique pick-up to drop-off pairs of rides made during this time window. This is also the number of nonzero elements of the temporal O'-D matrix that is derived from this network.

(3) *Network Density:* the average degree of the network's nodes, defined as $|E|/|V|$. This property represents the average number of unique drop-off locations per pick-up location (and vice versa) and is associated with the predictability of rides made during this time window, and is also related to the system's entropy.

(4) *Average Betweenness Centrality:* each node v in the network G has a calculate-able betweenness centrality score [84], representing the portion of "shortest paths" between all the node-pairs in the network, that pass through v. Formally, for a network node $v \in V$ this is defined as:

$$\sum_{s \neq v \neq t} \frac{\sigma_{s,t}(v)}{\sigma_{s,t}}, \tag{2}$$

where $\sigma_{s,t}$, is the total number of shortest paths from node s to node t and $\sigma_{s,t}(v)$ is the number of those paths that pass through v.

Averaging these values yields an estimation of the network's efficiency, with respect to the number of nodes whose adequate availability is required in order to preserve the network's ability to maintain efficient flow without increasing the length or durations of trips between arbitrary points [28, 85].

(5) *Average Closeness Centrality:* the closeness centrality of a node [86] is a measure of centrality in a network, calculated as the sum of the length of the shortest paths between the node and all other nodes in the graph. Thus the more central a node is, the closer it is to all other nodes. For a node $v \in V$, the measure is defined as:

$$\frac{1}{\sum_x d(v,x)} \tag{3}$$

Averaging the closeness centrality over all the network's nodes yields an estimation of the compactness of the network, that is – how short it is to travel between an arbitrary pair of network nodes.

(6) *Average Eigenvalue Centrality:* eigenvalue centrality [87] (also called eigencentrality or eigenvector centrality) is a measure of the influence of a node in a network. It assigns relative scores to all nodes in the network based on the concept that connections to high-scoring nodes contribute more to the score of the node in question than equal connections to low-scoring nodes.

For a given graph G with an adjacency matrix A the centrality score of a node $v \in V$, denoted as $x(v)$, is defined as

$$\frac{1}{\lambda} \sum_{u \in M(v)} x_u, \tag{4}$$

where $M(v)$ is a set of the neighbors of v and λ is the graph's largest positive real eigenvalue. This can be accurately estimated by taking the v^{th} component in the eigenvector that corresponds to the largest positive real eigenvalue.

The use of eigenvalues to analyze propagation phenomena over networks can be see for example in [88], where its usability for predicting the epidemic potential of viruses is demonstrated.

We use a linear regression to fit these features for the calculated potential utilization, as well as a multiple linear regression to fit the potential utilization for the entire set of network properties. As can be seen in Figure 10, these features show a

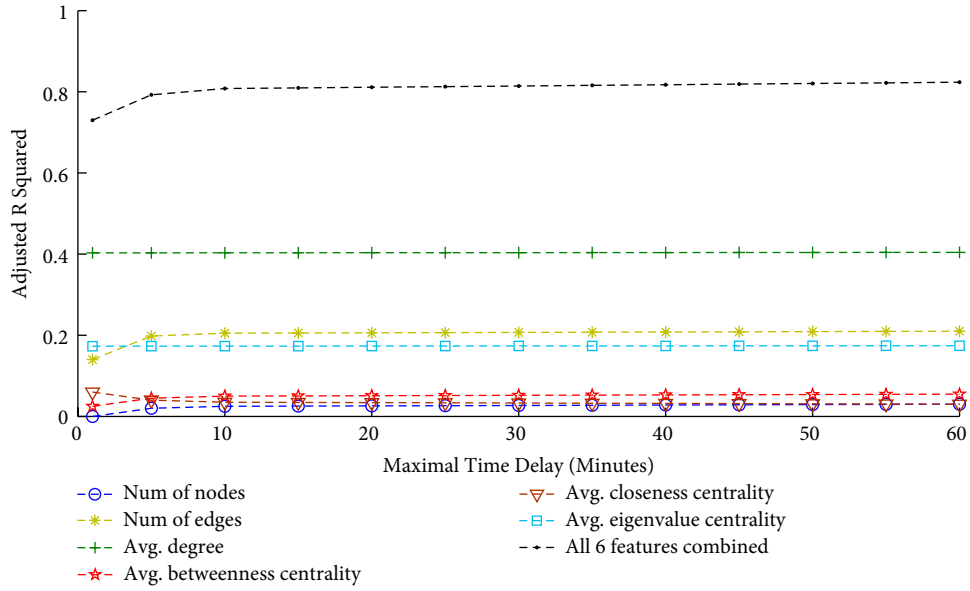

FIGURE 10: Adjusted R^2 of the correlation between seven features of the hourly rides network and the potential ride-sharing utilization for this network. Most features have low quality of fit, but the combined mixture of all seven results in a remarkably high correlation ($R^2 = 0.82$). Features are (1) the number of nodes in the network, (2) the number of edges, (3) the averaged degree, (4) the averaged betweenness centrality, (5) the averaged closeness centrality, and (6) the averaged eigenvector centrality.

high correlation with the potential utilization for this hourly network (the figure reports the adjusted R squared to account for the different number of predictors).

4.3. Ride-Sharing Potential Prediction. In the previous section, we have shown that the monthly rides can be partitioned into hourly aggregative snapshots, each of different characteristics (and specifically, network oriented ones), and different ride-sharing potentials. In addition, we have demonstrated the correlation between these network properties and the ride-sharing potentials of the rides the corresponding networks are implied from (as appears in Figure 10). In this section, we discuss whether this correlation can also be used for predictive purposes. Specifically, can we deduce from the current values of various network properties how the *change* in the ride-sharing potential compared to its current value.

In order to do so, we first analyze the evolution of various network properties of the hourly aggregative rides network $G_{T_n,T_{n+1}}$ over time. Figure 11 illustrates the evolution of the mean nodes' degree of the rides network as a function of time (that is, the average over all of the network's nodes' degrees, for all the dynamic hourly networks). For the sake of clarity, we have increased the time granularity used in the analysis, so that the hourly networks are now generated with 5-minute intervals, thus significantly overlapping, and subsequently generating a smoother and easier to read graph. The change from the monthly average of the mean degree as a function of time is portrayed, clearly showing a dominant daily pattern. However, on top of this pattern we can see significant hourly fluctuations, tens of percent in magnitude. This reveals the existence of strong volatility in the rides dynamics alongside the predicted daily and weekly dynamics.

A similar dynamics is observed when analyzing the evolution of the largest eigenvalue of the rides-network' adjacency matrix over time. The use of eigenvalues to analyze propagation phenomena over networks can be seen for example in [88, 89], where its usability for predicting the epidemic potential of viruses (both human and computer-based) is demonstrated. Additional mathematical analysis on the role of eigenvalues in the analysis of network structures can be found in [90]. This property, known to encapsulate various behavioral characteristics of the people whose mobility patterns the network is depicting, displays a clear (and easy to predict and understand) daily pattern, on top of which significant and erratic spikes are added, as can be seen in Figure 12. These spikes seem to appear sporadically, lacking any clear patterns or internal regularity, implying again the need for understanding the dynamic aspects of the network.

Now, let us perform a similar analysis over the potential ride-sharing utilization, looking at its evolution over time. The results of this analysis, presented in Figure 7, clearly demonstrate a similar dynamics to the couple of network properties mentioned earlier. Specifically, it can be seen that alongside the dominating daily pattern (and weaker, but still easy to see, weekly one), there are clear changes in the potential utilization. These changes take various shapes and forms, from sudden decrease in the daily peak (as can be seen around $X = 1400$), to changes in the intra-weekly peaks (the first week analyzed showing a 'U-shaped' form among its days, the second week showing an equal-peaks dynamics, and the third week showing an extremely high Monday and Tuesday, and weaker Wednesday, Thursday and Friday), and others. Surprisingly, the magnitude of these changes may even exceed the dominating daily pattern. For example, the change between the first Tuesday (around $X = 200$) and the third Tuesday ($X = 4100$) is 90% compared to the monthly average, whereas the average change in potential utilization between workdays and weekends is only 70%.

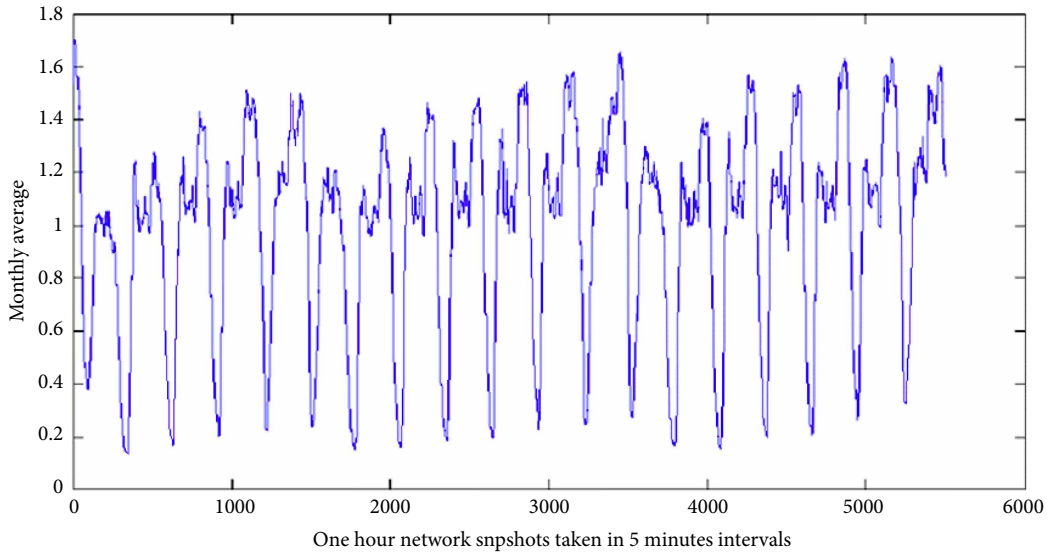

FIGURE 11: Dynamics of the mean degree of the rides network nodes. *X*-axis denotes the time, given in 5 minutes granularity. *Y*-axis denotes the change of the mean degree of the network compared to its monthly average.

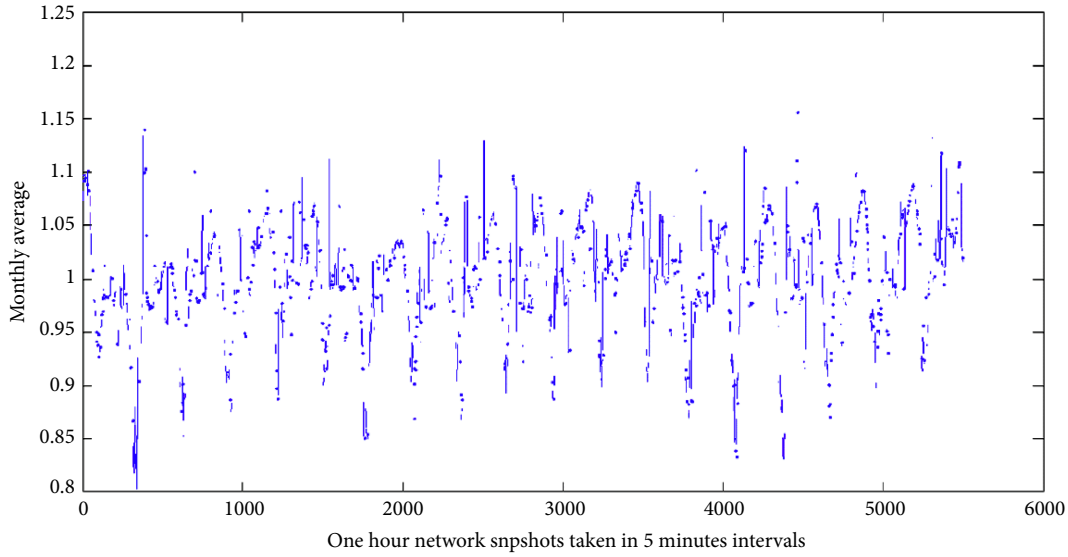

FIGURE 12: Dynamics of the largest eigenvalue of the rides-dynamic network over time. *X*-axis denotes the time, given in 5-minute granularity. *Y*-axis denotes the change of the largest eigenvalue of the network compared to its monthly average.

At this point, we ask the following question: "can we find a statistical correlation between *current* values of the rides network properties and *future* values of the potential ride-sharing utilization?". This question is of interest, as such a correlation would allow us to predict future changes in the potential utilization, providing valuable tools for both ride-sharing users, operators, and regulators.

We first address this question by comparing network properties values at time T with potential utilization of at time $T + 1$ (1 hour prediction). Figure 13 presents an example of such a comparison, in the form of a scatter plot showing for each point in time T a dot whose X-axis is the mean nodes' degree of the network $G_{T,T+1}$ and whose Y-axis is the change in the potential utilization of the rides between $T + 1$ and $T + 2$ compared to the rides between T and $T + 1$. That is, the change in the momentary ride-sharing utilization between "now" (time T) and "in an hour" (time $T + 1$). It is easy to see that this representation reveals a clear and strong negative correlation between the two.

Trying to increase our lookahead and predict the change in the dynamic ride-sharing utilization from a 2 hours timeframe, Figure 14 illustrates the correlation between the value of the largest eigenvalue of the rides network at time T and the change in the potential utilization between time T (aggregated to $T + 1$) and $T + 2$ (aggregated to $T + 3$). Again, a clear strong negative correlation is easily visible. For example, in times where the value of the largest eigenvalue of the rides network is smaller than 0.012, the potential ride-sharing utilization was

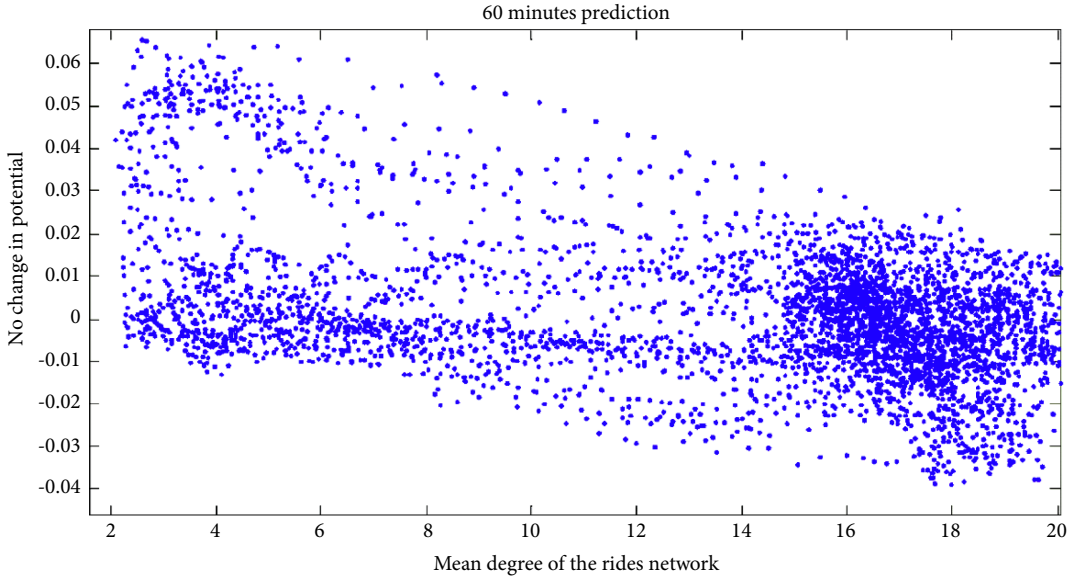

FIGURE 13: Change in potential ride-sharing utilization (Y-axis), 1 hour prediction, as a function of the mean degree of the rides network (X-axis).

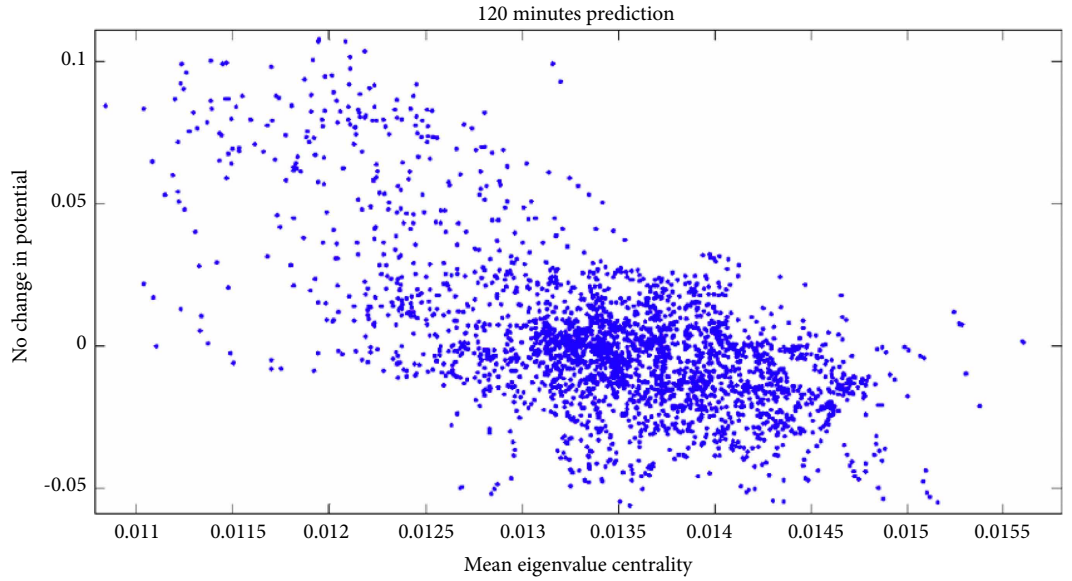

FIGURE 14: Change in potential ride-sharing utilization (Y-axis), 2 hours prediction, as a function of the largest eigenvalue of the rides network (X-axis).

statistically guaranteed (during the month of the observation) to significantly increase in the coming 2 hours. Similarly, largest eigenvalue of 0.014 would indicate a significant decrease in the ride-sharing potential within the next 2 hours.

Figures 13 and 14 are based on the analysis of the first 3 weeks of January 2013. These observations were then validated using the last week of January, as can be seen in Figures 15 and 16.

Once demonstrating the predictive power of the dynamic network's properties with respect to the network's future ride-sharing potential, we can now construct a multiple linear regression model that would fit all of these 6 properties. We have created 18 models, for 2 values of distance tolerance (400 m and 800 m, denoting the pick-up and drop-off distances that still allow rides to be merged), 3 values of time tolerance (30 s, 2 minutes and 5 minutes, denoting the time passengers would be willing to wait in order to merge their rides) and 3 values of prediction horizon (no prediction, 1 hour prediction and 2 hours prediction). The results include a scatter plot of the data, effects of the various properties, ANOVA, and other statistical analyses as appearing in Supplementary Figures 17–34.

The effectiveness of the prediction as a function of the prediction horizon (i.e., the distance between the point in time where the prediction is calculated and the point in time this

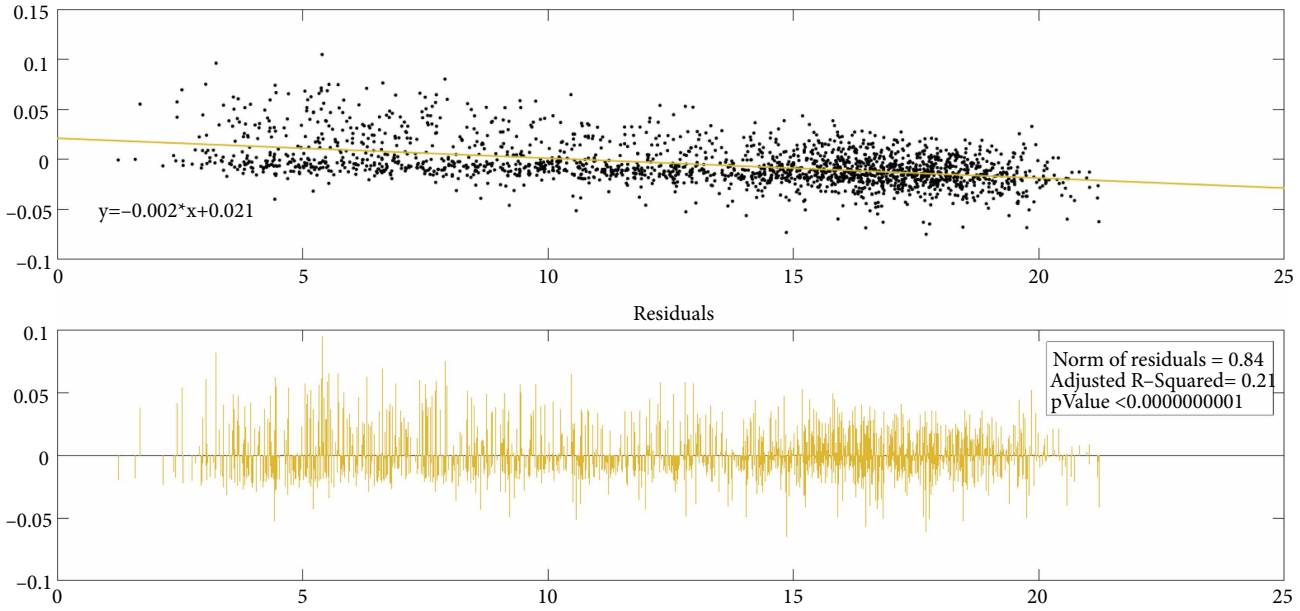

Figure 15: Change in potential ride-sharing utilization (Y-axis), 1 hour prediction, as a function of the mean degree of the rides network (X-axis), created for the last week of the data.

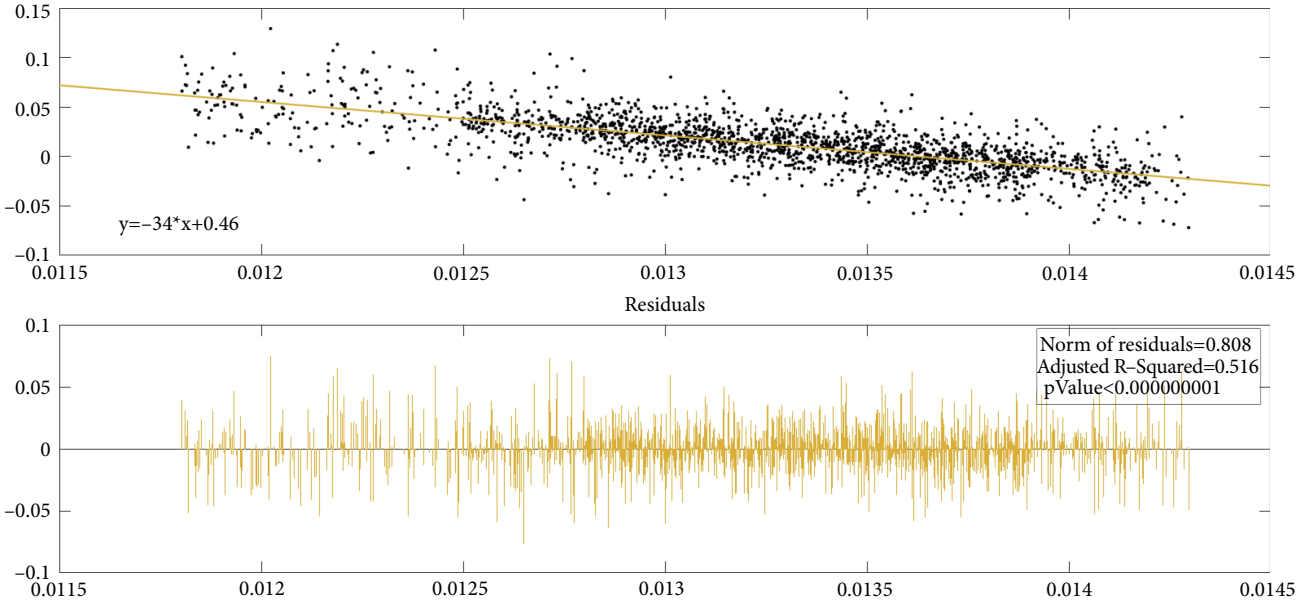

Figure 16: Change in potential ride-sharing utilization (Y-axis), 2 hours prediction, as a function of the largest eigenvalue of the rides network (X-axis), created for the last week of the data.

prediction refers to) is illustrated in Supplementary Figures 35–40, showing the R^2 of the model (both ordinal and adjusted) as a function of the time horizon (between 0 and 12 hours), for several values of distance tolerance and time tolerance. It can clearly be seen that in general (and as expected) the accuracy of the model decreases with the increase in the prediction horizon used (that is, when the model tries to predict the behavior of the system further into the future).

The effect of each feature, depicted by the adjusted response plot for its various values, is presented in Supplementary Figures 41–46, created for a scenario with distance tolerance of 800 meters, time tolerance of 5 minutes, and prediction horizon of 2 hours.

5. Summary and Future Work

As the popularity of ride-sharing systems grow, its users-base gradually transform from early adopters to mainstream consumers. Whereas the first are characterized by a keen affection

for innovative solution that are powered by cutting edge technologies and aim to disrupt the governing paradigm in the field, the latter are often interested mainly in the advantages these services can offer them with as smallest change in their habits as possible. With respect to ride sharing, these new users are willing to sustain far less wait-time and are extremely more susceptible to inconvenience than their preceding tech-savvy innovation-hungry early users. The key to a scalable mature ride-sharing infrastructure is found in the level of service such systems will provide, mainly measured by the availability of vehicles when they are needed. Alas, the availability maximization is immediately linked to a reduction in the financial savings that the service can offer. In other words, a further expansion of ride-sharing is being constrained among others by the ability to offer high utilization, defined as the ability to "merge" similar rides in a way that would not require the passengers to sustain more than a minimal delay in their trips.

This optimization problem was extensively discussed in previous literature (comprehensive literature review can be found in Section 2). However, the conventional approach to this problem assumed a static environment which needs to be optimized. By finding the optimal number of cars, or optimal pricing policy, the efficiency (or potential) of the system was assumed to be calculable in a robust way – a key component in the decision of operators where to deploy new systems, in the design of relevant urban legislations by municipal policy makers, and of course in the likelihood of passengers to use these services.

In this work we discussed the dynamic nature of ride-sharing systems. Specifically, we were interested whether ride-sharing utilization is stable over time (which coincides with the implicit assumption of most previous works in this field) or does it undergo significant and often rapid changes (which would imply the inherent inefficiency of schemes assuming a static nature). We modeled the ride-sharing utilization using the known New York Taxi dataset and clearly show that it is highly dynamic, and that any system that would be designed for the "average" utilization would be highly inefficient.

We then show that assuming a dynamic approach the taxi data can be modeled as a sequence of data-snapshots, resulting in a dynamic traffic-network model. Several recent works have shown that network features can effectively be used to predict a variety of events and properties, e.g., emergency situations, individuals' personality and spending behaviors [91, 92]. We used a similar technique in order to project the taxi data as into a feature space comprised of topological features of the dynamic network implied by this traffic. This (dynamic) feature space is then used to model the dynamics of ride-sharing utilization over time.

Using this approach we were able to demonstrate a clear correlation between the utilization of the ride-sharing system over time and several topological features of the network it creates. In addition, we demonstrated that the potential benefit of ride sharing expressed as the percentage of rides that can be shared with a limited discomfort for riders can also be predicted a few hours in advance. Such prediction can be used as a tool for an accurate short-term forecasting of the ride-sharing potential in cities and metropolitan areas.

Researchers in [8, 51, 93] and others have focused on addressing the computational challenges of trip-matching (an NP-hard optimization problem) in real-time and developed heuristics to quantify potential ride-sharing demand. These algorithms reroute trips in order to match them with similar, overlapping trips, explicitly capturing demand for ridesharing relative to passenger's willingness to experience prolonged travel time. However, finding an optimal solution to this problem is not computationally plausible (even under extreme limitations of the problem's space [94]), and even the calculation of approximation heuristics would be computationally intense when done ad-hoc. Therefore, the ability to use current traffic dynamics in order to predict properties of an efficient near-future ride-sharing scheme – such as the method we propose in this work – can be used to make this process significantly more efficient [95, 96].

Future work should focus on the analysis of the correlation we find in this paper, trying to detect traces of possible causalities. Are network properties merely correlated with ride-sharing utilization, or do they possess an active influence over it? Evidence of the latter would enable us to offer urban designers and policy makers an innovative tool for encouraging and facilitating the adoption of ride-sharing systems. Alternatively, incentives and fees could be better moderated, used as "remedies" in the case of a change in the travel patterns, in order to balance it and maintain a sustainable ride-sharing paradigm. Another approach could be the pipelining of the dynamic ride-sharing utilization forecast as the input of models intended to predict the benefits of ride-sharing on the overall traffic [97].

Recent works have demonstrated the benefit of tracking the network's dynamics in order to improve collaborative decision making [98, 99]. A possible continuation of the current work can analyze ride-sharing optimization as a case of decentralized decision-making process, using the technique that is presented here.

As the prediction of future ride-sharing potential is ultimately needed for optimization purposes (of the overall travel time, congestion or any other utilization metric) of a dynamic coverage problem, comparing the performance of any proposed method to the theoretical results that are available for various types of such decentralized collaborative coverage challenges (see [100–105] and specifically [106]) can also be of value.

Finally, as our suggested approach is agnostic to the actual route taken by the drivers it would be interesting to see whether the introduction of ride-sharing affects additional factors such as detours (that for a merged ride may become cost-effective), usage of toll-routes, etc.

Data Availability

The taxi data used to support the findings of this study, encompassing a dataset of over 14 million individual taxi trips taken in New York City, are accessible at the NYC Taxi repository [19].

Conflicts of Interest

The authors declare that they have no conflicts of interest.

Acknowledgments

This research was funded in part by the Israeli Institute of Technology graduate scholarship and Israel Science Foundation (ISF).

Supplementary Materials

Prediction results. (*Supplementary Materials*)

References

[1] A. Caragliu, C. Del Bo, and P. Nijkamp, "Smart cities in Europe," *Journal of Urban Technology*, vol. 18, no. 2, pp. 65–82, 2011.

[2] H. Chourabi, T. Nam, S. Walker et al., "Understanding smart cities: an integrative framework," in *Proceedings of the 45th Hawaii International Conference on System Science (HICSS)*, IEEE, USA, pp. 2289–2297, 2012.

[3] M. C. Gonzalez, C. A. Hidalgo, and A.-L. Barabasi, "Understanding individual human mobility patterns," *Nature*, vol. 453, no. 7196, pp. 779–782, 2008.

[4] F. Calabrese, M. Diao, G. Di Lorenzo, J. Ferreira Jr., and C. Ratti, "Understanding individual mobility patterns from urban sensing data: a mobile phone trace example," *Transportation Research Part C: Emerging Technologies*, vol. 26, pp. 301–313, 2013.

[5] A. Noulas, S. Scellato, R. Lambiotte, M. Pontil, and C. Mascolo, "A tale of many cities: universal patterns in human urban mobility," *PLoS One*, vol. 7, no. 5, Article ID e37027, 2012.

[6] http://www.waze.com, [Online; accessed 15-October-2014].

[7] Solving transport headaches in the cities of 2050, BBC Future [Online; accessed 15-October-2014].

[8] B. Cici, A. Markopoulou, E. Frias-Martinez, and N. Laoutaris, "Assessing the potential of ride-sharing using mobile and social data: a tale of four cities," in *Proceedings of the 2014 ACM International Joint Conference on Pervasive and Ubiquitous Computing*, ACM, USA, pp. 201–211, 2014.

[9] T. Altshuler, Y. Shiftan, R. Katoshevski, N. Oliver, A. S. Pentland, and Y. Altshuler, "Mobile phones for on-demand public transportation," in *NetSci*, 2014.

[10] D. Graziotin, "An analysis of issues against the adoption of dynamic carpooling," http://arxiv.org/abs/1306.0361.

[11] L. Alexander and M. Gonzalez, "Assessing the impact of real-time ridesharing on urban traffic using mobile phone data," 2015.

[12] S. Hobrink, "Explaining regional adoption differentials in Dutch car sharing markets," 2014.

[13] L. Coenen, P. Benneworth, and B. Truffer, "Toward a spatial perspective on sustainability transitions," *Research Policy*, vol. 41, no. 6, pp. 968–979, 2012.

[14] S. Shaheen, A. Cohen, and M. Chung, "North American carsharing," *Transportation Research Record: Journal of the Transportation Research Board*, vol. 2110, no. 1, pp. 35–44, 2009.

[15] lyft.com, http://www.lyft.com.

[16] uber.com, http://www.uber.com.

[17] side.cr, "(currently closed, and acquired by General Motors)," http://www.side.cr.

[18] D. Efthymiou, C. Antoniou, and P. Waddell, "Factors affecting the adoption of vehicle sharing systems by young drivers," *Transport Policy*, vol. 29, pp. 64–73, 2013.

[19] NYC Open Data Website, http://data.ny.gov/. Accessed September, 2014.

[20] Y. Altshuler, A. S. Pentland, and G. Gordon, "Social behavior bias and knowledge management optimization," *Social Computing, Behavioral-Cultural Modeling, and Prediction*, Springer, Cham, pp. 258–263, 2015.

[21] P. M. Krafft, J. Zheng, W. Pan et al., "Human collective intelligence as distributed bayesian inference," http://arxiv.org/abs/1608.01987.

[22] D. Lazer, A. S. Pentland, L. Adamic et al., "Computational social science," *Science*, vol. 323, no. 5915, pp. 721–723, 2009.

[23] E. Shmueli, V. K. Singh, B. Lepri, and A. S. Pentland, "Sensing, understanding, and shaping social behavior," *IEEE Transactions on Computational Social Systems*, vol. 1, no. 1, pp. 22–34, 2014.

[24] A. Almaatouq, A. Alabdulkareem, M. Nouh et al., "Twitter: Who gets caught? observed trends in social micro-blogging spam," in *Proceedings of the 2014 ACM Conference on Web Science, WebSci '14*, ACM, pp. 33–41, 2014.

[25] M. C. Gonzalez, C. A. Hidalgo, and A.-L. Barabasi, "Understanding individual human mobility pat-terns," *Nature*, vol. 453, no. 7196, pp. 779–782, 2008.

[26] Y. Altshuler, R. Puzis, Y. Elovici, S. Bekhor, and A. S. Pentland, "On the rationality and optimality of transportation networks defense: a network centrality approach," *Securing Transportation Systems*, pp. 35–63

[27] J. Armstrong and A. Khan, "Modelling urban transportation emissions: role of GIS," *Computers, Environment and Urban Systems*, vol. 28, no. 4, pp. 421–433, 2004.

[28] R. Puzis, Y. Altshuler, Y. Elovici, S. Bekhor, Y. Shiftan, and A. Pentland, "Augmented betweenness centrality for environmentally-aware traffic monitoring in transportation networks," *Journal of Intelligent Transportation Systems*, vol. 17, no. 1, pp. 91–105, 2013.

[29] B. Waclaw, *Statistical mechanics of complex networks*, http://arxiv.org/abs/0704.3702.

[30] S. Wassermann and K. Faust, *Social network analysis: Methods and applications*, Cambridge University Press, 1994.

[31] M. Granovetter, "The strength of weak ties," *American Journal of Sociology*, vol. 78, no. 6, pp. 1360–1380, 1973.

[32] R. Albert, H. Jeong, and A. Barabasi, "Error and attack tolerance of complex networks," *Nature*, vol. 406, no. 6794, pp. 378–382, 2000.

[33] J.-P. Onnela, J. Saramäki, J. Hyvönen et al., "Structure and tie strengths in mobile communication networks," *Proceedings of the National Academy of Sciences*, vol. 104, no. 18, pp. 7332–7336, 2007.

[34] R. Pastor-Satorras and A. Vespignani, "Epidemic spreading in scale-free networks," *Physical Review Letters*, vol. 86, no. 14, pp. 3200–3203, 2001.

[35] R. Pastor-Satorras and A. Vespignani, *Evolution and Structure of the Internet: A Statistical Physics Approach*, Cambridge Univ Pr, 2007.

[36] Y. Altshuler, M. Fire, N. Aharony, Y. Elovici, and A. Pentland, "How many makes a crowd? on the correlation between groups' size and the accuracy of modeling," in *International Conference on Social Computing, Behavioral-Cultural Modeling and Prediction*, Springer, pp. 43–52, 2012.

[37] Y. Altshuler, N. Aharony, M. Fire, Y. Elovici, and A. Pentland, "Incremental learning with accuracy prediction of social and individual properties from mobile-phone data," in *2012 International Conference on Privacy, Security, Risk and Trust and 2012 International Conference on Social Computing*, IEEE

[38] Y. Altshuler, E. Shmueli, G. Zyskind, O. Lederman, N. Oliver, and A. Pentland, "Campaign optimization through behavioral modeling and mobile network analysis," *IEEE Transactions on Computational Social Systems*, vol. 1, no. 2, pp. 121–134, 2014.

[39] Y. Altshuler, N. Aharony, A. Pentland, Y. Elovici, and M. Cebrian, "Stealing reality: when criminals become data scientists (or vice versa)," *IEEE Intelligent Systems*, vol. 26, no. 6, pp. 22–30, 2011.

[40] C. Jernigan and B. F. Mistree, "Gaydar: Facebook friendships expose sexual orientation," *First Monday*, vol. 14, no. 10, 2009.

[41] W. Pan, Y. Altshuler, and A. Pentland, "Decoding social influence and the wisdom of the crowd in financial trading network," in *Privacy, Security, Risk and Trust (PASSAT), 2012 International Conference on and 2012 International Conference on Social Computing (SocialCom)*, IEEE, pp. 203–209, 2012.

[42] A. Barabasi, "The origin of bursts and heavy tails in human dynamics," *Nature*, vol. 435, no. 7039, pp. 207–211, 2005.

[43] J. Candia, M. Gonzalez, P. Wang, T. Schoenharl, G. Madey, and A. Barabasi, "Uncovering individual and collective human dynamics from mobile phone records," *Journal of Physics A: Mathematical and Theoretical*, vol. 41, Article ID 224015, 2008.

[44] L. Alexander, S. Jiang, M. Murga, and M. C. Gonzalez, "Origin–destination trips by purpose and time of day inferred from mobile phone data," *Transportation Research Part C: Emerging Technologies*, vol. 58, no. Part B, pp. 240–250

[45] D. Brockmann, L. Hufnagel, and T. Geisel, "The scaling laws of human travel," *Nature*, vol. 439, no. 7075, pp. 462–465, 2006.

[46] Y.-A. de Montjoye, C. A. Hidalgo, M. Verleysen, and V. D. Blondel, "Unique in the crowd: the privacy bounds of human mobility," *Scientific Reports*, vol. 3, no. 1, 2013.

[47] C. Song, Z. Qu, N. Blumm, and A. Barabasi, "Limits of predictability in human mobility," *Science*, vol. 327, no. 5968, pp. 1018–1021, 2010.

[48] M. Furuhata, M. Dessouky, F. Ordóñez, M.-E. Brunet, X. Wang, and S. Koenig, "Ridesharing: the state-of-the-art and future directions," *Transportation Research Part B: Methodological*, vol. 57, pp. 28–46, 2013.

[49] K. Ghoseiri, *Dynamic rideshare optimized matching problem [thesis]*, University of Maryland, College Park, MD, 2012.

[50] L. Rayle, S. Shaheen, N. Chan, D. Dai, and R. Cervero, *App-based, on-demand ride services: comparing taxi and ridesourcing trips and user characteristics in San Francisco University of California Transportation Center (UCTC), Tech. rep., UCTC-FR-2014-08*, University of California Transportation Center, Berkeley, Calif., 2014.

[51] P. Santi, G. Resta, M. Szell, S. Sobolevsky, S. H. Strogatz, and C. Ratti, "Quantifying the benefits of vehicle pooling with shareability networks," *Proceedings of the National Academy of Sciences*, vol. 111, no. 37, pp. 13290–13294, 2014.

[52] J. Miller and J. P. How, *Predictive positioning and quality of service ridesharing for campus mobility on demand systems*, http://arxiv.org/abs/1609.08116.

[53] M. Ota, H. Vo, C. Silva, and J. Freire, "Stars: simulating taxi ride sharing at scale," *IEEE Transactions on Big Data*, vol. 3, no. 3, 2017.

[54] R. Tachet, O. Sagarra, P. Santi et al., "Scaling law of urban ride sharing," http://arxiv.org/abs/1610.09921.

[55] S. Banerjee, R. Johari, and C. Riquelme, "Dynamic pricing in ridesharing platforms," *ACM SIGecom Exchanges*, vol. 15, no. 1, pp. 65–70, 2016.

[56] K. Bimpikis, O. Candogan, and S. Daniela, "Spatial pricing in ride-sharing networks," *Operations Research*, vol. 67, no. 3, 2019.

[57] C. Dai, "Ridesharing recommendation: Whether and where should i wait?" in *International Conference on Web-Age Information Management*, Springer, pp. 151–163, 2016.

[58] J. Yuan, Y. Zheng, L. Zhang, and X. G. Xie Sun, "Where to nd my next passenger?" in *Ubicomp'11*, 2011.

[59] X. Li, G. Pan, Z. Wu et al., "Prediction of urban human mobility using large-scale taxi traces and its applications," *Frontiers of Computer Science*, vol. 6, no. 1, pp. 111–121, 2012.

[60] N. Agatz, A. Erera, M. Savelsbergh, and X. Wang, "Optimization for dynamic ride-sharing: a review," *European Journal of Operational Research*, vol. 223, no. 2, pp. 295–303, 2012.

[61] Y. Wang, R. Kutadinata, and S. Winter, "Activity-based ridesharing: increasing exibility by time geography," in *Proceedings of the 24th ACM SIGSPATIAL International Conference on Advances in Geographic Information Systems*, ACM, p. 12016.

[62] M. Stiglic, N. Agatz, M. Savelsbergh, and M. Gradisar, "The benefits of meeting points in ride-sharing systems," *Transportation Research Part B: Methodological*, vol. 82, pp. 36–53, 2015.

[63] P. Goel, L. Kulik, and K. Ramamohanarao, "Optimal pick up point selection for effective ride sharing," *IEEE Transactions on Big Data*, vol. 32, pp. 154–168, 2017.

[64] L. Alarabi, B. Cao, L. Zhao, M. F. Mokbel, and A. Basalamah, *A demonstration of sharek: an efficient matching framework for ride sharing systems*, in *Proceedings of the 24th ACM SIGSPATIAL International Conference on Advances in Geographic Information Systems*, ACM, p. 95, 2016.

[65] M. Stiglic, N. Agatz, M. Savelsbergh, and M. Gradisar, "Making dynamic ride-sharing work: the impact of driver and rider exibility," *Transportation Research Part E: Logistics and Transportation Review*, vol. 91, pp. 190–207, 2016.

[66] J. Alonso-Mora, S. Samaranayake, A. Wallar, E. Frazzoli, and D. Rus, "On-demand high-capacity ride-sharing via dynamic trip-vehicle assignment," *Proceedings of the National Academy of Sciences*, vol. 114, no. 3, pp. 462–467, 2017.

[67] E. D'Andrea, D. Di Lorenzo, B. Lazzerini, F. Marcelloni, and F. Schoen, "Path clustering based on a novel dissimilarity function for ride-sharing recommenders," in *IEEE International Conference on Smart Computing (SMARTCOMP)*, IEEE, pp. 1–8, 2016.

[68] C. Wu, E. Kamar, and E. Horvitz, "Clustering for set partitioning with a case study in ridesharing," in *2016 IEEE 19th International Conference on Intelligent Transportation Systems (ITSC)*, IEEE, pp. 1384–1388, 2016.

[69] D. Sánchez, S. Martínez, and J. Domingo-Ferrer, "Co-utile p2p ridesharing via decentralization and reputation management," *Transportation Research Part C: Emerging Technologies*, vol. 73, pp. 147–166, 2016.

[70] T. Altshuler, Y. Shiftan, R. Katoshevski et al., "The network dimension of ride sharing," in *International Conference on Computational Social Science (ICCSS)*, 2015.

[71] A.-L. Barabasi and R. Albert, "Emergence of scaling in random networks," *Science*, vol. 286, no. 5439, pp. 509–512, 1999.

[72] Z. Galil, "Efficient algorithms for finding maximum matching in graphs," *ACM Computing Surveys (CSUR)*, vol. 18, no. 1, pp. 23–38, 1986.

[73] B. Chandra and M. M. Halldorsson, "Greedy local improvement and weighted set packing approximation," *Journal of Algorithms*, vol. 39, no. 2, pp. 223–240, 2001.

[74] M. E. Ben-Akiva and S. R. Lerman, *Discrete Choice Analysis: Theory and Application to Travel Demand*, vol. 9, MIT Press, 1985.

[75] S. Erlander and N. F. Stewart, *The Gravity Model in Transportation Analysis: Theory and Extensions*, vol. 3, VSP, 1990.

[76] C.-H. Wen and F. S. Koppelman, "The generalized nested logit model," *Transportation Research Part B: Methodological*, vol. 35, no. 7, pp. 627–641, 2001.

[77] J. G. Wardrop, "Some theoretical aspects of road traffic research," *Proceedings of the Institution of Civil Engineers*, vol. 1, pp. 325–378, 1952.

[78] M. G. McNally, "The four step model," *Handbook of Transport Modelling*, vol. 1, pp. 35–41, 2007.

[79] T. L. Friesz, "Transportation network equilibrium, design and aggregation: key developments and research opportunities," *Transportation Research Part A: General*, vol. 19, no. 5, pp. 413–427, 1985.

[80] M. D. Meyer and E. J. Miller, *Urban Transportation Planning: A Decision-Oriented Approach*, Osgoode Course Casebooks, 2nd edition, 1984.

[81] H. Xu, F. Ordóñez, and M. Dessouky, "A traffic assignment model for a ridesharing transportation market," *Journal of Advanced Transportation*, vol. 49, no. 7, pp. 793–816, 2015.

[82] A. Lee and M. Savelsbergh, "Dynamic ridesharing: Is there a role for dedicated drivers?" *Transportation Research Part B: Methodological*, vol. 81, pp. 483–497, 2015.

[83] D. J. Fagnant and K. M. Kockelman, *Dynamic ride-sharing and optimal fleet sizing for a system of shared autonomous vehicles*, in *Transportation Research Board 94th Annual Meeting, no. 15–1962*, 2015.

[84] L. C. Freeman, "A set of measures of centrality based on betweenness," *Sociometry*, vol. 40, no. 1, pp. 35–41, 1977.

[85] Y. Altshuler, R. Puzis, Y. Elovici, S. Bekhor, and A. Pentland, "Augmented betweenness centrality for mobility prediction in transportation networks," in *International Workshop on Finding Patterns of Human Behaviors in NEtworks and MObility Data, NEMO11*, 2011.

[86] K. Stephenson and M. Zelen, "Rethinking centrality: methods and examples," *Social Networks*, vol. 11, no. 1, pp. 1–37, 1989.

[87] P. Bonacich, "Factoring and weighting approaches to status scores and clique identication," *Journal of Mathematical Sociology*, vol. 2, no. 1, pp. 113–120, 1972.

[88] B. A. Prakash, D. Chakrabarti, M. Faloutsos, N. Valler, and C. Faloutsos, *Got the flu (or mumps)? check the eigenvalue!*, http://arxiv.org/abs/1004.0060.

[89] D. Chakrabarti, Y. Wang, C. Wang, J. Leskovec, and C. Faloutsos, "Epidemic thresholds in real networks," *ACM Transactions on Information and System Security*, vol. 10, no. 4, pp. 1–26, 2008.

[90] S. Boccaletti, V. Latora, Y. Moreno, M. Chavez, and D.-U. Hwang, "Complex networks: structure and dynamics," *Physics Reports*, vol. 424, no. 4, pp. 175–308, 2006.

[91] Y.-A. de Montjoye, J. Quoidbach, F. Robic, and A. S. Pentland, "Predicting personality using novel mobile phone-based metrics," *Social Computing, Behavioral-Cultural Modeling and Prediction*, Springer, pp. 48–55, 2013.

[92] V. K. Singh, L. Freeman, B. Lepri, and A. S. Pentland, *Predicting spending behavior using socio-mobile features*, in *Proceedings of the International Conference on Social Computing (SocialCom)*, IEEE, pp. 174–179, 2013.

[93] S. Ma, Y. Zheng, and O. Wolfson, "T-share: a large-scale dynamic taxi ridesharing service," in *Proceedings of the 29th International Conference on Data Engineering (ICDE)*, IEEE, pp. 410–421, 2013.

[94] M. R. Garey, D. S. Johnson, and L. Stockmeyer, "Some simplied NP-complete graph problems," *Theoretical Computer Science*, vol. 1, no. 3, pp. 237–267, 1976.

[95] F. A. Kuipers and P. F. Van Mieghem, "Conditions that impact the complexity of QoS routing," *IEEE/ACM Transactions on Networking (TON)*, vol. 13, no. 4, pp. 717–730, 2005.

[96] Y. Naveh, Y. Richter, Y. Altshuler, D. L. Gresh, and D. P. Connors, "Workforce optimization: Identification and assignment of professional workers using constraint programming," *IBM Journal of Research and Development*, vol. 51, no. 3.4, pp. 263–279, 2007.

[97] O. Bahat and S. Bekhor, "Incorporating ridesharing in the static traffic assignment model," *Networks and Spatial Economics*, pp. 1–25, 2015.

[98] Y.-A. de Montjoye, A. Stopczynski, E. Shmueli, A. Pentland, and S. Lehmann, "The strength of the strongest ties in collaborative problem solving," *Scientific Reports*, vol. 4, no. 1, 2015.

[99] D. Lazer and A. Friedman, "The network structure of exploration and exploitation," *Administrative Science Quarterly*, vol. 52, no. 4, pp. 667–694, 2007.

[100] Y. Altshuler, V. Yanovsky, A. Bruckstein, and I. Wagner, "Efficient cooperative search of smart targets using uav swarms," *Robotica*, vol. 26, pp. 551–557, 2008.

[101] Y. Altshuler and A. M. Bruckstein, "Static and expanding grid coverage with ant robots: complexity results," *Theoretical Computer Science*, vol. 412, no. 35, pp. 4661–4674, 2011.

[102] J. Svennebring and S. Koenig, "Building terrain-covering ant robots: a feasibility study," *Autonomous Robots*, vol. 16, no. 3, pp. 313–332, 2004.

[103] S. Koenig, B. Szymanski, and Y. Liu, "Efficient and inefficient ant coverage methods," *Annals of Mathematics and Artificial Intelligence*, vol. 31, pp. 41–76, 2001.

[104] Y. Altshuler, I. Wagner, V. Yanovski, and A. Bruckstein, "Multi-agent cooperative cleaning of expanding domains," *International Journal of Robotics Research*, vol. 30, no. 8, pp. 1037–1071, 2010.

[105] E. Regev, Y. Altshuler, and A. M. Bruckstein, *The cooperative cleaners problem in stochastic dynamic environments*, http://arxiv.org/abs/1608.01987.

[106] Y. Altshuler, A. Pentland, S. Bekhor, Y. Shiftan, and A. Bruckstein, *Optimal dynamic coverage infrastructure for large-scale fleets of reconnaissance UAVs*, http://arxiv.org/1611.05735.

Hindawi
Journal of Advanced Transportation
Volume 2019, Article ID 9343705, 14 pages
https://doi.org/10.1155/2019/9343705

Review Article

Simulation-Based Connected and Automated Vehicle Models on Highway Sections: A Literature Review

Wooseok Do, Omid M. Rouhani, and Luis Miranda-Moreno

Department of Civil Engineering and Applied Mechanics, McGill University, 817 Sherbrooke Street West, Montreal, QC H3A 0C3, Canada

Correspondence should be addressed to Wooseok Do; wooseok.do@mail.mcgill.ca

Received 2 March 2019; Accepted 26 May 2019; Published 26 June 2019

Guest Editor: Claudio Roncoli

This study provides a literature review of the simulation-based connected and automated intelligent-vehicle studies. Media and car-manufacturing companies predict that connected and automated vehicles (CAVs) would be available in the near future. However, society and transportation systems might not be completely ready for their implementation in various aspects, e.g., public acceptance, technology, infrastructure, and/or policy. Since the empirical field data for CAVs are not available at present, many researchers develop micro or macro simulation models to evaluate the CAV impacts. This study classifies the most commonly used intelligent-vehicle types into four categories (i.e., adaptive cruise control, ACC; cooperative adaptive cruise control, CACC; automated vehicle, AV; CAV) and summarizes the intelligent-vehicle car-following models (i.e., Intelligent Driver Model, IDM; MICroscopic Model for Simulation of Intelligent Cruise Control, MIXIC). The review results offer new insights for future intelligent-vehicle analyses: (i) the increase in the market-penetration rate of intelligent vehicles has a significant impact on traffic flow conditions; (ii) without vehicle connections, such as the ACC vehicles, the roadway-capacity increase would be marginal; (iii) none of the parameters in the AV or CAV models is calibrated by the actual field data; (iv) both longitudinal and lateral movements of intelligent vehicles can reduce energy consumption and environmental costs compared to human-driven vehicles; (v) research gap exists in studying the car-following models for newly developed intelligent vehicles; and (vi) the estimated impacts are not converted into a unified metric (i.e., welfare economic impact on users or society) which is essential to evaluate intelligent vehicles from an overall societal perspective.

1. Introduction

With the advancement of the intelligent driving assistance system (IDAS), automobile drivers are becoming less required to perform simple driving tasks. An early stage of the IDAS is a cruise control (CC) system, and this evolves toward adaptive cruise control (ACC) and cooperative adaptive cruise control (CACC) systems. These systems mainly assist an acceleration control for longitudinal movements based on the gap distance and speed difference between preceding and current vehicles. In the meantime, connected and automated vehicles (CAVs) have gained increasing attention accompanied by tremendous investments from both public and private sectors [1, 2].

Self-driving (automated) vehicles could play a significant role in the future transportation system. Since this revolutionary concept was first introduced in 1920s, the CAV technology has evolved drastically over the last several decades. Despite the uncertainty as to when the CAV technologies will be publicly available, they will likely have enormous impacts on our transportation systems over the upcoming decades [3–8].

As of April 2009, Google's self-driving cars (Waymo) have been driven over eight million miles using a variety of platforms [9, 10]. Numerous manufacturers—including Audi, BMW, Cadillac, Ford, GM, Mercedes-Benz, Nissan, Toyota, Volkswagen, and Volvo—have begun testing automated vehicles, and they aim to sell such vehicles by 2020 [11, 12]. Meanwhile, partially automated vehicles are now available. The current models are equipped with ACC, collision avoidance, parking assist systems, and lane departure warning features [10, 13].

Researchers acknowledge that the development of CAVs will generate significant changes in our daily life and society as a whole. To estimate the impacts of CAVs, the vast majority

of researchers have been conducting a simulation-based analysis because (i) the real field data on the CAV's performance are limited [14–16] and (ii) many studies deal with high market shares for CAVs [17–19], which is hypothetical, far from the current reality. It is crucial to understand the impacts of CAVs early in their development to avoid costly mistakes before their widespread implementation.

We can broadly categorize simulation-based studies into micro and macro models according to a network scale and fundamental models of the simulation. Most of the micro simulation based studies reviewed in this paper develop their own ACC, CACC, AV, or CAV car-following models to estimate the impacts of these intelligent vehicles. That is primarily because no car-following model had existed to adequately describe the car-following characteristics of intelligent vehicles. Such studies develop the commonly used car-following models, e.g., IDM [20] and MIXIC [21], to mimic intelligent-vehicle characteristics. On the other hand, macro simulation model needs a traffic assignment procedure which can be applied by using activity-based models [22–25] or modified traditional four-step models [5]. Moreover, each simulation study has applied a different approach and examined a distinct performance measure(s) (e.g., micro stability, throughput, acceleration, and headway profiles; macro link traffic volume, link travel time, etc.). In this review paper, we focus mainly on the micro simulation based studies considering longitudinal dynamics.

There have been many newly developed car-following models to analyze the impacts of the intelligent (ACC, CACC, AV, and CAV) vehicles. However, the concepts of the intelligent vehicles, terminologies, vehicle performances, and evaluation criteria vary depending on the research topic. To the best of our knowledge, there have been no review studies summarizing the simulation-based intelligent-vehicle studies and their impact analyses. The primary contributions of this study are (i) to define intelligent-vehicle types with the hierarchical classification; (ii) to offer a summary of the simulation-based intelligent-vehicle studies and its impact; (iii) to discuss the implications from the previous literature and the limitations of previous studies.

The remainder of this paper is structured as follows. In the following section, we define the most commonly used intelligent-vehicle types and propose hierarchical classifications. Section 3 reviews intelligent-vehicle studies and introduce the commonly used car-following models for intelligent vehicles. The intelligent-vehicle's impacts and previous studies' limitations are described in Section 4. The paper concludes with key implications/lessons learned from the review results and our suggestion regarding potential future studies.

2. Intelligent-Vehicle Classifications and Definitions

Figure 1 illustrates the definitions of four key intelligent-vehicle types with the hierarchical classification reporting the related studies for each category, incorporating the sensing and communications of intelligent vehicles. The ACC is an advanced version of the earlier CC system. The primary function of the CC vehicle is to maintain a desired speed set by a driver. On the other hand, the ACC vehicle controls an acceleration based on a distance gap and a speed difference between preceding and current vehicles. In addition, the ACC systems can appropriately accelerate and decelerate with regard to preceding vehicles' speed changes. The CACC system includes a communication function, compared to ACC, that shares the acceleration, deceleration, a breaking capability, and vehicle positions through vehicle to vehicle (V2V) communications [26]. The communication allows the CACC vehicle to have a significantly shorter time headway (i.e., 0.5 seconds) compared to the ACC (i.e., 1.4 seconds). Moreover, the parameters are shared among the CACC-platooned vehicles, so, theoretically, they do not need to guarantee the minimum safety distance. Many previous studies show that CACC has the potential to improve both the traffic flow [27] and the string stability [28]. The CACC system is not commercially available for now but has been discussed in many studies due to its potential capacity increase under platoon driving. The IDAS's ultimate goal is that humans do not need to control vehicles at all. The USDOT [26] defines the fully automated vehicle as the vehicle capable of full-time automated driving under any road and environmental conditions, while CAVs contain all AV functions with the V2V and V2X functions. For highway sections, one of the key differences between CACC and CAV might be an automated lateral movement. Most of the CACC studies assume the lateral movement is made by human drivers. The above-mentioned vehicle concepts are completely new compared to the conventional car-following movements developed for human-driven vehicles. Therefore, the related terminologies and concepts in the reviewed literature varies and are not firmly classified.

We categorize the literature according to the intelligent-vehicle types. Such studies often use mixed definitions of the intelligent-vehicle types. Therefore, we define the intelligent-vehicle types used in each study and group them in the appropriate category.

3. Connected and Automated Vehicle Simulations

3.1. Simulation-Based Intelligent-Vehicle Studies. Tables 1 and 2 show the studies reviewed in this paper focusing on the simulation-based intelligent-vehicle modeling studies and their impact analyses. The review result shows that most of studies focus on the car-following model development for intelligent vehicles and examine their traffic impacts (e.g., throughput, stability, vehicle speed). Several studies estimate the energy and environmental impacts (e.g., fuel consumption and emission) and safety impacts using travel speed, time-to-collision (TTC), and post-encroachment-time (PET). Our literature review offers a comparative examination of the simulation-based models developed for the intelligent-vehicle analysis. The review is conducted examining the following criteria: (i) the objectives of the study, (ii) base model, (iii) simulation scenarios, (iv) analyzed vehicle types, (v) evaluation criteria, and (vi) main results.

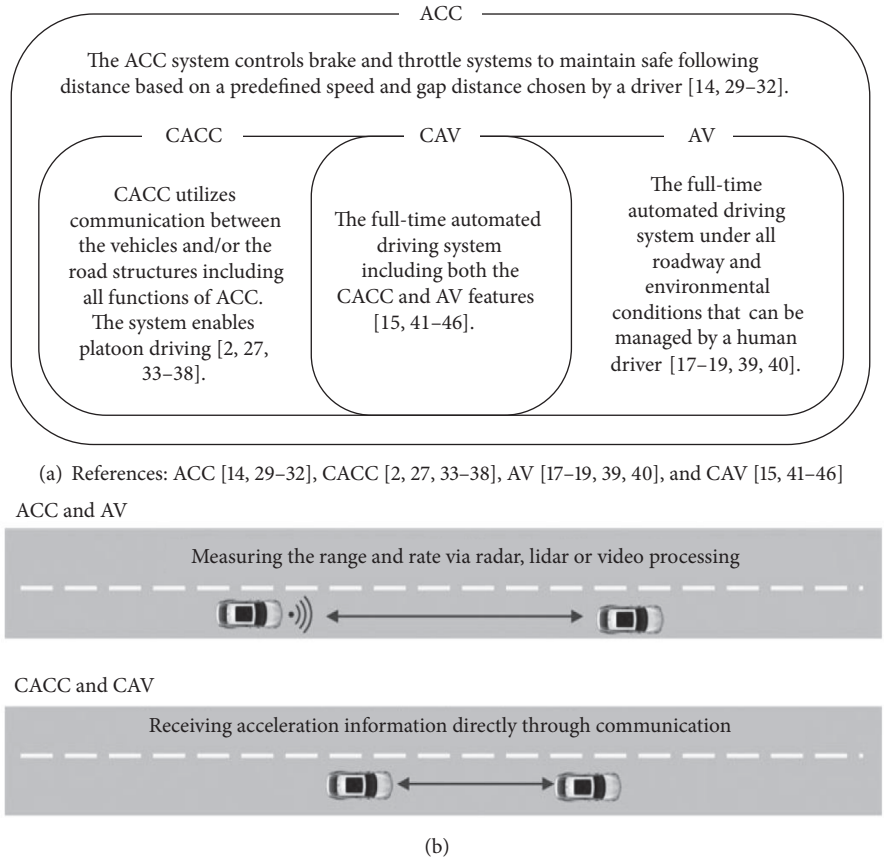

Figure 1: (a) intelligent-vehicle definitions with their classifications, (b) illustrations of sensing and communications by intelligent vehicles. *Source: Figure 1(b) [18].*

Because the use of intelligent vehicles on public roads will gradually increase under mixed-traffic situations with manual vehicles, many studies adopt a variety of scenarios regarding different market-penetration rates of intelligent vehicles. A small number of studies simulate only extreme 100% penetration rate of intelligent vehicles with no consideration of gradual growths [17, 32].

One interesting observation is that most analyzed vehicle types are limited to our four vehicle categories (see Figure 1). However, the studies barely consider manual vehicles equipped with V2V communication transponders, which send the current location and speed of the vehicle to the nearby intelligent vehicles. One study by Shladover, Su [27] defines these vehicle-awareness device (VAD) equipped manual vehicles as the "Here I Am" (HIA) vehicle. The result shows that the increase in the HIA vehicles can also contribute to the improvement of road capacity.

In terms of results, many of simulation-based studies found consistent outcomes in terms of traffic performance: throughput increases with higher intelligent-vehicle penetration rates, while some contradictory results exist for the ACC vehicles' performance. For instance, Kesting, Treiber et al. [14, 31] conclude that the ACC vehicle can improve road capacity under small penetration, but the results by VanderWerf, Shladover [32] and Shladover, Su [27] show the ACC vehicles' impact might be marginal. Meanwhile, a research gap exists regarding inconsistency in the previous studies' assumptions, scenarios, and evaluation criteria.

Our review result shows that the IDM and MIXIC models are the most often used models, as benchmark car-following models. Several studies tried to modify these models to explain the longitudinal movements of intelligent vehicles (e.g., IDM [14, 30, 31, 46] and MIXIC [45, 52, 62]). Both models and their applications are discussed in further detail in the following sections.

3.2. Car-Following Models for Intelligent Vehicles. Because of the newly introduced unprecedented systems, we need new car-following models to simulate intelligent vehicles. Conventional car-following models are developed based on human-driving characteristics. However, intelligent vehicles have different car-following characteristics. The accompanied sensor technology allows CAVs to see the down-stream traffic situations beyond human drivers' visibilities. Furthermore, the agile CACCs and CAVs communicate (e.g., V2V or V2X) with each other in order to improve traffic streams. Recently, there have been the research efforts to develop intelligent-vehicle car-following models by enhancing the conventional car-following models (e.g., IDM [14, 30, 31, 46] and MIXIC

Table 1: Simulation-based intelligent-vehicle studies: objectives, models, and scenarios.

Ref #	Objectives	Base model(s)	Scenarios
[32]	Develop the ACC and CACC car-following models and estimate their impact.	An error-based control law for the ACC and CACC. The lane change is under human control.	A 100% market-penetration rate of each vehicle type.
[29]	Examine the ACC vehicles' lane-changing effects compared to manual vehicles.	Manual vehicle: Pipes model [47]. ACC model from [48]. Comprehensive Modal Emissions Model (CMEM).	Position of ACC vehicles (2, 4, 6, 8th in the string of 10 vehicles). Market-penetration rate of ACC (5%, 10%, 15% and 30%).
[31]	Propose the ACC-based traffic-assistance system intended to improve traffic flow and road capacity.	IDM	Market-penetration rate of ACC (0%, 5%, 15% and 25%).
[14]	Propose the ACC-based traffic assistance system aimed at improving the traffic flow and road capacity.	IDM	Market-penetration rate of ACC (0%, 5%, 15% and 25%).
[30]	Propose the new ACC car-following model with its impact analysis	IDM with constant-acceleration heuristic (CAH).	Market-penetration rate of ACC (10%, 20%, 30%, 40%, and 50%).
[18]	Propose an analytical framework to estimate the AVs' impacts on highway sections.	Car-following model for manual vehicles in [49, 50]. First order control law for AVs.	Different combinations of manual vehicles, AVs, and CAVs (0-100 % by 10% gap).
[19]	Develop an improved cellular automaton as an AV modeling platform.	Cellular Automaton	The lane-changing rules in the same and opposite direction. Market-penetration rate of ACC (0%, 50%, and 100%).
[46]	Develop a cooperative IDM (CIDM) to examine the system performance under different proportions of the AVs.	The Full Velocity Difference Model (FVDM) and IDM.	Market-penetration rate of the AVs (0%, 5%, 15%, and 25%).
[45]	Propose an acceleration framework to address the limitations of micro-simulation models in capturing the changes in driver behavior in a mixed environment.	MIXIC model for the AV modeling. IDM for the CAV modeling.	Market-penetration rate of the CAVs and AVs (0%, 20%, 40%, 60%, 80%, and 100%).
[44]	Develop a micro-simulation framework for CAVs to analyze the impact on fuel consumption and travel time.	Optimal control for CAVs. Gipps model for manual vehicles [51].	Two single-lane merging roadways where CAVs communicate to each other.
[15]	Propose a hardware-in-the-loop (HIL) testing system for the CAV applications.	Hardware-in-the loop (HIL) testing.	Type I: String leader's smooth acceleration and deceleration between 20-30mph. Type II: Sharp brakes from 30mph to 10mph and quick recovery to 30mph. Type A: Perfect communication/radar. Type B: Compromised communication/radar (radar delay 100ms; radar noise = 0.05; DSRC Latency = 100ms and DSRC Packet Loss =10%).

Table 1: Continued.

Ref #	Objectives	Base model(s)	Scenarios
	Examine the impact of the CACC vehicles on traffic flow characteristics of a multilane highway.	IDM	Arrival rate scenarios: 7,000v/h (moderate), 8,000v/h (saturated), 9,000v/h (oversaturated), 10,000v/h (oversaturated). Penetration rates of CACC varied in multiples of 20% (truck is fixed in 10%).
[52]	Develop a simulation framework to facilitate the heavy-duty vehicle (HDV) platooning and establish the related concept and operations.	Carbon dioxide emission model [53]. The HDM platoon model with the ACC/CACC car-following model.	Average density, average travel time, and average travel speed.
[17]	Investigate AVs' impact on traffic performance.	Calibration on car following model (Wiedemann 99). Lane changing behavior based on a research project [54].	Each vehicle type of a 100% market-penetration rate.
[37]	Extend the CACC modeling framework to incorporate new algorithms describing the interactions between the CACC and manual vehicles in mixed traffic.	The CACC model reported in [55]. The anticipatory lane change (ALC) for lane changing.	Market-penetration rate of the CACC (0%, 20%, 40%, 60%, 80% and 100%).
[36]	Investigate the impact of the CACC vehicle string operation on the capacity of multilane highway with merging bottlenecks.	The ACC and CACC car-following models developed [33].	Market-penetration rate of the CACC (0%, 20%, 40%, 60%, 80% and 100%).
[56]	Propose a new algorithm for the CACC systems for collaborative driving based on the use of agent technology and information sharing.	Effective CACC (ECACC) algorithm consists of speed and distance control algorithms.	Market-penetration rate of the CACC (0%, 20%, 40%, 60%, 80% and 100%).
[27]	Estimate the effect on highway capacity of varying market-penetrations of vehicles with the ACC and the CACC.	The manual vehicle: NGSIM oversaturated freeway flow model [57]. ACCs: Proprietary to Nissan. CACCs: Car-following behavior was described [33].	The ACC and CACC vehicles 10 % increase proportion.
[21]	Investigate the impact of the CACC on traffic-flow characteristic.	MIXIC model	Market-penetration rate of the CACC (0%, 20%, 40%, 60%, 80% and 100%).
[58]	Develop the models of both ACC and CACC control systems based on real experimental data.	IDM	Ten consecutive CACC and five consecutive ACC vehicles. A mixed case, where the two first followers are ACC-equipped and the next seven are CACC-equipped.

Table 1: Continued.

Ref #	Objectives	Base model(s)	Scenarios
[59]	Estimate the emissions and energy use (i.e., fuel consumption) associated with an Automated Highway System (AHS) using advanced simulation modeling tools.	Smart AHS framework developed at PATH program.	Congestion levels (LOS A - F).
[60]	Analyze roundabout safety level in the circumstances where different numbers of the AVs are mixed with manual vehicles.	Safety impact: Surrogate Safety Assessment Model (SSAM). Manual vehicles: Wiedemann 74. AVs: VISSIM parameter adjustment.	Market-penetration rate of the AVs (0%, 10%, 25%, and 50%).
[61]	Develop the decision-making CAV control algorithm in the VISSIM for safety evaluations.	Safety impact: SSAM. CAV: External driver model API written in C++. Manual vehicles: Wiedemann 99.	Market-penetration rate of the CAVs (0%, 25%, 50%, 75%, and 100%). Daily based estimation, Monday to Friday.

[45, 52, 62]). In this section, we summarize the commonly used car-following models adapted for intelligent vehicles.

3.2.1. Intelligent Driver Model (IDM). In this section, we discuss the IDM, first developed by Treiber, Hennecke [20]. The IDM is the most commonly used model for the intelligent-vehicle simulations because it is one of the simplest and accident-free models producing realistic acceleration profile in a single lane situation [63]. The IDM is closer to the ACC vehicles than to human-driven vehicle characteristics because it does not have an explicit reaction time and is given in a continuously differentiable acceleration function [63]. By changing some parameters, we can use the IDM itself as ACC or a human-driven vehicle model. Additionally, the modified IDM is applied to simulate CAVs [46]. The basic function of IDM is as follows:

$$a_{IDM}(s, v, \Delta v) = \frac{dv}{dt} = a\left[1 - \left(\frac{v}{v_0}\right)^{\delta} - \left(\frac{s^*(v, \Delta v)}{s}\right)^2\right] \quad (1)$$

$$s^*(v, \Delta v) = s_0 + vT + \frac{v\Delta v}{2\sqrt{ab}} \quad (2)$$

where s denotes the current distance to the preceding vehicle, s_0 denotes the minimum gap, $s*(v, \Delta v)$ denotes desired (safety) gap, v denotes the current speed, v_0 is the desired (safety) speed, Δv is speed difference between the current vehicle and the preceding vehicle, δ is the parameter that decides the magnitude of acceleration decrease depending on the velocity v, T denotes the constant desired gap, and a and b denote comfortable acceleration and deceleration rates, respectively.

The IDM results in plausible acceleration and deceleration rates in most situations. However, when the current vehicle gap is significantly lower than the desired gap, the deceleration rate becomes unrealistically high. In fact, when it comes to the human-driven vehicles, drivers assume that the preceding vehicle will not suddenly stop with the hardest deceleration without any reason. Therefore, the current gap smaller than the desired gap distance is considered a relatively mild-critical situation [64]. To address this issue, Kesting, Treiber [30] combined the IDM and the Constant Acceleration Heuristics (CAH) to limit the unrealistic deceleration rates. The fundamental assumption of the CAH model is that the preceding vehicle will not change its acceleration suddenly in following few seconds.

There are three underlying conditions of the CAH: (i) the acceleration of the vehicle under consideration and the preceding vehicle will not change in the applicable future (generally, a few seconds); (ii) no safe time headway or minimum distance is required at any moment; and (iii) drivers react without delay (zero reaction time) [30].

For given actual values of the gap s, current speed v, the preceding vehicle speed v_1, and its acceleration a_1, the maximum acceleration a_{CAH} that prevents crashes is given by

$$a_{CAH}(s, v, v_1, a_1) = \begin{cases} \dfrac{v^2 \widetilde{a_l}}{v_1^2 - 2s\widetilde{a_l}} & \text{if } v_1(v - v_1) \le -2s\widetilde{a_l}, \\ \widetilde{a_l}\dfrac{(v - v_1)^2\,\theta(v - v_1)}{2s} & \text{otherwise}, \end{cases} \quad (3)$$

where the effective acceleration $\widetilde{a_l} = \min(a_1, v)$ is used to avoid artefacts that may be caused by preceding vehicles with higher acceleration capabilities. The condition $v_1(v - v_1) \le -2s\widetilde{a_l}$ is true if the vehicles have stopped at the time that the minimum gap s = 0 is reached. Otherwise, negative approaching rates do not make sense to the CAH and are therefore eliminated by the Heaviside step function Q.

Table 2: Simulation-based intelligent-vehicle studies: analyzed vehicle types, evaluation criteria, and main results.

Ref #	Analyzed vehicle types	Evaluation criteria	Main results
[32]	Manual vehicle, ACC, CACC	Throughput	Throughput of the manual, ACC, and CACC vehicles were, respectively, 2,050, 2,200, and 4,550 vehicles/h.
[29]	Manual vehicle, ACC	Fuel consumptions and environmental effect (CO, HC, CO2, NOx)	The smooth response of the ACC vehicles has a beneficial effect on the environment. These benefits vary with the levels of the disturbance, the position of the ACC vehicle in the string of manually driven vehicles and the ACC vehicle penetration.
[31]	Manual vehicle, ACC	Throughput	A small proportion (5%) of ACC vehicles can improve the traffic flow. An increasing proportion of ACC vehicles reduces traffic congestion.
[14]	Manual vehicle, ACC	Throughput	ACC vehicles improve the traffic stability and the road capacity. 25% of ACC eliminates traffic congestion during simulation (the cumulated travel time without ACC vehicles is 4,000 hours, but with 25% ACC vehicles 2,500 hours).
[30]	Manual vehicle, ACC	Throughput	1% more ACC vehicles will lead to an increase in the road capacities by about 0.3%.
[18]	Manual vehicle, CAV, AV	Throughput	Increasing CAVs will have significant implications on the road capacity of highways. Road capacity efficiency will be dependent on the level of automation. The lane capacity increases from 2,046 to 6,450 vehicles/hour/lane with CAVs increases from 0% to 100%.
[19]	Manual vehicle, AV	Throughput	AVs could considerably improve traffic flow. The lane-changing frequency between neighboring lanes evolves with traffic density. AV lane changing seems to be much less pronounced than that of the AV car-following.
[46]	Manual vehicle, CAV	Average speed dispersion, travel time, space mean speed	Increasing percentage of AVs will reduce the total travel time and smooth traffic oscillations.
[45]	Manual vehicle, connected vehicle, AVs	Stability and throughput	CAVs can improve string stability, and automation is more effective in preventing shockwave formation and propagation. Substantial throughput increases under certain penetration scenarios.
[44]	Manual vehicle, CAV	Fuel consumption, travel time, throughput	CAVs can contribute to significant fuel consumption and travel time reduction. CAVs allow for more stable traffic patterns even for high density traffic.
[15]	Manual vehicle, CAV	Speed, vehicle position profile	Effectiveness of the CACC in absorbing certain disturbance and oscillation of speeds. Speed oscillation decreases as vehicle position in the string increases. Perfect communication/radar contributes string stability.
	Manual vehicle, CACC	Throughput	A low-to-moderate penetration rate of CACC, the CACC impact is not statistically significant (advantages observed with a 40% or more CACC). A very large improvement is noticed at a high penetration rate of CACC, especially in high traffic conditions.

Table 2: Continued.

Ref #	Analyzed vehicle types	Evaluation criteria	Main results
[52]	Manual vehicle, HDV with ACC, CACC functions	Fuel consumption Space mean speed	The increasing HDV platooning in traffic flow results in more dramatic improvements on traffic efficiency. Deceleration of the first HDV to a low speed during platoon formation will increase the formation time to a large extent in medium and heavy traffic.
[17]	Manual vehicle, AV	Average density Average travel time Average travel speed	The average density of autobahn segment remarkably improved (8.09%) during p.m. peak hours in the AV scenario. The average travel speed enhanced relatively by 8.48%. The average travel time improved by 9.00% in the AV scenario.
[37]	Manual vehicle, CACC	Throughput	Freeway capacity is 90% higher in a 100% CACC penetration compared to 0%. The capacity increase is insignificant under low to medium CACC market-penetrations (e.g., 20–60%) in the absence of additional management strategies.
[36]	Manual vehicle, CACC	Bottleneck capacity	The freeway capacity increases quadratically as the CACC increases, with a maximum of 3080 vehicles/hour/lane at 100% CACC penetration. The disturbance from the on-ramp traffic can reduce the freeway capacity by up to 13% but the bottleneck capacity still increases in as CACC increase. There is very little gain in merge bottleneck capacity as CACC penetration increases from 0% to 20% when the on-ramp demand is high. A rapid increase in bottleneck capacity from 80% to 100% CACC penetration, especially with high on-ramp inputs.
[56]	Manual vehicle, CACC	Throughput	The congestion reduction is higher when the market-penetration rate of the CACC-equipped vehicle increases. At a low penetration rate, the effect of the CACC on traffic dynamics is not significant.
[27]	Manual vehicle, ACC, CACC, and Here-I-Am (HIA) vehicle	Highway throughput	The use of ACC was unlikely to change lane capacity significantly. The CACC can increase capacity greatly after its market-penetration reached moderate to high percentages (4000 vehicles/hour if all are the CACC or vehicle awareness device-VAD equipped). The capacity benefits of CACC can be accelerated at somewhat lower market-penetrations, if the rest of the vehicles are equipped with VADs.
[21]	Manual vehicle, CACC	Throughput	The CACC can improve traffic-flow characteristics. A low market-penetration rate of the CACC (< 40%) would not have an impact on the throughput.
[58]	Four ACC and CACC experimental vehicles	Speed, distance gap, time gap	The IDM controller in the experimental test vehicles does not perceptibly follow the speed changes of the preceding vehicle. Strings of consecutive ACC vehicles are unstable, amplifying the speed variations of preceding vehicles. Strings of the consecutive CACC vehicles overcome these limitations, providing smooth and stable car following responses.
[59]	Manual vehicle Non-platooned AVs Platooned AVs	Fuel consumption Emissions (HC, CO, NOx)	The AHS has much lower average fuel consumption operating under congested conditions, because of its smoother traffic flow, but slightly lower average fuel consumption at free-flow. The AHS operating at 60 mph has substantially lower emissions per vehicle-mile traveled than non-automated traffic at the same average speed. Vehicles that platoon in an AHS can expect additional 5 - 15% fuel savings and emission reduction due to the aerodynamic drafting effect.

Table 2: Continued.

Ref #	Analyzed vehicle types	Evaluation criteria	Main results
[60]	Manual vehicle, Heavy commercial vehicle-HGV, AVs	Average travel speed	An increase of travel speed and decrease of average stop delay with the increase of percentage of the AVs. Increases in estimated crash number at roundabouts when the AVs percentage is increased in terms of rear-end conflict.
[61]	Manual vehicle CAV	Conflicts based on the threshold values of TTC (1.5 seconds) and PET (5 seconds).	The CAVs bring about compelling benefit to road safety as traffic conflicts significantly reduce even at relatively low market-penetration rates (12–47%, 50–80%, 82–92% and 90–94% for 25%, 50%, 75% and 100% CAV penetration rates respectively).

By combining acceleration from the IDM and the CAH, Kesting, Treiber [30] proposed the ACC model as formulated in (4). The ACC model produces different acceleration rates based on the IDM or the CAH depending on the following conditions. The ACC model produces the same acceleration if both the IDM and the CAH reach the same acceleration output. If the IDM produces the unrealistically high deceleration, while the CAH deceleration is in comfortable deceleration range, the situation is considered to be mildly critical, and the ACC acceleration stays above the CAH acceleration minus the comfortable deceleration. If both the IDM and the CAH result in acceleration significantly below −b, the situation is seriously critical, and the ACC acceleration must not be higher than the maximum of the IDM and CAH acceleration. The ACC acceleration should be a continuous and differentiable function of the IDM and CAH acceleration.

$$a_{ACC} = \begin{cases} a_{IDM} & a_{IDM} \geq a_{CAH}, \\ (1-c)\, a_{IDM} + c\left[a_{CAH} + b \tanh\left(\frac{a_{IDM} - a_{CAH}}{b}\right)\right] & otherwise. \end{cases} \quad (4)$$

The ACC model contains one additional parameter c compared to the IDM. c is named as a coolness factor. When $c = 0$, the ACC model reverts to the IDM, while if $c = 1$, the sensitivity of gap changes vanishes under small gaps and no velocity difference exists. Kesting, Treiber [30] have assumed c =0.99 (see Table 1).

Zhou, Qu [46] developed the cooperative intelligent demand model (CIDM) using the IDM as the benchmark model and examined the system performance of CAVs. Communication of the CAV is applied by using the concept of spatial anticipation in the human driver model (HDM) [65, 66]. The HDM anticipation is applied to the CIDM which splits the IDM's a_n into (5) based on (1).

$$a_n\left(\Delta x, v_n, \Delta v\right) = a_n^{free} + \sum_{m}^{n-1} a_{nm}^{int}\left(\Delta x_{nm}, v_n, \Delta v_{nm}\right) \quad (5)$$

The base IDM (1) consists of two parts: one is the acceleration term comparing the current speed v to the desired speed $a_{free} = a(1 - (v/v_0)^{\delta})$, and another one is the breaking term $a_{break} = -a(s^*(v, \Delta v)/s)^2$ that compares the current distance with the desired distance s^*. In (5), a_n^{free} is the same definition of $a_{free}(v)$, and a_{mn}^{int} is the same definition of a_{break} in (1) with the consideration of V2V interaction.

3.2.2. The MICroscopic Model for Simulation of Intelligent Cruise Control (MIXIC). To estimate the impact of intelligent vehicles, the modeling framework should be able to analyze different assumptions of intelligent-vehicle characteristics according to different functionalities. Furthermore, the modeling frameworks should be capable of estimating their impacts on traffic performance, safety, fuel consumption, emission, and noise emission. With consideration of these requirements, a stochastic simulation model MIXIC is developed by Van Arem, De Vos [62]. As an early developed intelligent-vehicle model, the MIXIC is one of the most applied models for the cooperative intelligent-vehicle simulations. The reasons behind its widespread application are the following: (i) The MIXIC model incorporates the V2V communication by sharing speed, acceleration, and/or braking capabilities between the preceding and current vehicles. Such model capability allows better simulations of the characteristics of CACC. (ii) The model is calibrated for different two-, three-, and four-lane situations, which results in a well-adjusted traffic flow model, corresponding to real-life situations. Additionally, the MIXIC results were found reliable where the detailed calibration of vehicles' performances is not available [62]. In this section, we discuss the basic MIXIC model and its applications.

For the basic MIXIC model [21], the acceleration system can be divided into two distinct components: (i) the acceleration controller delivering reference values and (ii) a vehicle model transforming the reference values into actually realized values. Therefore, the reference acceleration is determined by a controller and then fed into the vehicle model.

The reference acceleration (6) can be computed based on the difference between current and intended speed (a_{ref_v}) or the distance and the speed (a_{ref_d}) differences between the current vehicle and the preceding vehicle. The acceleration demand is given by the most restrictive one of the two. The acceleration (2m/s^2) and deceleration (-3m/s^2) are limited for driver comfort.

$$a_{ref} = \min\left(a_{ref_v}, a_{ref_d}\right) \tag{6}$$

where v_{int} and v denote the intended and the current speed of the CACC vehicle in meters per second. The reference acceleration demand based on speed difference is given by

$$a_{ref_v} = k \bullet \left(v_{int} - v\right) \tag{7}$$

where k as a constant speed-error factor.

The distance-based reference acceleration computation is slightly more complex. Let v_p denote the speed of the preceding vehicle and let r and r_{ref} denote the current and reference clearances relative to the preceding vehicle in meters, respectively. Let a_p denote the acceleration of the preceding vehicle. The reference acceleration based on the distance and speed difference between current and preceding vehicles is given by

$$a_{ref_d} = k_a \bullet a_p + k_v \bullet \left(v_p - v\right) + k_d \bullet \left(r - r_{ref}\right) \tag{8}$$

with k_a, k_v, and k_d being constant factors frequently used in previous studies [45, 67] as 1, 0.58s^{-1}, and 0.1s^{-2}, respectively.

The reference clearance r_{ref} is defined as the maximum value among the safety following distance (r_{safe}), the following distance according to the system time setting (r_{system}), and a minimum allowed distance (r_{min}), set at 2 meters.

$$r_{ref} = \max\left(r_{safe}, r_{system}, r_{min}\right) \tag{9}$$

The safe following distance (r_{safe}) is computed using the current vehicle speed (v), deceleration capability of the preceding vehicle (d_p), and the current vehicle (d).

$$r_{safe} = \frac{v^2}{2} \bullet \left(\frac{1}{d_p} - \frac{1}{d}\right) \tag{10}$$

For simplicity, the MIXIC model assumes a communication delay to be zero. In addition, the current and preceding vehicles can share braking capabilities using a V2V communication. The communication information includes the precise speed, acceleration, maximum braking capability, warnings regarding hazards in front, and fault warnings. The following distance according to the system time-gap setting is given by

$$r_{system} = t_{system} \bullet \mathrm{v} \tag{11}$$

where t_{system} is assumed as 0.5 seconds if the preceding vehicle has the CACC function and 1.4 seconds otherwise.

Talebpour and Mahmassani [45] developed the CAV model based on the MIXIC model considering sensor detection ranges of CAVs. The study uses individual sensors to create the input data for the MIXIC model. The assumed sensors are Smart-Micro Automotive Radar (UMRR-00 Type 30) with 90 m ± 2.5% detection range and ±35 horizontal Field of View (FOV). Each sensor updates the sensing information every 50 milliseconds and can track up to 64 objects.

The fundamental assumption of the study is that the speed of AVs is low enough to allow it to stop at the sensor detection range since an autonomous vehicle can observe vehicles only in its sensor detection range. This is equivalent to the assumption that there is a vehicle at a complete stop right outside of the sensor detection range. Moreover, if a preceding vehicle is spotted, it is reasonable to assume that the speed of the autonomous vehicle should be low enough to allow stopping if its preceding vehicle decides to decelerate with its maximum deceleration rate and reach a full stop. Considering the maximum of the possible deceleration for the autonomous vehicle and its leader, we can calculate the maximum of the safe speed using the following equations:

$$\Delta X_n = \left(X_{n-1} - X_n - l_{n-1}\right) + v_n\tau + \frac{v_{n-1}^2}{2a_{n-1}^{decc}} \tag{12}$$

$$\Delta X_n = \min\left(SensorDetectionRange, \Delta X_n\right) \tag{13}$$

$$v_{max} = \sqrt{-2a_i^{decc}\Delta \mathrm{X}} \tag{14}$$

where n and $n-1$ denote the autonomous vehicle and its leader, respectively. X_n is the location of vehicle n, l_n is the length of vehicle n, v_n is the speed of vehicle n, τ is the reaction time of vehicle n, and a_n^{decc} is the maximum deceleration of vehicle n. Then, the acceleration of a vehicle can be calculated by

$$\begin{aligned} a_n^d(t) = {} & k_a a_{n-1}(t-\tau) + k_v\left(v_{n-1}(t-\tau) - v_n(t-\tau)\right) \\ & + k_d\left(s_n(t-\tau) - S_{ref}\right) \end{aligned} \tag{15}$$

where S_n is the spacing and s_{ref} is the maximum of the following three values: the minimum distance (s_{min}), the following distance based on the reaction time (s_{system}), and the safe following distance (s_{safe}). In the study by Talebpour and Mahmassani [45], the minimum distance is set at 2.0 meters and s_{system} and s_{safe} are calculated as follows.

$$s_{safe} = \frac{v_{n-1}^2}{2}\left(\frac{1}{a_n^{decc}} - \frac{1}{a_{n-1}^{decc}}\right) \tag{16}$$

$$s_{system} = v_n\tau \tag{17}$$

Finally, the acceleration of the autonomous vehicle can be calculated using the following equation:

$$a_n(t) = \min\left[a_n^d(t), k\left(v_{max} - v_n(t)\right)\right] \tag{18}$$

where k is a model parameter which is the same as the basic MIXIC model [45].

4. Discussions

In this section, we summarize the literature review results regarding intelligent vehicle's impacts according to different vehicle types and performance measures. Additionally, the limitations and implications from previous studies are discussed. An increasing number of researchers have been studying intelligent vehicles with a recognition of its potential impacts on the future transportation system. However, important future impacts/developments remain uncertain, i.e., the capacity increase, the market-penetration growth, safety issues, public acceptance, regional economic impact, and/or future policies. Under such uncertainties, many researchers conduct simulation-based intelligent-vehicle analysis based on their own assumptions. However, the concept, assumptions, and even terminologies across various studies are inconsistent and even conflicting because the real-life data acquisition is not accessible at present. Our review results offer the following insights into simulation-based intelligent-vehicle studies.

First, we notice that most studies predict that the throughput could be increased with growing market-penetration rates of intelligent vehicles under the mixed-traffic condition with manual vehicles [14, 18, 19, 27, 30–32, 36, 37, 45]. However, the results are contradictory regarding vehicle types. The ACC studies conducted by Kesting, Treiber et al. [14, 31] show that the small portion (5%) of ACCs can still improve lane capacity. Furthermore, approximately 25% of the ACC eliminates traffic congestion during their simulation. In addition, Kesting, Treiber [30] estimate the road capacity elasticity of the ACC penetration: 1% more ACCs can increase road capacity by about 0.3%. Conversely, a few other studies have been skeptical regarding the ACC vehicles' impacts on road capacity. VanderWerf, Shladover [32] show that the ACC road capacity impact (i.e., 2,200 vehicles/hour/lane) could be minor compared to manual vehicles (i.e., capacity 2,050 vehicles/hour/lane) while the CACC could offer a significant impact (i.e., capacity up to 4,550 vehicles/hour/lane). Moreover, Shladover, Su [27] conclude that ACCs are not likely to change lane capacity significantly while the CACC can substantially contribute with moderate to high penetration rates (e.g., approximately 4,000 vehicles/hour/lane when all vehicle are the CACC or VAD-equipped vehicles).

Meanwhile, most CACC and CAV simulation studies estimate a positive road capacity increase with increasing market-penetration rates. Olia, Razavi [18] simulate the CAVs under mixed-traffic conditions with the assumption of increasing 10% gap of CAVs. The result shows a 100% penetration rate of CAVs could increase road capacity from 2,046 to 6,450 vehicles/hour/lane. Liu, Kan [37] conduct multilane and mixed-traffic highway simulations by increasing CACCs' gap by 20%. The results show that the freeway capacity could be approximately 90% higher with a 100% CACC penetration rate, compared to 0%. Although researchers conduct micro simulations based on different assumptions, they concede that vehicle connectivity (V2V) is one of the key factors in improving road capacity which could allow short headways while maintaining high-speed levels.

Second, both longitudinal and lateral movements of intelligent vehicles could offer benefits in terms of reducing energy and environmental costs. Ioannou and Stefanovic [29] estimate the environmental effects (i.e., CO, HC, CO_2, NOx, and fuel consumption) caused by lateral movements of the ACC vehicles based on different market-penetration rates and the position of the ACC vehicle in a string of 10 vehicles. Their results show that the smooth lane change feature has a positive effect on environment. Barth [59] estimates emissions and energy consumption under the automated highway system (AHS) operation at various congestion levels (LOS A-F). The study result shows that an AHS has a slightly lower average fuel consumption (5-15%) than a nonautomated highway operating at free flow conditions, but much lower average fuel consumption, under congested conditions because of smoother traffic flows of AVs. Additionally, platooned vehicles in an AHS can expect additional 5-15% fuel savings and emission reductions due to aerodynamic-drafting effects. Analyzing the AV impacts on GHG emissions and energy use, Wadud, MacKenzie [4] developed several illustrative scenarios and showed that AVs can reduce GHG emissions and the energy use by nearly half. However, the study did not employ empirical data or micro simulation for the estimation and simply used the results from previous simulation studies. Rios-Torres and Malikopoulos [44] develop a micro simulation framework for CAVs to estimate fuel consumption and travel time. The result shows that CAVs can significantly reduce fuel consumption and travel time.

Third, none of the parameters in the AV or CAV simulation models is calibrated by the real field data. However, there have been ongoing efforts trying to connect intelligent-vehicle simulations (e.g., CACC or low-automation level AVs) to actual field experiments. Bu, Tan [33] develop a V2V-based CACC experimental system retrofitted on two Infinity FX45s models that are originally equipped with the ACC systems. The experimental result indicates that the CACC-equipped vehicles can perform better than the ACC vehicles by operating with a 0.6 to 1.1 second-gap, compared to a range of 1.1 to 2.2 seconds with the ACC. The shorter gap by the CACC implies a potential highway capacity increase. Milanés, Shladover [2] used the dedicated short-range communication (DSRC) equipped with four Infinity M56s models (ACC equipped) to test the CACC systems under various road situations (different vehicle gaps, cut-in and -out of manual vehicles) on public roads. The CACC vehicles clearly show their potential in increased highway capacity and traffic flow stability.

Fourth, since the first car-following concept was introduced by Pipes [47] and Reuschel [68], traffic engineers and traffic psychologists have developed various car-following models to explain human-driven vehicle characteristics [69]. However, a research gap exists for modeling machine-driven car-following characteristics. This gap leads to a high dependency on a few previously developed car-following models (e.g., IDM or MIXIC) in the literature. Furthermore, we found that the vast majority of simulation-based studies aim to measure only the longitudinal performance of intelligent vehicles. Note that the introduced IDM and MIXIC models

are also limited to the analysis of a longitudinal movement's impacts. In fact, very few studies focus on the impacts of the lateral movement of intelligent vehicles [29, 37]. This can be because lateral movements are expected to have relatively lower benefits than those of longitudinal movements. As a result, existing models are limited to the explanation of intelligent vehicles' lateral movements.

Finally, as our review shows, many studies are dependent on simulation-based intelligent-vehicle analysis. Additionally, the intelligent-vehicle impacts have been calculated according to various performance measures (e.g., throughput, environmental effect, energy consumption, and safety). However, there is much less attention to their broader impacts, combining these impacts into a unified metric (e.g., the overall economic impact or social welfare impacts). Without such overarching criteria, we are unable to provide a clear optimal pathway about how to implement and regulate AVs when comparing intelligent-vehicle alternatives to each other.

5. Conclusion

With the fast growth in intelligent-vehicle technologies, the conventional transportation system will experience drastic changes. This evolutionary transportation system is challenging researchers and practitioners to estimate intelligent-vehicle impacts on road transportation and society. In this paper, we review and summarize the simulation-based impact analysis studies for intelligent vehicles. The present study is, therefore, timely and significant in terms of both understanding the current stage of intelligent-vehicle analysis and predicting the future impacts.

In our literature review, we found that the concept of intelligent vehicle is simulated based on a variety of assumptions. Furthermore, there are no firmly defined terminologies for each vehicle type. To offer insights, we define and classify the commonly used intelligent vehicles into four categories (ACC, CACC, AV, and CAV). One important note is that different studies use their own assumptions for the intelligent vehicles' capabilities. This can lead to inconsistent conclusions.

More than a half of intelligent-vehicle studies adopt the road capacity as the primary performance measure. Intuitively, one of the most effective functions of intelligent vehicles is the vehicle connections that enable high-speed operations under small headway gaps. This is suggested as a solution that could considerably increase road capacity. Despite inconsistent results, most studies agreed that vehicle connectivity can significantly contribute to the road capacity increase. In addition to the connectivity, the general agreement of most studies is that the increase in the market-penetration rate of intelligent vehicles highly improves roadway capacity.

Regarding simulation models, the most frequently adapted car-following models are the IDM [20] and MIXIC model [62]. However, the IDM assumes unrealistically high deceleration rates when the current vehicle's gap to the preceding vehicle is much smaller than the desired gap. To overcome this issue, Kesting, Treiber [30] adapt the CAH model and develop the ACC acceleration control model. On the other hand, the MIXIC model is simulated for the CACC by Van Arem, Van Driel [21] and Talebpour, Mahmassani [45]. However, we should note that none of parameters for the AV or CAV is calibrated based on real field data since level 3 or higher levels of AVs are still immature [16]. Therefore, no adequate empirical data for the calibration of intelligent vehicles is available at present.

Our findings indicate that the impact analysis of intelligent vehicles is still in a preliminary stage involving many uncertainties. Although new models have been developed to capture the car-following and lane-changing characteristics of intelligent vehicles, empirical data are needed for the model calibration. Furthermore, a set of standardized driving characteristics of intelligent vehicles is necessary for future research studies as most studies use different assumptions on the key features of intelligent vehicles.

Conflicts of Interest

The authors declare that there are no conflicts of interest regarding the publication of this paper.

References

[1] D. González, J. Pérez, V. Milanés, and F. Nashashibi, "A review of motion planning techniques for automated vehicles," *IEEE Transactions on Intelligent Transportation Systems*, vol. 17, no. 4, pp. 1135–1145, 2016.

[2] V. Milanes, S. E. Shladover, J. Spring, C. Nowakowski, H. Kawazoe, and M. Nakamura, "Cooperative adaptive cruise control in real traffic situations," *IEEE Transactions on Intelligent Transportation Systems*, vol. 15, no. 1, pp. 296–305, 2014.

[3] K. Bimbraw, "Autonomous cars: Past, present and future a review of the developments in the last century, the present scenario and the expected future of autonomous vehicle technology," in *Proceedings of the 2015 12th International Conference on Informatics in Control, Automation and Robotics (ICINCO'15)*, IEEE, 2015.

[4] Z. Wadud, D. MacKenzie, and P. Leiby, "Help or hindrance? The travel, energy and carbon impacts of highly automated vehicles," *Transportation Research Part A: Policy and Practice*, vol. 86, pp. 1–18, 2016.

[5] Y. Zhao and K. M. Kockelman, "Anticipating the regional impacts of connected and automated vehicle travel in Austin, Texas," *Journal of Urban Planning and Development*, vol. 144, no. 4, Article ID 04018032, 2018.

[6] D. J. Fagnant and K. M. Kockelman, "Dynamic ride-sharing and fleet sizing for a system of shared autonomous vehicles in Austin, Texas," *Transportation*, vol. 45, no. 1, pp. 143–158, 2018.

[7] T. Seo and Y. Asakura, "Endogenous market penetration dynamics of automated and connected vehicles: Transport-oriented model and its paradox," *Transportation Research Procedia*, vol. 27, pp. 238–245, 2017.

[8] B. Kloostra and M. J. Roorda, "Fully autonomous vehicles: analyzing transportation network performance and operating scenarios in the greater Toronto area, Canada," in *Proceedings of the TRB 2017 Annual Meeting*, 2017.

[9] S. Anthony, Google's self-driving car passes 700,000 accident-free miles, can now avoid cyclists, stop at railroad crossings Extreme Tech, 2014.

[10] D. J. Fagnant and K. Kockelman, "Preparing a nation for autonomous vehicles: Opportunities, barriers and policy recommendations," *Transportation Research Part A: Policy and Practice*, vol. 77, pp. 167–181, 2015.

[11] D. J. Fagnant, K. M. Kockelman, and P. Bansal, "Operations of shared autonomous vehicle fleet for Austin, Texas, market," *Transportation Research Record*, vol. 2536, pp. 98–106, 2015.

[12] P. Tientrakool, Y.-C. Ho, and N. F. Maxemchuk, "Highway capacity benefits from using vehicle-to-vehicle communication and sensors for collision avoidance," in *Proceedings of the Vehicular Technology Conference (VTC Fall)*, IEEE, 2011.

[13] S. Trommer, V. Kolarova, E. Frädrich et al., Autonomous driving: The impact of vehicle automation on mobility behaviour, 2016.

[14] A. Kesting, M. Treiber, M. Schönhof, and D. Helbing, "Adaptive cruise control design for active congestion avoidance," *Transportation Research Part C: Emerging Technologies*, vol. 16, no. 6, pp. 668–683, 2008.

[15] J. Ma, F. Zhou, Z. Huang, and R. James, "Hardware-in-the-loop testing of connected and automated vehicle applications: a use case for cooperative adaptive cruise control," in *Proceedings of the 2018 21st International Conference on Intelligent Transportation Systems (ITSC '18)*, IEEE, 2018.

[16] D. Milakis, B. Van Arem, and B. Vanwee, "Policy and society related implications of automated driving: A review of literature and directions for future research," *Journal of Intelligent Transportation Systems: Technology, Planning, and Operations*, vol. 21, no. 4, pp. 324–348, 2017.

[17] E. Aria, J. Olstam, and C. Schwietering, "Investigation of automated vehicle effects on driver's behavior and traffic performance," *Transportation Research Procedia*, vol. 15, pp. 761–770, 2016.

[18] A. Olia, S. Razavi, B. Abdulhai, and H. Abdelgawad, "Traffic capacity implications of automated vehicles mixed with regular vehicles," *Journal of Intelligent Transportation Systems*, vol. 22, no. 3, pp. 244–262, 2018.

[19] Y. Liu, J. Guo, J. Taplin, and Y. Wang, "Characteristic analysis of mixed traffic flow of regular and autonomous vehicles using cellular automata," *Journal of Advanced Transportation*, vol. 2017, Article ID 8142074, 10 pages, 2017.

[20] M. Treiber, A. Hennecke, and D. Helbing, "Congested traffic states in empirical observations and microscopic simulations," *Physical Review E: Statistical, Nonlinear, and Soft Matter Physics*, vol. 62, no. 2, pp. 1805–1824, 2000.

[21] B. Van Arem, C. J. G. Van Driel, and R. Visser, "The impact of cooperative adaptive cruise control on traffic-flow characteristics," *IEEE Transactions on Intelligent Transportation Systems*, vol. 7, no. 4, pp. 429–436, 2006.

[22] D. J. Fagnant and K. M. Kockelman, "The travel and environmental implications of shared autonomous vehicles, using agent-based model scenarios," *Transportation Research Part C: Emerging Technologies*, vol. 40, pp. 1–13, 2014.

[23] P. M. Boesch, F. Ciari, and K. W. Axhausen, "Autonomous vehicle fleet sizes required to serve different levels of demand," *Transportation Research Record*, vol. 2542, no. 1, pp. 111–119, 2016.

[24] T. D. Chen and K. M. Kockelman, "Management of a shared autonomous electric vehicle fleet: Implications of pricing schemes," *Transportation Research Record*, vol. 2572, no. 1, pp. 37–46, 2016.

[25] J. Liu, K. M. Kockelman, P. M. Boesch, and F. Ciari, "Tracking a system of shared autonomous vehicles across the Austin, Texas network using agent-based simulation," *Transportation*, vol. 44, no. 6, pp. 1261–1278, 2017.

[26] L. Greer, J. L. Fraser, D. Hicks, M. Mercer, and K. Thompson, Intelligent Transportation Systems Benefits, Costs, And Lessons Learned: 2018 Update Report. United States. Dept. of Transportation. ITS Joint Program Office; 2018.

[27] S. E. Shladover, D. Su, and X.-Y. Lu, "Impacts of cooperative adaptive cruise control on freeway traffic flow," *Transportation Research Record*, vol. 2324, no. 1, pp. 63–70, 2012.

[28] D. A. Reece and S. A. Shafer, "A computational model of driving for autonomous vehicles," *Transportation Research Part A: Policy and Practice*, vol. 27, no. 1, pp. 23–50, 1993.

[29] P. A. Ioannou and M. Stefanovic, "Evaluation of ACC vehicles in mixed traffic: Lane change effects and sensitivity analysis," *IEEE Transactions on Intelligent Transportation Systems*, vol. 6, no. 1, pp. 79–89, 2005.

[30] A. Kesting, M. Treiber, and D. Helbing, "Enhanced intelligent driver model to access the impact of driving strategies on traffic capacity," *Philosophical Transactions of the Royal Society A: Mathematical, Physical & Engineering Sciences*, vol. 368, no. 1928, pp. 4585–4605, 2010.

[31] A. Kesting, M. Treiber, M. Schönhof, and D. Helbing, "Extending adaptive cruise control to adaptive driving strategies," *Transportation Research Record*, vol. 2000, no. 1, pp. 16–24, 2007.

[32] J. VanderWerf, S. Shladover, N. Kourjanskaia, M. Miller, and H. Krishnan, "Modeling effects of driver control assistance systems on traffic," *Transportation Research Record*, no. 1748, pp. 167–174, 2001.

[33] F. Bu, H.-S. Tan, and J. Huang, "Design and field testing of a cooperative adaptive cruise control system," in *Proceedings of the 2010 American Control Conference*, IEEE, 2010.

[34] K. C. Dey, L. Yan, X. Wang et al., "A review of communication, driver characteristics, and controls aspects of cooperative adaptive cruise control (CACC)," *IEEE Transactions on Intelligent Transportation Systems*, vol. 17, no. 2, pp. 491–509, 2016.

[35] J. Ding, H. Pei, J. Hu, and Y. Zhang, "Cooperative adaptive cruise control in vehicle platoon under environment of i-VICS," in *Proceedings of the 2018 21st International Conference on Intelligent Transportation Systems (ITSC '18)*, IEEE, 2018.

[36] H. Liu, X. Kan, S. E. Shladover, X.-Y. Lu, and R. E. Ferlis, "Impact of cooperative adaptive cruise control on multilane freeway merge capacity," *Journal of Intelligent Transportation Systems: Technology, Planning, and Operations*, vol. 22, no. 3, pp. 263–275, 2018.

[37] H. Liu, X. Kan, S. E. Shladover, X.-Y. Lu, and R. E. Ferlis, "Modeling impacts of Cooperative Adaptive Cruise Control on mixed traffic flow in multi-lane freeway facilities," *Transportation Research Part C: Emerging Technologies*, vol. 95, pp. 261–279, 2018.

[38] S. Yu and Z. Shi, "The effects of vehicular gap changes with memory on traffic flow in cooperative adaptive cruise control strategy," *Physica A: Statistical Mechanics and its Applications*, vol. 428, pp. 206–223, 2015.

[39] C. Goodin, J. T. Carrillo, D. P. McInnis et al., "Unmanned ground vehicle simulation with the virtual autonomous navigation environment," in *Proceedings of the 2017 International Conference on Military Technologies (ICMT '17)*, IEEE, 2017.

[40] X. Mao, Y. Xu, S. Mita, H. Chin, and H. Tehrani, "Navigating automated vehicle through expressway toll gate," in *Proceedings of the 2018 IEEE Intelligent Vehicles Symposium (IV)*, IEEE, 2018.

[41] P. Fernandes and U. Nunes, "Platooning of autonomous vehicles with intervehicle communications in SUMO traffic simulator," in *Proceedings of the 13th International IEEE Conference on Intelligent Transportation Systems*, IEEE, 2010.

[42] D. Jia, D. Ngoduy, and H. L. Vu, "A multiclass microscopic model for heterogeneous platoon with vehicle-to-vehicle communication," *Transportmetrica B: Transport Dynamics*, pp. 1–25, 2018.

[43] A. Kemeny, E. Icart, A. Sepchat, F. Colombet, S. Espié, and J-R. Chardonnet, "Large scale collaborative autonomous vehicle simulation and analysis using smartphones," in *Proceedings of the Driving Simulation Conference 2018 Europe VR*, 2018.

[44] J. Rios-Torres and A. A. Malikopoulos, "Impact of connected and automated vehicles on traffic flow," in *Proceedings of the 2017 IEEE 20th International Conference on Intelligent Transportation Systems (ITSC '17)*, IEEE, 2017.

[45] A. Talebpour and H. S. Mahmassani, "Influence of connected and autonomous vehicles on traffic flow stability and throughput," *Transportation Research Part C: Emerging Technologies*, vol. 71, pp. 143–163, 2016.

[46] M. Zhou, X. Qu, and S. Jin, "On the impact of cooperative autonomous vehicles in improving freeway merging: a modified intelligent driver model-based approach," *IEEE Transactions on Intelligent Transportation Systems*, vol. 18, no. 6, pp. 1422–1428, 2017.

[47] L. A. Pipes, "An operational analysis of traffic dynamics," *Journal of Applied Physics*, vol. 24, no. 3, pp. 274–281, 1953.

[48] A. Bose and P. Ioannou, *Analysis of Traffic Flow with Mixed Manual And Intelligent Cruise Control Vehicles: Theory and Experiments*, 2001.

[49] M. Fellendorf, "VISSIM: A microscopic simulation tool to evaluate actuated signal control including bus priority," in *Proceedings of the 64th Institute of Transportation Engineers Annual Meeting*, Springer, 1994.

[50] R. Wiedemann, Simulation des Strassenverkehrsflusses. Kalsruhe. Traffic Engineering, University of Karlsruhe, 1974.

[51] B. Ciuffo, V. Punzo, and M. Montanino, "Thirty years of Gipps' car-following model: Applications, developments, and new features," *Transportation Research Record*, vol. 2315, no. 1, pp. 89–99, 2012.

[52] Q. Deng, "A general simulation framework for modeling and analysis of heavy-duty vehicle platooning," *IEEE Transactions on Intelligent Transportation Systems*, vol. 17, no. 11, pp. 3252–3262, 2016.

[53] T. Oguchi, M. Katakura, and M. Taniguchi, "Carbondioxide emission model in actual urban road vehicular traffic conditions," *Doboku Gakkai Ronbunshu*, vol. 2002, no. 695, pp. 125–136, 2002.

[54] U. Leyn and P. Vortisch, "Calibrating VISSIM for the German highway capacity manual," *Transportation Research Record*, vol. 2483, pp. 74–79, 2015.

[55] H. Yeo, Asymmetric microscopic driving behavior theory, 2008.

[56] G. M. Arnaout, H. Arbabi, and S. Bowling, "Effective cooperative adaptive cruise control algorithm for intelligent transportation systems," *International Journal of Robotics and Automation*, vol. 30, no. 3, 2015.

[57] H. Yeo and A. Skabardonis, "Parameter estimation for NGSIM freeway flow algorithm," in *Proceedings of the 10th International Conference on Applications of Advanced Technologies in Transportation*, 2008.

[58] V. Milanés and S. E. Shladover, "Modeling cooperative and autonomous adaptive cruise control dynamic responses using experimental data," *Transportation Research Part C: Emerging Technologies*, vol. 48, pp. 285–300, 2014.

[59] M. Barth, "An emissions and energy comparison between a simulated automated highway system and current traffic conditions," in *Proceedings of the 2000 IEEE Intelligent Transportation Systems (ITSC' 00)*, IEEE, 2000.

[60] A. D. Tibljaš, T. Giuffrè, S. Surdonja, and S. Trubia, "Introduction of Autonomous Vehicles: Roundabouts design and safety performance evaluation," *Sustainability*, vol. 10, no. 4, p. 1060, 2018.

[61] A. Papadoulis, M. Quddus, and M. Imprialou, "Evaluating the safety impact of connected and autonomous vehicles on motorways," *Accident Analysis & Prevention*, vol. 124, pp. 12–22, 2019.

[62] B. Van Arem, A. De Vos, and M. J. Vanderschuren, The microscopic traffic simulation model MIXIC 1.3, 1997.

[63] M. Treiber and A. Kesting, *Traffic Flow Dynamics. Traffic Flow Dynamics: Data, Models and Simulation*, Springer, Berlin, Germany, 2013.

[64] M. Treiber, A. Kesting, and D. Helbing, "Understanding widely scattered traffic flows, the capacity drop, and platoons as effects of variance-driven time gaps," *Physical Review E: Statistical, Nonlinear, and Soft Matter Physics*, vol. 74, no. 1, Article ID 016123, 2006.

[65] M. Treiber, A. Kesting, and D. Helbing, "Influence of reaction times and anticipation on stability of vehicular traffic flow," *Transportation Research Record*, vol. 1999, no. 1, pp. 23–29, 2007.

[66] M. Treiber, A. Kesting, and D. Helbing, "Delays, inaccuracies and anticipation in microscopic traffic models," *Physica A: Statistical Mechanics and its Applications*, vol. 360, no. 1, pp. 71–88, 2006.

[67] B. Van Arem, A. De Vos, and M. J. W. A. Vanderschuren, The microscopic traffic simulation model MIXIC 1.3. 1997.

[68] A. Reuschel, "Fahrzeugbewegungen in der Kolonne," *Osterreichisches Ingenieur Archiv*, vol. 4, pp. 193–215, 1950.

[69] M. Saifuzzaman and Z. Zheng, "Incorporating human-factors in car-following models: a review of recent developments and research needs," *Transportation Research Part C: Emerging Technologies*, vol. 48, pp. 379–403, 2014.

Hindawi
Journal of Advanced Transportation
Volume 2019, Article ID 8151582, 11 pages
https://doi.org/10.1155/2019/8151582

Research Article

Modified Traffic Flow Model with Connected Vehicle Microscopic Data for Proactive Variable Speed Limit Control

Jie Fang[1], **Huixuan Ye**[1] **and Said M. Easa**[2]

[1] *Transportation Department, Fuzhou University, Fuzhou, Fujian, China*
[2] *Department of Civil Engineering, Ryerson University, Toronto, Ontario, Canada*

Correspondence should be addressed to Jie Fang; fangjie@fzu.edu.cn

Received 16 February 2019; Revised 16 April 2019; Accepted 22 May 2019; Published 10 June 2019

Guest Editor: Md. A. S. Kamal

Most previous prediction based Variable Speed Limit (VSL) control strategies focused on improving traffic mobility based on the macroscopic traffic data. Nowadays, the emerging technologies provide access to the microscopic traffic flow data, which better captures the details of traffic flow dynamics in the VSL controlled environment. Thus, in this paper, the microscopic traffic flow data were utilized as a supplement to predict the evolutions of traffic flow parameters. The proposed VSL control algorithm adopts the Model Predictive Control (MPC) framework, which employs a modified version of the classic traffic flow model METANET to take advantage of the microscopic data in traffic flow predictions. The microscopic traffic simulation software VISSIM was used to establish an experimental simulation platform and perform real time traffic responsive control based on field data. The proposed control strategy was evaluated against the no-VSL control and macroscopic-based VSL controlled scenario. The results show that utilizing the proposed modified METANET model reduced the error in speed prediction accuracy and improved system mobility performance.

1. Introduction

Urban freeways provide efficient and convenient traffic service for road users and play a significant role in accelerating the development of regional economy [1]. With the rapid economic development, the great increase in car-ownership has aggravated the traffic congestion. Thus, traffic mobility and safety have become major challenges in freeway operations. Due to the restriction of urban space and the high cost of infrastructure construction, the problems may not be solved simply by expanding road facilities. To ease traffic congestion, some traffic control measures have been adopted, such as Route Guidance [2, 3], Ramp Metering [4, 5], and Variable Speed Limits (VSL). Among these measures, VSL control draws widely attentions. It determines a dynamic speed limit according to the current traffic flow states, climatic, road environments, etc. The main benefits of VSL control are as follows: (1) improves traffic operations through regulating the mainstream traffic flow and delaying the forthcoming traffic breakdown for potential capacity gain and higher level of service, (2) mitigates the speed differences between individual vehicle for fewer traffic collisions, and (3) reduces the vehicle stop frequencies for vehicle emission and air pollution [6–8].

The MPC control framework has recently been widely adopted in proactive freeway control simulations implementing VSL. The essential core of the MPC framework is the included traffic state prediction model for process control. For this approach, the performance of VSL control strategy depends heavily on the accurate prediction of traffic-flow parameters, which will be used for quantitatively determining the dynamic speed limits. To adapt the limitation of the traditional data collection methods, existing VSL control methods adopt macroscopic traffic flow data that can be easily collected, such as speed, volume, and density. Enabled by the fast-emerging technologies, such as internet of vehicles, the real-time microscopic traffic data, such as the acceleration rate, can be collected by the in-vehicle or roadside sensors [9]. This newly available data source may better capture the details of traffic flow dynamics in the VSL controlled environment.

Thus, in this paper, a VSL control strategy based on a modified METANET model utilizing the microscopic traffic data was proposed. In the modified model, the microscopic data are used in the prediction model as a supplement to predict the evolution of the traffic dynamics. By analyzing higher resolution data, such as the individual acceleration rate and headway at second-by-second level, the responding and evolving of the traffic flow to the control measure can be modeled more accurately, thus improves the prediction accuracy. The modified model with proposed control strategy was implemented in a simulated freeway to validate their feasibility and control performance.

The next sections present a brief literature review of existing VSL control strategies, followed by the descriptions of the basic and modified METANET models. The following sections present the model validation through an application of the proposed control strategy using VISSIM simulation and the conclusions.

2. Literature Review

The studies of VSL control in Europe and North America, traced back to 1990s, have provided valuable state-of-the-art and practical experiences [10]. Various VSL control strategies have been proposed and can be grouped into three categories: rule-based VSL control strategies, feedback controller-based VSL control strategies, and model-based VSL control strategies.

The rule-based control strategies use real-time traffic measurements as a basis for real-time control. The decision tree strategy can be categorized as rule-based control strategy, which is the earliest to be developed for VSL control. It uses an algorithm that defines an indicator, such as density, as a criterion for determining whether to start the VSL control. Decision tree-based strategies are straightforward for field implementation. Lee et al. [11] proposed a real-time conflict prediction model and showed that the precursors of conflict could be decided in an objective manner to replace the subjective classification mode used in the analysis. In 2006, Lee et al. [12] proposed a VSL strategy that reduced the speed limit when the potential conflict exceeded a preset threshold. The optimal speed limit was selected based on several thresholds associated with safety. The results suggested that the number of potential conflicts were decreased, but travel time was increased.

In 2011, Carlson et al. [13] designed a simple local feedback controller Mainstream Traffic Flow Control (MTFC) to improve traffic-flow efficiency. The control strategy was evaluated using simulation and the performance of the controller was shown to approach the optimal control effect. In 2013, the same group of authors [14] proposed two simple feedback controllers that relied on readily available real-time measurements for local MTFC via VSL. The results showed that the feedback controllers had satisfactory control effects. Recently, Iordanidou et al. [15, 16] proposed an extended feedback-based VSL control strategy, considering multiple-bottleneck locations, and obtained good results.

The Model Predictive Control- (MPC-) based VSL control strategy is a model-based VSL control strategy, of which the model has predictive function. The limitation of the rule-based control strategies is that traffic conditions may have already broken down before VSL is deployed. Thus, Model Predictive Control (MPC) has emerged as a new approach to address this limitation. The MPC is a valuable, widely used framework for VSL control of freeways [17]. In model experiment, future traffic conditions (e.g., congestion) are foreseen before they even occur, and VSL strategies are deployed to reduce traffic volume in the expected congestion area, see, for example, Khondaker et al. [18]. The framework uses a model to predict future traffic states. The MPC-based VSL control strategies consider future traffic conditions and quantitatively evaluate the impact of VSL control on traffic-flow dynamics to keep traffic flow at high efficiency, especially during congested periods. In 2005, Zhang et al. [19] used MPC to design a roadway controller that reduced traffic congestion. In 2009, Zegeye et al. [20] used MPC to evaluate the impact of dynamic speed limit control and the results showed a reduction in total time spent. In 2010, Ghods et al. [21] solved the problem of real-time optimal control of traffic flow in a freeway network with a promising approach by casting the underlying dynamic control problem in an MPC framework. Hadiuzzaman et al. proposed a modified Cell Transmission Model (CTM) based on Daganzo's original model [22] and used MPC to alter the speed limit dynamically [23, 24]. In 2017, Han et al. [25] developed a fast MPC based approach for VSL coordination to resolve freeway jam waves. This MPC approach is based on a more accurate discrete first-order model that keeps the linearity property of the classical discrete first-order model and takes capacity drop into consideration. The simulation results demonstrated that the proposed control strategy resolved the jam wave with a real-time feasible computation speed [26].

As a macroscopic modeling tool, the METANET model, developed by Papageorgiou et al. [10], and its extensions are widely used. One of the pioneering MPC-based VSL control strategies was proposed by Hegyi [27] and Hegyi et al. [28, 29]. The authors modified the METANET model, for example, by proposing a revised the desired speed term. The new desired speed is the minimum of the targeted speed based on the current traffic conditions and the displayed speed limit. The MPC framework was adopted to determine the optimal speed limit. Hence, Hegyi et al. [29] proposed an extended METANET model with modeling of dynamic speed limits and mainstream origins. The results showed that the VSL can prevent traffic breakdown and maintain a higher outflow. In 2010, Carlsonet al. [30] incorporated VSL in the METANET model as an additional control component leading to an extended optimal control formulation. The results showed that traffic-flow efficiency was substantially improved when VSL control measures were used. In 2012, Hadiuzzaman et al. [23] replaced the fundamental diagram with the VSL control variable in the relaxation term of the METANET model, the proposed traffic dynamics with the control strategy were implemented in a freeway corridor using the MPC framework. The analysis was carried out in VISSIM and the results showed that VSL was mostly effective during congestion periods in terms of mobility. In 2014, Sun et al. [31] proposed a new extension of METANET model in

which traffic state variables were modeled and predicted. In addition, VSL values were optimized using MPC. Yu et al. [32] proposed an extended METANET model, in which the desired speed term was modified to minimize the total crash risk. The results showed that traffic safety improved and speed homogeneity was enhanced. The MPC based VSL control have been proven effective in the preceding researches.

However, most previous VSL control strategies predicted traffic-flow states using collected macroscopic traffic data to determine the VSL control signal. Due to lack of microscopic traffic flow data, the prediction accuracy maybe compromised in certain circumstances, such as low density (free flow). With the development of new sensoring and communication technologies, microscopic traffic data can be collected and incorporated into the formulation of the basic METANET model for better modeling the responding and evolving of the traffic flow under VSL controlled environment. Thus, in this paper, a modified METNET model incorporating microscopic traffic data will be proposed to establish an MPC based proactive VSL control strategy that further improves the prediction accuracy and freeway operation efficiency.

3. Methodology

3.1. Model Formulation

3.1.1. Macroscopic METANET Model. In this paper the authors adopted the MPC framework that incorporates the METANET model and its extensions, which are valuable tools widely used to make accurate prediction of traffic-flow variables. The METANET model is deterministic, discrete-time, discrete-space, and macroscopic, making it very suitable for model-based traffic control [27].

According to the conservation equation of fluid motion,

$$\frac{\partial_\rho}{\partial_t} + \frac{\partial_q}{\partial_x} = H' - S' \tag{1}$$

where H' = average inflow from onramp at position x (veh) and S' = average outflow of the off-ramp at position x (veh).

If the number of lanes of segment i is λ_i and the length of segment i is L_i, (1) becomes

$$\frac{\lambda_i \left[\rho_i (k+1) - \rho_i (k)\right]}{T} + \frac{q_i (k) - q_{i-1} (k)}{L_i} = \frac{h_i (k) - s_i (k)}{L_i} \tag{2}$$

After adjustment, the conservation equation of vehicles is obtained as

$$\rho_i (k+1) = \rho_i (k) + \frac{T}{L_i \lambda_i} \left(q_{i-1} (k) - q_i (k) + h_i (k) - s_i (k)\right) \tag{3}$$

where $\rho_i(k)$ = density of segment i at time k (veh/km/ln); $q_i(k)$ = traffic flow of segment i at time k (veh/h); $h_i(k)$ = on-ramp flow of segment i at time k (veh/h) and $s_i(k)$ = off-ramp flow of segment i at time k (veh/h).

The outflow of segment i is equal to the density multiplied by the average speed and the number of lanes of that segment. That is,

$$q_i (k) = \rho_i (k) \cdot v_i (k) \cdot \lambda_i (k) \tag{4}$$

When adjusting towards the desired speed, there will a brief delay related to the drivers' reaction time and vehicle acceleration capability. In other words, to reach the desired speed at position $\triangle x$ ahead, a certain time and spacing are required for the vehicle to adjust according to the observation of the downstream traffic-flow state. If the adjustment time is $\triangle t$, then

$$v (x, t + \triangle t) = U \left[\rho (x + \triangle x, t)\right] \tag{5}$$

Applying Taylor series expansion to each side of (5), then

$$v (x, t) + \triangle t \cdot \frac{\partial v (x, t)}{\partial t} = U \left[\rho (x, t)\right] + \triangle x \cdot \frac{dU \left[\rho\right]}{d\rho} \cdot \frac{\partial \rho (x, t)}{\partial x} \tag{6}$$

In previous researches, $\triangle x$ was set to be an average value of $1/(2\rho)$ based on the empirical data [10, 27], while $(dU[\rho]/d\rho)$ is the sensitivity of adjusting towards the anticipated speed, considering segment density. Defining $(dU[\rho]/d\rho) = \gamma(x, t)$, (6) becomes

$$v (x, t) + \triangle t \cdot \frac{\partial v (x, t)}{\partial t} = U \left[\rho (x, t)\right] + \frac{\gamma (x, t)}{2\rho} \cdot \frac{\partial \rho (x, t)}{\partial x} \tag{7}$$

where

$$\frac{\partial v (x, t)}{\partial t} = \frac{\partial v}{\partial x} \cdot \frac{\mathrm{d}x}{\mathrm{d}t} + \frac{\partial v}{\partial t} \tag{8}$$

Based on (8), (7) can be written as

$$\frac{\partial v}{\partial t} = \frac{1}{\triangle t} \left\{U \left[\rho\right] + \frac{\gamma}{2\rho} \cdot \frac{\partial \rho}{\partial x} - v\right\} - v \cdot \frac{\partial v}{\partial x} \tag{9}$$

After discretizing and rearranging (9), one obtains

$$v_i (k+1) = v_i (k) + \frac{T}{\tau_{i(k)}} \left(U \left[\rho_i (k)\right] - v_i (k)\right) - \frac{T}{L_i} v_i (k) \left[v_i (k) - v_{i-1} (k)\right] + \frac{\gamma_{i(k)} T}{\tau_{i(k)} L_i} \cdot \frac{\rho_{i+1} (k) - \rho_i (k)}{\rho_i (k) + \kappa} \tag{10}$$

$$U \left[\rho_i (k)\right] = v_{free,i} \cdot \exp \left[-\frac{1}{a_m} \left(\frac{\rho_i (k)}{\rho_{crit}}\right)^{a_m}\right] \tag{11}$$

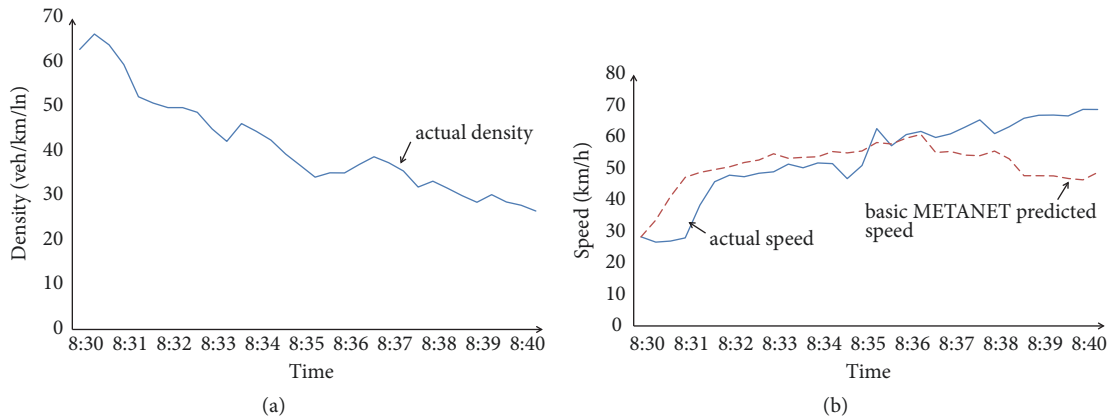

Figure 1: Variation of density corresponding actual and basic METANET predicted speeds: (a) actual density and (b) actual speed and basic METANET predictions.

where $U[\rho_i(k)]$ = desired speed of segment i (km/h), $\gamma_{i(k)}$ = a parameter with negative value, sensitivity of adjusting towards the anticipated speed of segment i at time k, $\tau_{i(k)}$ = driver adjustment delay coefficient of segment i, κ = positive compensation coefficient to avoid the error brought by too-small $\rho_i(k)$, $v_{free,i}$ = free-flow speed of segment i (km/h), a_m = model parameter of segment, and ρ_{crit} = critical density (veh/km/ln).

In the basic METANET model, $\gamma_{i(k)}$, $\tau_{i(k)}$, and κ are treated as constant model parameter. Thus, (10) becomes

$$v_i(k+1) = v_i(k) + \frac{T}{\tau}\left(U\left[\rho_i(k)\right] - v_i(k)\right) - \frac{T}{L_i}v_i(k)\left[v_i(k) - v_{i-1}(k)\right] + \frac{\gamma T}{\tau L_i} \cdot \frac{\rho_{i+1}(k) - \rho_i(k)}{\rho_i(k) + \kappa} \quad (12)$$

3.1.2. Proposed Macroscopic METANET Model with Microscopic Connected Vehicle Data. The term$\triangle x$ in (6) indicates the lag of speed adjustments. In the basic METANET model, $\triangle x$ is assumed to an empirical averaged value of $1/(2\rho)$, and $(dU[\rho]/d\rho)$ was replaced as a constant system parameter. In other words, the distance required for speed adjustment was set to be half of the headway, by simply assuming averaged vehicle headway as the ideal situation. However, this assumption is not always consistent with field implementation. Although this assumption is relatively accurate under high density, under low density circumstances the large averaged headway will cause significant model mismatches, as illustrated in Figure 1.

As noted in Figure 1, before 8:35 am, the density is comparatively higher and the prediction error of the basic METANET model is lower than 35%. On the other side, after 8:35 am, prediction error of the basic METANET model grows larger as the density decreases. Noticing this model mismatches, an extra model parameter κ was introduced into the basic METANET model as compensation coefficient to reduce the error in the low-density region [10]. Nonetheless, the error of speed prediction at low density may still be large in some cases, as shown in Figure 1(b). Therefore, a model modification utilizing the microscopic data was proposed to overcome this mismatch in this paper.

In the basic METANET model, since the actual individual vehicle status is unknown, the vehicle is assumed to be equally distributed along the road segment (by taking the segment averaged headway). Thus, the distance required for speed adjustment $\triangle x$ was set to half of the headway, which clearly will not represent all the circumstances in the real world. This distance required for speed adjustment should be a function of the current traffic condition: influenced by the interactions between individual vehicles, or in the other words, individual vehicle spacing when the traffic is congested and affected by the individual driving characteristic (acceleration/deceleration status) when the traffic is light. Therefore, taking advances of the state-of-the-art technologies, microscopic data were collected in this study to derive a modified METANET model, which utilized the microscopic data to model this dynamic term. In the field, when the density is high, the distance for speed adjustment is mainly influenced by the interactions between vehicles, as indicated by the headway. Thus, the term$\triangle x$ is expressed mathematically as a hybrid sigmoid function of the individual headway and acceleration, as follows:

$$S_h(y) \cdot h_i + S_{acc}(y) \cdot F(acc) \quad (13)$$

$$S_h(y) = \frac{1}{1+e^{-y}} \quad (14)$$

$$S_{acc}(y) = \frac{e^{-y}}{1+e^{-y}} \quad (15)$$

$$y = \tan\left[\left(\frac{\rho_i(k)}{\rho_0} - \rho^{\wedge}\right)\pi\right] \quad (16)$$

$$F(acc) = \frac{v_{i+1}^2(k) - v_i^2(k)}{2 \times acc_i(k)} \quad (17)$$

where h_i = averaged individual headway of vehicles in segment i(km), $F(acc)$ = distance function of averaged

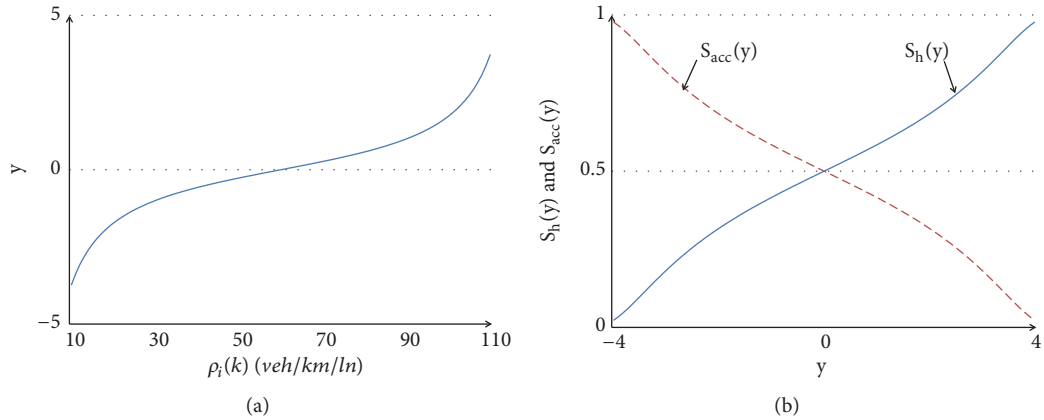

FIGURE 2: Interpretation of the term $\triangle x$: (a) the formulated sensitivity y along density $\rho_i(k)$ and (b) RELATIONSHIPS between $S_h(y)$, $S_{acc}(y)$, and y.

individual acceleration of vehicles(km), $S_h(y), S_{acc}(y)$ = coefficient related to density, $\rho_i(k)$ = density of segment i at time k(veh/km/ln), $\rho^{\wedge}, \rho_0$ = model parameter for shaping the sigmoid function, y = function of density, $v_i(k)$ = mean speed of segment i at time k(km/h), and $acc_i(k)$ = averaged individual acceleration of vehicles of segment i at time k(km/h^2).

The mathematical interpretation of established sigmoid model (13) is illustrated in Figure 2.

As demonstrated in Figure 2(a), in data set the density ranges from 10 to 110 while y ranges approximately from -4 to 4. The value of $S_h(y)$ and $S_{acc}(y)$ are continuous between 0 and 1. As shown in Figure 2(b), when the density is relatively large, the sensitivity depends mainly on $S_h(y)$, as observed in the field. And going the other way around as the density decreases. This means for better representing of the traffic flow dynamics, the formulated sensitivity term was mainly influenced by the individual vehicle at large densities and by the vehicle acceleration status in the low-density region. The formulated sensitivity term is less sensitive when the density is either too large or too low, and otherwise when the density is moderate. Noted that through this modification, the extra constant model parameter κ in the basic MEATNET model was neglected since no compensation is needed. The proposed microscopic METANET model improved the prediction accuracy, as shown in Figure 3, and the speed predicted by the modified METANET model is closer to the actual data.

Then, the density and volume of segment i at the next time step are determined using (3) and (4). The speed is determined by the modified model:

$$\begin{aligned} v_i(k+1) = {} & v_i(k) + \frac{T}{\tau}\left(U\left[\rho_i(k)\right] - v_i(k)\right) \\ & - \frac{T}{L_i} v_i(k)\left[v_i(k) - v_{i-1}(k)\right] + \frac{\gamma T}{\tau L_i} \\ & \cdot \left[\frac{1}{1+e^{-y}} \cdot h_i + \frac{e^{-y}}{1+e^{-y}} \cdot F(acc)\right] \\ & \cdot \left[\rho_{i+1}(k) - \rho_i(k)\right] \end{aligned} \tag{18}$$

where y is given by (16).

In the MPC-based VSL control strategy proposed in this paper, (19) is derived from the proposed microscopic METANET model. The desired speed $U[\rho_i(k)]$ is replaced by the speed limit $u_i(k)$. Thus, the prediction speed under the VSL control is determined by

$$\begin{aligned} v_i(k+1) = {} & v_i(k) + \frac{T}{\tau}\left(u_i(k) - v_i(k)\right) \\ & - \frac{T}{L_i} v_i(k)\left[v_i(k) - v_{i-1}(k)\right] + \frac{\gamma T}{\tau L_i} \\ & \cdot \left[\frac{1}{1+e^{-y}} \cdot h_i + \frac{e^{-y}}{1+e^{-y}} \cdot F(acc)\right] \\ & \cdot \left[\rho_{i+1}(k) - \rho_i(k)\right] \end{aligned} \tag{19}$$

3.1.3. Constraints. The constraints of the METANET model by Cao et al. [33] are adopted in this paper. Let V_{min}, V_{max} and V_d be the minimum speed, maximum speed, and maximum speed difference. Then, based on safety, driver compliance, traffic-flow characteristics, and other considerations, the speed limit is determined based on the following constraints:

(1) To guarantee drivers' safety, the optimal speed limit must be lower than the maximum speed:

$$u_i(k) \le \mathrm{V}_{\max} \tag{20}$$

(2) To maintain operating efficiency, the optimal speed limit must be higher than the minimum speed:

$$u_i(k) \ge \mathrm{V}_{\min} \tag{21}$$

(3) For safe operation, the difference in the speed limits of two consecutive time steps should be less than the maximum difference:

$$u_i(k) - u_i(k+1) \le \mathrm{V}_{\mathrm{d}} \tag{22}$$

(4) Not all vehicle drivers are able to drive at the speed limit. Therefore, to ensure that the speed limit is

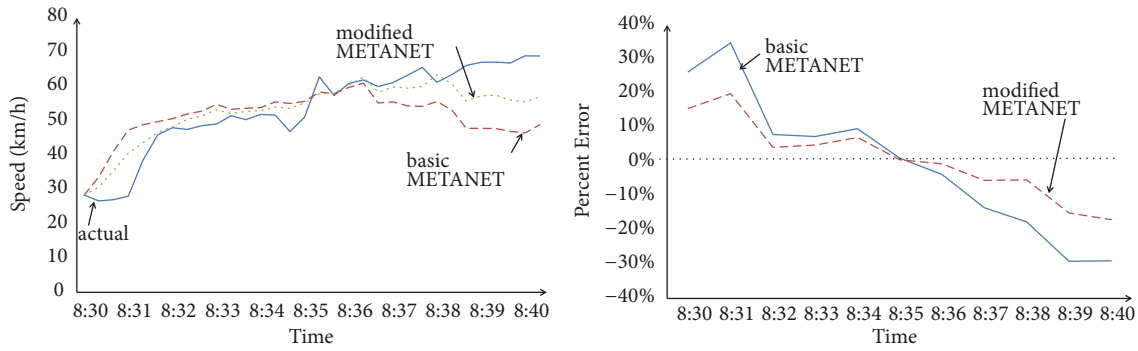

Figure 3: Comparison of speeds of basic and modified METANET models: (a) actual and predicted speeds and (b) percentile prediction error of basic and modified METANET model.

more suitable for actual traffic conditions, the difference between the optimal speed limit and the speed detected downstream should be less than the maximum difference:

$$\left|u_i(k) - v_{i+1}(k-1)\right| \leq \mathrm{V_d} \tag{23}$$

3.2. Model Validations. To calibrate the proposed model modification, the parameters of the basic and modified METANET (18) and (19) were first calibrated using field data. The data for the modified model were collected on a typical freeway (Whitemud Drive freeway, Edmonton, Canada). The actual data were collected for 100 continuous days. Fifty days of the data were used for model calibration, where model performance was measured using the error between predicted and actual values. The optimal parameters that produced the minimum error were selected.

The other 50 days of data were used for model validation. These data and the optimal parameters were used in the prediction model to predict traffic-flow state. As shown in Figure 3, before 8:35 am, the speed predicted by the modified METANET model is lower than the speed predicted by the basic METANET model, which is closer to the actual speed. The largest percentage of prediction error reduction is 14.9%. After 8:35 am, the speed predicted by the modified METANET model is generally larger than that predicted by the basic METANET model, which is also closer to the actual speed. The largest errors of the basic METANET model for the high and low-density ranges are 34.7% and -29.1%, respectively, while those of the modified model are 19.8% and -17.0%, respectively. The results show that the modified model has reduced the errors of the basic METANET model for the two density ranges by 14.9% and 14.1% in average.

3.3. Model Predictive Control. In this paper, an MPC framework is used to solve the problem of optimal speed limit for implementing proactive VSL control. In MPC, the time horizon is k discrete time steps. As shown is Figure 4, at each time step k, the optimal speed limits are computed over a prediction horizon N_p. The current traffic state variables are used as input to determine the optimal speed limits. Based on collected traffic data, for every input, the VSL-controlled future traffic states over the N_p horizon are predicted by the prediction model at the current time. The control input implements a control interval T_C, which is selected to improve traffic conditions.

As shown in Figure 5, the traffic flow in segment i is continuous, namely, it follows the conservation equation of fluid motion. The speed, density, and volume are temporal and spatial variables for each freeway segment. Thus, the three traffic-flow variables are functions of time and position. The variables $\rho_i(k)$ and $q_i(k)$ represent the density and volume at a certain moment and position, respectively, while t is time and x is coordinate of the position along the driving direction.

The objective function of VSL optimization was set as the weighted sum of total time spent (TTS) and total travel distance (TTD), in order to improve the mobility of the network, as suggested by Cao et al. [33] and couple other previous studies. The speed limits associated with the minimum objective function are selected as the optimal speed limits. The traffic states are updated dynamically after adopting the optimal speed limits, which are then forwarded to the framework again for optimizing the control input in the next time step. The objective function is given by

$$J = \sum_{j=1}^{N_p} \sum_{i=1}^{M} \left(\alpha_{TTS} T \lambda_i L_i \rho_i (k-1+j) - \alpha_{TTD} T \lambda_i L_i \rho_i (k-1+j)\, v_i (k-1+j)\right) \tag{24}$$

where N_p = total time step, M = number of segments, T = time step of the evolution of traffic flow, λ_i = number of lanes of segment i, L_i = length of segment i (km), $\rho_i(k-1+j)$ = density of segment i at time $k-1+j$ (veh/km/ln), $v_i(k-1+j)$ = mean speed of segment i at time $k-1+j$ (veh/km/ln), and α_{TTS} and α_{TTD} = weighting factors for TTS and TTD, respectively.

4. Application

4.1. Simulation Experiment. To evaluate and analyze the MPC-based VSL control strategy using the modified METANET model, an urban freeway corridor is selected as the experimental simulation site. The selected freeway

Table 1: Comparison of the objective function for no VSL, basic and modified METANET-VSL controls.

Time	Objective Function		
	No VSL	Basic METANET	Modified METANET
6:30-6:50	392.3	381.1	381.1
6:50-7:10	610.0	798.6	806.5
7:10-7:30	2739.6	2539.9	2505.5
7:30-7:50	5527.7	2932.8	3465.9
7:50-8:10	8613.2	2589.7	2515.2
8:10-8:30	9445.6	2617.7	1049.4
8:30-8:50	3779.2	736.5	624.9
Total	31107.6	12596.3	11348.5

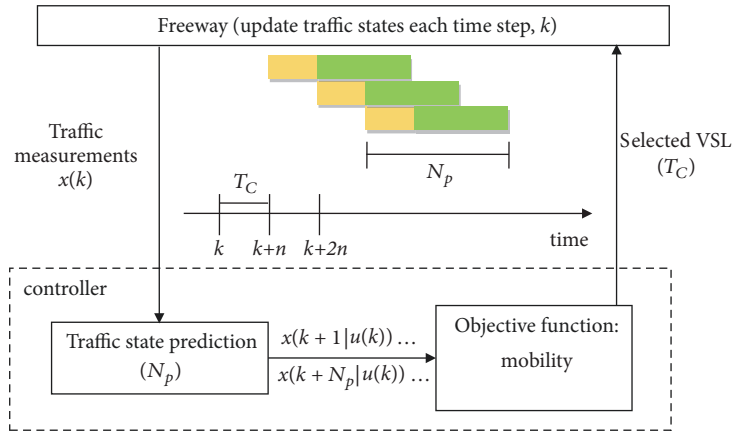

Figure 4: MPC-based control framework.

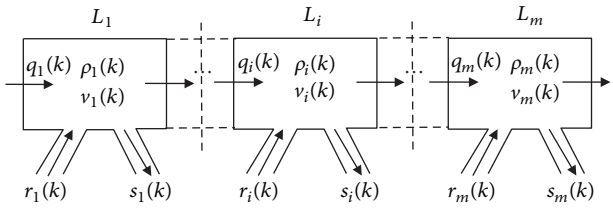

Figure 5: Schematic diagram of the METANET model.

is about 9 km long with three lanes in each direction. For modeling, the corridor is further divided into 13 segments including five on-ramps (r_1, r_2, r_3, r_4, and r_5) and six off-ramps (s_1, s_2, s_3, s_4, s_5, and s_6), and the VSL board locations are marked, as shown in Figure 6.

The traffic data were collected on-site using loop detectors installed in each segment, and the experiment was conducted for a peak-hour period of two and a half hour. The VISSIM simulation software was selected to establish the network simulation platform. The authors chose 10 random simulation seeds in the experiment, and the all simulation results in this paper are based on the average of the 10 different scenarios. The simulation resolution is 5 per second in this paper, since a higher resolution will lead to high computational load. Using MATLAB, the MPC-based VSL control strategy that includes the modified METANET model was implemented on the simulated site. The simulation platform was calibrated by minimizing the difference between actual and predicted traffic state variables.

In the experiment, three different control scenarios were evaluated in the simulation platform: (1) no control, (2) VSL control based on the basic METANET model, and (3) VSL control based on the modified METANET model.

4.2. Analysis Results. The basic demand profile of the experiment site is shown in Figure 7 as the volume variations in the uncontrolled scenario. On the profile, two bottlenecks can be recognized around segments L_4 and L_8. At Segment L_4, parts of the vehicles entering the mainline freeway through on-ramp r_1 want to leave the mainline through off-ramp s_2. The weaving segment in-between results in chaotic traffic operation and serious congestion. A similar weaving section exists around segment L_8, and significant capacity drop can be observed as well.

The evaluation results of the objective function for No-VSL, basic METANET-VSL, and modified METANET-VSL controls (using an interval of 20 s) are shown in Table 1 and Figure 8. As illustrated, under free-flow condition (before 7:00 AM), traffic conditions of the three tested scenarios are nearly identical. After 7:10 am, the traffic demand continued to increase. In both METANET-VSL controlled scenarios,

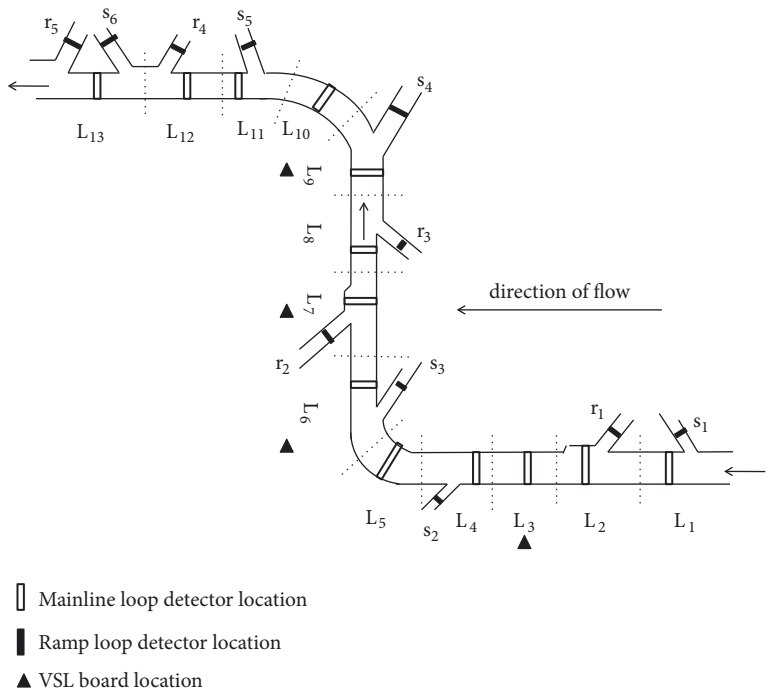

Figure 6: Schematic diagram of expressway segments.

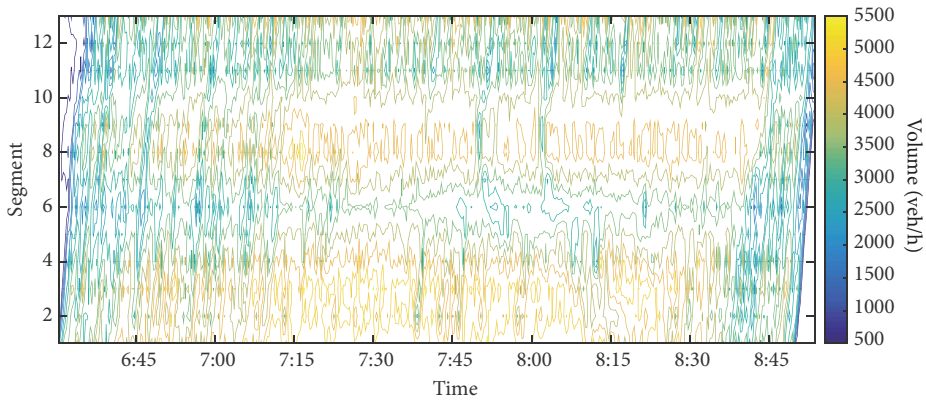

Figure 7: Volume variation at different segments without control.

the adopted traffic flow model was able to predict the forthcoming traffic breakdown and determined to advise reduced speed limit in advance for overall speed stability (6:50 to 7:10 AM). Thus, in the time slice, the objective function values in both controlled scenario were worse than the uncontrolled case. In addition, since the proposed model modification captures the speed dynamics more accurately during the density oscillation, the proposed modified control scenario determines to maintain a lower VSL value at 7:30 to 7:50 AM. As a result, the objective function performance in that time slice is not as good as the basic METANET controlled scenario, which mistakenly predicted the traffic flow has recovered and raised the VSL. Instead, the proposed modified VSL control maintained a more stable and sustainable traffic flow, which avoids the traffic breakdown occurred later in the basic METANET controlled scenario shortly after 8:00 AM. Overall speaking, the combined TTS and TTD for the basic and proposed modified METANET controlled scenario were reported to be 12,596.3 and 11,348.5, indicating an improvement of 10% in terms of the mobility performance and even more significant when comparing with the uncontrolled scenario. Clearly, the modified METANET-based VSL control strategy plays a better role in improving traffic mobility.

For segment densities, a comparison of no-VSL and basic and modified METANET-VSL controls is shown in Figure 9. The density of Segment L_8 increased significantly since around 7:30 am and remained high until nearly the end of the study period. The congestion propagates upstream to L_7 and such. It can be observed that both the severity and duration of the congestion has been significantly reduced

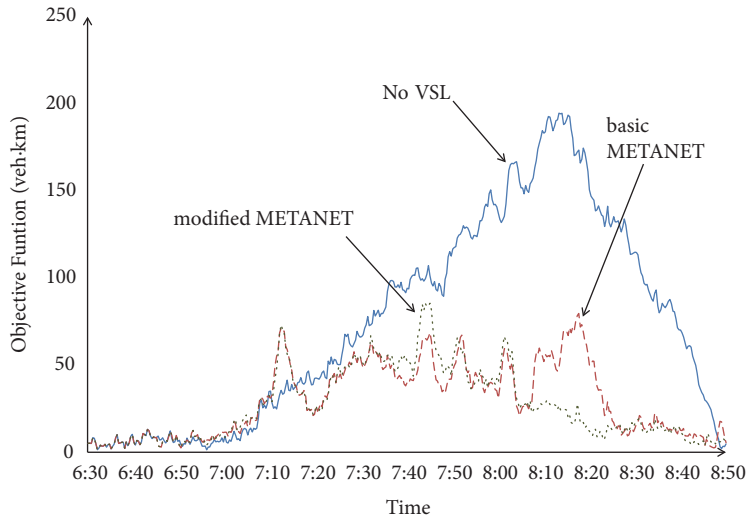

Figure 8: Comparison of the objective function for No VSL, basic, and modified METANET-VSL controls.

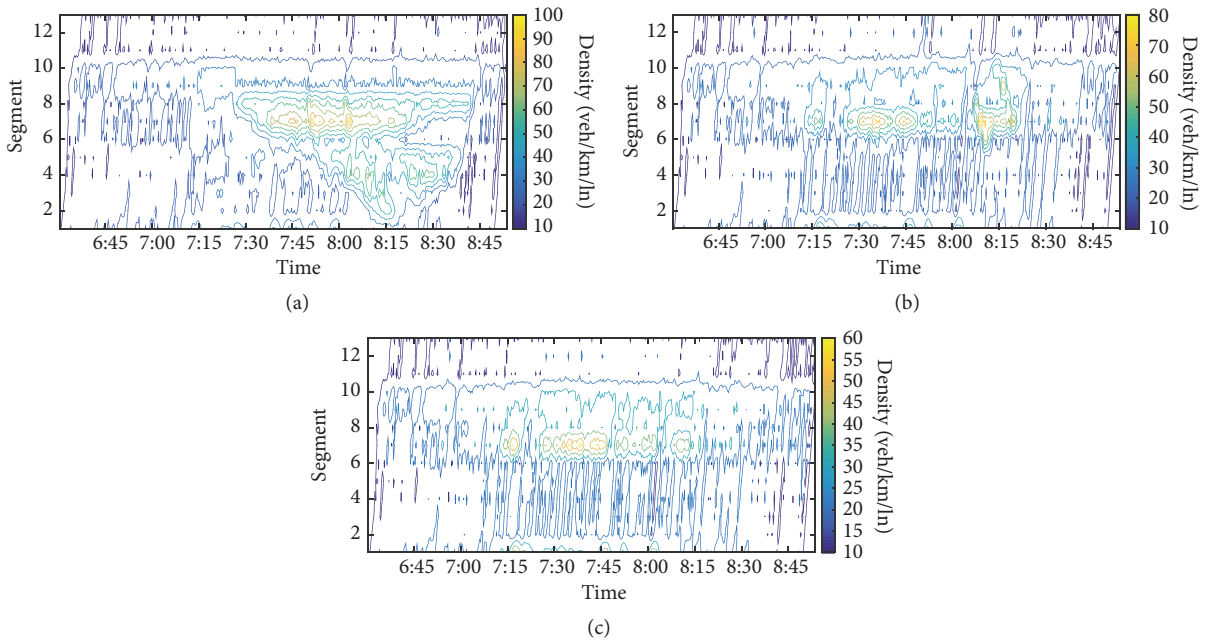

Figure 9: Comparison of segment densities of No-VSL, basic, and modified METANET-VSL controls: (a) no-VSL control; (b) basic METANET model; (c) modified METANET model.

by the deployed VSL control strategy, especially in the two identified bottlenecks (segment L_4 and L_8). From 8:00 to 8:15 am, the density of segment L_8 has been maintained at approximately 70 veh/km/ln for basic METANET model control and around 40 veh/km/ln for proposed modified METANET VSL control.

By capturing the variations of the speed dynamics, the METANET-model activated the VSL to prevent capacity drop and relieve traffic congestion. Taking Segment L_8 as an example, under modified-METANET control, comparison between the speed limit and the actual speed was shown in Figure 10. Before 6:50 am, the modified-METANET VSL control was not activated since the traffic congestion did not emerge before 7:00 am. Before that congestion, the modified-METANET model had predicted the speed drop and lowered the speed limit in advance. As a result, the modified-METANET model improved the minimum segment speed to approximately 40km/h and shortened the congestion duration. After the congestion relieved, the speed limit recovered gradually.

5. Conclusions

This paper proposed a modified METANET model that utilizes the microscopic traffic-flow data. A MPC framework-based control strategy incorporates the proposed modified

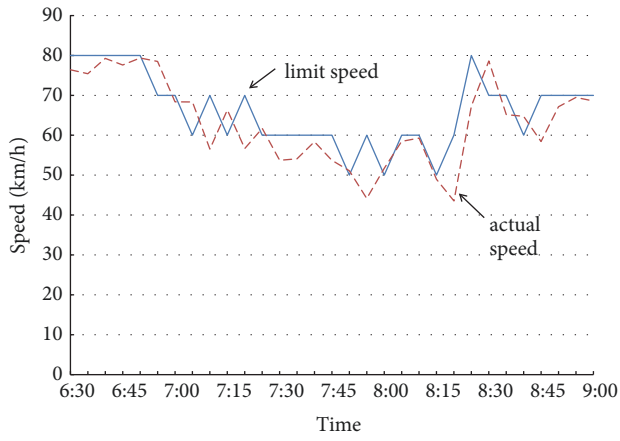

Figure 10: Comparison between limit speed and actual speed under modified METANET control.

model was established to capture the variations of traffic flow dynamics, which enables the VSL control to prevent dramatic decline of link speed beforehand and gains improvement on the freeway mobility performance.

The proposed formulation of the anticipation term in the modified METANET model is more reasonable and comprehensive. The proposed modification takes in the microscopic traffic-flow data, such as individual vehicle headway and accelerations, to better interpreted the progress of drivers adjusting toward the anticipated speed. The proposed modified model can produce more accurate prediction results, which provides a more reliable basis for achieving further improvement in VSL control applications. The modified METANET model has reduced the prediction error by up to 14.9% and 14.1% for the low and high-density ranges, respectively.

As a result, traffic mobility was substantially improved along with the reduced prediction error. The VISSIM software was used to establish a field data based experimental simulation platform for model validations. To evaluate the control benefits, the traffic-flow states of the modified METANET-based VSL control strategy were compared with those of the No-VSL control and basic METANET-based VSL controlled scenario. The modified METANET model has achieved substantial improvements in terms of mobility performance. The simulation results demonstrated that the modified METANET model reduced segment density, increased segment speed, and shortened the congestion period, indicates the improved freeway mobility. More initiatives to aid the speed prediction of the model should continue to be explored in the future.

Data Availability

The data used to support the findings of this study may be released upon application to the authors, who can be contacted at fangjie@fzu.edu.cn.

Conflicts of Interest

The authors declare that they have no conflicts of interest.

References

[1] H. Dai, E. Yao, N. Lu et al., "Freeway network connective reliability analysis based complex network approach," *Procedia Engineering*, vol. 137, pp. 372–381, 2016.

[2] N. Cui, B. Chen, K. Zhang, Y. Zhang, X. Liu, and J. Zhou, "Effects of route guidance strategies on traffic emissions in intelligent transportation systems," *Physica A: Statistical Mechanics and its Applications*, vol. 513, pp. 32–44, 2019.

[3] Y. E. Hawas, G. Thandavarayan, B. Basheerudeen, and M. Sherif, "Testbed evaluation of real-time route guidance in inter-vehicular communication urban networks," *IEEE Access*, vol. 7, pp. 1470–1485, 2019.

[4] A. Janota, P. Holečko, M. Gregor, and M. Hruboš, "Ramp-metering algorithms evaluated within simplified conditions," *Journal of Civil & Environmental Engineering*, vol. 13, no. 2, pp. 112–119, 2017.

[5] Y. Li, N. Duan, and X. Yang, "Analysis balance parameter of optimal ramp metering," *IOP Conference Series: Materials Science and Engineering*, vol. 359, no. 1, article 012007, 2018.

[6] M. Papageorgiou, E. Kosmatopoulos, and I. Papamichail, "Effects of variable speed limits on motorway traffic flow," *Transportation Research Record*, no. 2047, pp. 37–48, 2008.

[7] R. Jiang, A. B. Lucky, and E. Chung, "Calibration and operational analysis of variable speed limits for high flow conditions," in *Proceedings of the IEEE Forum on Integrated and Sustainable Transportation Systems, FISTS '11*, pp. 221–226, 2011.

[8] M. Islam, M. Hadiuzzaman, J. Fang, T. Qiu, and K. El-Basyouny, "Assessing mobility and safety impacts of a variable speed limit control strategy," *Transportation Research Record*, vol. 2364, pp. 1–11, 2013.

[9] Z. Xu, T. Wei, S. Easa, X. Zhao, and X. Qu, "Modeling relationship between truck fuel consumption and driving behavior using data from internet of vehicles," *Computer-Aided Civil and Infrastructure Engineering*, vol. 33, no. 3, pp. 209–219, 2018.

[10] M. Papageorgiou, J.-M. Blosseville, and H. Hadj-Salem, "Modelling and real-time control of traffic flow on the southern part of boulevard peripherique in Paris: Part I: modelling," *Transportation Research Part A: General*, vol. 24, no. 5, pp. 345–359, 1990.

[11] C. Lee, B. Hellinga, and F. Saccomanno, "Real-time crash prediction model for application to crash prevention in freeway traffic," *Transportation Research Record: Journal of the Transportation Research Board*, no. 1840, pp. 67–77, 2003.

[12] C. Lee, B. Hellinga, and F. Saccomanno, "Evaluation of variable speed limits to improve traffic safety," *Transportation Research Part C: Emerging Technologies*, vol. 14, no. 3, pp. 213–228, 2006.

[13] R. C. Carlson, I. Papamichail, and M. Papageorgiou, "Local feedback-based mainstream traffic flow control on motorways using variable speed limits," *IEEE Transactions on Intelligent Transportation Systems*, vol. 12, no. 4, pp. 1261–1276, 2011.

[14] R. C. Carlson, I. Papamichail, and M. Papageorgiou, "Comparison of local feedback controllers for the mainstream traffic flow on freeways using variable speed limits," *Journal of Intelligent Transportation Systems: Technology, Planning, and Operations*, vol. 17, no. 4, pp. 268–281, 2013.

[15] G.-R. Iordanidou, I. Papamichail, C. Roncoli, and M. Papageorgiou, "A feedback-based approach for mainstream traffic flow control of multiple bottlenecks on motorways," *IFAC Proceedings Volumes*, vol. 47, no. 3, pp. 11344–11349, 2014.

[16] G.-R. Iordanidou, C. Roncoli, I. Papamichail, and M. Papageorgiou, "Feedback-based mainstream traffic flow control for

multiple bottlenecks on motorways," *IEEE Transactions on Intelligent Transportation Systems*, vol. 16, no. 2, pp. 610–621, 2015.

[17] M. Burger, M. Van Den Berg, A. Hegyi, B. De Schutter, and J. Hellendoorn, "Considerations for model-based traffic control," *Transportation Research Part C: Emerging Technologies*, vol. 35, pp. 1–19, 2013.

[18] B. Khondaker and L. Kattan, "Variable speed limit: a microscopic analysis in a connected vehicle environment," *Transportation Research Part C: Emerging Technologies*, vol. 58, pp. 146–159, 2015.

[19] J. Zhang, A. Boitor, and P. Ioannou, "Design and evaluation of a roadway controller for freeway traffic," in *Proceedings of the 8th International IEEE Conference on Intelligent Transportation Systems '05*, pp. 543–548, IEEE, 2005.

[20] S. K. Zegeye, B. De Schutter, H. Hellendoorn, and E. Breunesse, "Reduction of travel times and traffic emissions using model predictive control," in *Proceedings of the 2009 American Control Conference, ACC '09*, pp. 5392–5397, IEEE, 2009.

[21] A. H. Ghods, L. Fu, and A. Rahimi-Kian, "An efficient optimization approach to real-time coordinated and integrated freeway traffic control," *IEEE Transactions on Intelligent Transportation Systems*, vol. 11, no. 4, pp. 873–884, 2010.

[22] C. F. Daganzo, "The cell transmission model: a dynamic representation of highway traffic consistent with the hydrodynamic theory," *Transportation Research Part B: Methodological*, vol. 28, no. 4, pp. 269–287, 1994.

[23] M. Hadiuzzaman, T. Z. Qiu, and X.-Y. Lu, "Variable speed limit control design for relieving congestion caused by active bottlenecks," *Journal of Transportation Engineering*, vol. 139, no. 4, pp. 358–370, 2012.

[24] M. Hadiuzzaman and T. Z. Qiu, "Cell transmission model based variable speed limit control for freeways," *Canadian Journal of Civil Engineering*, vol. 40, no. 1, pp. 46–56, 2013.

[25] Y. Han, A. Hegyi, Y. Yuan, S. Hoogendoorn, M. Papageorgiou, and C. Roncoli, "Resolving freeway jam waves by discrete first-order model-based predictive control of variable speed limits," *Transportation Research Part C: Emerging Technologies*, vol. 77, pp. 405–420, 2017.

[26] A. Muralidharan and R. Horowitz, "Computationally efficient model predictive control of freeway networks," *Transportation Research Part C: Emerging Technologies*, vol. 58, pp. 532–553, 2015.

[27] A. Hegyi, *Model Predictive Control for Integrating Traffic Control Measures*, TRAIL Research School, Netherlands, 2004.

[28] A. Hegyi, B. de Schutter, and J. Hellendoorn, "Optimal coordination of variable speed limits to suppress shock waves," *IEEE Transactions on Intelligent Transportation Systems*, vol. 6, no. 1, pp. 102–112, 2005.

[29] A. Hegyi, B. De Schutter, and H. Hellendoorn, "Model predictive control for optimal coordination of ramp metering and variable speed limits," *Transportation Research Part C: Emerging Technologies*, vol. 13, no. 3, pp. 185–209, 2005.

[30] R. C. Carlson, I. Papamichail, M. Papageorgiou, and A. Messmer, "Optimal motorway traffic flow control involving variable speed limits and ramp metering," *Transportation Science*, vol. 44, no. 2, pp. 238–253, 2010.

[31] R. Sun, J. Hu, X. Xie, and Z. Zhang, "Variable speed limit design to relieve traffic congestion based on cooperative vehicle infrastructure system," *Procedia: Social and Behavioral Sciences*, vol. 138, pp. 427–438, 2014.

[32] R. Yu and M. Abdel-Aty, "An optimal variable speed limits system to ameliorate traffic safety risk," *Transportation Research Part C: Emerging Technologies*, vol. 46, pp. 235–246, 2014.

[33] J. Cao, D. Hu, Y. Luo, T. Z. Qiu, and Z. Ma, "Exploring the impact of a coordinated variable speed limit control on congestion distribution in freeway," *Journal of Traffic and Transportation Engineering*, vol. 2, no. 3, pp. 167–178, 2015.

Hindawi
Journal of Advanced Transportation
Volume 2018, Article ID 4251701, 10 pages
https://doi.org/10.1155/2018/4251701

Research Article

Context-Aware Intelligent Traffic Light Control through Secure Messaging

Mükremin Özkul,[1] **Ilir Capuni**,[2] **and Elton Domnori**[1]

[1]*Department of Computer Engineering, Epoka University, Tirana 1039, Albania*
[2]*Advanced Computing Research Center, University of New York Tirana, Tirana 1000, Albania*

Correspondence should be addressed to Mükremin Özkul; mozkul@epoka.edu.al

Received 29 May 2018; Revised 28 September 2018; Accepted 22 October 2018; Published 5 November 2018

Guest Editor: Jackeline Rios-Torres

In this paper, we propose STCM, a context-aware secure traffic control model to manage competing traffic flows at a given intersection by using secure messages with real-time traffic information. The vehicle is modeled as a virtual sensor which reports the traffic state, such as its speed and location, to a traffic light controller through a secure and computationally lightweight protocol. During the reporting process, a vehicle's identity and location are kept anonymous to any other vehicle in the system. At an intersection, the traffic light controller receives the messages with traffic information, verifies the identities of the vehicles, and dynamically implements and optimizes the traffic light phases in real-time. Moreover, the system is able to detect the presence of emergency vehicles (such as ambulances and fire fighting trucks) in the communication range and prioritize the intersection crossing of such vehicles to in order to minimize their waiting times. The simulation results demonstrate that the system significantly reduces the waiting time of the vehicles in both light and heavy traffic flows compared to the pretimed signal control and the adaptive Webster's method. Simulation results also yield effective robustness against impersonating attacks from malicious vehicles.

1. Introduction

With the increase in the number of vehicles on roads, traffic congestion is becoming a serious problem in urban areas as it increases travel times and fuel consumption [1]. Traffic light control systems manage incompatible traffic flows by restricting the free flow of the traffic using distinct time intervals or phases at road intersections and at pedestrian crossings. Besides ensuring the safe crossing of traffic, traffic signal control systems try to reduce the waiting times of vehicles at an intersection by appropriately adjusting the timing of the light sequences.

Traditional traffic light control systems use fixed-cycles that are computed as an approximation of the traffic flow based on the historical traffic flow data at an intersection. Such a pattern is followed regardless of the real-time traffic state throughout the day. On the other hand, an adaptive light control system uses the real-time traffic data coming from fixed roadside sensors, such as loop detectors or video cameras, and adopts traffic light timings continuously based on real-time traffic information.

Recently, vehicular mobile wireless ad hoc networks (VANETs) have been a primary focus of study to develop applications that would increase the road safety and the efficiency of traffic flows. In this context, significant research of VANETs has been carried out where vehicles are used as sensor nodes to create intelligent traffic light systems (ITL).

An ITL dynamically changes the traffic light timings based on the traffic information gathered from the vehicles in the VANETs. The traffic along routes with higher vehicle density are prioritized with longer green light timing compared to other routes.

In this collaborative system, the correctness of claimed identity (i.e., the characteristics of the vehicle) and location information is an important issue since it affects the functionality of the scheduling algorithm.

In the literature, existing ITL control systems ignore security control mechanisms assuming that data coming from the vehicles (such as identity, location, and other reported information) are authentic and reliable. However, a vehicle can try to cheat or deceive the control system by broadcasting false traffic information or pretending to be

multiple vehicles in order to increase the apparent number of vehicles observed by the ITL. In this way, the vehicle receives an increased portion of the green light timing. A further weakness in ITL control systems is that private data may be exposed by each vehicle's identity and made publicly available during information dissemination.

Our goal is to design an ITL control system which reduces the time required to cross an intersection and is able to prioritize the movement of emergency vehicles at given intersections without compromising the privacy of the participants.

To achieve this goal, we are aiming to achieve the following properties.

(1) **Security:** the system must be robust against attacks from malicious participants; i.e., a vehicle should not be able to manipulate the decisions of the traffic controller on the light timings and sequences or to claim multiple identities.

(2) **Privacy:** the anonymity of a vehicle should be preserved at all times. The identity of the vehicle v and its related information such as location and speed should be known only to a trusted authority.

(3) **Veracity:** the authenticity and integrity of the messages sent by a vehicle should easily be verified by a trusted authority with a computationally efficient and lightweight protocol.

(4) **Efficiency:** the system adapts promptly to real-time changes in the state of the traffic and minimizes the waiting time that vehicles spend at an intersection.

(5) **Scalability:** the system should scale regardless of the increase in the number of vehicles at an intersection.

2. Related Work

In a fixed-timing traffic light control system, a precalculated pattern is periodically repeated based on the historical traffic data. These systems do not operate in real-time and are only efficient when the traffic flow is stable and regular at the intersection during the day. However, there are several circumstances that may alter the traffic state such as accidents or maintenance work on specific roads. As a result, a prefixed control system is not able to respond to the traffic demand in real-time.

Traffic light control systems have been widely studied in the literature and adopted in practice. One approach is to use physical sensors and devices (e.g., loop detectors, video cameras with content-analysis capabilities, and wireless sensors) to detect the presence of and to classify the vehicles [2] in order to forecast vehicle density at an intersection. Using this approach [3, 4], the traffic light controller optimizes the phase timings based on the real-time inputs coming from the loop detectors installed in the proximity of or immediately before the stop line for the intersection. Loop detectors detect the presence of and count the number of vehicles that pass over them. Data collected in real-time are sent to the light controller which adjusts the traffic cycles based on the vehicle density at an intersection.

Even though an adaptive system reduces the waiting time of vehicles compared to a fixed time control, the infrastructure used in the systems entails high installation, maintenance, and operational costs and needs frequent human intervention. Moreover, loop detectors are not reliable under adverse weather conditions (e.g., the performance of the video cameras is reduced in rainy or foggy conditions or at night since visual contact with vehicles is restricted), they are ineffective in oversaturated traffic conditions (e.g., whenever the vehicle queue grows beyond the installed infrastructure), and they are not able to detect the passage of emergency vehicles approaching an intersection.

Due to the drawbacks in using road sensors, recently, vehicle actuated systems have been introduced to develop intelligent traffic lights using wireless communications. In such systems, vehicles play a crucial role in the decision-making process as they become the source of information. Through vehicular ad hoc networks (VANET), vehicles share traffic information with each other or with roadside units (RSUs) within their transmission range using Dedicated Short-Range Communications (DSRC). A vehicle, acting as a virtual sensor, is equipped with an on-board unit and periodically sends messages including the vehicle's ID, current speed, and location. Such information can be sent exclusively to the roadside unit through a vehicle-to-infrastructure (V2I) communication as in [5] or such messages may be shared with other vehicles through a vehicle-to-vehicle (V2V) communication, as proposed in [6], before they reach the roadside unit.

The roadside unit continuously collects the data and by using dynamic programming, an optimal light phase sequence is determined to reduce the total queue length at the intersection. To optimize the computation several approaches have been proposed. In [7], the authors proposed a model in which speed and position data are gathered from the vehicles' broadcast messages and used to divide the traffic into vehicle *platoons*; each platoon is then treated separately to optimize the traffic flow. Recently, in [8], a virtual *wait area* in front of the road intersection is defined for each traffic flow and the vehicles inside this area are considered ready to cross the intersection. Each vehicle uses multihop communications and advertises itself within the transmission range by broadcasting a message. The size of the vehicle queue in each wait area is computed using the broadcast data of the vehicles.

Roadside units might not be available at every intersection, especially in rural areas, raising the need for a self-coordination process among vehicles. The issue has been discussed for the first time in [9], proposing an adaptive traffic signal system based on car-to-car communication and the creation a virtual traffic light (VTL) controller. The advantage of the VTLs on the other intelligent systems is that they do not require the installation and maintenance costs of permanent infrastructure. The vehicles autonomously elect a leader vehicle which coordinates the traffic lights at the intersection. The coordinator election in a VTL has been discussed in [10] and an optimized distributed algorithm has been proposed in [11].

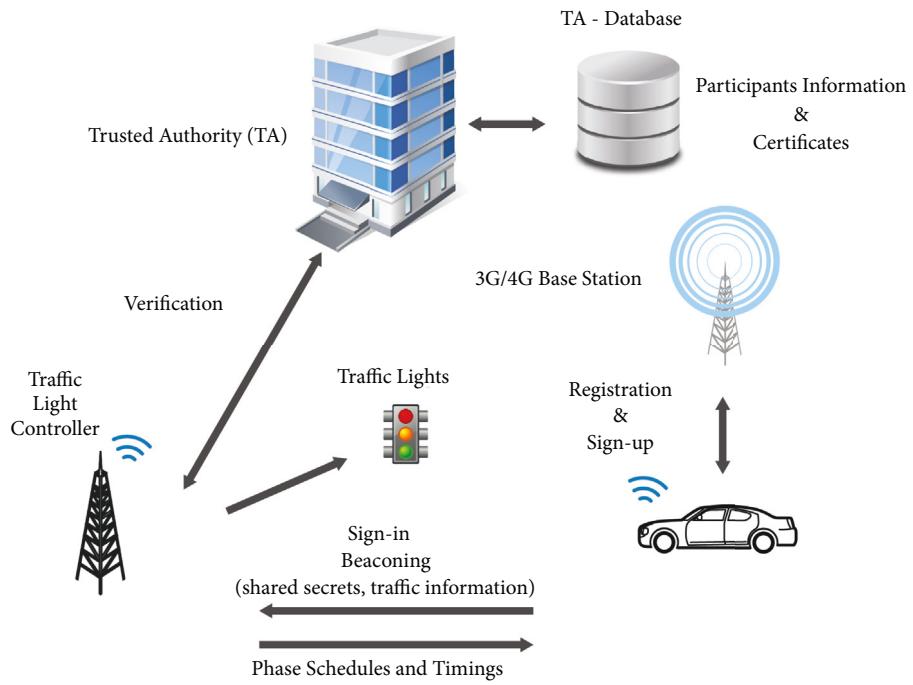

Figure 1: The system architecture with communication protocol.

The use of VTL becomes problematic once the number of vehicles increases over a certain threshold. The system approaches a lack of scalability by facing two issues: (a) the election process for the coordinator could be problematic in VTLs showing poor performances (as discussed in [12]) and (b) the coordinator should afford all the computation required to collect the data, take a decision, and forward it to the other vehicles in the network.

The involvement of vehicles in the decision process, beside computation, has raised another issue: that of the reliability of the data they share. Adversary vehicles can collude to get a higher priority and time to cross through an intersection. Although the proposed intelligent controls in [7, 9–11] are more efficient in terms of reducing vehicle delay times and increasing traffic flow than the prefixed controls and actuated systems, the security issues of the models are not addressed at all. The aforementioned intelligent traffic systems operate under the assumption that data from participating vehicles is fully accurate; i.e., that all identity and location reports from the vehicles are veracious. However, a malicious vehicle can try to cheat a traffic light control by simply broadcasting a bogus identity, e.g., impersonating an emergency vehicle or pretending to be multiple vehicles by replaying the messages of other vehicles to increase the green time allotted to the cheating vehicle's road section. Therefore, an accurate and reliable method of real-time information verification is a key aspect in implementing an efficient and intelligent traffic light controller.

Recently, several secure message delivery protocols for VANETs have been proposed. In [13], the authors propose a privacy-preserving framework for continuous tracking and verification of the vehicles using a computationally lightweight cryptography. In the model, each vehicle announces its location periodically through anonymous beacons to the nearby vehicles, which collect and report the received beacons to a location authority. The location authority processes the reported beacons to verify and infer the positions of the vehicles. In our system, information about location is not saved by the transportation authority. In the VANETs, anonymous authentication schemes to verify the authenticity of vehicles as presented in [14, 15] are a well-adapted method that avoids revealing real identities by using multiple certificates and pseudo identities.

To address these problems, we propose a traffic light control system using secure messages of vehicles in VANET. A vehicle only sends anonymous messages to announce its presence to a traffic controller in a way that the movements of a vehicle are not tractable and the real identity is hidden from the vehicles. The reliable messages obtained from the vehicles provide the basis of efficient light timing for a traffic controller.

3. System Layout

In this section we outline the system and the notation that will be employed during the analysis and implementation.

The system architecture and the communication protocol are represented as seen in Figure 1. The system consists of a trusted authority (TA) which maintains a database of registered vehicles and communicates with the vehicles via a 3G/4G network and Traffic Light Controllers (TLC) installed at road intersections. Once a vehicle starts, it needs to go through a sign-up process with the TA. Once this phase is completed, the vehicles mostly communicate with the TLCs.

TLCs do not communicate with each other; hence they do not share information (except with the TA). This

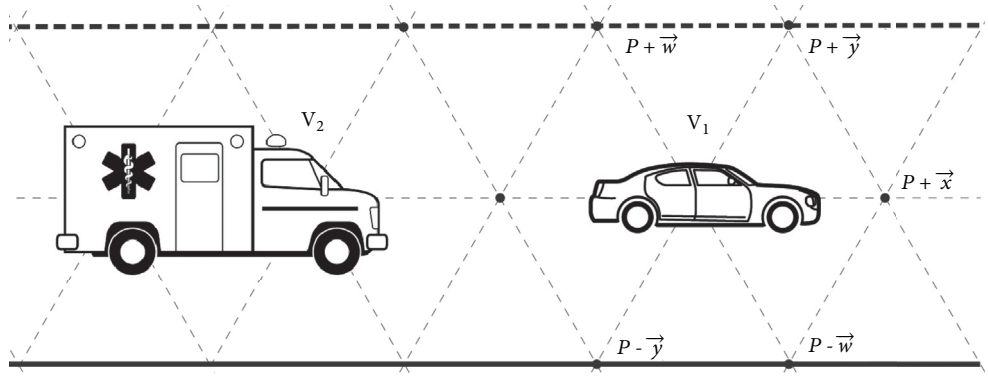

Figure 2: The grid system. V_1 shows a standard vehicle located in a single site P and V_2 shows a longer vehicle, an ambulance, modeled by using two adjacent sites.

communication strategy preserves the private information of each participant, both their true identity and location at each instant of time.

We will use a two-dimensional triangular grid with a fixed coordinate system as shown in Figure 2. This model is introduced in [16]. Each point $\overrightarrow{p} = (x, y)$ of this system is called a *site* and may contain at most one object. A vehicle is an object of specific kind; it is an automaton which is self-propelled. As an automaton, its state information includes data such as the unique ID given by the trusted authority, current location, speed obtained by the on-board units, time, its vehicle category, etc. Each vehicle is equipped with a wireless communication unit (such as Dedicated Short-Range Communications (DSRC) and a temper proof Global Positioning System receiver (GPS)) and has 3G/4G capability. The vehicles can move to one of the six neighboring sites and can change and update their state by applying a rule from the rule set. The *movable set* M_v of a vehicle v contains the set of neighboring empty sites in the direction of the traffic flow where a vehicle can go in the next update. An empty movable set M_v of a vehicle v means that v cannot apply movement rules.

A list of consecutive sites between grid boundaries with the same movement direction is called a *lane*, and a set of neighboring lanes (facing independent directions) is called a *road*.

A road *intersection* I is a set of sites which connects the lanes with different traffic directions. The set of inbound lanes in an intersection I define the incoming traffic flow, and the set of outbound lanes define the outgoing traffic flow.

The traffic controller manages the traffic flow into and through the intersection by updating the rules to each traffic flow using time intervals. The sets of these rules are called *phases*. These rules define the movable sets which were mentioned above. In a *red phase*, a vehicle has an empty M_v, whereas a *green phase* results in a nonempty M_v.

Phases allow at most two flows to proceed simultaneously into and through the intersection without conflicting with each other. The resulting decisions made by TLC are displayed by the classical traffic lights.

Let P_{ij} be a pair of unconflicting flows i and j, where $i, j \in \{1, 2, \ldots, 8\}$, as seen in Figure 3(a). During an active phase, flows are allowed to cross the intersection transition to the next phase in the sequence. From this time the controller restarts the phase sequence, which is called a *traffic light cycle* configuration $C_t = \{P_{15}, P_{26}, P_{37}, P_{48}\}$, at time t, as follows:

$$\mathscr{P}_{15} \longrightarrow \mathscr{P}_{26} \longrightarrow \mathscr{P}_{37} \longrightarrow \mathscr{P}_{48}. \quad (1)$$

Note that a light cycle is flexible in the sense that there are no constraints on the phase sequences and timings or the time intervals between the phases. The controller can reorder the current phase C_t at an emergency event or use a different phase sequence on the next cycle C_{t+1}.

3.1. Encoded Data. Initially, a vehicle is registered to the trusted authority (TA), which manages the sign-in process, distributes digital certificates and a set of pseudo IDs to the vehicles, keeps the identity information of the vehicles in its database, and is totally trusted by all the vehicles.

When a vehicle starts, it initiates communication using traffic controllers or through the cellular network and establishes a symmetric key with the TA. First, a vehicle v sends a registration request at time t^0 to the TA which verifies the identity, id of v, and returns the triplet $(K_v; r_v; o_v)$ to the vehicle, where K_v is a short-term symmetric key, and r_v and o_v are two random integers. Both parties initialize a counter n to the value r_v and increment it by o_v at every message sent by v. A time dependent secret $s_v(t)$ serves for the TA to verify the identity of the vehicle v and the integrity of the messages it sends. The secret is computed and encrypted as follows.

First,

$$s_v(t) = E_{K_v}\{r_v + no_v\}. \quad (2)$$

Then at every τ_b seconds, the vehicle periodically broadcasts a beacon in which it sends location and speed to TLCs in the communication range through the wireless IEEE 802.11p standard. The beacon message is calculated as follows:

$$\mathscr{B} = \left\langle E_{K_v}\{(l \parallel s) \oplus s_v(t)\}, t_{stamp}, \sigma \right\rangle \quad (3)$$

where l is the location of the vehicle on the grid system, s is the vehicle speed which is appended to the location information, and both l and s are XOR'ed with the encoded data $s_v(t)$, t_{stamp} is used to prevent a message replay attack, and the σ is the beacon digest obtained by using a hash function, e.g., SHA-1.

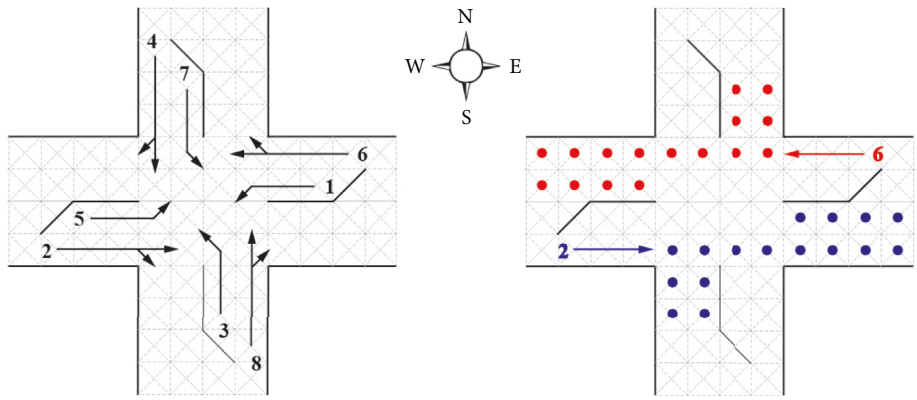

FIGURE 3: (a) Traffic flows at the intersection. (b) The sites with dots show the movable set for the phase sequence P_{26}.

4. Traffic Light Controller

In the system, the vehicles act like virtual sensors and perform the task of reporting the traffic information to a traffic controller in the communication range.

The traffic controller is physically centered at the intersection and has access to the TA database. It receives beacons from the vehicles to detect their presence, determine their location and speed, and monitor the traffic state in real-time. Whenever a beacon is received, it must be verified for veracity. For each message b received, the traffic controller determines the vehicle v which the message belongs to as follows:

(1) Define t_{beacon} the time the beacon b is received.

(2) For each $w \in \mathcal{S}$, where $\mathcal{S}$ is the set of vehicles to be verified, compute

$$i = \left\lfloor \frac{t_{beacon} - t_w^0}{\tau_b} \right\rfloor, \tag{4}$$

where i represents the index of the precomputed encoded data value and t_w^0 represents the time when TA has received the sign-up request from the vehicle w.

(3) It retrieves the secret value x_w^i that matches x_v^i.

If there is a match, the traffic controller identifies v to be the vehicle that has sent the beacon and includes the vehicle in the set of authenticated vehicles $\mathcal{V}$ which are in the vehicle queue to cross the intersection.

4.1. Phase Scheduling. The traffic controller dynamically executes the phase sequence according to assigned priority to each direction or skips a green phase as necessary, e.g., in the case of prioritizing the passage of emergency vehicles. Valid beacons allow the traffic controller to define the traffic state at a time t, such that the traffic controller has the exact number of waiting vehicles, the length of vehicle queues, the types of vehicles, and the vehicular density in a traffic flow on each road section.

When all phases of a current cycle are executed, the traffic controller computes the new phase timings to each flow as follows:

$$T_{phase} = n_l + \frac{c \cdot t_c}{s} \tag{5}$$

where n_l is a time constant used to compensate vehicle stop-and-go movements caused by the phase changes, c is the number of sites occupied with vehicles, t_c is the time per vehicle to enter the intersection, and s is the mean speed on the road.

The phase timings are granted to each traffic flow based on of the number of vehicles at the road intersection, therefore assigning more phase timing to traffic flow with a higher density. To prevent vehicles waiting very long in traffic flow with low density an upper time limit t_{max} is set for each phase timing.

A phase to traffic flow can be skipped in the next cycle if there is no vehicle within the communication distance. Priority of the traffic flows is also defined at this stage. Whenever an emergency vehicle is detected, the respective traffic flow is given highest priority to cross independent of the present traffic state at the intersection.

Then, the traffic controller periodically broadcasts the phase timing information (every 1 second), which also includes information about the time remaining for the current phase, the phase sequence, and times through beacons at the intersection.

4.2. Emergency and Public Transport. Emergency vehicles need to reach their destination as quickly as possible. Therefore, they need to be given higher priority at an intersection. Such vehicles warn and announce their presence to the others with visual and sound alarms in the neighborhood, so that a nonemergency vehicle is to yield and allow the emergency vehicle to pass through the intersection.

Even though vehicles should always respond in a timely way to the alarms and give the right of way to emergency vehicles, sometimes careless drivers may miss or ignore the alarm, hence causing delays to response times of emergency vehicles. In our model, an emergency vehicle approaching the

intersection is identified by the beacons it broadcasts, after which the active phase is interrupted if necessary or the phase time is extended to provide the safe passage of the emergency vehicle without any significant delay.

First, a priority index k = (0-highest, 1-high, 2-normal, 3-low, 4-lowest) is set in the traffic rule set to detect the emergency vehicles approaching the intersection. The emergency vehicles have the highest priority, while a nonemergency vehicle such as a truck has the lowest priority. A further classification of the vehicles can be defined into several different categories; e.g., medical, police and security, fire, and rescue, as in the work [17], depending on their importance. If an emergency vehicle is detected in the traffic flow served by the current green phase, the controller simply extends the phase time until the vehicle passes through the intersection in a way that creates a green wave effect for the quick passage of the vehicle to its destination. For the cases in which the vehicle is present in a flow other than the served green phase, the current phase is interrupted and the green phase is granted to the flow where the vehicle is approaching. Finally, the phase sequence is restored to its initial configuration before the emergency event.

The traffic controller virtually extends the phase time for vehicles such as buses or taxis used in the public transportation structure. Here, depending on the size of the vehicle and the time of the day, the traffic controller doubles or triples the time assigned per vehicle.

5. Security and Privacy Analysis

In this section, we analyze the security aspect of the traffic light control system. We pay particular attention to message alteration, replay attacks, and identity impersonation of a vehicle.

5.1. Message Alteration. In the system, a vehicle cannot claim to be another vehicle, since at the initial sign-up the TA requires a valid digital certificate. Therefore, a vehicle cannot deny having sent a beacon because a verifiable signature guarantees the beacon's integrity. Furthermore, the identity of a vehicle and its report is verified with the encoded, s_v, data upon receiving the reports.

In a message alteration attack, an adversary tries to change or modify the information in a beacon of its neighbors. However, a beacon at time t always includes the encoded data to TA, and the identity of a vehicle is verified with the encoded data s_v upon receiving the beacon by the traffic controller. Since only the vehicle v can create the valid encoded data s_v at the time t, a trusted authority can verify the validity and integrity of the information in the beacon.

5.2. Replay Attacks. In this attack, an adversary vehicle uses and replays the beacons which are sent by its neighbors at an earlier time. It then tries to increase the number of vehicles in the traffic flow or impersonates an emergency vehicle to have priority crossing.

However, the traffic controller first determines the time the encoded data is generated and compares with the t_{stamp} of the received beacon.

If the time is outside the allowable time interval of τ_b, an adversary replays a beacon it recorded at an earlier time, validation of the t_{stamp} will fail, and the beacon will be treated as old and and then simply discarded.

In a case for which a beacon is successfully replayed in the window of τ_b, only the first valid beacon is processed and the others are dropped without processing. Moreover, each beacon has a different time dependent secret of s_v for two consecutive time instants t and $t + 1$. If the same encoded data were detected, the time registered would not match. Therefore, the code contained in the beacon along with the t_{stamp} guarantees the freshness of the beacon. Thus, the system is secure against any replay attack.

5.3. Sybil Attacks. In Sybil [18] attacks, an adversary vehicle claims multiple identities and impersonates another. Recall that the decision of the traffic light controller is based on the numbers and the types of vehicles gained, from the broadcast beacons of the vehicles. Therefore, a dishonest vehicle may present multiple identities with the intent of increasing the number of vehicles at an intersection. At the sign-in, each vehicle receives a set of pseudo IDs and a symmetric key by trusted authority using a valid digital certificate. For this type of attack to succeed, a vehicle must obtain a number of valid certificates of other vehicles or fabricate a valid certificate which is virtually impossible with the use of digital signature certificates. This attack only is effective when the security of the TA is compromised.

A vehicle must obtain a number valid of certificates of other vehicles as fabricating a valid certificate or a pseudonym is not possible with public-key-based digital signatures. An adversary vehicle is not able to use multiple identities at once.

5.4. Privacy. Pseudonym changing techniques are the main solution adopted to provide privacy and anonymity in VANETs. In the system, each vehicle is assigned multiple certificates with pseudo identities by the TA. At the initial sign-in phase a vehicle's certificate is verified, and then a symmetric key is established with the TA and the vehicle. Then, instead of using one fixed certificate, each message is signed using pseudonym certificates by the vehicle.

6. Simulation

In this section, the performance of our proposed system is evaluated against the prefixed time and actuated Webster's traffic control in terms of average vehicle waiting times. Then, the system security is tested under the influence of adversary vehicles which broadcast bogus beacons or impersonate truthful vehicles by simply replaying their beacons.

6.1. Simulation Settings. Our proposal is evaluated through OMNET++ wireless simulator, a discrete-event network simulator based on C++ [19], and Simulation of Urban Mobility (SUMO) [20], a realistic open source traffic simulator for vehicular traffic. SUMO generates the vehicular traffic and is used to obtain the traffic information, including speed and location, from the vehicles. OMNET++ implements a framework for simulating wireless communications and uses

Table 1: The simulation parameters for waiting times.

Parameter	Value
Number of vehicles per two-lane road	500 - 1800 per hour
Beacon transmission rate	1 x per second
Transmission range	$\cong 200m.$
Road length	100 sites at each approach
Simulation duration	70 min.

the IEEE 802.11p protocol stack at both the physical and Media Access Control (MAC) protocol layers. VEINS [21] is a framework for vehicular network simulations, which through TraCI [22] serves as an interface between SUMO and OMNET++ and maps the vehicles as a mobile network node in OMNET++.

The prefixed time control is set to have 45 seconds of green time and 3 seconds offset for the phase changes. Webster's equation is used to compute the optimal cycle time C_o which minimizes vehicle delays at an intersection for the adaptive traffic lights control and is defined as follows:

$$C_o = \frac{1.5L + 5}{1 - \sum Y_i} \tag{6}$$

where Y_i is the ratio of an upstream flow rate to the saturation flow at the same approach for the phase i and L is unusable offset times per cycle including all-red periods. Here, the green phase is given time in proportion to the degree of the saturation on its approach.

The main simulation parameters are summarized in Table 1.

The simulation map is based on a four-leg road intersection. At the intersection, a roadside unit is positioned, receives the traffic information from the vehicles, and broadcasts the cycle information to the vehicles. All the roads have two lanes in the same traffic direction and have a total length of 1 km upstream and downstream of the intersection.

At each road, the maximum speed limit is set to 40 km/h. A random distribution of the speed is specified for the vehicles between the range 25 km/h to 40 km/h. The typical passenger car length is equal to 5 m., and intervehicle distance at full stop is set to 2.5 m. The vehicles periodically broadcast beacons at intervals of 1 second whereas a RSU is set to broadcast at an interval of 1 second for dissemination of phase timings at the intersection.

6.2. System Performance. In the simulation, several vehicle densities are used to evaluate the effects of density over the vehicle waiting times at the intersection. First, the traffic flow is set to a constant 600 vehicles/hour for the north-south flow, defined as the $\mathscr{P}_{48}$, while east-west traffic flow density is varied from light to high density levels several times during the simulation. The east-west flow has four different vehicle density rates, 500, 800, 1000, and 1400 v/h (vehicles/hour), defined as the $\mathscr{P}_{26}$, which is considered to be light and medium vehicle density levels. The simulation starts with the 500 v/h east-west vehicle density and then is switched to the next level at 10 min. intervals, and then from the peak density level it reverts to the initial light density

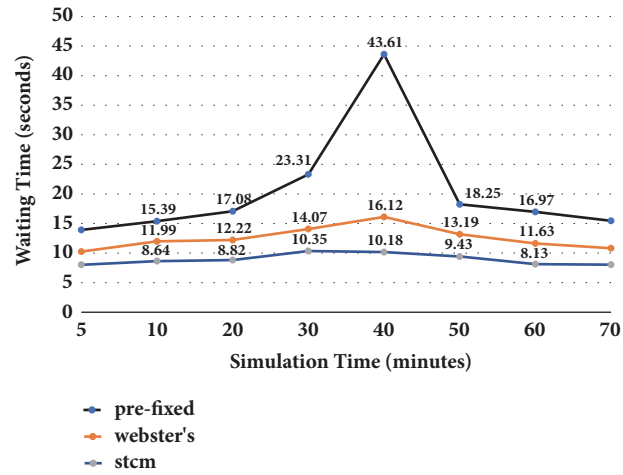

Figure 4: The comparison of the light control systems under light and medium traffic flows.

level. Second, the model is tested under heavy vehicle density levels where the east-west traffic flow density is set to 1400, 1800, and then back 1400 v/h. The simulation is run in a period of 70 minutes where the initial 5 minutes is defined as the warm up period after which the measurements are recorded. The average vehicle waiting time is expressed in seconds and represent the time a vehicle takes to cross the last 250 meters of an intersection (this is the average distance of wireless communication), and the results are plotted at 5 min. intervals in all the traffic light control systems.

Figure 4 shows the performance evaluation of the model in light and medium traffic flows compared to the prefixed time method and adaptive Webster's method, in terms of average vehicle waiting times.

From the results, it can be observed that as the vehicle density increases the average vehicle waiting times also increase in all methods. However, our model exhibits a linear increase compared to the fixed time and Webster's control systems. This is due to the vehicles need to wait more than one green phase at the intersection, resulting in an exponential increase of the vehicle delay times. Moreover, as seen in Figure 5, the model recovers faster in heavy vehicle densities than in the other two systems since the density drops toward a medium level over time.

The magnitude of the waiting times reduction obtained using our model varies in the range of 35% in the light vehicle densities and 25% in heavy densities with the other methods considered here.

6.3. System Security. In this section, the effect of adversary vehicles on the average waiting times is tested in the system. Recall that a green phase timing depends proportionally on the number of vehicles (vehicles that truthfully participate in the system by periodically broadcasting the encoded data, penetration level) in the respective road section.

Figure 6 shows the results of the vehicle waiting times under several rates of adversary vehicles in the traffic flows. Here, the north-south bound vehicles always broadcast correct information; whereas in the east-west flow the number

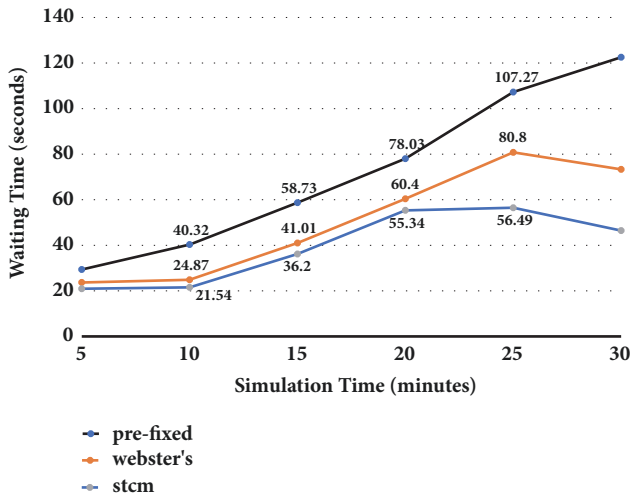

Figure 5: The comparison of the light control systems under heavy traffic flow.

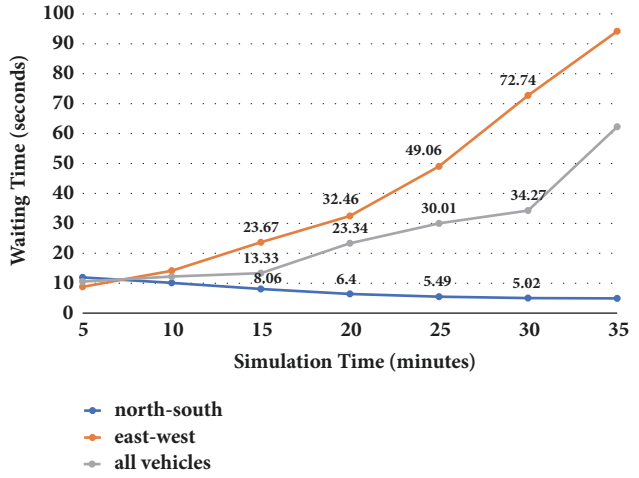

Figure 6: The system performance under adversary vehicles.

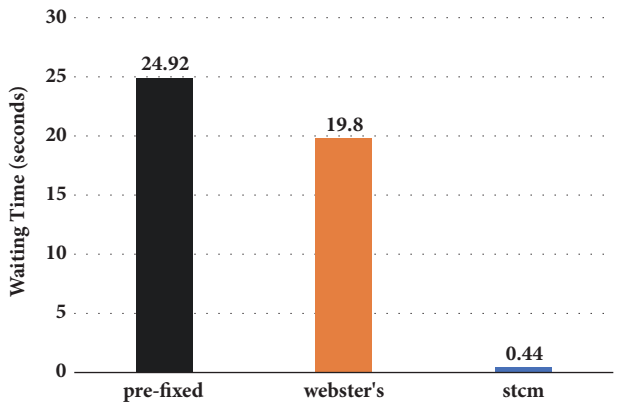

Figure 7: Emergency vehicles waiting times.

of the truthful vehicles is decreased over time during the simulation. The waiting times for all vehicles between the 70% and 90% penetration levels are similar to those for the 100% levels. There is, however, an increase in average waiting times under the penetration levels of 50% and lower.

Specifically, the waiting times of east-west flow dramatically increase as the levels of truthful vehicles goes below 50%. Therefore, the result indicates that the system is not affected by the bogus messages since the adversary vehicles are not considered in determining the signal timing, which causes an increase of the waiting times. Note that the north-south waiting times improve over time since the number of the vehicles increases proportionally relative to the east-west flow.

6.4. Emergency and Public Transport. Figure 7 shows the average waiting times of the emergency vehicle which cross the intersection. The emergency vehicles make up 1.5% of all vehicles and are entered into the simulation with Poisson arrival rate. A vehicle usually experiences some peak waiting times whenever it is caught up at a red phase in the prefixed and Websters' control methods, whereas our system consistently exhibits minimum waiting times throughout the simulation. However, the average waiting times per vehicle increase, up to 30% in some cases as compared with the results in which no emergency vehicle exists due to extended and interrupted phases to the flows to prioritize the emergency vehicles. This can be considered an acceptable trade-off given the benefits of near elimination of the waiting times of the emergency vehicles.

Note that the simulation scenario assumes the vehicle queue at the road section on which an emergency vehicle is present is within the boundaries of the communication distance.

In the next simulation, the size of the public vehicles, buses, is virtually increased at every 12 minutes from 1 site to 9 sites in a simulation of one hour. The east-west flow has a density of 800 v./h and contains additional traffic of 60 buses per hour, whereas north-south flow is set to 600 v./h with no public vehicles present. Figure 8 shows the effect of virtual resizing on wait times of vehicles. The results show the decrease in wait times in east-west flow as the size of the buses increases. Naturally, north-south flow wait times are affected inversely with a trade-off that favors public transport vehicles.

7. Conclusions

In this paper, we presented a traffic light control system which operates on the exchange of messages between the vehicles and a traffic light controller. The system maintains the anonymity of the vehicles at all times and uses a computationally lightweight encryption protocol. At the same time the system allows a trusted authority to identify the vehicles including those that are used in cases emergency and public transportation.

The simulation results show that the system is efficient in optimizing the waiting times of the vehicles and significantly reduces the waiting time of emergency vehicles. Furthermore, the system is robust against network attacks from adversary vehicles, and the vehicles that try to cheat the system with bogus messages to gain some advantage over the intersection

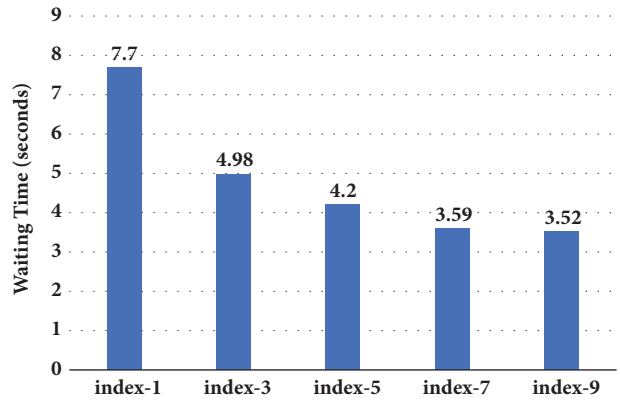

FIGURE 8: Public transport vehicle; bus; wait times with different site values.

crossing end up with a disadvantage in terms of longer waiting times.

Clearly, in real life application, not all the vehicles are registered within the TA. The system needs a certain number of vehicles to actively participate in order for the system to be beneficial and efficient. As the results depicted in Figure 6 imply, if the participation rate is less than 60% the performance of the system degrades.

Even though not explicitly shown in the paper, the system can easily be deployed at urban intersections where the commuter pedestrian traffic is high. Here, the participants with a mobile unit with wireless capabilities, such as a smartphone or a tablet, can participate by simply using a mobile application or some specific carry on device.

Moreover, the traffic controller is able to dynamically prioritize the traffic flows based on the vehicle types present in traffic in real-time by simply changing the index values set in the system. During rush hours, public transport vehicles like buses and other similar vehicles can be given higher passage priorities to encourage the usage of public transportation and consequently reduce the number of private vehicles in traffic.

For the ease of presentation, we have assumed that vehicles do send the GPS coordinates to the TLC. However, it is easy to see that sending the type of vehicle and its size and proving its location by replaying the messages of the neighboring vehicles is sufficient. Unfortunately, this would impose some cumulative delays and overall loss of efficiency in the system.

Data Availability

No data were used to support this study

Conflicts of Interest

The authors declare that they have no conflicts of interest.

References

[1] D. Schrank and T. Lomax, *Urban Mobility Report*, Texas Transportation Institute, 2005.

[2] S. Atev, H. Arumugam, O. Masoud, R. Janardan, and N. P. Papanikolopoulos, "A vision-based approach to collision prediction at traffic intersections," *IEEE Transactions on Intelligent Transportation Systems*, vol. 6, no. 4, pp. 416–423, 2005.

[3] N. Hounsell, J. Landles, R. Bretherton, and K. Gardner, "Intelligent systems for priority at traffic signals in London: the INCOME project," in *Proceedings of the Ninth International Conference on Road Transport Information and Control*, pp. 90–94, London, UK.

[4] R. Akçelik, M. Besley, and E. Chung, *An evaluation of scats master isolated control [Msc. thesis]*, 2001.

[5] C. Priemer and B. Friedrich, "A decentralized adaptive traffic signal control using V2I communication data," in *Proceedings of the 2009 12th International IEEE Conference on Intelligent Transportation Systems (ITSC)*, pp. 1–6, St. Louis, October 2009.

[6] V. Gradinescu, C. Gorgorin, R. Diaconescu, V. Cristea, and L. Iftode, "Adaptive traffic lights using car-to-car communication," in *Proceedings of the 2007 IEEE 65th Vehicular Technology Conference (VTC '07)*, pp. 21–25, April 2007.

[7] K. Pandit, D. Ghosal, H. M. Zhang, and C.-N. Chuah, "Adaptive traffic signal control with vehicular Ad Hoc networks," *IEEE Transactions on Vehicular Technology*, vol. 62, no. 4, pp. 1459–1471, 2013.

[8] M. Bani Younes and A. Boukerche, "Intelligent Traffic Light Controlling Algorithms Using Vehicular Networks," *IEEE Transactions on Vehicular Technology*, vol. 65, no. 8, pp. 5887–5899, 2016.

[9] N. Maslekar, J. Mouzna, M. Boussedjra, and H. Labiod, "CATS: an adaptive traffic signal system based on car-to-car communication," *Journal of Network and Computer Applications*, vol. 36, no. 5, pp. 1308–1315, 2013.

[10] F. Hagenauer, P. Baldemaier, F. Dressler, and C. Sommer, "Advanced leader election for virtual traffic lights," *ZTE Commun*, vol. 12, no. 1, pp. 11–16, 2014.

[11] A. Bazzi, A. Zanella, and B. M. Masini, "A distributed virtual traffic light algorithm exploiting short range V2V communications," *Ad Hoc Networks*, vol. 49, pp. 42–57, 2016.

[12] V. V. Gayah, X. Gao, and A. S. Nagle, "On the impacts of locally adaptive signal control on urban network stability and the macroscopic fundamental diagram," *Transportation Research Part B: Methodological*, vol. 70, pp. 255–268, 2014.

[13] F. Malandrino, C. Borgiattino, C. Casetti, C.-F. Chiasserini, M. Fiore, and R. Sadao, "Verification and inference of positions in vehicular networks throughanonymous beaconing," *IEEE Transactions on Mobile Computing*, vol. 13, no. 10, pp. 2415–2428, 2014.

[14] Y. Sun, R. Lu, X. Lin, X. Shen, and J. Su, "An efficient pseudonymous authentication scheme with strong privacy preservation for vehicular communications," *IEEE Transactions on Vehicular Technology*, vol. 59, no. 7, pp. 3589–3603, 2010.

[15] X. Lin, X. Sun, P.-H. Ho, and X. Shen, "GSIS: a secure and privacy-preserving protocol for vehicular communications," *IEEE Transactions on Vehicular Technology*, vol. 56, no. 6 I, pp. 3442–3456, 2007.

[16] M. Ozkul and I. Capuni, "An autonomous driving framework with self-configurable vehicle clusters," in *Proceedings of the 3rd International Conference on Connected Vehicles and Expo, ICCVE 2014*, pp. 463–468, Austria, November 2014.

[17] M. B. Younes, A. Boukerche, and A. Mammeri, "Context-Aware traffic light self-scheduling algorithm for intelligent transportation systems," in *Proceedings of the 2016 IEEE Wireless*

Communications and Networking Conference, WCNC 2016, Qatar, April 2016.

[18] J. R. Douceur, "The sybil attack," in *Peer-to-Peer Systems*, vol. 2429 of *Lecture Notes in Computer Science*, pp. 251–260, Springer, Berlin, Germany, 2002.

[19] A. Varga and R. Hornig, "An overview of the omnet++ simulation environment in," in *Proceedings of the 1st International Conference on Simulation Tools and Techniques for Communications*, pp. 60-10, 2008, http://dl.acm.org/citation.cfm.

[20] M. Behrisch, L. Bieker, J. Erdmann, and D. Krajzewicz, "Sumo - simulation of urban mobility: An overview in," in *Proceedings of the in SIMUL, 2011*, pp. 63–68, 2011.

[21] C. Sommer, R. German, and F. Dressler, "Bidirectionally coupled network and road traffic simulation for improved IVC analysis," *IEEE Transactions on Mobile Computing*, vol. 10, no. 1, pp. 3–15, 2011.

[22] A. Wegener, M. Piórkowski, M. Raya, H. Hellbrück, S. Fischer, and J. Hubaux, "Traci: An interface for coupling road traffic and network simulators," in *Proceedings of the 11th Communications and Networking Simulation Symposium, CNS '08*, pp. 155–163, ACM, New York, NY, USA, April 2008.

Hindawi
Journal of Advanced Transportation
Volume 2018, Article ID 7835010, 15 pages
https://doi.org/10.1155/2018/7835010

Research Article

Modeling Microscopic Car-Following Strategy of Mixed Traffic to Identify Optimal Platoon Configurations for Multiobjective Decision-Making

Mudasser Seraj,[1] **Jiangchen Li**,[1] **and Zhijun Qiu**[1,2]

[1]*Department of Civil and Environmental Engineering, University of Alberta, Edmonton, Alberta, Canada*
[2]*Intelligent Transportation System Research Center, Wuhan University of Technology, Wuhan, Hubei, China*

Correspondence should be addressed to Zhijun Qiu; zhijunqiu@ualberta.ca

Received 31 May 2018; Revised 16 August 2018; Accepted 10 September 2018; Published 27 September 2018

Guest Editor: Guoyuan Wu

Microscopic detail of complex vehicle interactions in mixed traffic, involving manual driving system (MDS) and automated driving system (ADS), is imperative in determining the extent of response by ADS vehicles in the connected automated vehicle (CAV) environment. In this context, this paper proposes a naïve microscopic car-following strategy for a mixed traffic stream in CAV settings and specified shifts in traffic mobility, safety, and environmental features. Additionally, this study explores the influences of platoon properties (i.e., intra-platoon headway, inter-platoon headway, and maximum platoon length) on traffic stream characteristics. Different combinations of MDS and ADS vehicles are simulated in order to understand the variations of improvements induced by ADS vehicles in a traffic stream. Simulation results reveal that grouping ADS vehicles at the front of traffic stream to apply Cooperative Adaptive Cruise Control (CACC) based car-following model will generate maximum mobility benefits for upstream vehicles. Both mobility and environmental improvements can be realized by forming long, closely spaced ADS vehicles at the cost of reduced safety. To achieve balanced mobility, safety, and environmental advantages from mixed traffic environment, dynamically optimized platoon configurations should be determined at varying traffic conditions and ADS market penetrations.

1. Introduction

Vehicles with diverse levels of integrated connectivity and automated control systems are considered to be pushing a technological leap towards diminished trip delay, fuel efficiency, reduced emission, and enhanced safety of road traffic. Although a purely automated vehicle-based traffic stream could take decades to become a reality, introducing and gradually increasing market shares of automated driving system-based vehicles in traffic streams would enable us to perceive and harness the potential gains from these technologies. Varied perceptions of mixed traffic streams and their collaborative motion dynamics hindered both researchers and practitioners from progressing with these technologies. Furthermore, the ideal compositions of automated vehicles in mixed traffic conditions remain unfamiliar to most. In response to these problems, this study proposes a simple yet effective car-following strategy for mixed traffic stream and measures the resulting impact on mobility, safety, and the environment. Additionally, the car-following strategy involved platoon development in a connected automated vehicle (CAV) environment and the study explores various platoon configurations to determine platoon parameters at different traffic states to obtain utmost benefits.

Numerous studies have been conducted by acclaimed researchers and practitioners to interpret the complex dynamics of combined traffic movements [1–6]. While these studies transcended in conceiving the levels of impact of automated driving technologies through simplified to complex macroscopic and mesoscopic modeling, the motivation of the present was shaped by the need of modeling microscopic car-following behavior in heterogeneous traffic in order to study macroscopic consequences from mobility, safety, and environmental perspectives. With that intention, this study

gives insights into a wide variation of distinct forms of impact while simulating automated-control-enabled vehicles on ideal locations and distributions along traffic stream. These insights into mixed traffic movements and platoon characteristics will motivate researchers to consider other unattended aspects of mixed traffic dynamics (e.g., lane-changing, gap acceptance, and merging) in order to rectify perceived benefits. Similarly, traffic operational authorities can take these lessons into account to impose different control strategies (e.g., dynamic aggregated controls for manually driven vehicles, dynamic personalized controls on connected vehicles) on traffic to attain maximum improvements with regard to reduced travel time, collision rates, greenhouse gas emissions, etc.

The rest of the paper is organized as follows: The next section summarizes the existing literature on car-following models and strategies for mixed traffic and also touches on studies that identify the different form of impact that automated vehicles have on traffic. The proposed car-following strategy is described in the following section. The description of simulation procedures and the discussion on obtained results are covered, respectively, in two subsequent sections. The following section proposed an approach to obtain dynamic optimal platoon configuration for specific traffic state. The last section provides the synopsis of findings of the study and also gives recommendations for future research.

2. Literature Review

As the primary aim of this study relates to car-following strategy for mixed traffic environment, the literature related to car-following models for both forms (i.e., manual, automated) of driving system is explored here. Numerous microscopic car-following models have been proposed to imitate driving pattern of manual driving system [7–12]. Among the proposed stimulus-response-based car-following models, the intelligent driver model (IDM) is widely used in literature to depict manual driving dynamics. The ability of this model to define numerous microscopic (e.g., desired velocity and acceleration/deceleration limits) and macroscopic (e.g., capacity, capacity drop, and fundamental diagram) phenomena made it the prevalent model. On the other hand, due to rapid growth of CAV technology, the longitudinal control models for automated vehicles were also examined by researchers [13–18]. These studies provide us with structures to work on car-following strategy in mixed traffic environment and identify the extents of potential paradigm shifts.

A clear distinction of the driving system is dictated by the operational authority. While the manual driving system (MDS) represents driving systems controlled by humans, the motion dynamics of vehicles with the automated driving system (ADS) are mandated by distinct levels of automation. ADS vehicles' longitudinal movements are commonly portrayed with adaptive cruise control (ACC) and cooperative adaptive cruise control (CACC). Many studies have analyzed the contributions of longitudinal control system of ADS vehicles on traffic mobility [19–28]. While mobility was the main focus of these studies, the impact of traffic movement from safety and environmental perspective was often ignored. Yeo et al. [29] proposed an integrated car-following and lane changing model to perform microsimulation of oversaturated freeway traffic. The proposed algorithm considered complex dynamic interactions at a microscopic level to replicate vehicle movements. However, the aptitude of this model to capture possible consequences was not tested. Wang et al. [30] proposed a car-following control for autonomous vehicle and identified the impact, focusing mainly on traffic flow characteristics. Liberis et al. [31] took a macroscopic approach to identify traffic mobility parameters in a heterogeneous traffic environment. The authors used the market penetration rate of connected vehicles to estimate traffic states. Moreover, other researchers studied the impact of introducing ADS based vehicles with conventional vehicles [32–36] on flow and mobility. Reviews of these studies provide us with the opportunity to constructively examine the contributions of earlier studies, identify the necessities to improve current knowledge, and uncover the latent insights to progress promptly with CA technology.

While the mobility attributes of traffic flow were widely discussed in many studies, the safety and environmental aspects, which are equally if not more important, were relatively unexplored by a majority of the studies. The impact of automated vehicles on both safety and mobility was discussed by Fernandes and Nunes [37]. They studied platooning of ADS vehicles with different communication schemes at various flow rates to improve roadway capacity. Several studies assessed the safety aspects of CAV based traffic. According to the National Highway Traffic Safety Administration (NHTSA), a complete adaptation of CAV based traffic movements would annually prevent 439,000–615,000 crashes [38]. Li et al. [39] evaluated the impact of CACC control on reducing rear-end collisions on freeways. The study shows a reduction in safety improvements with increasing market share of ADS vehicles. Rahman and Abdel-Aty [40] compared potential improvement in longitudinal safety due to varying market penetration of connected vehicles. According to the analysis presented, the managed-lane CAC control outperformed multilane control with regard to traffic safety. The report of Zabat et al. [41] stated that the presence of boundary layer along closely spaced vehicles would reduce aerodynamic drag, resulting in reduced fuel consumption and less emission. Platoon-wide environment-friendly CACC system was studied by Wang et al. [42] and their objective assessment attained 2% fuel saving with 17% emission reductions. Mamouei et al [43] argued that fuel-economy based ACC control model would not lead to highly conservative driving dynamics of traffic.

Although the reviewed studies had remarkable contributions that helped to clarify the roles and influences of ADS vehicles in traffic, the inadequacy of multiobjective decision-making approach to address ADS vehicles' potential has influenced this research further to investigate the complex interdependencies of mixed traffic. This research seeks to contribute on three research gaps identified from the literature. These gaps are (i) the significance of ADS vehicles' position and distributions along traffic stream, (ii) the variations of traffic flow attributes (i.e., mobility, safety, and environmental) resulting from structural changes of

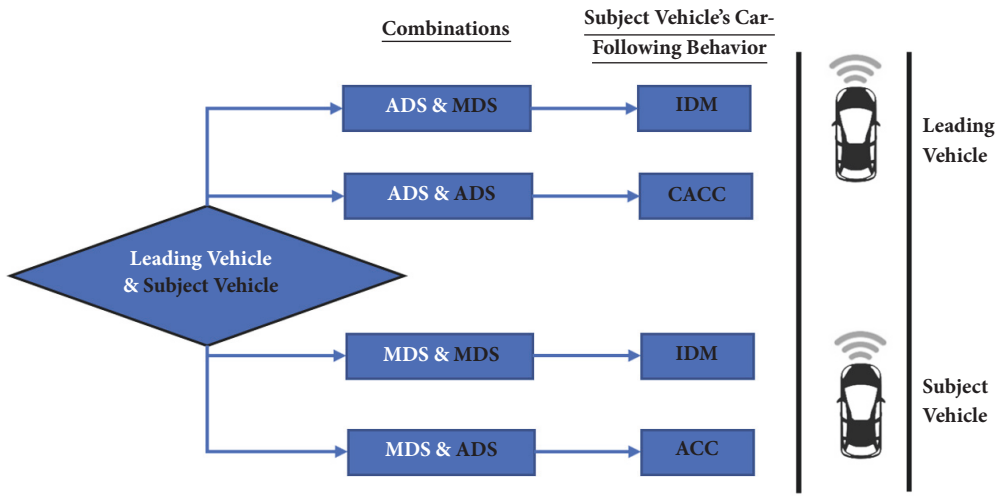

Figure 1: Proposed car-following strategy for mixed traffic.

CACC platoons, and (iii) adjusting platoon configurations dynamically to obtain balanced benefits from considered traffic attributes.

3. Proposed Car-Following Strategy for Individual Vehicle

Interactions and behaviors of vehicles at microscopic levels have macroscopic implications. Factors like maximum accelerations, comfortable decelerations, preferred time headways, etc. are directly linked to traffic mobility, safety, and environmental aspects. Car-following models provide individual vehicles' acceleration from dynamic interactions with adjacent vehicles, control constraints to generate velocity, and position to determine vehicle trajectory. The car-following models of vehicles in mixed traffic were schemed here to simulate real-traffic movements. As mentioned earlier, the existence of two types of vehicle driving system was considered for combined traffic. The proposed driving strategy identified all potential combinations of leading vehicle and subject vehicle based on driving systems to determine suitable car-following models.

The proposed car-following mechanism presumed that MDS vehicles would maintain conventional car-following behavior irrespective of the leading vehicle's driving system [Figure 1]. In this regard, intelligent driver model (IDM) [10] was chosen to represent manual drivers' car-following behavior. Extensive applications of this model across different studies developed this model as a perfect example to simulate MDS vehicles' car-following behavior. An enhanced version of traditional IDM was used to determine a realistic longitudinal control decision of MDS vehicles (see (1)). Discretized kinematic equations were used for all vehicles irrespective of the driving system to determine vehicle's velocity and position (see (2) and (3)).

$$\dot{v}(t+\Delta t) = a\left[1-\left(\frac{v(t)}{v_0}\right)^4 - \left(\frac{s_0+\max\left[0, v(t)\times T + (v(t)\times\Delta v(t))/2\sqrt{ab}\right]}{s}\right)^2\right] \quad (1)$$

$$v(t+\Delta t) = v(t) + a(t)\times\Delta t \quad (2)$$

$$p(t+\Delta t) = p(t) + v(t)\times\Delta t + \frac{1}{2}a(t)\times\Delta t^2 \quad (3)$$

where $\dot{v}$ is acceleration of vehicle (m/s^2), v is velocity (m/s), p is vehicle position (m), a is maximum acceleration (set as 3 m/s^2), v_0 is desired velocity (35 m/s), s_0 is leading gap at jam density (5 m), b is desirable deceleration (-3 m/s^2), Δv is velocity difference with leading vehicle, and T is preferred time headway (2.5 sec).

To demonstrate the car-following mechanism of ADS vehicles, both ACC and CACC based car-following were implemented. A MDS based leading vehicle would prompt ADS vehicle to follow ACC with relatively high preferred time headway. Provided that the leading vehicle had ADS, the subject vehicle would choose CACC based car-following. Whether the subject vehicle would join the CACC platoon depends on the leading vehicle's platoon ID. Platoon ID is an identification number assigned to an ADS vehicle that represents its order of position in the platoon. If an ADS vehicle is a part of a platoon, it will have a fixed platoon ID; otherwise its platoon ID will contain a platoon ID = 0 (zero). While travelling through roads, the built-in communication technology of ADS vehicles would enable them to identify the leading vehicles driving system as well as platoon ID. If the platoon ID of the leading vehicle was equal to the maximum platoon length, then the subject vehicle would form a new platoon by maintaining inter-platoon headway and as a leader of the new platoon. In addition, if the leading vehicle's platoon ID was lower than maximum platoon length, the subject vehicle would join the platoon by maintaining intra-platoon headway. We adopted the ACC and CACC car-following models developed in [17]. The accelerations of the subject

vehicle were determined with respect to relative position and velocity. The following equation was used to determine the acceleration of the subject vehicle:

$$\dot{v}(t+\Delta t) = k_1\left(\Delta p(t) - v(t)\times T - s_0\right) + k_2\Delta v(t) \quad (4)$$

where k_1, k_2 are control constants for relative distance and speed, respectively ($k_1, k_2 > 0$) and $\Delta p(t)$ is position difference with leading vehicle. The stability of the proposed ACC system was proved in [17]. Suitable k_1, k_2 values were chosen according to [17] to implement realistic simulation accounting for the sensitivity of these factors. Similar approach of dual consensus was taken by Wang et al. [18] where both position and velocity consensus were considered to determine acceleration/deceleration decision. While both ACC and CACC car-following models used (4) to determine acceleration values for ADS vehicles, higher preferred time headways (T = 1.5 sec) distinguish ACC mode with CACC mode ($T \leq 1.0$ sec).

4. Simulation Procedures

A microscopic simulation structure was built on MATLAB to replicate vehicles' motion on a two-lane directional highway. The simulation environment was grounded on numerical analysis-based car-following behavior. All previously mentioned motion dynamic equations were coded to follow proposed car-following strategy. A stream of 20 vehicles following a controlled leading vehicle was simulated for numerous scenarios. The time headways between the vehicles in traffic stream were manipulated to simulate distinct traffic flow rates. In the simulation environment, the acceleration of the first vehicle was controlled consciously to generate multiple shockwaves and to observe the reaction of the vehicles behind it. Each simulation ran for 1000 time steps and 20 times for each scenario. The preferred time headway (T) for MDS vehicles was considered as a normally distributed variable with mean value of 2.5 sec and standard deviation of 0.5 sec. Multiple runs for each scenario were executed to ensure that the obtained outcome was free from anomaly. The average values of 20 runs were listed for analysis. In the beginning of the simulation, the first vehicle was travelling at 25 m/s for 210 time steps and then accelerated at 0.167 m/s^3 rate for 60 time steps followed by steady state (acceleration/deceleration rate = 0 m/s^3, velocity = 35 m/s) for 120 time steps. Finally, the controlled vehicle at front decelerated again at 0.167m/s^3 rate for 60 time steps to regain 25m/s velocity and moved with constant velocity for the remaining time steps. The maximum velocity was set to 35 m/s. The combinations generated from the following variables sets were simulated to represent various traffic states encountered in roadways as well as to identify the variations on improvements obtained by introducing the ADS vehicles in the connected automated vehicle (CAV) environment:

(a) Initial flow rate (veh/hr): (i) 1400, (ii) 1800, (iii) 2400

(b) ADS market share (%): (i) 25, (ii) 50, (iii) 75

(c) Maximum platoon length (vehicle): (i) 3, (ii) 4, (iii) 5, (iv) 6

(d) Inter-platoon headway (sec): (i) 2, (ii) 4, (iii) 6, (iv) 8

(e) Intra-platoon headway (sec): (i) 0.5, (ii) 0.75, (iii) 1.0, (iv) 1.25

The variables sets were restricted by the above values to limit the analysis and discussions within manageable ranges while covering a wide range of variations in traffic conditions. Platoon parameters (i.e., maximum platoon length, inter-platoon headway, and intra-platoon headway) were varied within reasonable ranges to identify observable trends. Two distinct driving systems were simulated by assigning specific values of driving system (0 for MDS, 1 for ADS). The driving system values assigned for vehicles were used to implement the proposed car-following strategy on the CAV environment. Assigned driving system values were also useful to adopt proper sets of motion dynamic equations.

5. Analysis, Results, and Findings

5.1. Impact of ADS Vehicles Location and Distribution. Before analyzing the mobility, safety, and environmental aspects of ADS vehicles on traffic, the influences of ADS vehicles location and distribution in traffic stream were explored. It was hypothesized that the positions of ADS vehicles in traffic stream dictated their impacts on the remaining vehicles. To prove this hypothesis, the proposed car-following strategy was simulated by allotting ADS vehicles at diverse combinations of positions with gradually increasing the initial flow rate and ADS market share. To clearly comprehend the significance of vehicle position more clearly and to reduce the intricacy of comprehension, only two features were analyzed: acceleration fluctuation of MDS vehicle in the vehicle group and variations of maximum traffic flow at varying traffic state. Since numerous combinations of ADS vehicles' distribution are viable at different penetration rates of ADS vehicles, only a handful of combinations were selected to cover most possible variations.

Initially, these distributions were generated by placing ADS vehicles as far apart as possible (--% Comb-1) in the vehicle stream while maintaining target ADS market share. Gradually, ADS vehicles were grouped together in different combinations. The purpose of placing ADS vehicles in such an order was to visualize and measure the impact of ADS vehicles location and distribution along the vehicle stream. The combinations are listed in Table 1. The first column of the table shows percentages of ADS vehicles in the traffic stream. The numbers in second column of Table 1 identify the position ID of ADS vehicles in the traffic stream. Other vehicles, except the positions mentioned in the table, were MDS vehicles. The last column of the table provides distinct combination name of each distribution of ADS vehicles. These combinations were simulated on developed simulation environment by virtually placing ADS vehicles in the mentioned position IDs of the vehicle stream and by following proposed car-following strategy for mixed traffic. The listed combinations in Table 1 were assumed to represent varying ranges of ADS vehicles distribution on vehicle group. Analyzing these sets of vehicle location and distribution

Table 1: List of ADS vehicle combinations simulated for different market penetrations.

ADS Market Share	Distribution of ADS vehicles (position)	Combination Name
25%	4, 8, 12, 16, 20	25% Comb-1
	4, 5, 10,11, 16	25% Comb-2
	5, 6, 7, 13, 14	25% Comb-3
	9, 10, 11,12 17	25% Comb-4
	2, 3, 4, 5, 6	25% Comb-5
	16, 17, 18, 19, 20	25% Comb-6
50%	2, 4, 6, 8, 10, 12, 14, 16, 18, 20	50% Comb -1
	2, 3, 6, 7, 10, 11, 14, 15, 18, 19	50% Comb -2
	2, 3, 4, 8, 9, 10, 14, 15, 16, 20	50% Comb -3
	2, 3, 4, 5, 10, 11, 12, 13, 18, 19	50% Comb -4
	2, 3, 4, 5, 6, 7, 8, 9, 10,11	50% Comb -5
75%	2, 3, 4, 6, 7, 8, 10, 11, 12, 14, 15, 16, 18, 19, 20	75% Comb-1
	2, 3, 4, 5, 6, 9,10, 11, 12, 13, 16, 17, 18, 19, 20	75% Comb-2
	2, 3, 4, 5, 6, 9, 10, 11, 12, 13, 16, 17, 18, 19, 20	75% Comb-3

provided the opportunity to shed light on resulting impacts due to ADS vehicles' position on traffic stream.

From the analysis, the simulation outcomes of the initial flow rate of 1800 veh/hr with different ADS market penetration are provided in Figure 2 to demonstrate the influences of ADS vehicles position and distribution along the stream from both microscopic and macroscopic perspective. Figure 2(a) represents the variations of maximum flow rates resulting from the proposed car-following strategy at listed combinations. Figure 2(b) shows the average coefficient of variations (CoV) of acceleration of MDS vehicles in the simulated vehicle stream. Boxplots for a specific combination were plotted from the maximum flow rate and average CoV of acceleration data of simulated scenarios with varying platoon parameters, as listed before. Macroscopic analysis on maximum flow rates at different ADS vehicle shares (Figure 2(a)) identified the pattern of gradual increment with increasing ADS shares in the traffic. Observations of different combinations revealed that combinations with scattered ADS vehicles lead to lower maximum flow rates in comparison to combinations with grouped ADS vehicles. Additionally, grouping ADS vehicles at the front of the vehicle stream (i.e., 25% Comb-6, 50% Comb-5, and 75% Comb-3) resulted in 6.7-11.5% higher maximum flow rates in comparison to the scattered distribution of ADS vehicles (i.e., 25% Comb-1, 50% Comb-1, and 75% Comb-1). Analysis on microscopic characteristics of MDS vehicles was undertaken by measuring the average CoV of acceleration at different market shares and combinations of ADS vehicles. The resulting analysis showed a gradual decreasing CoV of acceleration with increasing shares of ADS vehicles. Similar to macroscopic analysis, the maximum amount of decrease in CoV (1.69–6.63%) was observed from combinations with ADS vehicles at the front of the traffic stream grouped together. Specific analysis on maximum platoon length's influence on acceleration fluctuations of MDS vehicles revealed that increasing maximum platoon length reduced the average coefficient of variation of acceleration for ADS vehicles. Similar analysis on the other two platoon parameters (i.e., inter-platoon headway and intra-platoon headway) demonstrated a reciprocal relation with acceleration fluctuations (increasing inter- and intra-platoon headway increased the average CoV of acceleration).

The analysis of the remaining initial flow rates and ADS market share revealed that creating platoons of ADS vehicles by positioning them at the front of traffic stream would be beneficial to the rest of vehicles in the traffic stream. Furthermore, increasing market shares of ADS vehicles could gradually reduce the acceleration fluctuation of MDS vehicles. Finally, increasing the flow rates could inversely influence traffic flow improvements with a specific ADS location and distribution combination. The notion of traffic flow improvements guided the authors in this study to explore mobility improvement potentials of the proposed car-following strategy by placing ADS vehicles at ideal positions along the traffic stream.

5.2. Impact on Mobility. Since creating platoons of ADS vehicles was found to be the most effective way of acquiring associated benefits, influences of ADS vehicles on traffic mobility were examined with respect to three key variables of platooning: intra-platoon headway, inter-platoon headway, and maximum platoon length. Combinations of these three variables within listed sets were utilized to generate various platoon scenarios for simulation and analysis. The impact of these platoon structures on mobility was measured and compared with the help of two parameters: Average Travel Time (ATT) (see (5)) and Average Travel Distance (ATD) (see (6)). Later, case scores were computed by providing equal weights to ATT and ATD (see (7)). Different cases of platoon configurations were simulated and evaluated through case scores. Higher dispersion from base-case (0% ADS share) scores indicated higher mobility improvements. The objective of this analysis was to identify the optimal platoon configuration to improve mobility by increasing ATD and reducing ATT. The following equations were used to identify the mobility gains.

$$ATT = \frac{\sum_{j=1}^{J} ATT_j}{J} = \sum_{i=1}^{I} \frac{\left(p_{i,j} - p_{i,j-1}\right)}{v_{i,j}} \quad (5)$$

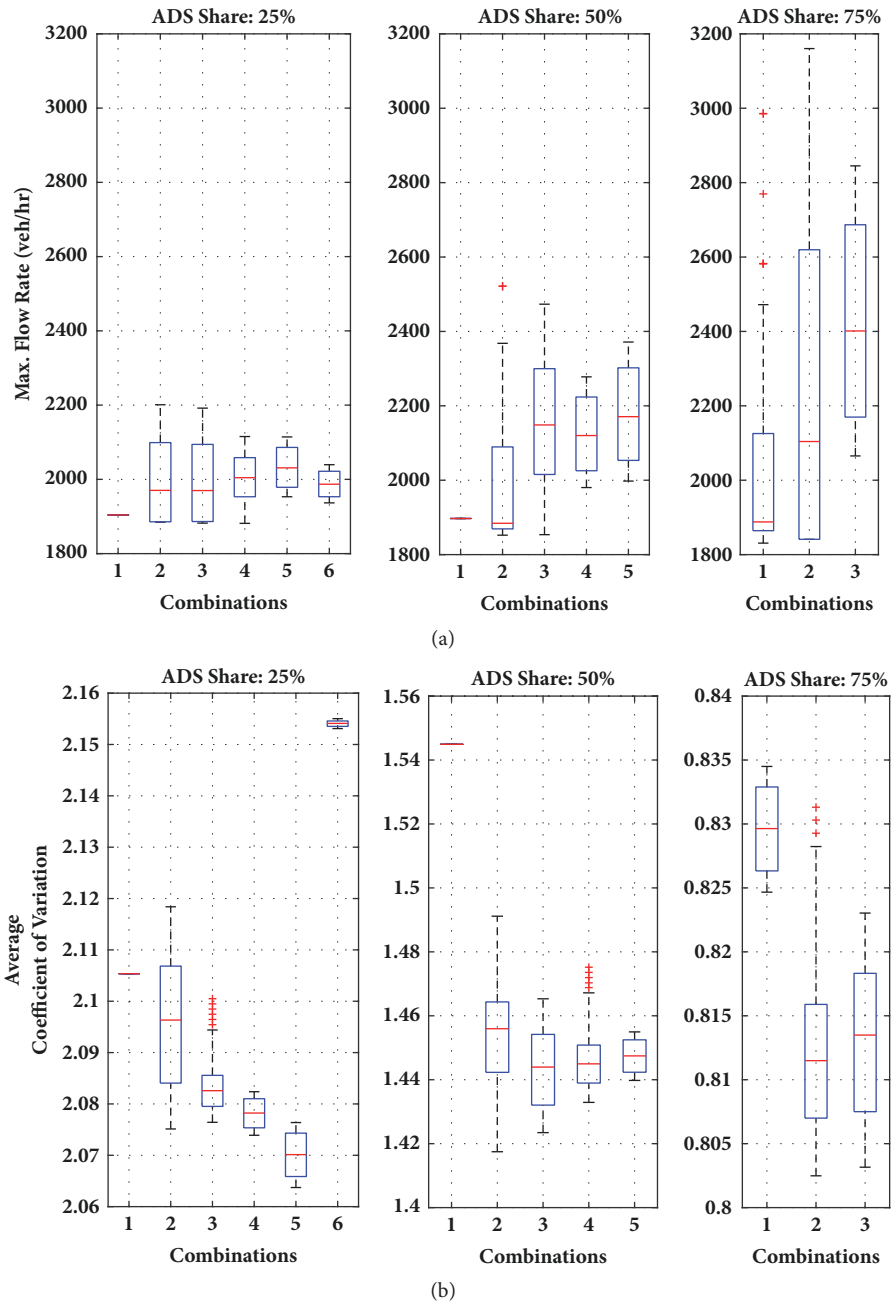

FIGURE 2: Influences of ADS vehicles' position on (a) maximum flow rate and (b) average coefficient of variation of accelerations.

$$ATD = \frac{\sum_{J=1}^{J} ATD_j}{J}, \quad ATD_j = \frac{\left(p_{I,j} - p_{1,j}\right)}{I} \tag{6}$$

$$Score_{Case\,k} = \frac{\sum_{J=1}^{J} v_{1,j}\left(ATD_{j,Case\,k}\right)}{J} - \left(ATT_{Case\,k}\right) \tag{7}$$

Here, i is vehicle index ($I = 21$), j is time index (J = 1000), $v_{i,j}$ is velocity of vehicle i at time step j, $p_{i,j}$ is position of vehicle i at time step j, and $Score_{SCase\,k}$ is score of case k. Aforementioned (Section 4) platoon variables (i.e., maximum platoon length, inter-platoon headway, and intra-platoon headway) were explored to generate distinct platoon scenarios. The combinations of these parameter sets produced 64 distinct platoon configuration cases that were simulated for different traffic flows and ADS market shares to detect the capability of mobility improvements. Moreover, the limits of mobility improvements due to variation of platoon configurations were also revealed in this analysis. Obtained mobility improvements from base cases at different traffic states are presented in Figure 3(a). The three-quarter circles showed comparative mobility progresses at different flow

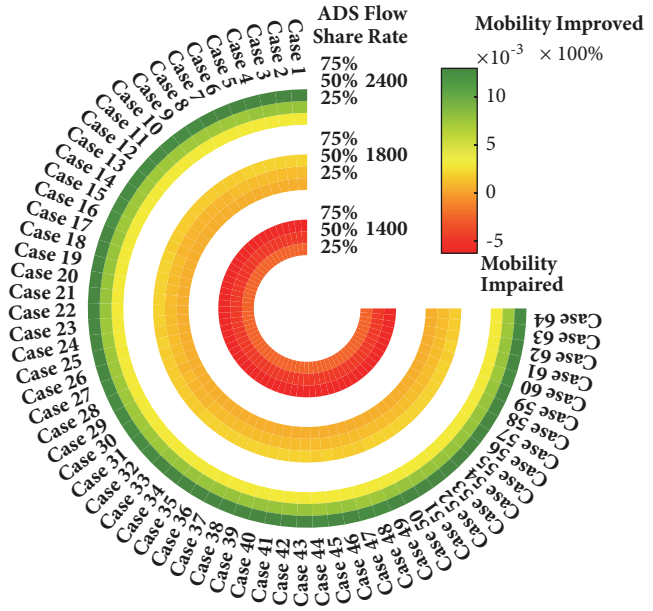

(a)

Case	Intra Platoon Headway	Inter Platoon Headway	Max. Platoon Length	Mobility Improvement	Case	Intra Platoon Headway	Inter Platoon Headway	Max. Platoon Length	Mobility Improvement
1	0.50	2	3	0.200%	33	0.50	2	5	0.204%
2	0.75	2	3	0.196%	34	0.75	2	5	0.200%
3	1.00	2	3	0.193%	35	1.00	2	5	0.196%
4	1.25	2	3	0.190%	36	1.25	2	5	0.192%
5	0.50	4	3	0.189%	37	0.50	4	5	0.198%
6	0.75	4	3	0.186%	38	0.75	4	5	0.194%
7	1.00	4	3	0.182%	39	1.00	4	5	0.190%
8	1.25	4	3	0.179%	40	1.25	4	5	0.186%
9	0.50	6	3	0.178%	41	0.50	6	5	0.193%
10	0.75	6	3	0.175%	42	0.75	6	5	0.189%
11	1.00	6	3	0.172%	43	1.00	6	5	0.185%
12	1.25	6	3	0.168%	44	1.25	6	5	0.181%
13	0.50	8	3	0.168%	45	0.50	8	5	0.188%
14	0.75	8	3	0.164%	46	0.75	8	5	0.184%
15	1.00	8	3	0.161%	47	1.00	8	5	0.180%
16	1.25	8	3	0.158%	48	1.25	8	5	0.176%
17	0.50	2	4	0.202%	49	0.50	2	6	0.204%
18	0.75	2	4	0.198%	50	0.75	2	6	0.200%
19	1.00	2	4	0.194%	51	1.00	2	6	0.196%
20	1.25	2	4	0.191%	52	1.25	2	6	0.192%
21	0.50	4	4	0.194%	53	0.50	4	6	0.198%
22	0.75	4	4	0.190%	54	0.75	4	6	0.194%
23	1.00	4	4	0.186%	55	1.00	4	6	0.190%
24	1.25	4	4	0.183%	56	1.25	4	6	0.186%
25	0.50	6	4	0.186%	57	0.50	6	6	0.193%
26	0.75	6	4	0.182%	58	0.75	6	6	0.189%
27	1.00	6	4	0.178%	59	1.00	6	6	0.185%
28	1.25	6	4	0.175%	60	1.25	6	6	0.181%
29	0.50	8	4	0.178%	61	0.50	8	6	0.188%
30	0.75	8	4	0.174%	62	0.75	8	6	0.184%
31	1.00	8	4	0.170%	63	1.00	8	6	0.180%
32	1.25	8	4	0.167%	64	1.25	8	6	0.176%

(b)

Figure 3: Variations of mobility benefits due to varying platoon configurations at (a) different flow rates and ADS shares and (b) specific flow rate (1800 veh/hr) and ADS share (75%).

rates and ADS market shares simulated for the analysis. The color bar in Figure 3(a) indicated the extent of generated mobility score improvements. Figure 3(b) reveals detailed analysis for a specific flow rate and ADS share. For clear understanding of the impact of platoon configurations at a specific traffic state, mobility improvements at initial flow rate of 1800 veh/hr and 75% ADS share are provided in Figure 3(b) as an example. As observed in Figure 3(b), sixty-four (64) separate platoon configurations are generated from listed parameter set (Section 4). Parameters for each case are listed in the table in Figure 3(b). The mobility improvement column was calculated by comparing the base case (flow rate = 1800 veh/hr, ADS share = 0%) with the corresponding cases and transforming the value into a percentage. Negative percentages indicate impaired mobility and positive percentages denote improved mobility resulting from a specific platoon configuration. When inspecting Figure 3(b), it was found that maximum mobility benefits (0.204% improvement on case score) could be obtained from Case 33 (platoon configuration: intra-platoon headway = 0.50 sec, inter-platoon headway = 2 sec, and max. platoon length = 5) and Case 49 (platoon configuration: intra-platoon headway = 0.50 sec, inter-platoon headway = 2 sec, and max. platoon length = 6) for that specific traffic state. A declining trend of mobility gains was captured with increasing inter and intra-platoon headway. Additionally, increasing maximum platoon length parameter showed expansion with regard to mobility which came to a halt at maximum platoon length = 5.

An exploration of Figure 3(a) revealed that increasing ADS market could bring broader mobility enhancement at higher flow rates (yellow to green bands on 2400 veh/hr flow rate). Increased ADS share at low flow rates had a diminishing effect on mobility (light red to deep red bands on 1400 veh/hr flow rate). Another finding of this analysis was that the closely spaced ADS vehicles with long platoons would generate more mobility improvements. Hence, the maximum mobility benefit was experienced in Case 33 and Case 49. Although the analysis concluded that closely spaced, long ADS platoons could attain higher mobility benefits, close proximity of ADS platoons and long chain of ADS vehicles in these platoon configurations would severely restrict merging vehicles from neighboring lanes, on-ramps, side roads, etc.

Analysis on platoon parameters at different traffic state revealed that, with other parameters being constant, increasing platoon length resulted in improved mobility gains. Similar investigation on inter-platoon headway presented that increase in inter-platoon headway would reduce traffic mobility if other two parameters remain constant at a specific traffic state. Analysis of intra-platoon headways coincides with the insights of inter-platoon headway analysis. Therefore, compactness of ADS vehicles would bring more mobility benefits in roadway sections with minimal conflict points (e.g., spans between on/off-ramps on freeways and sections between intersections in arterial). The notion of conflict points led to the next section of this study, examining the impact of ADS vehicles on traffic safety.

5.3. Impact on Safety. Although Cases 33 and 49 were found to be an obvious choice among 64 tested platoon configuration cases with respect to mobility enhancements, all aforementioned cases were examined again to identify the potential impact on traffic safety. Findings from ADS vehicles location and distribution influenced the simulation of safety improvements by placing a series of ADS vehicles at the front of traffic stream to obtain optimal benefits. Since no merging traffic was considered, the safety enhancements were examined as a measure of potentials to reduce rear-end collision risks. Three safety surrogate measures were considered in this regard: time-to-collision (TTC), time exposed time-to-collision (TET), and time integrated time-to-collision (TIT).

TTC, TET, and TIT, introduced by Hayward, Minderhoud, and Bovy [44, 45], were widely used by traffic safety researchers. The time required for two successive vehicles in the same lane to hit if they maintain their current velocity is represented by TTC. Higher TTC would indicate safer traffic condition. TTC can be used to evaluate safety of a traffic environment, since lower TTC is indicative of potential dangerous situation [46]. Both TET and TIT are derived from TTC to measure safety improvements from macroscopic standpoint. Since TET is the summation of instances when TTC are lower than threshold value, the lower TET value is expected at safer traffic conditions. TET value was measured by (9) where TTC values for each vehicle at each time stamp ($TTC_{i,j}$) were compared with the threshold TTC (TTC^*) value to calculate TET value for each scenario. TIT measures the value of TTC lower than the threshold TTC. Similar to TET, a higher TIT value indicates higher safety concerns. The values of these parameters were measured using the following equations:

$$TTC_{i,j} = \begin{cases} \dfrac{p_{i-1,j} - p_{i,j} - L}{v_{i,j} - v_{i-1,j}} & if\ v_{i,j} > v_{i-1,j} \\ Inf & if\ v_{i,j} \le v_{i-1,j} \end{cases} \tag{8}$$

$$\begin{aligned} TET &= \sum_{j=1}^{J} TET_j, \\ TET_j &= \sum_{i=1}^{I} \delta_j \Delta j, \quad \delta_j = \begin{cases} 1 & \forall 0 < TTC_{i,j} < TTC^* \\ 0 & else \end{cases} \end{aligned} \tag{9}$$

$$\begin{aligned} TIT &= \sum_{j=1}^{J} TIT_j, \\ TIT_j &= \sum_{i=1}^{I} \left[\frac{1}{TTC_{i,j}} - \frac{1}{TTC^*} \right] .\Delta j \\ &\qquad \forall 0 < TTC_{i,j} < TTC^* \end{aligned} \tag{10}$$

The threshold TTC values to measure TET and TIT were set as 2.5 sec, similar to standard perception reaction time. Resulting changes with regard to safety are displayed in Figure 4. Figure 4(a) presents total TET and average TIT values over the simulation period on base cases which

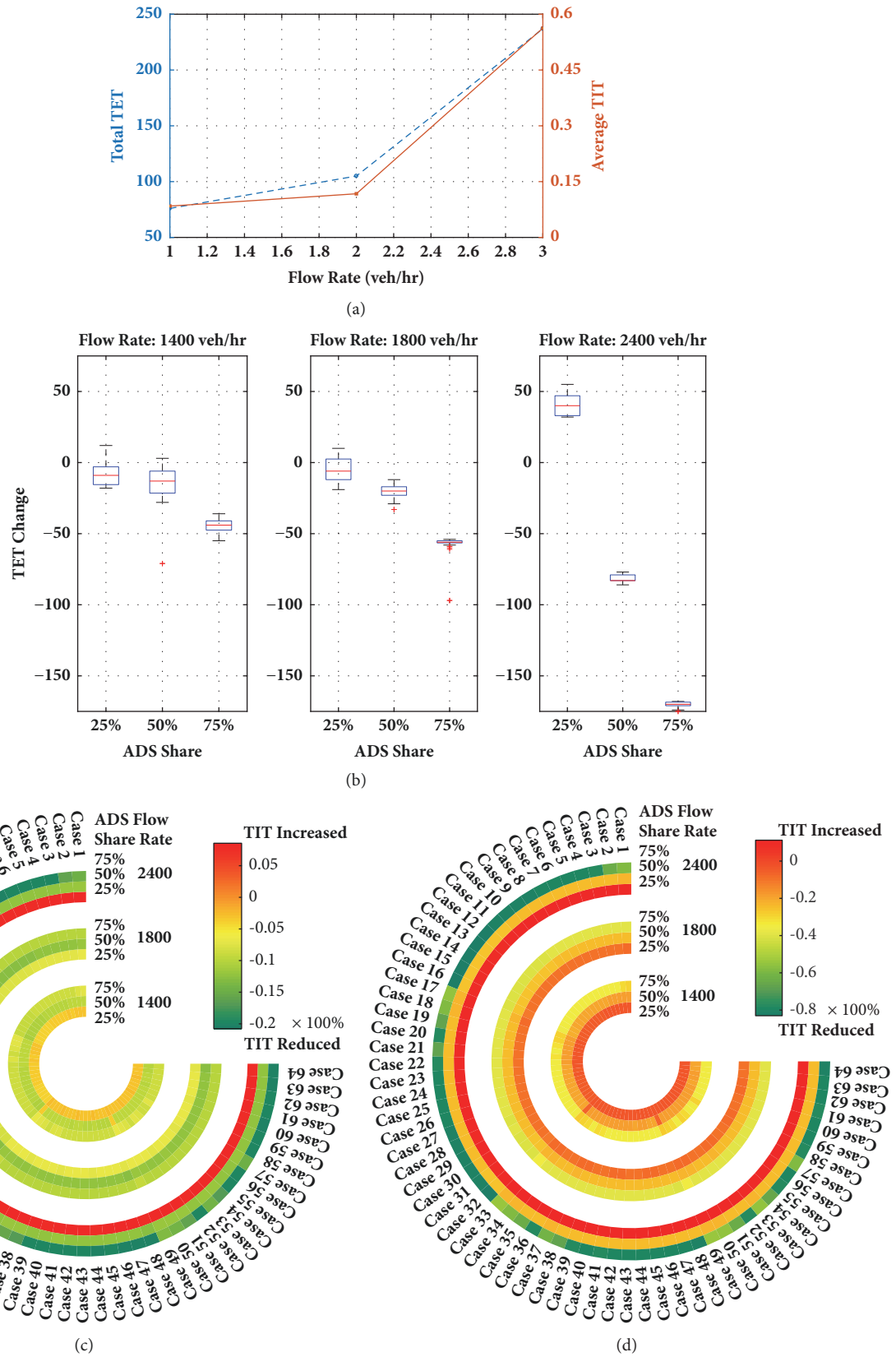

FIGURE 4: (a) Base-case safety parameter values at varying flow rates. (b) Changes in total TET, (c) variations of average TIT values considering MDS vehicles only, and (d) variations of average TIT values considering all vehicles, due to varying platoon configurations at different flow rates and ADS shares.

were utilized to measure safety improvements gained with the introduction of ADS vehicles. Figure 4(b) displays the range of changes on total TET values at different traffic states with varying platoon structures. Increasing ADS shares showed a gradual decline of total TET values. The extent of declination was much higher in higher flow rates. However, an exception was observed at high flow rates and lower ADS shares (flow rate = 2400 veh/hr, ADS share = 25%) where total TET value increased from base traffic states. Therefore, it can be stated that higher ADS share is required to bring noticeable safety improvements with increasing flow rates. Figures 4(c) and 4(d) show analysis results of average TIT changes. As shown in earlier figure (Figure 3(a)), both factional circles revealed resulting improvements on average TIT parameters. Figure 4(c) shows resulting safety improvements of the vehicle stream for different platoon configurations, ADS shares, and flow rates by comparing with base average TIT values. This analysis considered average TIT values of MDS vehicles only in the traffic stream. Average TIT values of MDS vehicles in the CAV environment were compared with corresponding vehicles on base case for this analysis. The average TIT reduction of MDS vehicles was found to be within the range of -20.76%–8.55%. Additionally, higher safety gains were achieved with shorter platoons including ADS vehicles sparsely spaced.

On the other hand, Figure 4(d) shows the analysis by comparing average TIT values of all vehicles with base case. For this analysis, it was assumed that there was no collision risk for ADS vehicles (average TIT values = 0 for ADS vehicles), irrespective of platoon configurations. Comparison between Figures 4(c) and 4(d) shows significantly higher improvements on average TIT values for all vehicles over MDS vehicles. The range of average reduction is much higher in Figure 4(d). Detailed analysis of safety enhancement for a specific traffic state provided further insights on the impact of platoon configurations. For instance, simulation results of 1800 veh/hr flow rate with 75% ADS share traffic state revealed that increasing ADS vehicles' stretch over the traffic stream resulted in greater safety benefits for the remaining vehicles. Hence, the maximum safety gain was attained from Case 16 (-10.23% reduction on average TIT of MDS vehicles) for this specific traffic state. Although a similar pattern was observed for other traffic states, unexpectedly high safety concerns were experienced for some cases (dark red strip in Figure 4(c) for 2400 veh/hr with 25% ADS share). Moreover, maximum safety gains on MDS vehicles were obtained on 50% ADS share at 1800 veh/hr flow. The findings from safety impact analysis have led us to conclude that increasing ADS vehicles with increasing flow rates would improve safety of all vehicles if ADS vehicles form short, sparse platoon in start of traffic stream. Although rear-end collision risk for MDS vehicles would proportionately reduce with increasing ADS share at comparatively high and low flow rate, this correlation between safety gain and ADS share did not hold true for flow rates near capacity level.

Exploring the evolution pattern of platoon parameters provided important insights into safety feature. While other parameters (i.e., inter-platoon headway and max. platoon length) remain the same, continuous increment of intra-platoon headway showed reduction on rear-end collision expectation. Inter-platoon headway followed similar pattern to intra-platoon headway. However, range of safety improvement in both parameters depends on maximum platoon length. Magnitude of safety gains was much higher at small platoons (i.e., max. platoon length = 3) than big platoons (i.e., max. platoon length).

5.4. Impact on Environment. Environmental implications of proposed car-following mechanism were measured with respect to fuel consumption and emission reduction. While numerous models were available and utilized in the literature [47–49], the integrational simplicity of the VT-micro model [50–52] with car-following model persuaded us to implement this model. Output from car-following models can be directly used on the VT-micro model as input to estimate environmental impact due to vehicle dynamics which makes this model a perfect candidate for this analysis. According to the VT-micro model, the fuel consumption of or emission rate of i^{th} vehicle at time step j can be measured using the following equations:

$$\ln\left(MOE_{i,j}\right) = \begin{cases} \sum_{l=0}^{3}\sum_{m=0}^{3} K_{l,m} \times v_{i,j}^{l} \times a_{i,j}^{m} & if\ a \geq 0 \\ \sum_{l=0}^{3}\sum_{m=0}^{3} K'_{l,m} \times v_{i,j}^{l} \times a_{i,j}^{m} & if\ a < 0 \end{cases} \tag{11}$$

where $MOE_{i,j}$ is measure of effectiveness with respect to fuel consumptions, CO_2 emissions, and NO_x emissions for vehicle i at time j and $K_{l,m}$ are regression coefficients for MOEs at powers l and m. The values of regression coefficients are obtained from [50]. $v_{i,j}^{l}$ is velocity of vehicle i at time j with power l. $a_{i,j}^{m}$ is acceleration of vehicle i at time j with power m.

Analysis using the VT-micro model for the base case (0% ADS share) measured average fuel consumptions, CO_2 emissions, and NO_x emissions of the vehicles in simulated traffic stream at different flow rates, which is presented in Figure 5(a). Simulation results indicated that the lowest fuel consumption, CO_2 emission, and NO_x emission at base traffic state occurred at 1800 veh/hr flow rate. Therefore, low flow rates do not necessarily ensure low environmental impact. The transformation in environmental impact resulting from varying shares of ADS vehicles is demonstrated in Figures 5(b), 5(c), and 5(d). Gradual increments of ADS share showed a continuous reduction in fuel consumption. However, CO_2 and NO_x emissions for the traffic stream followed a different trend. As previous figures, the fractional circles displayed changes in average environmental parameters resulting from varying platoon structures and traffic states (i.e., flow rates and ADS shares). For a specific traffic state (i.e., flow rate and ADS share), the effect on environment demonstrated similar patterns to the impact on mobility. As an example, we can examine the platoon structures for 1800 veh/hr flow rate with 75% ADS share. The observations of this specific traffic state revealed that environmental benefits kept increasing with the gradual compaction of ADS vehicle in traffic stream. For instance, maximum reduction on fuel consumption was obtained for Case 33 and Case 49 (platoon configuration:

Base Case (0% ADS Share)				
Parameters	Unit	Flow Rate (veh/hr)		
		1400	1800	2400
Fuel Consumption	Litre/ 100km	8.57	8.52	8.66
CO_2 Emission	Kg/ 100km	19.71	19.64	19.9
NO_x Emission	g/ 100km	28.03	27.96	27.33

(a)

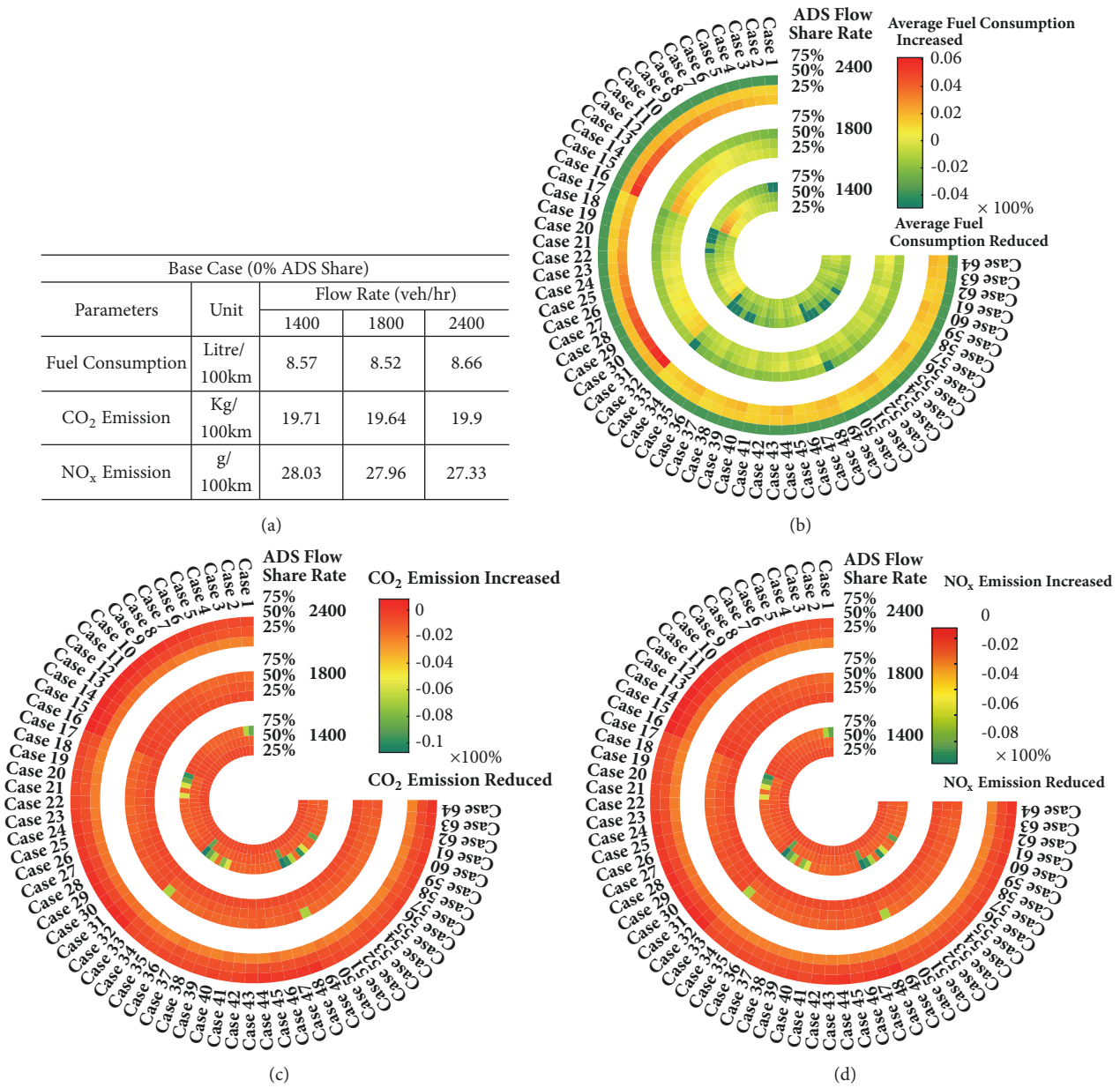

FIGURE 5: Observed variations of (a) environmental parameters at base case, (b) fuel consumption, (c) CO_2 emission, and (d) NO_x emission for varying platoon structures at different traffic state.

intra-platoon headway = 0.50 sec, inter-platoon headway = 2 sec, and max. platoon length = 5 and 6, respectively) which reduced average fuel consumption by 4.87% from the base case, whereas Cases 48 and 64 (platoon configuration: intra-platoon headway = 1.25 sec, inter-platoon headway = 8 sec, and max. platoon length = 5 and 6] reduced fuel consumption by 1.42% and 1.44%, respectively. A similar pattern was observed for the other two parameters (i.e., CO_2 emission and NO_x emission) for this traffic state. Detailed analysis of the environmental impact identified a proportional relation between fuel consumption reduction and ADS share at all simulated traffic flow rates. However, the extent of improvements varied at different flow rates. As for CO_2 and NO_x emission, the relation between emission reduction and ADS share was found to be proportionate at lower flow rates (i.e., 1400, 1800 veh/hr). At high flow rate (i.e., 2400 veh/hr), higher reduction was obtained at low ADS share. Out analysis of the environmental impact of ADS vehicles and formed platoons provided us with the insights of fuel consumption, CO_2 emission, and NO_x emission characteristics in order to make informed decision regarding platoon structures with an aim to attain optimal environmental benefits.

Close inspection of platoon parameters revealed similar inclinations to mobility. Unlike mobility gains, the degree of environmental gains was significantly higher at larger platoon sizes (i.e., max. platoon length = 5,6) in comparison to smaller

platoons (i.e., max. platoon length = 3,4). Furthermore, the increments of intra and inter-platoon headway values showed steady declination of environmental benefits at a specific traffic state with other parameters being constant.

6. Identification of Optimal Platoon Parameter Set

An analysis of proposed car-following strategy delivered insights regarding mobility, safety, and environmental improvement potentials due to presence of ADS vehicles at mixed traffic conditions. One key finding of the analysis was that the expectation to obtain multiobjective improvements (i.e., mobility, safety, and environmental) from single platoon configuration was impractical. Since mobility and environmental developments maintained a reciprocal relationship with safety enhancements, a suboptimal platoon configuration could be determined to procure maximum gains from these three features. Another compelling outcome of prior analysis involved recognizing the fact that both traffic flow rates and ADS market shares impacted obtained benefits. Hence, achieving maximum mobility, safety, and environmental advantages from fixed suboptimal platoon configuration at different flow rates was unrealistic. To this end, it was necessary to present an approach that identified dynamic suboptimal platoon configurations for multiobjective decision-making purposes.

Influenced by Khondaker and Kattan [53], an analysis was performed to identify the suboptimal platoon configurations to maximize mobility, safety, and environmental gains generated by ADS vehicles. Collective influences from these three features were measured by placing different weights on them to get resulting variations on improvements (Figure 6(b)). Four sets of multiobjective functions were investigated to obtain suitable platoon structure. Sets for platoon variables were chosen from earlier analyses to identify suboptimal configurations.

The optimization of platoon variables for different multiobjective function identified each features' (i.e., mobility, safety, and environmental) individual and collective inclinations. To obtain clear and precise insights of these trends, the group of vehicles with 1800 veh/hr flow rate and 75% ADS market penetration is demonstrated in Figure 6. The improvements obtained due to ADS vehicles were scaled within [0 1] using extreme values from prior analysis of all the features (Figure 6(a)). For mobility improvements, the scenario scores were scaled within the above-mentioned range. Extreme average TIT values measured in safety impact analysis were applied to measure safety scores of different platoon configurations. Similarly, environmental score was calculated by assigning equal weights to three components of environmental impact (i.e., fuel consumption, CO_2 emission, and NO_x emission) while scaling them within the range of 0 and 1. This action was performed due to variations of units in measures of effectiveness and to bring them in the same scale for optimization. Reviews of individual features identified a gradual reduction of mobility and environmental improvements with an increase of intra and inter-platoon headway. However, safety improvements showed opposite pattern. Figure 6(b) shows the results of a set of objective functions with predefined weight put on mobility, safety, and environmental aspect. The goal of this analysis is to obtain suboptimal platoon configurations for predefined objective sets and also to identify the objective function with maximum benefits from the assorted weight sets. Analysis of combined impacts identified that maximum benefits for all objective functions were achieved with the platoon configuration of intra-platoon headway = 0.50 sec, inter-platoon headway = 2 sec, and maximum platoon length = 5/6 vehicles. The objective of this analysis was to present an approach to identify suboptimal platoon configurations suitable for specific flow rates and ADS market share with specific motivation to assist in multiobjective decision-making.

7. Conclusion and Future Extensions

The objective of the study was to obtain rationalized insight on mixed traffic movements and evaluate the impact that ADS vehicles will supposedly have on traffic. While the potential of connectivity and automated controls is astounding, the extent of harnessing the benefits depends on discerning their influences on traffic. In this regard, we have proposed a naïve car-following mechanism for mixed traffic and analyzed their motion dynamics to determine the possible improvements. Initially, the location and distributions of ADS vehicles along the traffic stream were discovered to be moving forward with established framework to obtain the highest rewards. The mobility, safety, and environmental gains obtained from CAV traffic stream were examined for varying traffic flow, ADS market penetration, and platoon configurations with the intention of determining the limits of these potential improvements. The final stage of this study was the analysis to obtain optimal platoon configurations to achieve maximum collective improvements.

The findings of the research show that, to obtain maximum mobility benefits, close and compact platoons are favorable in roadway sections without side frictions. However, segments with on-ramps, off-ramps, side roads, etc. need to be researched in the future to account for side frictions and their consequences on collective mobility, safety, and environmental gains. Identifying suboptimal platoon configurations for varying flow rates and market shares of ADS vehicles will assist traffic operation authorities to propose traffic state responsive dynamic platoon structures. Utilizing these platoon configurations will make the best use of ADS vehicles on prevailing traffic conditions to obtain maximum gains. Future research based on this study will account for vehicles with conflicting movements (i.e., lane changing, merging traffic from on-ramps, diverging traffic towards off-ramp, etc.) and propose potential improvements.

Data Availability

The data used to support the findings of this study are available from the corresponding author upon request.

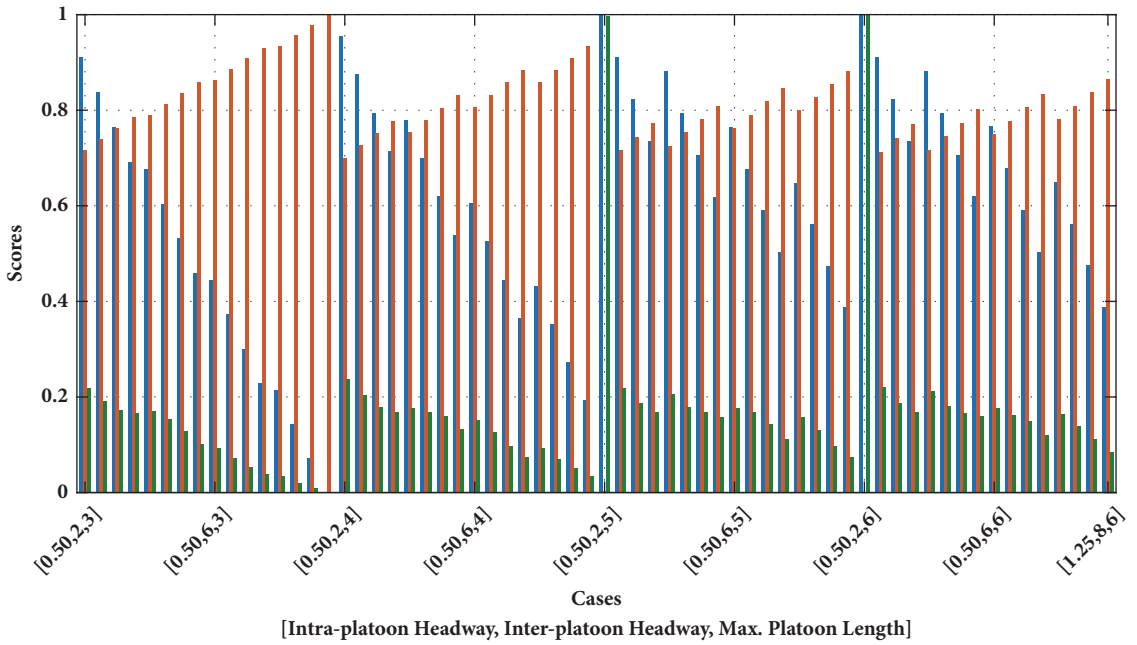

(a)

Obj	Mobility	Safety	Environment
Obj_1	0.33	0.33	0.33
Obj_2	0.5	0.25	0.25
Obj_3	0.25	0.5	0.25
Obj_4	0.25	0.25	0.5

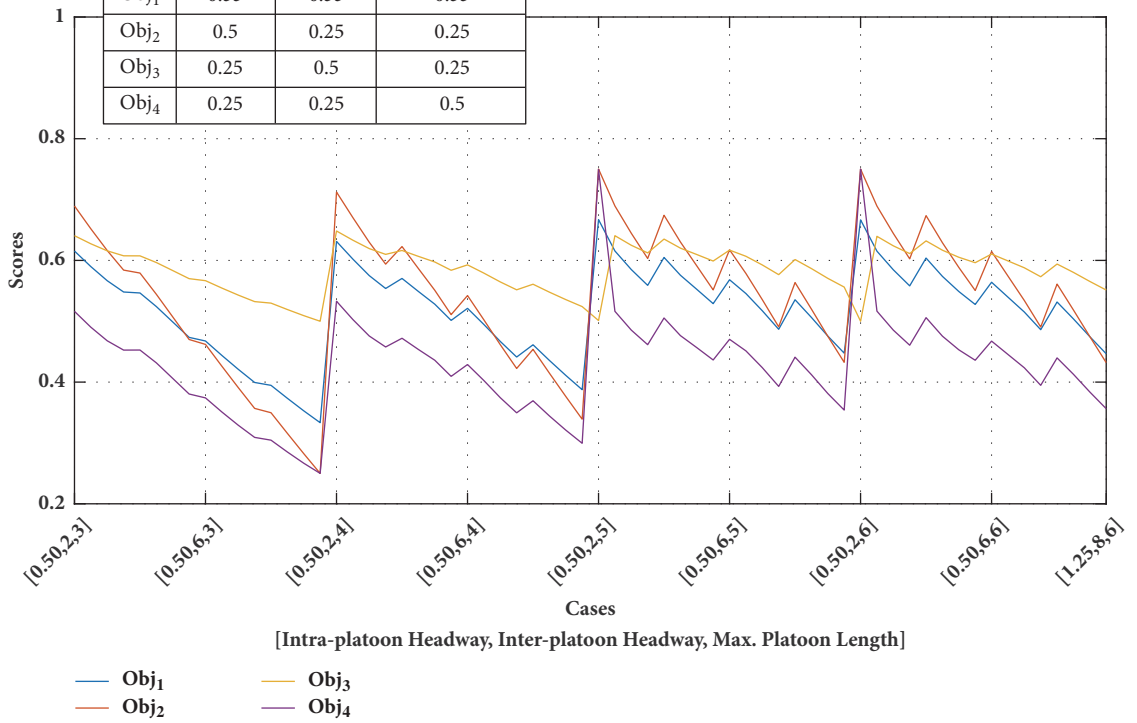

(b)

Figure 6: Observed variations of (a) individual features due to diverse platoon variables listed and (b) listed multiobjective function sets resulting from changing platoon variables.

Disclosure

The contents of this paper reflect the views of the authors who are responsible for the facts and the accuracy of the data presented herein. The contents do not necessarily reflect the official views or policies of the City of Edmonton and Transport Canada. This paper does not constitute a standard, specification, or regulation.

Conflicts of Interest

The authors declare that they have no conflicts of interest.

Acknowledgments

This research work was jointly supported by the Natural Sciences and Engineering Research Council (NSERC) of Canada, City of Edmonton, and Transport Canada.

References

[1] S. Fakharian, "Evaluation of Cooperative Adaptive Cruise Control (CACC) Vehicles on Managed Lanes Utilizing Macroscopic and Mesoscopic Simulation," *Transp. Res. Rec. J. Transp. Res. Board*, vol. no, p. 16, 2016.

[2] A. Ghiasi, O. Hussain, Z. Qian, and X. P. Li, "A mixed traffic capacity analysis and lane management model for connected automated vehicles: A Maekov chain method," *Transportation Research Part B: Methodological*, vol. 106, pp. 266–292, 2017.

[3] Y. Liu, J. Guo, J. Taplin, and Y. Wang, "Characteristic Analysis of Mixed Traffic Flow of Regular and Autonomous Vehicles Using Cellular Automata," *Journal of Advanced Transportation*, vol. 2017, Article ID 8142074, 10 pages, 2017.

[4] A. Talebpour and H. S. Mahmassani, "Influence of connected and autonomous vehicles on traffic flow stability and throughput," *Transportation Research Part C: Emerging Technologies*, vol. 71, pp. 143–163, 2016.

[5] N. Bekiaris-Liberis, C. Roncoli, and M. Papageorgiou, "Highway traffic state estimation per lane in the presence of connected vehicles," *Transportation Research Part B: Methodological*, vol. 106, pp. 1–28, 2017.

[6] D. Chen, S. Ahn, M. Chitturi, and D. A. Noyce, "Towards vehicle automation: Roadway capacity formulation for traffic mixed with regular and automated vehicles," *Transportation Research Part B: Methodological*, vol. 100, pp. 196–221, 2017.

[7] R. E. Chandler, R. Herman, and E. W. Montroll, "Traffic dynamics: studies in car following," *Operations Research*, vol. 6, pp. 165–184, 1958.

[8] W. Helly, "Simulation of bottlenecks in single-lane traffic flow," in *Theory of traffic flow*, pp. 207–238, Elsevier, Amsterdam, 1961.

[9] M. Bando, K. Hasebe, A. Nakayama, A. Shibata, and Y. Sugiyama, "Dynamical model of traffic congestion and numerical simulation," *Physical Review E: Statistical, Nonlinear, and Soft Matter Physics*, vol. 51, no. 2, pp. 1035–1042, 1995.

[10] M. Treiber, A. Hennecke, and D. Helbing, "Congested traffic states in empirical observations and microscopic simulations," *Physical Review E: Statistical, Nonlinear, and Soft Matter Physics*, vol. 62, no. 2, pp. 1805–1824, 2000.

[11] P. G. Gipps, "A behavioural car-following model for computer simulation," *Transportation Research Part B: Methodological*, vol. 15, no. 2, pp. 105–111, 1981.

[12] L. Evans and R. Rothery, *Experimental measurement of perceptual thresholds in car following. Highway Research Board, Washington District of Columbia, United States*, 1973.

[13] L. C. Davis, "Optimality and oscillations near the edge of stability in the dynamics of autonomous vehicle platoons," *Physica A: Statistical Mechanics and its Applications*, vol. 392, no. 17, pp. 3755–3764, 2013.

[14] P. Y. Li and A. Shrivastava, "Traffic flow stability induced by constant time headway policy for adaptive cruise control vehicles," *Transportation Research Part C: Emerging Technologies*, vol. 10, no. 4, pp. 275–301, 2002.

[15] G. Orosz, J. Moehlis, and F. Bullo, "Delayed car-following dynamics for human and robotic drivers," in *Proceedings of the ASME 2011 International Design Engineering Technical Conferences and Computers and Information in Engineering Conference, IDETC/CIE 2011*, pp. 529–538, USA, August 2011.

[16] L. Xiao and F. Gao, "Practical string stability of platoon of adaptive cruise control vehicles," *IEEE Transactions on Intelligent Transportation Systems*, vol. 12, no. 4, pp. 1184–1194, 2011.

[17] S. G. Hu, H. Y. Wen, L. Xu, and H. Fu, "Stability of platoon of adaptive cruise control vehicles with time delay," *Transportation Letters*, pp. 1–10, 2017.

[18] Z. Wang, G. Wu, and M. Barth, "Developing a distributed consensus-based Cooperative Adaptive Cruise Control (CACC) system," *J. Adv. Transp*, vol. 2017, 2017.

[19] M. Fountoulakis, N. Bekiaris-Liberis, C. Roncoli, I. Papamichail, and M. Papageorgiou, "Highway traffic state estimation with mixed connected and conventional vehicles: Microscopic simulation-based testing," *Transportation Research Part C: Emerging Technologies*, vol. 78, pp. 13–33, 2017.

[20] Q. Xin, N. Yang, R. Fu, S. Yu, and Z. Shi, "Impacts analysis of car following models considering variable vehicular gap policies," *Physica A: Statistical Mechanics and its Applications*, vol. 501, pp. 338–355, 2018.

[21] J. Sun, Z. Zheng, and J. Sun, "Stability analysis methods and their applicability to car-following models in conventional and connected environments," *Transportation Research Part B: Methodological*, vol. 109, pp. 212–237, 2018.

[22] B. Van Arem, C. J. G. Van Driel, and R. Visser, "The impact of cooperative adaptive cruise control on traffic-flow characteristics," *IEEE Transactions on Intelligent Transportation Systems*, vol. 7, no. 4, pp. 429–436, 2006.

[23] G. N. Bifulco, L. Pariota, F. Simonelli, and R. D. Pace, "Development and testing of a fully adaptive cruise control system," *Transportation Research Part C: Emerging Technologies*, vol. 29, pp. 156–170, 2013.

[24] J. Yi and R. Horowitz, "Macroscopic traffic flow propagation stability for adaptive cruise controlled vehicles," *Transportation Research Part C: Emerging Technologies*, vol. 14, no. 2, pp. 81–95, 2006.

[25] I. A. Ntousakis, I. K. Nikolos, and M. Papageorgiou, "On Microscopic Modelling of Adaptive Cruise Control Systems," *Transportation Research Procedia*, vol. 6, pp. 111–127, 2015.

[26] A. I. Delis, I. K. Nikolos, and M. Papageorgiou, "Macroscopic traffic flow modeling with adaptive cruise control: development and numerical solution," *Computers & Mathematics with Applications*, vol. 70, no. 8, pp. 1921–1947, 2015.

[27] L. Ye and T. Yamamoto, "Modeling connected and autonomous vehicles in heterogeneous traffic flow," *Physica A: Statistical Mechanics and its Applications*, vol. 490, pp. 269–277, 2018.

[28] W.-X. Zhu and H. M. Zhang, "Analysis of mixed traffic flow with human-driving and autonomous cars based on car-following model," *Physica A: Statistical Mechanics and its Applications*, vol. 496, pp. 274–285, 2018.

[29] H. Yeo, A. Skabardonis, J. Halkias, J. Colyar, and V. Alexiadis, "Oversaturated freeway flow algorithm for use in Next Generation Simulation," *Transportation Research Record*, no. 2088, pp. 68–79, 2008.

[30] N. Chen, M. Wang, T. Alkim, and B. van Arem, "A Robust Longitudinal Control Strategy of Platoons under Model Uncertainties and Time Delays," *Journal of Advanced Transportation*, vol. 2018, Article ID 9852721, 13 pages, 2018.

[31] N. Bekiaris-Liberis, C. Roncoli, and M. Papageorgiou, "Highway traffic state estimation with mixed connected and conventional vehicles," *IEEE Transactions on Intelligent Transportation Systems*, vol. 17, no. 12, pp. 3484–3497, 2016.

[32] V. A. C. van den Berg and E. T. Verhoef, "Autonomous cars and dynamic bottleneck congestion: the effects on capacity, value of time and preference heterogeneity," *Transportation Research Part B: Methodological*, vol. 94, pp. 43–60, 2016.

[33] P. Tientrakool, Y.-C. Ho, and N. F. Maxemchuk, "Highway capacity benefits from using vehicle-to-vehicle communication and sensors for collision avoidance," in *Proceedings of the IEEE 74th Vehicular Technology Conference, VTC Fall*, The Hilton San Francisco Union Square, San Francisco, USA, September 2011.

[34] J. Vander Werf, S. Shladover, M. Miller, and N. Kourjanskaia, "Effects of Adaptive Cruise Control Systems on Highway Traffic Flow Capacity," *Transportation Research Record*, vol. 1800, pp. 78–84, 2002.

[35] D. Ni, J. Li, S. Andrews, and H. Wang, "Preliminary estimate of highway capacity benefit attainable with IntelliDrive technologies," in *Proceedings of the 13th International IEEE Conference on Intelligent Transportation Systems, ITSC 2010*, pp. 819–824, Portugal, September 2010.

[36] T.-H. Chang and I.-S. Lai, "Analysis of characteristics of mixed traffic flow of autopilot vehicles and manual vehicles," *Transportation Research Part C: Emerging Technologies*, vol. 5, no. 6, pp. 333–348, 1997.

[37] P. Fernandes and U. Nunes, "Platooning with IVC-enabled autonomous vehicles: Strategies to mitigate communication delays, improve safety and traffic flow," *IEEE Transactions on Intelligent Transportation Systems*, vol. 13, no. 1, pp. 91–106, 2012.

[38] N. H. T. S. Administration, "FMVSS No. 150 Vehicle-To-Vehicle Communication Technology For Light Vehicles," Off. Regul. Anal. Eval. Natl. Cent. Stat. Anal., no. 150, 2016.

[39] Y. Li, H. Wang, W. Wang, L. Xing, S. Liu, and X. Wei, "Evaluation of the impacts of cooperative adaptive cruise control on reducing rear-end collision risks on freeways," *Accident Analysis & Prevention*, vol. 98, pp. 87–95, 2017.

[40] M. S. Rahman and M. Abdel-Aty, "Longitudinal safety evaluation of connected vehicles' platooning on expressways," *Accident Analysis & Prevention*, vol. 117, pp. 381–391, 2018.

[41] M. Zabat, N. Stabile, S. Farascaroli, and F. Browand, "The Aerodynamic Performance Of Platoons: A Final Report," Calif. Partners Adv. Transit Highw, 1995.

[42] Z. Wang, G. Wu, P. Hao, K. Boriboonsomsin, and M. Barth, "Developing a platoon-wide Eco-Cooperative Adaptive Cruise Control (CACC) system," in *Proceedings of the 28th IEEE Intelligent Vehicles Symposium, IV 2017*, pp. 1256–1261, USA, June 2017.

[43] M. Mamouei, I. Kaparias, and G. Halikias, "A framework for user- and system-oriented optimisation of fuel efficiency and traffic flow in Adaptive Cruise Control," *Transportation Research Part C: Emerging Technologies*, vol. 92, pp. 27–41, 2018.

[44] J. C. Hayward, "Near-Miss Determination Through," *Highw. Res. Board*, pp. 24–35, 1971.

[45] M. M. Minderhoud and P. H. L. Bovy, "Extended time-to-collision measures for road traffic safety assessment," *Accident Analysis & Prevention*, vol. 33, no. 1, pp. 89–97, 2001.

[46] K. Vogel, "A comparison of headway and time to collision as safety indicators," *Accident Analysis & Prevention*, vol. 35, no. 3, pp. 427–433, 2003.

[47] M. Barth et al., "Development of a Comprehensive Modal Emissions Model," *Natl. Coop. Highw. Res. Progr*, 2000.

[48] J. Koupal, H. Michaels, M. Cumberworth, C. Bailey, and D. Brzezinski, "EPAs plan for MOVES: a comprehensive mobile source emissions model," in *Proceedings of the 12th CRC On-Road Veh. Emiss. Work*, San Diego, CA.

[49] S. Hausberger, J. Rodler, P. Sturm, and M. Rexeis, "Emission factors for heavy-duty vehicles and validation by tunnel measurements," *Atmospheric Environment*, vol. 37, no. 37, pp. 5237–5245, 2003.

[50] K. Ahn, *Microscopic Fuel Consumption and Emission Modeling*, Virginia Tech University, 1998.

[51] K. Ahn, H. Rakha, A. Trani, and M. van Aerde, "Estimating vehicle fuel consumption and emissions based on instantaneous speed and acceleration levels," *Journal of Transportation Engineering*, vol. 128, no. 2, pp. 182–190, 2002.

[52] T.-Q. Tang, Z.-Y. Yi, and Q.-F. Lin, "Effects of signal light on the fuel consumption and emissions under car-following model," *Physica A: Statistical Mechanics and its Applications*, vol. 469, pp. 200–205, 2017.

[53] B. Khondaker and L. Kattan, "Variable speed limit: a microscopic analysis in a connected vehicle environment," *Transportation Research Part C: Emerging Technologies*, vol. 58, pp. 146–159, 2015.

Hindawi
Journal of Advanced Transportation
Volume 2018, Article ID 4276593, 12 pages
https://doi.org/10.1155/2018/4276593

Research Article

Potentialities of Autonomous Vehicles for Online Monitoring of Motorway Traffic Volume

Hyun-ho Chang[1] and Byoung-jo Yoon[2]

[1]*Graduate School of Environmental Studies, Seoul National University, Seoul, Republic of Korea*
[2]*Department of Urban Engineering, Incheon National University, Incheon, Republic of Korea*

Correspondence should be addressed to Byoung-jo Yoon; bjyoon63@inu.ac.kr

Received 23 April 2018; Revised 25 July 2018; Accepted 16 August 2018; Published 6 September 2018

Academic Editor: Md. A. S. Kamal

The fact that real-time autonomous vehicle (AV) traffic volume can be collected without a field detector by virtue of advanced global positioning system (GPS) and wireless communication technologies can render a promising solution to online monitoring of traffic volume in the upcoming AV era. To demonstrate this opportunity, this paper proposes a new method to monitor real-time motorway traffic volumes for road locations where no detector is installed using AV traffic volume. The modeling concept is based on the obvious fact that AV traffic volume is a direct portion of total traffic volume. The capabilities of the method are demonstrated through an experimental study using real-world GPS-enabled smartphone vehicle navigation data. The results show that online motorway traffic volume can be effectively monitored throughout the day with 5.69% average error at the 14.91% penetration rate of AVs during the daytime. Therefore, it is expected that AVs can at least be used as complementary means for the role of vehicle detectors in the near future due to the fact that the detection range of AVs is not spatially constrained.

1. Introduction

Real-time traffic volume is essential for traffic control and management in intelligent transportation systems (ITS). Since the introduction of ITS, various vehicle detectors that are based on in-roadway and over-roadway sensor technologies have been utilized to monitor traffic flow variables (i.e., volume, speed, and density). Typically, the spatially consecutive and dense deployment of vehicle detectors is utilized for the instant and accurate monitoring of the variables due to the fact that the spatial coverage of current detectors ranging from conventional inductive loop to radar sensing is constrained to fixed point or fixed short length. This surveillance strategy requires extensive budgets and resources in order to guarantee the reliability of monitored information. In addition, vehicle detectors are operated without the change of their locations in many cases after they are installed in the field.

To address these obstacles from the perspective of ITS infrastructure management and the constrained spatial coverage of vehicle detectors, several investigations to produce the three traffic variables for unmeasured points or road sections using advanced data have been introduced in our literature review. The existing studies have been focused on travel speed or density, showing remarkable and distinguished estimation accuracy according to the data used. Despite the importance of traffic volume, however, any method for dynamic traffic volume still has not been reported even under the condition of advanced data. As such, dynamic traffic volume estimation for unmeasured locations is a new research topic for solving the spatially constrained and fixed coverage of vehicle detectors and then for reducing the budgets and resources for surveillance infrastructure in modern and near future ITS.

Fortunately, it is expected that AVs play a key role as a new moving probe source by virtue of an advanced global positioning system (GPS) and communication technologies for their driving. To mine this promising opportunity, the aim of this study is to initiatively demonstrate the potential of autonomous vehicles (AVs) for producing dynamic traffic volumes for an unmeasured location by using a novel method. The proposed method in this paper is to develop

a new concept that contracts and then expands AV traffic volumes into overall traffic volumes. In addition, based on the analysis results, some findings and research directions for the online monitoring of traffic volume in the present and near future era are discussed.

2. Literature Review

Despite advanced vehicle detection technologies in modern ITS, it seems that the measurements are insufficient due to constrained space coverage (i.e., fixed point or short-length detection area) and the high costs of installation and maintenance. To address these hindrances, academic investigations to dynamically estimate three traffic flow variables (i.e., volume, speed, and density) have been conducted using advanced (probe) data. Note that the literature review of this paper is focused on academic research in which real-world advanced data was employed to produce the three variables.

For the dynamic measurement of travel speed or time, four types of probes have been employed: automatic vehicle identification (AVI) [1], vehicle-based GPS mobile sensor [2, 3], cellular phone (CP) [4–6], and GPS-enabled CP [7, 8].

Probe data that is collected from AVI or vehicle-based GPS mobile sensor systems was employed as a direct portion of vehicle travels in [1–3]. AVI probe data from the San Antonio TransGuide system was employed for estimating average link travel time in [1]. The study demonstrated that a low sampling rate, less than 1%, can represent average link travel time effectively. Travel speed was estimated using GPS-based taxi probe data in [2, 3]. The two studies indicated that imperfect probe data can be used for monitoring traffic status in practice. The results of the two studies in [1, 2] are similar to [9, 10] in terms of a minimum sampling rate of 1~3%.

CP probe data based on tracking CP footprints in a cellular communication network was used to measure travel speed and time between freeway locations in [4–6]. The potentialities of a CP-based system for monitoring traffic status were demonstrated. Despite the reliable measurement accuracy of the CP probe, research indicated in [4] that the noise of the CP probe should be addressed successfully. The noise problem occurs when travel speed is low. Thus, CP-based monitoring systems are suitable for a high-speed roadway such as a motorway [5]. The measurement accuracy was highly improved through an advanced tracking algorithm in [6]. The CP-based system only measures traffic status between two fixed cells (i.e., antennas), as the system totally relies on the geographical configuration of cells. Therefore, the CP-based system is not suitable for measuring traffic status in an urban road network.

Noticeably, two studies demonstrated that the spatiotemporal dotted trajectory of an individual GPS-enabled smartphone can be employed as an effective traffic probe to measure accurate traffic status in [7, 8]. The two studies proved that a 2-3% penetration of GPS probes in the driver population is sufficient to measure accurate traffic speed [7]. The uncertainty of speed measurements caused by the noise of a GPS signal was effectively addressed in [8]. The study showed that the behaviors of speed measured by smartphone trajectory are statistically the same as those of actual speed. The strength of the trajectory probe is suitable for various measurements of traffic status without spatial constraints.

A few studies for estimating traffic density [11] and hourly traffic volume [12, 13] have been reported. A combination method of a kinematic wave model and a probability model for dynamically estimating traffic density was developed based on reconstructing individual vehicle trajectory using heterogeneous data (loop detector, AVI probe, and GPS probe data) in [11]. An innovative methodology for estimating hourly traffic volumes using cellular-phone call count and its probability crossing intercell boundaries was proposed in [12, 13]. The two studies demonstrated that cellular-phone call data can be employed for inferring hourly traffic volumes, where the resulting estimation error was 20%. Despite the initiative efforts, it can be seen that more accuracy should be achieved with more short time length such as a level of five-minute data aggregation for the applications of ITS.

Based on the literature review on the dynamic estimation of the traffic variables using advanced probe data, several studies for traffic speed and density have reached an acceptable level in terms of estimation accuracy. However, more investigations of traffic volume need to be performed at a level of acceptable accuracy. In a strict sense, research for estimating dynamic traffic volumes has not been reported or highly correlated using advanced probe data that is a direct portion of traffic volume. In addition, the dynamic evolution of traffic volume behaves like a chaotic system [14, 15]. That is, a time-series of traffic volume data naturally reveals intensive and wide fluctuations in ergodic and nonperiodic manners. This fact makes it difficult to directly estimate reliable traffic volumes by using either direct low probe data from a GPS-enabled vehicle or indirect probe data from a GPS-enabled mobile phone. More importantly, a new approach should be developed, which is capable of adaptively recognizing the temporal evolution of traffic volumes even in the case when the penetration rate of probe data available to traffic volume is low. In this context, the direct monitoring of dynamic traffic volume using the trajectory probe data of AV is one of new research directions in modern ITS.

3. Methodology

3.1. Approach Concept. The operation of AVs should be supported with advanced GPS and communication technologies. That is, AVs that are on a driving service can be considered a moving GPS probe in a road network. It is also surely expected that detailed point-to-point operation trajectory data can be stocked by virtue of the GPS technology, and then the trajectory data can be transferred to an advanced data centre through the communication technology online. This develops the assumption that AV probe volume is a direct portion of total traffic volume or at least is very highly related to that in some way. If this assumption is reasonable, then traffic volume at a target road location can be produced using a suitable relationship between probe volumes and traffic volumes that are collected from the nearby locations of the target road location. Moreover, the AV trajectory data is not spatially constrained unlike existing vehicle detectors, and thus, the probe volume can be accurately monitored at any

road location. This implies in turn that traffic volume at any road location (used by AVs) can be effectively monitored using the probe volume. Therefore, it is expected that AVs render golden opportunities against the traffic surveillance system of modern and future ITS.

To demonstrate the potential of AVs for the real-time monitoring of traffic volume, a new method to produce dynamic traffic volume at any road location using AV probe volume data is proposed in this study. The method is developed on the basic concept that probe volume data provide key information to solve the uncertainty problem in the direct monitoring of traffic volume. This modeling approach is also supported by the fact that probe volume is at least a direct portion of traffic volume. The method consists of two modeling concepts: contraction and expansion of probe volume. In the contraction method, time-series probe volume data are adjusted into suitable data by eliminating its unnecessary random noise. The method also adaptively interpolates zero probe volume values into useful values, because zero probe volume values inevitably occurs when either traffic volume and/or the penetration rate of AV is low. In the expansion method, an adjusted probe volume at a road location where a traffic volume estimation is desired is converted into a traffic volume value by using a relationship between adjusted probe volumes and traffic volumes. As such, the combination of the two methods can solve the problem of direct monitoring traffic volume efficaciously by diminishing the number of uncertainties that inevitably occurs in solving this problem.

3.2. Contraction Method. It is natural that the temporal evolution of AV probe volume reveals more wide relative variations than that of overall traffic volume under the condition that the penetration rate (0.0~1.0) of AV to traffic volume is less than 1.0. This is because the probe volume is a sort of random sample with a given penetration rate. In this case, undesirable estimation results (i.e., over- and under-estimation problems) are unavoidable when a time series of probe volume data that includes the random-sampling variation in itself is directly used for the monitoring of traffic volume without any filtering process. This problem becomes more serious when the sampling variability of collected temporal probe volumes increases under the condition of low AV penetration rates and/or low traffic volumes. Zero probe volumes can also occur frequently, even when traffic volumes are low and AV penetration rates are not low.

To address this problem effectively and to ensure the reliability of traffic volume monitoring, two processes that adjust raw probe volumes into suitable probe volumes are essentially required as follows: unnecessary random variations that intrinsically exist in raw probe volumes should be filtered; and zero probe volume values should also be interpolated with useful values. The two processes are concurrently conducted by a contraction method proposed in this study.

The contraction method is devised based on the assumption that the temporal variation of actual traffic volumes is highly related to that of raw probe volumes. This assumption could be reasonable if the raw probe volume that include random-sampling variation is a part of the traffic volume.

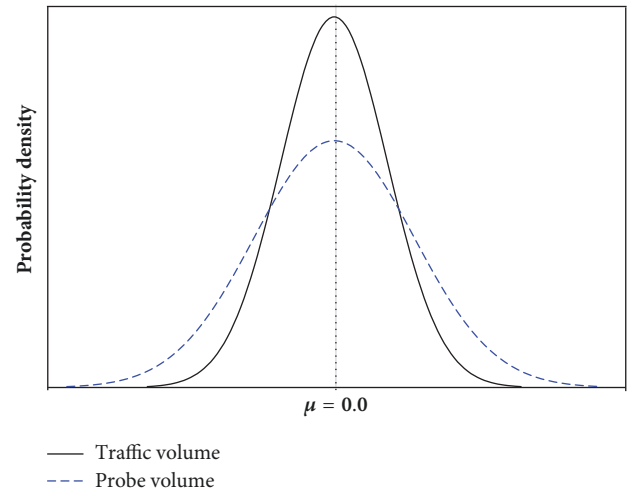

Figure 1: Distributions of relative variation.

Thus, the unnecessary variation of raw probe volumes can be removed by using the distribution of relative variation (RV) of raw temporal probe volumes and that of RV of temporal traffic volumes. To measure time-series RV values, time-series values and moving-average values for traffic volume and probe volume are defined as follows. Let $s = \{tg, up, dn\}$ be the target location (tg) and the upstream and downstream of tg, respectively. Let $x = \{q, p\}$ be a set of traffic volume (q, vehicles per length of time interval) and probe volume (p, vehicles per length of time interval). Let X = {Q, P} be time-series sets of x. Note that a form of time series (i.e., a series of time intervals) at the present time interval (t) toward the past is defined as $T = [(t), (t-1), \ldots, (t-d)]$, where d is the embedding size of time series. Let $X_s = [x_s(t), x_s(t-1), \ldots, x_s(t-d)]$ be a time series of x for s. Let $X_s^b = [x_s^b(t), x_s^b(t-1), \ldots, x_s^b(t-d)]$ be a time series of moving-average values for X and s, where each element of X_s^b (i.e., $x_s^b(i)$) is calculated as $[\sum_{k=0}^{m} x_s(i-k)]/[m+1]$ with m (≥ 1), ($\forall x, s$, and $i \in$ T). Let $R_s^X = [r_s^x(t), r_s^x(t-1), \ldots, x_s^x(t-d)]$ be a time series of RV values for X and s. Thus, each element of R_s^X is computed using each element of X_s and that of X_s^b (where if $s = tg$, then X $\neq$ Q), as follows:

$$r_s^x(i) = \frac{x_s(i) - x_s^b(i)}{x_s^b(i)}, \quad \forall s, x, i, \ i \in \mathrm{T} \tag{1}$$

Figure 1 shows the RV distributions of traffic and probe volumes (i.e., R_s^Q and R_s^P), where the variance of probe volume is greater than that of traffic volume. The RV distribution of probe volume can be adjusted similar to that of traffic volume using the standard deviation. This statistical principle is employed to modify a variation of temporal probe volumes. Let σ_s^X be the standard deviation of R_s^X (where if $s = tg$, then X $\neq$ Q). Let $P_s^a = [p_s^a(t), p_s^a(t-1), \ldots, p_s^a(t-d)]$ be a time series of adjusted probe volumes for s. Finally, each element of P_s^a is estimated based on each component of P_s^b and the rate of σ_s^Q to σ_s^P as

$$p_s^a(i) = p_s^b(i) \times \left[1.0 + r_s^p(i) \times \frac{\sigma_s^Q}{\sigma_s^P}\right], \quad \forall s, i,\ s \neq tg,\ i \in \mathrm{T} \tag{2}$$

Thus, each probe volume (i.e., $p_s(i)$) is contracted into $p_s^a(i)$ by removing unnecessary random-sampling variation. Additionally, $p_s^a(i)$ is effectively generated in the case of a low value of $p_s(i)$, and $p_s(i)$ is also interpolated with a useful value even when $p_s(i)$=0.0, if $p_s^b(i) > 0.0$, $\sigma_s^P > 0.0$, and $\sigma_s^Q > 0.0$.

Due to the fact that no traffic volume is collected at the target location, it is impossible to directly compute the adjusting factor (i.e., the rate of σ_s^Q to σ_s^P). Therefore, it is assumed that σ_{tg}^P (i.e., the standard deviation of R_{tg}^P) is more similar to σ_s^P when P_{tg}^b is nearer to P_s^b, ($s \neq tg$), from the viewpoint of RV distribution of probe volume. This can be supported by the rational reasoning that penetration rates of AV between the three locations are similar or at least not significantly different, and then the similarity of P_s^b values between different locations highly relies on Q_s^b values even though Q_{tg}^b cannot be estimated. Based on this assumption, closeness (c_s) between P_{tg}^b and P_s^b can be a direct solution to combine the two adjusting-factor values of upstream and downstream locations into an adjusting-factor value for tg. Euclidean distance metric that is one of direct and widely applied techniques to determine the degree of similarity in the time-series analysis of discrete dynamical system [15] is used in this study, and c_s between P_{tg}^b and P_s^b is calculated as

$$c_s = \left[\left|p_{tg}^b(t) - p_s^b(t)\right|^2 + \cdots + \left|p_{tg}^b(t-d) - p_s^b(t-d)\right|^2\right]^{1/2}, \quad s \neq tg \tag{3}$$

The inverse of c_s (i.e., $c_s^{-1} > 0.0$) that is effectively utilized in pattern selection-based traffic volume forecasting [15, 16] is employed to weight the two adjusting-factor values of upstream and downstream locations. According to this consideration, a value of adjusting factor (i.e., the rate of σ_{tg}^Q to σ_{tg}^P) for tg at (t) is estimated using a weighted average function, which combines the two adjusting-factor values by c_s^{-1}. Finally, a contracted probe volume ($p_{tg}^a(t)$) for tg at (t) is computed as

$$p_{tg}^a(t) = p_{tg}^b(t) \times \left[1.0 + r_{tg}^p(t) \times \frac{\sum_s \left(\left(\sigma_s^Q/\sigma_s^P\right) \times c_s^{-1}\right)}{\sum_s c_s^{-1}}\right], \quad s \neq tg \tag{4}$$

As such, $p_{tg}(t)$ is modified into $p_{tg}^a(t)$ by using the two adjusting-factor values (i.e., σ_s^Q/σ_s^P) and the inverse of c_s (i.e., c_s^{-1}). Furthermore, $p_{tg}^a(t)$ is robustly estimated when a value of $p_{tg}(t)$ is very low, and $p_{tg}(t)$ is also interpolated with a useful value even when $p_{tg}(t)$=0.0, if $p_{tg}^b(t) > 0.0$, $r_{tg}^p(t) > 0.0$, and $\sigma_s^P > 0.0$.

3.3. Expansion Method. To expand the contracted probe volume (i.e., $p_{tg}^a(t)$) to a traffic volume (i.e., $\widehat{q}_{tg}(t)$) for the target location (tg) at time interval (t), a weighted power curve is employed to determine a relationship between contracted probe volumes (i.e., $p_s^a(i)$, , $s \neq tg, i \in \mathrm{T}$) and traffic volumes (i.e., $p_s(i)$, , $s \neq tg, i \in \mathrm{T}$) in this study. The expansion method is stated according to two parts: a weighting function and the determination of an optimal fitting curve. From the perspective of temporal development of traffic flow, it is self-evident that the temporal evolution of traffic flow nearer to (t) is more related to traffic flow at (t) [14–16]. This is considered with the bisquare weighting function that was introduced to explain nonstationary relationships between spatial elements in [17]. Let $W_s = [w_s(t), w_s(t-1), \ldots, w_s(t-d)]$ be a series of weight values (0.0~1.0) for T. The variation of weight value according to the proximity of time is illustrated in Figure 2(a), which can be efficaciously used in the case that the penetration rate of AV varies according to the time periods of day (e.g., peak and off-peak time). The bisquare function for temporal nonstationarity can be expressed as

$$w_i = \left[1 - \left(\frac{i}{d}\right)^2\right]^2, \quad i = [0, 1, \ldots, d] \tag{5}$$

In order to find an optimal power curve, traffic volume data and contracted probe volume data for upstream and downstream locations are used as a dependent variable and an independent variable, respectively. The dependent and independent variables are defined as follows. Let $\mathrm{Q} = [\mathrm{Q}_{up}, \mathrm{Q}_{dn}]$ and $\mathrm{P} = [\mathrm{P}_{up}^a, \mathrm{P}_{dn}^a]$ be sets of traffic volumes and adjusted probe volumes for the upstream and downstream locations, respectively. In addition, let $\mathrm{W} = [\mathrm{W}_{up}, \mathrm{W}_{dn}]$ be a set of weight values for the two locations. For the convenience of the description of the expansion method, these definitions are redefined with the number of observations (N=2×(d+1)). Let $\mathrm{Q} = [q_1, q_2, \ldots, q_N]$ and $\mathrm{P} = [p_1, p_2, \ldots, p_N]$ be dependent and independent variables, and let $\mathrm{W} = [w_1, w_2, \ldots, w_N]$ be a set of weight values.

The temporal evolution of traffic volume states reveals intensive variation in ergodic and nonperiodic manners [14, 15]. Hence, it is natural that the temporal variation of probe volumes varies more steeply and widely than that of traffic volumes, even though the probe is a direct part of traffic volume. Thus, if a linear regression model is employed, then unacceptable results (e.g., repetitive overestimations and underestimations, and even negative estimations) can occur by failing the directionality of relationship between P and Q. To prevent these undesirable results, a power curve with versatility in curve fitting (ranging from logarithmic, linear, to positively exponential types) is used to understand the relationship between the two variables as shown in Figure 2(b). The power curve for the members of [P, Q] (i.e., $[p_i, q_i], i \in N$) is defined as

$$q_i = \alpha \cdot p_i^{\beta} + \gamma \tag{6}$$

where α (>0.0) and β (>0.0) are the coefficient and exponent of p_i, respectively; γ ($0.0 \leq \gamma \leq \gamma_{max}$) is a constant term; $\gamma_{max} = \min\{\overline{q}_s\}$; and $\overline{q}_s$ is an average of elements of Q_s, where $s =$

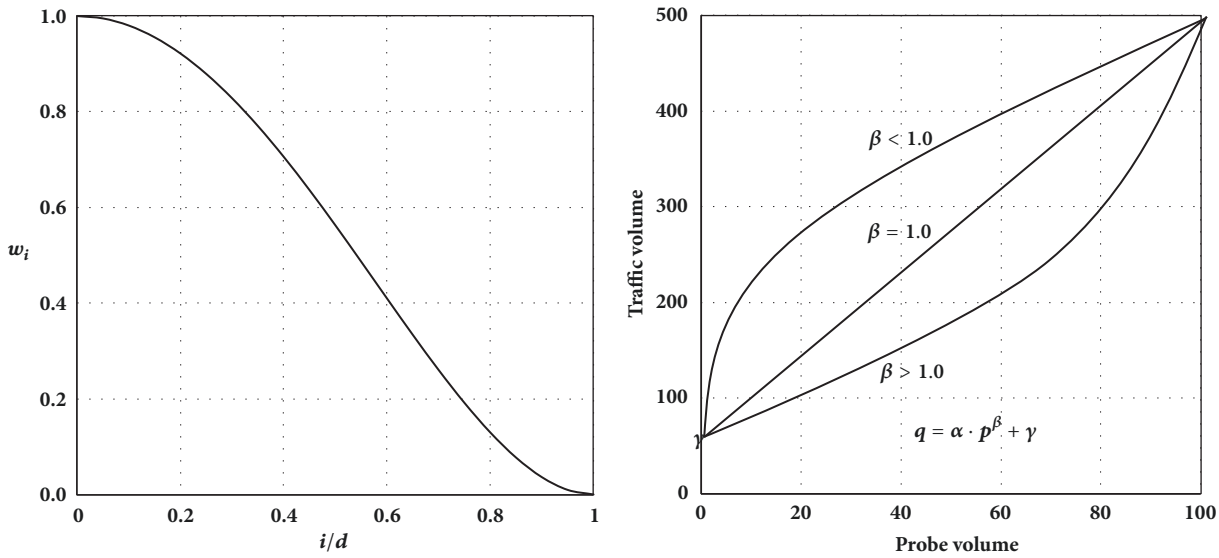

(a) Weight curve by time proximity

(b) Versatility of curve fitting

Figure 2: Power curve for expansion of probe volume.

$\{up, dn\}$. To prevent negative estimations, α is greater than 0.0 and γ is greater than or equal to 0.0. β is greater than 0.0 and γ is less than or equal to γ_{max}, since traffic volumes do not decrease according to the increase of probe volumes. For an optimal curve that minimizes total estimation error, a local error for each observation can be expressed as

$$\epsilon_i = q_i - \left(\widehat{\alpha} \cdot p_i^{\widehat{\beta}} + \widehat{\gamma}\right) \tag{7}$$

where $\widehat{\alpha}$, $\widehat{\beta}$, and $\widehat{\gamma}$ are optimal α, β, and γ values, respectively, and ϵ_i is the estimation error for observation i, $i \in N$.

As mentioned, temporal traffic volumes fluctuate widely, and then the quantity of traffic volume varies from low to high levels. Thus, a family of the residual sum of squares that are widely employed as an objective function for determining an optimal fitting can have a 'bias and variation problem' in the case of low traffic volumes [18]. That is, the low traffic volume can be over- or underestimated, due to its low contributions in decision-making of an optimal curve fitting.

To handle this problem effectively, the sum of a weighted absolute relative error is used as an objective function of a minimization problem to determine an optimal power curve. The absolute relative error also provides an unbiased basis [18], and thus, it is widely used as a performance measure in the area of time-series estimation and prediction. Here, a minimization problem for determining an optimal expansion curve is defined as

$$\begin{aligned} \text{Min.} \quad & \frac{\sum_{i=1}^{N} w_i \times \left| q_i - \left(\widehat{\alpha} \cdot p_i^{\widehat{\beta}} + \widehat{\gamma}\right)\right| / q_i}{\sum_{i=1}^{N} w_i} \\ \text{S.T.} \quad & 0.0 < \widehat{\alpha}, \\ & 0.0 < \widehat{\beta}, \\ & 0.0 \le \widehat{\gamma} \le \gamma_{max} \end{aligned} \tag{8}$$

Once, the estimated values of $\widehat{\alpha}$, $\widehat{\beta}$, and $\widehat{\gamma}$ for an optimal curve are identified through solving the minimization problem, a traffic volume for tg at (t) is directly produced as

$$\widehat{q}_{tg}(t) = \widehat{\alpha} \cdot p_{tg}^{a}(t)^{\widehat{\beta}} + \widehat{\gamma} \tag{9}$$

where $\widehat{q}_{tg}(t)$ and $p_{tg}^{a}(t)$ is the estimated traffic volume and the adjusted probe volume for tg at (t), respectively.

4. Results and Potentialities

4.1. Study Design. In order to demonstrate the potential of GPS probe data collected by autonomous vehicles, a case study was conducted using two types of data: GPS probe volume data and traffic volume data. The GPS probe data that was collected by a smartphone vehicle navigation system is most similar to the probe data of autonomous vehicles under the present conditions, due to the fact that the vehicle-probe volume is a direct portion of traffic volume. In this context, it seems at least that the used probe data contains the characteristics of probe data that are collected through autonomous vehicles, even though the features of mixed traffic flow with general vehicles and autonomous vehicles have not been investigated with real-world data so far.

The used motorway data is shown in Figure 3. The test bed is a part of the Seoul External Circulation Motorway 100, one of the main motorways in South Korea. The target road location consists of four lanes, and the upstream road section includes one interchange and one junction and the distance is 11.6 km. The downstream road section contains two interchanges and four junctions and the distance is 25.6 km. It can be seen that the test-bed conditions are unfavorably severe for the experimental condition, whereas the test-bed conditions are desirable to demonstrate the potential of the

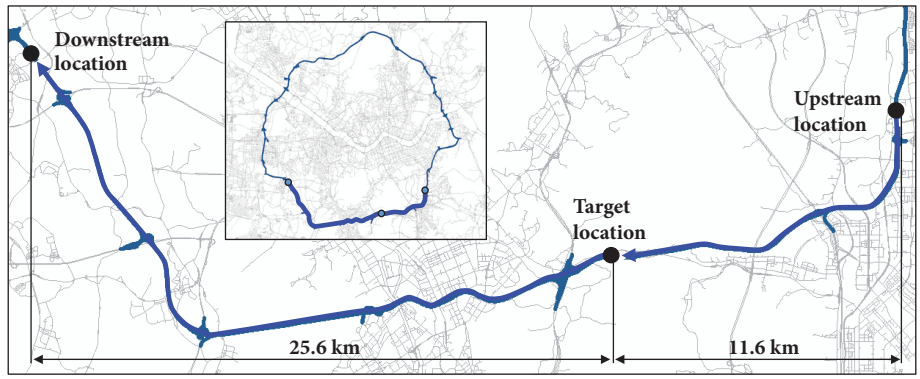

Figure 3: Test bed.

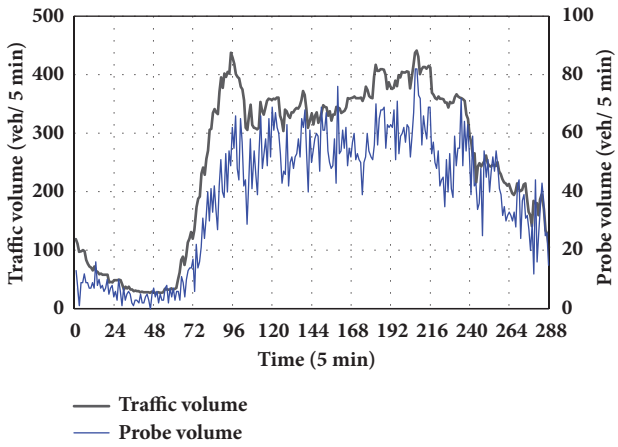

Figure 4: Temporal variation of traffic and probe volumes.

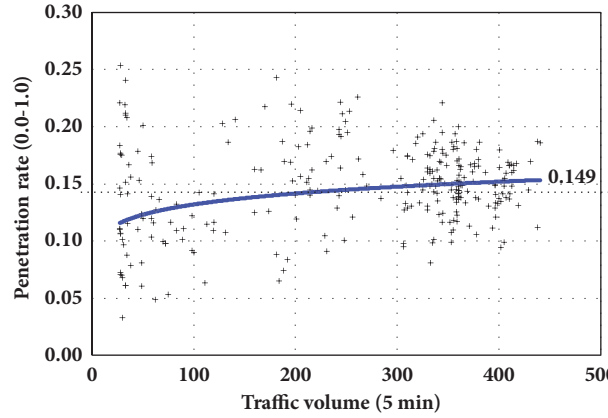

Figure 5: Penetration rate according to traffic volume.

proposed method in this paper. One-week individual point-to-point trajectory data was collected on December 24-30, 2016. The individual data was aggregated with a 5-minute interval. In addition, traffic volume data with a 5-minute aggregation was collected by an electronic toll collection system.

The temporal evolution of the two types of data are shown in Figure 4. The traffic volume varies from 27 to 442, and its temporal development reveals intensive variation in terms of relative percentage difference (RPD) (%), $[x(t+1) - x(t)]/x(t) \times 100$. RDP values range widely from -21.10 to 39.27. Regarding the probe volume ranges from 0 to 82, the RDP values vary from -100.0 to 800.0 except for a zero probe volume. As such, it is obvious that the temporal evolution of probe volumes exhibits more intensive and steep variation than that of traffic volumes by means of RDP. Despite these intensive variations, the statistical correlation between the two types of data is up to 0.933. This fact directly indicates that the probe volume is a direct portion of traffic volume and can reflect the features of traffic volume in some way.

Figure 5 shows the penetration rate (PR) of probe volume to traffic volume, where PR = [probe volume / traffic volume]. PR widely varies spanning from 0.06 to 0.25 with an average of 0.149. It seems that the evolution behavior of PR according to traffic volume is near to a mixed state but also has a closed boundary condition. The width of variation becomes narrower when traffic volumes increase, due to the fact that the sampling variability decreases when either the sample size (i.e., probe volume) increases or the variance of population (i.e., traffic volume) decreases. Moreover, a trend curve of PR shows logarithmic growth and increases when traffic volumes increase. This is because drivers have a tendency to use more vehicle navigation systems when their travel distance increases and because traffic congestion usually occurs at daytime.

To measure the performance of the propose method in this paper, the following four performance measures were carefully selected. Absolute percentage error (APE, %) and relative percentage error (RPE, %) provide a useful basis for comparison when traffic volume varies widely [15, 16]. APE and RPE have a weakness in the case of low traffic volume, as the relative temporal variation of low traffic volume is high. In this vein, straight error for lane (SEL, vehicles per lane), which can be useful in practice, is introduced in this study. The hit rate, one of crucial performance measures for real-life applications, was also utilized with RPE and SEL. In addition, the mean of APEs was employed to analyze and identify the optimal parameter values (i.e., d and m values)

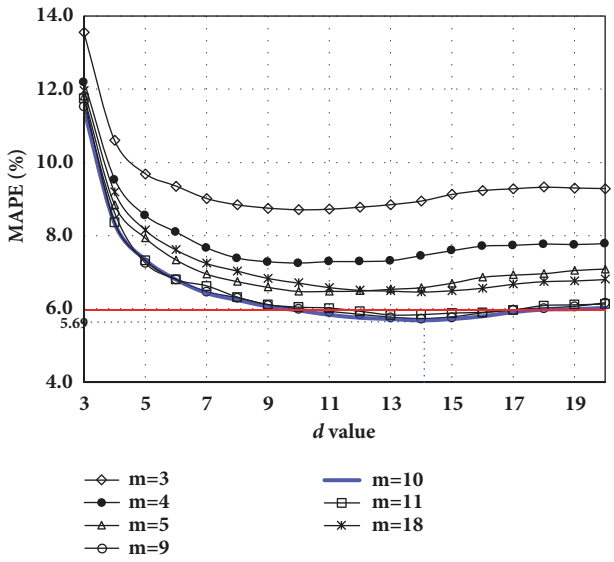

Figure 6: Effects of m and d values on estimation error rates.

of the presented method. APE, RPE, and SEL are expressed as

$$\text{APE}\,(\%) = \frac{\left|\hat{y}_i - y_i\right|}{y_i} \times 100, \quad y_i > 0.0 \tag{10}$$

$$\text{RPE}\,(\%) = \frac{\left(\hat{y}_i - y_i\right)}{y_i} \times 100, \quad y_i > 0.0 \tag{11}$$

$$\text{SEL}\,(\text{veh}) = \frac{\left(\hat{y}_i - y_i\right)}{l} \tag{12}$$

where y_i and $\hat{y}_i$ is the observed value and the estimated value of sample i, respectively, and l is the number of lanes.

4.2. Results and Findings. The proposed model was developed based on the combination of the contraction and conversion method (C2C). Hence, the performances of the C2C method are highly dependent on the m and d values in terms of estimation accuracy. The m and d values contribute key roles to contract the temporal variation of probe volumes, and the d value highly influences the determination of optimal curve fitting. The effects of the combination of the two parameter values on estimation accuracy are shown with estimation error rates in Figure 6. As for the m value, the estimation error curve steeply decreases (m=3⟶9) and then stays (m=9⟶11) at the optimal error space and then increases (m=11⟶18) when the d values are greater than 9. This indicates that a locality of temporal evolution of probe or traffic volumes exists in terms of moving average, even though the temporal development of probe and traffic volumes reveals intensive and steep variations. Regarding the d value, the estimation error exponentially decreases to the optimal error space and then gradually increases when the d value increases with little variation. This indirectly implies that a locality of temporal evolution of probe or traffic volumes exists in terms of determination of optimal relationship between probe and traffic volumes, whether the boundary condition is obvious or not. The optimal error space is very stable within a minimal error +0.5%, which indicates that suitable parameter values can be analyzed and determined within the margin of error on a daily or monthly basis in advance.

In addition, the optimal m and d values of 10 and 14, respectively, were selected for more analysis.

Two relationships between α and β values according to γ values are shown in Figures 7(a)-7(b), where the explanatory power of probe volume data is divided into two regimes with an obvious boundary condition. As for γ=0.0, the β value exponentially decreases when the α value increases, showing a high relationship with the R^2 value of 0.93. The cases of $\beta < 1.0$ reach to 83.02%. This means that the relationships between probe and traffic volumes are logarithmic in many cases. This fact also indicates that negative estimations inevitably arise in the case of very low probe volume if a linear relationship is used, which is directly connected to the prediction failure. Regarding the case of $\gamma > 0.0$, the β value steeply decreases according to the increment of the α value, and the two parameters are more highly connected than the upper relationship by means of R^2. The cases of $\beta > 1.0$ are up to 91.90%. This indicates that the relationships between probe and traffic volumes are upward in many cases. This fact also implies that the underestimation problem unavoidably occurs when probe volume is very low if a single linear relationship is employed. Therefore, it can be seen in our case that if a linear model is used, estimation failure inevitably occurs in the case of low traffic volume except for a few cases of $\gamma > 0.0$.

Figure 8 demonstrates the time-series variations of raw probe volumes and contracted probe volumes. Extreme variations, which can cause undesirable estimation results, are adjusted within the range of temporal variations of traffic volumes. The standard deviation of the RDP (SDRDP) of raw probe volume is 76.94%, whereas that of filtered probe volume is 7.73%. Similarly, adjustment gain is up to 89.95% [=(76.94-7.73)/76.94×100]. The SDRDP value of adjusted probe volume is also similar to that of traffic volume (7.45%). This suggests that extreme estimations can be effectively prevented through the contraction of temporal variation of probe volumes.

The relationships between probe volumes and traffic volumes for the before and after cases are shown in Figure 9. The contraction method effectively improves the relationship of the two variables in terms of R^2, where the R^2 value increases from 0.84 to 0.95. It can be seen at least that this result is acceptable, even considering that the natural attribute of R^2 increases when the number of observations increases. Specifically, the effect of variation contraction is distinguished in the case when traffic volumes are less than 100. This is because temporal traffic volumes exhibit less variation than that of probe volumes as shown in Figure 4. In the same context, the explanatory power of probe volumes is remarkably improved when traffic volumes are greater than 300.

The analysis results are summarized with three traffic volume regimes in Table 1, showing noticeable performances.

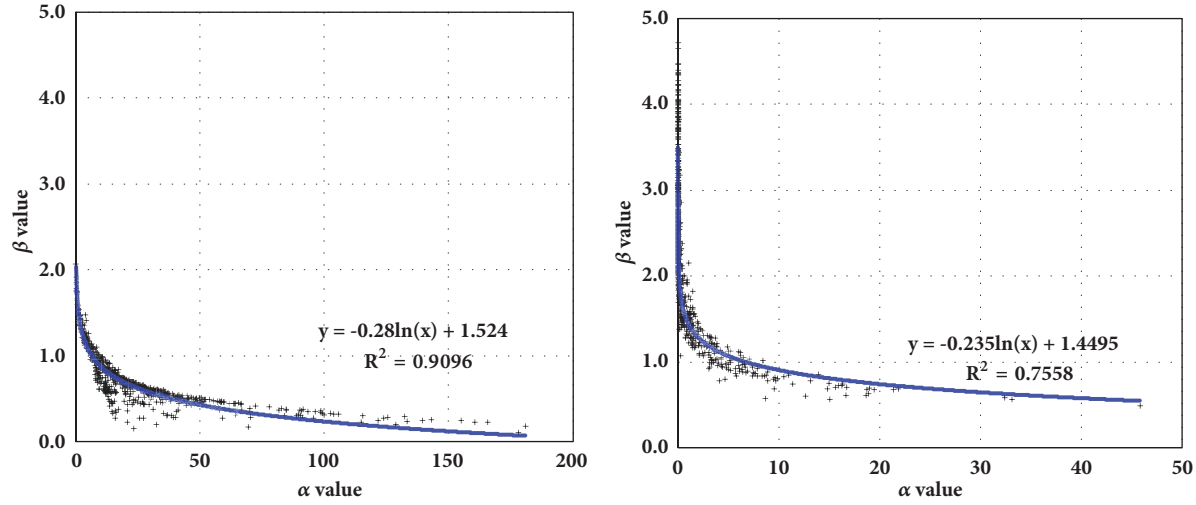

(a) γ =0.0 (b) γ >0.0

FIGURE 7: Relationships between α and β values according to γ values.

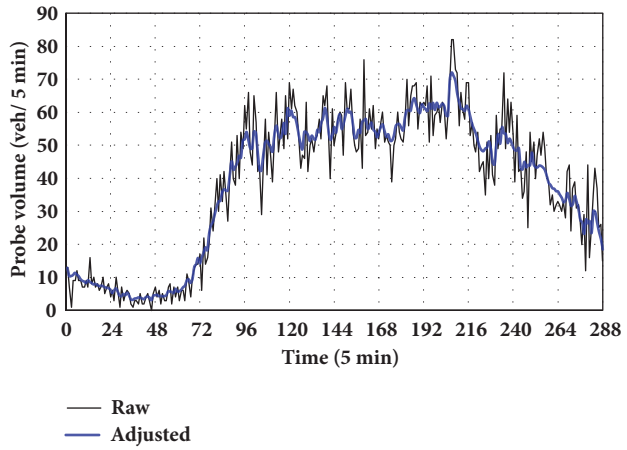

FIGURE 8: Temporal comparison of before and after contraction.

For all regimes, it can be seen that the accuracy performance of the C2C method is at least comparable to those of modern vehicle detectors in terms of the mean of APE (MAPE, %), 5.69%. Note that the accuracy performances of traffic counting for inductive loop, laser scanner, weight-in-motion (WIM) piezoelectric, and WIM quartz detectors in the case of 5-minute data aggregation were reported as 10.6, 24.1, 7.4, and 17.6% by means of MAPE, respectively [19]. The worst performances for APE and RPE measures are shown in the low-volume regime, excluding SEL as shown in Figures 10 and 11. The APEs are greater than 20% for several cases, which is undesirable from the standpoint of forecasting. Note that the tolerable detection error in the case of vehicle detectors should not vary from actual volumes by more than 20.0% [12]. Despite these undesirable performances, forecasting for the low regime can be also acceptable with the maximal SEL of 4.73, which is almost equal to one vehicle per one minute in practice. The hit rate within RPE±10.0% does not reach 90.0% for all regimes, whereas the hit rate within SEL±10 vehicles are up to 98.86%. On the contrary, in the cases of middle and heavy volume regimes, the APE values are less than 10.0% in most cases as shown in Figure 10, where the temporal variation of estimations concurs with that of the observations. The hit rate within RPE±10% is also up to 91.27%. In addition, the hit rate within RPE±20.0% for the middle and heavy regimes reaches 99.61% (Figure 11(a)). Moreover, the worst cases that span to -32.32% or +32.60% occur in the late-night hours, even though they are acceptable in terms of SEL within ±3.0 vehicles (Figure 11(b)). Note that the accuracy performances of the proposed method for the case of low traffic volume are comparable to those of pattern selection-based single-interval forecasting [15, 16] in terms of MAPE. Therefore, traffic volumes estimated from AV probe volumes can also be regarded as a promising option for traffic volume detection.

4.3. Present and Future Potentialities. For more real-world applications in the present and near future, more analysis for the potential of the C2C method was conducted through both the data-aggregation level and the penetration rate of AVs. Figure 12 shows the performances of the hit rate within RPE±10% according to data-aggregation levels. Note that accuracy performances (MAPE) for inductive loop, video image, laser scanner, WIM piezoelectric, and WIM quartz detectors in the case of 15-minute data aggregation were reported as 9.4, 34.1, 19.8, 5.7, and 12.3, respectively [19]. As for the 10-minute aggregation level, the hit rate reached 88.39% with the MAPE of 4.85% for all regimes and was up to 94.65% with the MAPE of 3.77% when traffic volume (vehicles/ 10 min) is greater than 200. In regard to the 15-minute and 30-minute aggregation levels, it can be seen that the performance of the C2C method is obviously comparable to the required detection accuracy for modern vehicle detectors. Accordingly, it is expected that the C2C method for directly monitoring traffic volumes can at least be feasible

Table 1: Summary of the results.

Performance Measures		All regimes Cases (volume)	Low regime 481 (<100)	Middle regime 532 (<300)	Heavy regime 1003 (300≤)
APE (%)	Mean	5.69	9.93	6.08	3.45
	Max.	32.60	32.60	21.62	15.74
	Median	3.98	8.41	5.04	2.73
RPE (%)	Mean	0.17	0.47	0.22	-0.01
	Max.	32.60	32.60	21.62	15.74
	Min.	-32.32	-32.32	-19.53	-12.53
	SD	7.91	12.51	7.67	4.42
	HR±10%	83.28	57.80	80.45	97.01
	HR±20%	96.83	87.94	98.87	100.00
SEL (veh)	Mean	-0.01	0.02	0.12	-0.10
	Max.	14.00	4.73	12.87	14.00
	Min.	-12.07	-6.02	-12.07	-11.89
	SD	3.45	1.49	3.74	3.92
	HR±5 veh	85.07	99.79	82.52	79.36
	HR±10 veh	98.86	100.00	98.87	98.31

Note: SD stands for standard deviation.

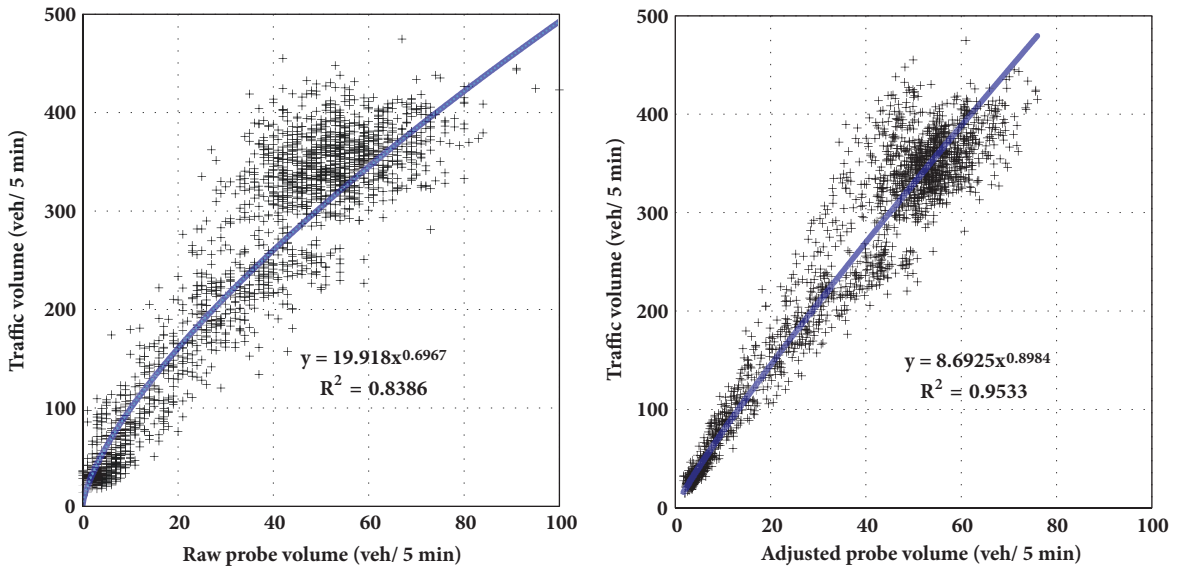

(a) Before adjustment (b) After adjustment

Figure 9: Efficacy of the contraction method.

as complementary means for the role of vehicle detectors if vehicle trajectory data is available with the penetration rate of 0.15%. Moreover, the levels of estimation reliability can be flexibly considered and employed according to the various tactics of traffic operation and control.

In order to demonstrate the potentialities of AV probe volume according to the penetration rate of AVs in the near future, we conducted a random simulation to generate temporal probe volume data. The penetration rate of the probe data used in our case study was employed for the basis of the probability of random selection (rather than a simple random sampling) to consider actual sampling rate. In addition, it is not easy for a random-sampling method to realistically mimic the temporal evolution of probe volumes while considering that of traffic volumes, due to the chaotic behaviors of traffic flow as mentioned before. The probability of selection was computed as

$$p_{sel} = \frac{PR_d}{PR_r} \tag{13}$$

where p_{sel} (0.0~1.0) is the probability of selection, PR_r (0.0-1.0) is the real-world penetration rate of probe volume to

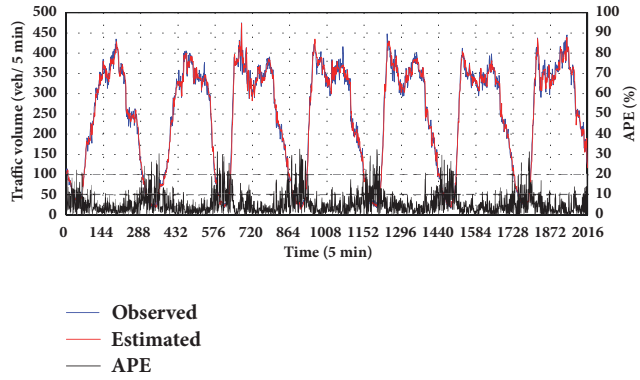

Figure 10: Temporal comparison of actual and estimated traffic volumes.

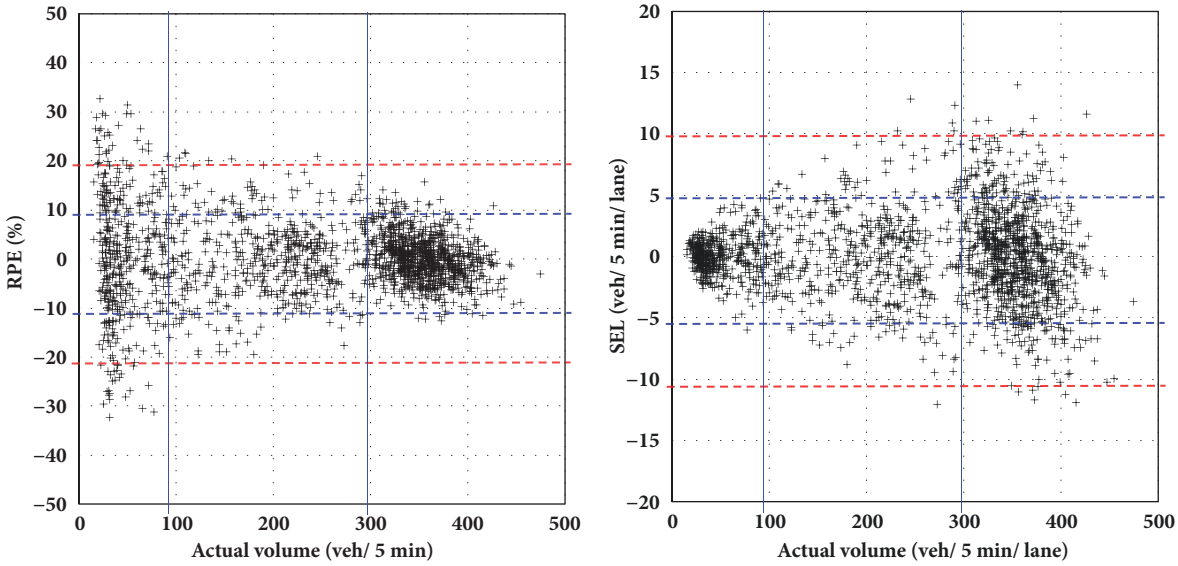

(a) Distribution of RPEs

(b) Distribution of SELs

Figure 11: Distributions of estimation errors according to traffic volumes.

traffic volume, and RP_d ($0.0 \leq PR_d \leq PR_r$) is a desired penetration rate. Thus, a random sample value for each time interval (t) was generated by using p_{sel} and a probe volume at (t). 14 scenarios of p_d from 0.01 to 0.14 were repeated twenty times for each probe volume data for the day time (06:00-24:00).

Figure 13 shows the performances of the C2C method according to each scenario with the median of 20 MAPE values. The estimation errors exponentially decrease when the penetration rate increases. The span of errors also decreases from 1.80% to 0.16% as the penetration rate increases. Based on the results, it can be seen that the monitoring accuracy of 93.77% can be accomplished within the maximum average error of 6.63% at the penetration rate of 0.05. In addition, it seems that the penetration rate of 0.10 can yield the monitoring accuracy of 94.78%. These analysis results suggest that the direct monitoring of real-time traffic volumes can be realized since the introduction of AVs to real roadways. There are also obvious possibilities that the monitoring accuracy can be improved dramatically according to the results of this study, where the error curve does not converge within a minimum error space. Furthermore, the probe volume of autonomous vehicles can be combined with that of a smartphone car navigation system (or a vehicle-GPS system) to guarantee the monitoring accuracy of real-time traffic volume until the market occupancy of AVs reaches a suitable level.

5. Conclusion Remarks

It is expected that autonomous vehicles can render new solutions to fundamental hindrances and unsolved academic issues in modern ITS. One of the fundamental hindrances is vehicle detectors that are essential for real-time traffic surveillance, which requires extensive budgets and resources in order to guarantee the reliability of monitored information. In addition, their spatial coverage of detection is constrained to fixed point or fixed short length.

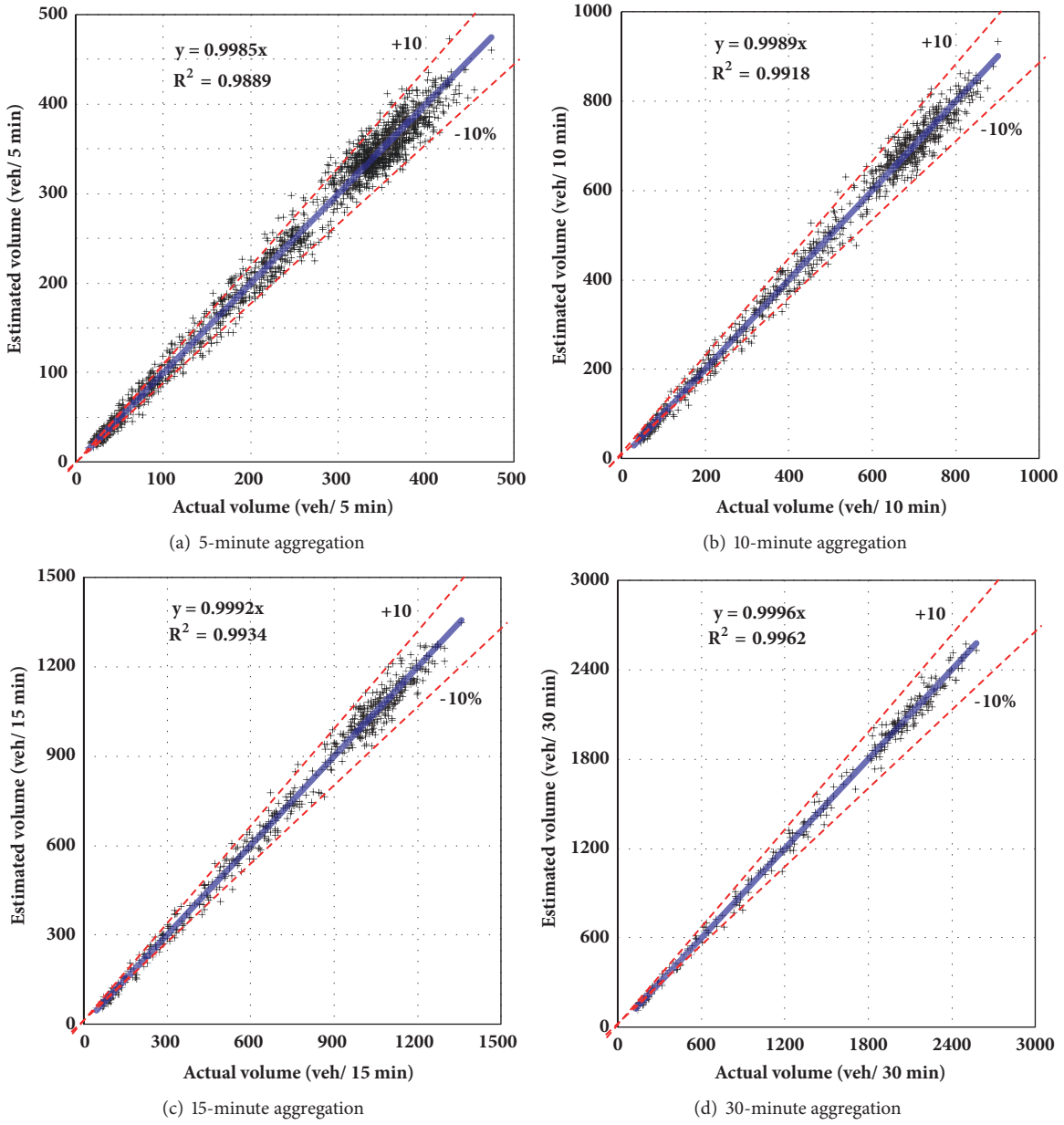

(a) 5-minute aggregation

(b) 10-minute aggregation

(c) 15-minute aggregation

(d) 30-minute aggregation

Figure 12: Predictability of the proposed model according to the aggregation level.

To realize this opportunity, a new concept for direct real-time monitoring was initiatively introduced in this paper. Using real-world probe volume data collected from a smartphone car navigation system, the potentialities of autonomous vehicles for direct monitoring of traffic volumes for road locations where real-time traffic volumes are desired were demonstrated with a novel and practical approach. The results were noticeable in terms of explanation of temporal variation of real-life traffic volumes. It turned out that the monitoring accuracy of the developed method is at least comparable to the actual detection accuracy of modern vehicle detectors, and it can reliably meet the required detection accuracy of vehicle detectors. Therefore, it can be seen that the direct monitoring of traffic volume is one of promising approaches to solve the current hindrance of traffic volume surveillance. In addition, the developed method is instantly feasible when probe volume data is available at least with the penetration rate of 0.05.

This study contributes a first step in proposing a promising solution to the direct monitoring of real-time traffic volumes. Despite the meaningful results of this research, there are other opportunities in direct real-time monitoring of traffic flow for unobserved road locations with advanced methodologies. We are still conducting investigations to improve the performance of the method and are searching for new potentialities in modern ITS.

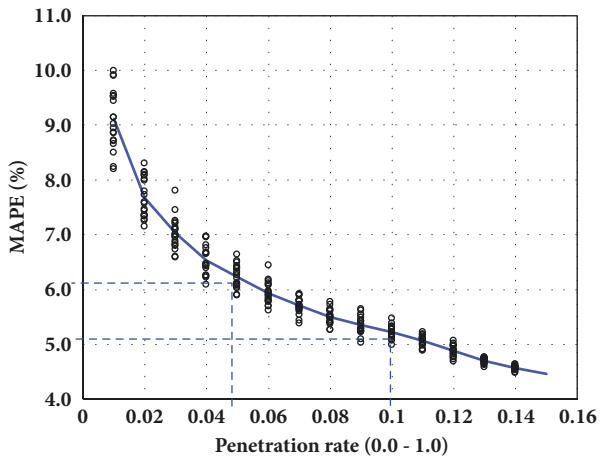

Figure 13: Predictability according to penetration rate.

Data Availability

The smartphone vehicle navigation data used to support the findings of this study were provided only for academic research by SK Telecom.

Conflicts of Interest

The authors declare that they have no conflicts of interest.

Acknowledgments

This work was supported by the University of Incheon (International Cooperative) Research Grant in 2014.

References

[1] F. Dion and H. Rakha, "Estimating dynamic roadway travel times using automatic vehicle identification data for low sampling rates," *Transportation Research Part B: Methodological*, vol. 40, no. 9, pp. 745–766, 2006.

[2] X. Li, W. Shu, M. Li, H.-Y. Huang, P.-E. Luo, and M.-Y. Wu, "Performance evaluation of vehicle-based mobile sensor networks for traffic monitoring," *IEEE Transactions on Vehicular Technology*, vol. 58, no. 4, pp. 1647–1653, 2009.

[3] X. Zhan, S. Hasan, S. V. Ukkusuri, and C. Kamga, "Urban link travel time estimation using large-scale taxi data with partial information," *Transportation Research Part C: Emerging Technologies*, vol. 33, pp. 37–49, 2013.

[4] H. Bar-Gera, "Evaluation of a cellular phone-based system for measurements of traffic speeds and travel times: a case study from Israel," *Transportation Research Part C: Emerging Technologies*, vol. 15, no. 6, pp. 380–391, 2007.

[5] K. Sohn and K. Hwang, "Space-based passing time estimation on a freeway using cell phones as traffic probes," *IEEE Transactions on Intelligent Transportation Systems*, vol. 9, no. 3, pp. 559–568, 2008.

[6] A. Janecek, D. Valerio, K. A. Hummel, F. Ricciato, and H. Hlavacs, "The Cellular Network as a Sensor: From Mobile Phone Data to Real-Time Road Traffic Monitoring," *IEEE Transactions on Intelligent Transportation Systems*, vol. 16, no. 5, pp. 2551–2572, 2015.

[7] J. C. Herrera, D. B. Work, R. Herring, X. Ban, Q. Jacobson, and A. M. Bayen, "Evaluation of traffic data obtained via GPS-enabled mobile phones: the Mobile Century field experiment," *Transportation Research, Part C: Emerging Technologies*, vol. 18, no. 4, pp. 568–583, 2010.

[8] G. Guido, V. Gallelli, F. Saccomanno, A. Vitale, D. Rogano, and D. Festa, "Treating uncertainty in the estimation of speed from smartphone traffic probes," *Transportation Research Part C: Emerging Technologies*, vol. 47, no. 1, pp. 100–112, 2014.

[9] M. Chen and S. I. J. Chien, "Determining the number of probe vehicles for freeway travel time estimation by microscopic simulation," *Transportation Research Record*, no. 1719, pp. 61–68, 2000.

[10] M. Chen and S. I. J. Chien, "Dynamic freeway travel time prediction using probe vehicle data," *Transportation Research Record*, no. 1768, pp. 157–161, 2001.

[11] W. Deng, H. Lei, and X. Zhou, "Traffic state estimation and uncertainty quantification based on heterogeneous data sources: A three detector approach," *Transportation Research Part B: Methodological*, vol. 57, pp. 132–157, 2013.

[12] N. Caceres, L. M. Romero, F. G. Benitez, and J. M. Del Castillo, "Traffic flow estimation models using cellular phone data," *IEEE Transactions on Intelligent Transportation Systems*, vol. 13, no. 3, pp. 1430–1441, 2012.

[13] N. Caceres, L. M. Romero, and F. G. Benitez, "Inferring origin-destination trip matrices from aggregate volumes on groups of links: A case study using volumes inferred from mobile phone data," *Journal of Advanced Transportation*, vol. 47, no. 7, pp. 650–666, 2013.

[14] E. I. Vlahogianni, M. G. Karlaftis, and J. C. Golias, "Statistical methods for detecting nonlinearity and non-stationarity in univariate short-term time-series of traffic volume," *Transportation Research Part C: Emerging Technologies*, vol. 14, no. 5, pp. 351–367, 2006.

[15] B. Yoon and H. Chang, "Potentialities of data-driven non-parametric regression in urban signalized traffic forecasting," *Journal of Transportation Engineering*, vol. 10, 2014.

[16] H. Chang and B. Yoon, "High-speed data-driven methodology for real-time traffic flow predictions: practical applications of ITS," *Journal of Advanced Transportation*, vol. 2018, Article ID 5728042, 11 pages, 2018.

[17] F. Fotheringham, C. Brunsdon, and M. Charlton, *Geographically weighted regression: the analysis of spatially varying relationship*, Wiley, Chichester, England, 2003.

[18] D. Mohamad, K. Sinha, T. Kuczek, and C. Scholer, "Annual average traffic prediction model for county roads," *Transportation Research Record*, no. 1617, pp. 69–77, 1998.

[19] P. Bellucci and E. Cipriani, "Data accuracy on automatic traffic counting: The SMART project results," *European Transport Research Review*, vol. 2, no. 4, pp. 175–187, 2010.

Hindawi
Journal of Advanced Transportation
Volume 2018, Article ID 5679064, 10 pages
https://doi.org/10.1155/2018/5679064

WILEY | Hindawi

Research Article

A Separation Strategy for Connected and Automated Vehicles: Utilizing Traffic Light Information for Reducing Idling at Red Lights and Improving Fuel Economy

Lin-heng Li, Jing Gan, and Wen-quan Li

School of Transportation, Southeast University, China

Correspondence should be addressed to Lin-heng Li; leelinheng@seu.edu.cn

Received 6 March 2018; Revised 16 June 2018; Accepted 17 July 2018; Published 29 July 2018

Academic Editor: Md. A. S. Kamal

Vehicle platoon composed of a group of connected and automated vehicles (CAVs), a coordinated movement strategy, has been widely proposed to address a range of traffic problems. The motion of vehicle in the platoon passing signalized intersections can significantly affect their total trip time and fuel consumption. With the development of advanced communication technology such as V2V and V2I, CAVs can automatically obtain and use the upcoming traffic light timing information to find optimal velocity profiles that can avoid idling at red lights. This paper proposes an optimal velocity control and separation strategy for the platoon to minimize the trip time and reduce fuel consumption as much as possible. Simulation results show that with the introduction of the velocity control and separation strategy, the total trip time and fuel consumption decrease by 19.2% and 18.1%, respectively. Thus the effectiveness of the proposed strategy is demonstrated.

1. Introduction

In the connected and automated vehicles (CAVs) system, vehicles are capable of sharing information and sensing local environment with each other via the advanced communication technologies (e.g., V2V and V2I). The vehicles' information (e.g., location and velocity) and the road transportation infrastructure information (e.g., the traffic light timing, including the phase cycle length, the green phase length, and the start of the first green phase) will be obtained by every vehicle. After receiving such information, the internal decision-making mechanism will make corresponding driving decisions and then achieve the level of automatic driving. Under this circumstance, all CAVs will be platooned through communication and automated control technologies [1]. With CAV platooning, consecutive vehicles are similar to two concatenated carriages of a train and thus shall have much less time headway compared with a pair of conventional human driven vehicles.

All these potential benefits are linked to the expectation that CAVs can significantly improve traffic capacity, efficiency, and safety [2–5]. Studies by Lioris et al. have shown that traffic capacity at signalized intersections could be doubled when vehicles on the road are connected to an intelligent network without changing the signal control [6, 7]. Chang and Edara also examined whether the road traffic efficiency could be further improved under CAVs environment [8].

World Oil Outlook 2016, issued by Organization of Petroleum Exporting Countries (OPEC), predicted that most of the oil consumed today and in the future will come from the road transportation sector. By 2040, the road transportation sector will represent 44% of global oil demand [9]. All the benefits provided by vehicle platooning are also linked to reduce fuel consumption. Lammert et al. conducted a comprehensive investigation on the effect of platooning on fuel consumption of class 8 vehicles, and they found saving of up to 6% for the leading vehicle and 10% for the following vehicle [10]. Alam et al. proposed a particular test to study the fuel reduction that heavy duty vehicle platooning enables and the analysis with respect to the influence of a commercial adaptive cruise control on the fuel consumption [11]. Tsugawa et al. presented an automated truck platoon that has been developed under a national ITS project named Energy ITS;

the results in their study show that the fuel can be saved by about 14 % [12].

Even if vehicle platooning has a certain advantage in traffic capacity improvement and fuel-saving, a huge wastage of traffic capacity and fuel will occur due to the stoppage at signalized intersection during its red phase. Idling at red lights will decrease traffic capacity and increase fuel consumption from many aspects:

(**1**) **Stop-and-go motion.** X. Zhang et al. proved that fuel consumption and exhaust gas emission can remarkably decrease when the acceleration and deceleration of vehicles are pretty gentle; idling at red light or traveling in a mode of stop-and-go will consume more fuel and emit more greenhouse gases comparing with the vehicles in free flow [13]. Research by Wan N et al. emphasized that, due to vehicles' stop-and-go motion, they need to consume more energy than that during cruising [14].

(**2**) **Intersection delays.** Intersection delays may include queue delay and control delay. Ch. Ravi Sekhar et al. estimated delay and fuel loss during idling at signalized intersections. The simulation results showed that heavy delays and a huge wastage of fuel at intersections are caused due to stoppage of vehicles during the red phase of the signals, because many vehicles need to stop as a consequence of their arrival either during the red interval or during the green interval when the queue of vehicles that had formed during the previous red interval has not yet fully dissipated [15].

(**3**) **Congestion.** On the other hand, heavy delays at intersections may result in traffic congestion especially in heavy volume arterial corridor, which will cause a large amount of financial loss, including more traffic capacity and fuel loss. INRIX, a joint traffic data company in London, quantitatively analyzed the impact of traffic congestion on Britain, France, Germany, and the United States. In 2013, the four countries lost 200 billion dollars caused by traffic congestion, accounting for 0.8% of the total GDP of the four countries.

Therefore, a number of benefits can be obtained in limiting the idling time at red light. These benefits include increasing traffic efficiency, saving in fuel use, reduction in exhaust emissions, and even vehicle life extension. In recent years, the exponential increase in the number of vehicles in urban city has resulted in congestion and more fuel consumption at intersections. Traffic efficiency improvement and fuel economy have been paid more attention than ever. Thus, from the perspective of traffic efficiency improvement, travel comfort, and traffic energy conservation, it is of great importance to keep the traffic flow smooth and reduce red light idling.

Besides the fuel wastage at intersection due to the operation of signals, fuel consumption can also be affected by other factors along the entire trip, such as cruising speed, the intervehicle distance, and traffic conditions [16]. With the advanced control system installed on CAVs, all the vehicles can realize autonomous velocity control along the entire trip. Motivated by the problems mentioned above, this paper investigates one optimal platoon velocity control and separation strategy defined to find the optimal velocity profiles on signalized arterials that can avoid idling at red lights and improve fuel economy along the entire trip.

The rest of this paper is organized as follows. Section 2 introduces the conceptualization of vehicle platoon and analyzes the optimization goals in this study. Section 3 proposes the optimal platoon separation and velocity control strategy used in this paper to minimize the trip time and reduce the fuel consumption. The simulation results are presented and discussed in Section 4, and conclusion is given in Section 5.

2. Problem Statement

In this section, the conceptualization of the vehicle platoons in a short length is firstly introduced. Then the objective function of reducing the platoons idling at red lights is formulated. Finally, the formula for the minimum fuel consumption is introduced.

2.1. Conceptualization of Vehicle Platoons. Maiti et al. provided a detailed concept of vehicle platoon [1]. A vehicle platoon generally consists of one leader vehicle and a number of follower vehicles. The leader vehicle takes all decisions on behalf of the whole platoon and controls all the platoon members accordingly; all vehicles in the same platoon share the same velocity. Each platoon has its own ID. And the size of platoon is a dynamic property, which implies the current number of vehicles in platoon; the maximum size of a platoon means the maximum number of vehicles grouping together in a platoon. Each vehicle in a platoon also has its vehicle ID. As mentioned above, the role of a vehicle can be divided into leader vehicle and follower vehicle; the role may get updated by platoon operations (e.g., separation or merging), which means follower vehicle may change into leader vehicle when doing the separation operation, and leader vehicle will also become follower vehicle when the merging operation happens.

A platoon of CAVs is actually a network of dynamical systems, S. E. Li et al. presented a four-component framework to model, analyze, and synthesize a platoon of CAVs from the perspective of multiagent consensus control [17]. When a platoon is driving on the road, the leader vehicle can communicate with the transportation infrastructure relying on the V2I technology. The leader vehicle transmits the platoon's position, size, destination, and other traffic parameters to the transportation infrastructure, to avoid idling at red lights; the leader vehicle can obtain feedback velocity information from the control center who can give feedback on optimal velocity to the leader vehicle according to the green light duration and traffic flow information. When the leader vehicle receives the velocity information, it will transfer this velocity information to other follower vehicles immediately through V2V technology. Therefore vehicles in the same platoon can share the same velocity and then achieve unified operation; the platoon driving schematic diagram can be shown in Figure 1. As for the quality of information flow exchange among vehicles, some scholars addressed the internal stability and scalability issue for platoon under different information topologies; e.g., Y. Zheng et al. have studied the influence of information flow topology on the

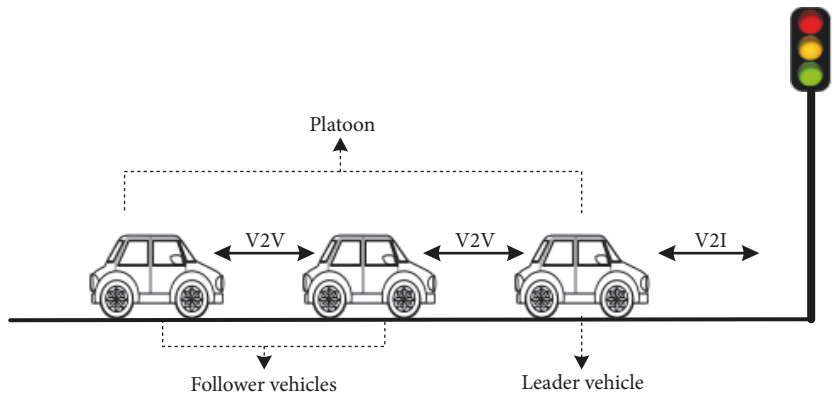

FIGURE 1: Platoon driving schematic diagram.

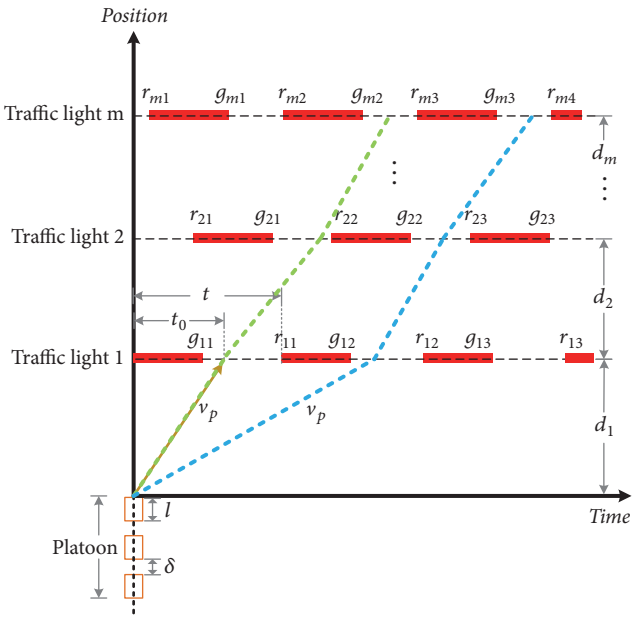

FIGURE 2: Schematic of the trajectory and velocity of leader vehicle.

internal stability and scalability of homogeneous vehicular platoon [18].

2.2. Idling at Red Light. The process of vehicle stopping at the red light and leaving when the light turns green is actually the stop-and-go motion, as mentioned in Section 1; in order to enhance vehicles' safety, energy efficiency, and mobility, the idling at the red light should be reduced as much as possible.

The schematic of the candidate trajectory and velocity of the leader vehicle at each intersection is shown in Figure 2; the green and the blue dotted lines denote the candidate trajectories of the leader vehicle in a platoon at different velocity, with the parameters defined as follows:

(1) The traffic light information of ith intersection is represented by $\{r_{ij}, g_{ij}\}; i = 1, 2, \cdots m$, $j = 1, 2 \cdots \infty$, where r_{ij} is the start of jth red phase and g_{ij} is the start of jth green phase at ith signalized intersection.

(2) d_i is the distance between consecutive intersections, that is, the distance between the i-1st traffic light and the ith traffic light (called ith segment); in particular, for a platoon, d_1 is the distance to the first upcoming traffic light and the d_2 is the distance between the first upcoming traffic light and the second traffic light, which can be estimated from the vehicle's GPS and the traffic light's location information.

(3) Let l denote average length of a vehicle and δ represent Gap distance between a pair of consecutive vehicles in a platoon

Our goal is to find a permit velocity of platoon which aids in minimizing idling at the red light. The problem of idling at the red light can be transformed into the platoon's waiting time at the traffic light. Based on the signal timing information and platoon information, total waiting time of all vehicles at all traffic lights can be calculated as

$$Z = \sum_{k=1}^{n} \sum_{i=1}^{m} \left\{ t_r^i - \mathrm{mod} \left[\frac{d_i + \theta v_p^i(k) + (k-1)(l+\delta)}{v_p^i(k)\, t_{cycle}^i} \right] \right\} \quad (1)$$

where

Z is the sum of the platoon's waiting time at all the traffic lights;

k is the vehicles' ID number in a platoon, $k = 1, 2, \cdots n$;

i is the traffic lights' number during the trip, $i = 1, 2, \cdots m$;

t_r^i is the red light duration in the ith traffic light, $t_r^i = g_{ij} - r_{ij}$;

θ is the compensation time, for the case of $r_{i1} \neq 0$;

$v_p^i(k)$ is the passing velocity of kth vehicle in a platoon at ith signalized intersection;

t_{cycle}^i is the cycle of traffic signals at the ith traffic light; $t_{cycle}^i = g_{i,j} - g_{i,j-1}$ or $r_{i,j} - r_{i,j-1}$.

Vehicles in the same platoon share the same velocity; *i.e.*, $v_p^i(k) = v_p^i$, where v_p^i denotes the passing velocity of a platoon at ith signalized intersection whose unit is m/s. Specifically, Z only takes a result greater than 0; that is, when the operation result of Z is less than 0, the final result of Z is equal to 0.

2.3. Fuel Consumption. Before studying the influence of idling at red light and velocity on fuel consumption, we introduce the fuel consumption model. Many efforts have been made to understand the relationship between traffic activities and fuel consumption rate; many researchers modeled fuel consumption as a function of vehicle load and average speed [19–22]. There are a number of microscopic fuel consumption models; we use the model proposed by Kamal et al. [23]. This is because of its simplicity; calculating the fuel consumption only uses the instantaneous velocity of platoon. Based on this model, optimal velocity could be found to minimize fuel consumption. Kamal et al. sampled sufficient data from a passenger size vehicle and fitted it into a third order polynomial curve that approximates the relation between fuel consumption rate and velocity. In this model, the fuel consumption rate $\dot{m}$ is estimated as

$$\dot{m} = \alpha_0 + \alpha_1 v_p^i + \alpha_2 \left(v_p^i\right)^2 + \alpha_3 \left(v_p^i\right)^3 \tag{2}$$

where α_0, α_1,α_2, and α_3 are corresponding coefficients, whose values are presented in Table 3.

Hence, during the whole trip, for each vehicle in the same platoon, the fuel consumption can be calculated as

$$J = \left[\alpha_0 + \alpha_1 v_p^i + \alpha_2 \left(v_p^i\right)^2 + \alpha_3 \left(v_p^i\right)^3\right] t_i(k) \tag{3}$$

where $t_i(k)$ represents the trip time of kth vehicle of platoon in ith segment.

Assuming that all the vehicles run at constant speed in each segment ignoring the acceleration or deceleration process, then, for all vehicles in a platoon passing all the intersections without idling, the total fuel consumption can be calculated as

$$J = \sum_{k=1}^{n}\sum_{i=1}^{m}\left[\frac{\alpha_0}{v_p^i} + \alpha_1 + \alpha_2 v_p^i + \alpha_3 \left(v_p^i\right)^2\right] \cdot \left[d_i + (k-1)(l+\delta)\right]. \tag{4}$$

2.4. Optimization Problem and Complexity Analysis. The objective of this paper is to minimize two performance indexes $Z = f(v_p^i(k))$ and $J = f(v_p^i(k))$, *i.e.*, the waiting time at red lights and fuel consumption, by determining velocity profiles $v_p^i(k) = \{v_1, v_2, \ldots v_m\}$ for each vehicle at each segment subject to certain constraints, which will be introduced in detail in Section 3. Obviously, the total waiting time at all the traffic light can be reduced to 0 as long as all the vehicles pass with a suitable velocity to ensure no idling at red light.

Y. Zheng et al. analyzed the complexity of a known green light optimal velocity (GLOV) problem, finding, e.g., optimal velocity that can avoid idling at red lights and minimize the trip time [24]. The complexity analysis shows that GLOV with binary velocity choices belongs to NP-complete, which means it cannot be numerically solved in polynomial time unless P=NP. Intuitively, it is much more difficult to solve this problem with more velocity choices; the number of possible solutions will increase exponentially.

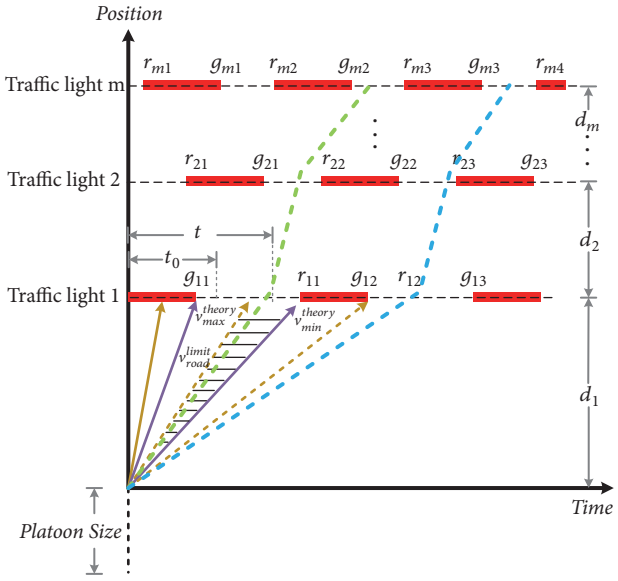

FIGURE 3: Allowable velocity bound for platoon.

In order to ensure effective solution to our proposed problem, approximation algorithm is proposed in the following optimization strategy. We consider finding optimal velocity profiles for each platoon to save fuel consumption as much as possible while ensuring the improvement of traffic efficiency, that is, to let the maximum number of vehicles pass without idling at red light as much as possible even if the current velocity does not guarantee the lowest fuel consumption.

3. Optimization Strategy

This section focuses on the introduction and analysis of optimization strategy to solve the problem defined in Section 2.

3.1. Allowable Bounds Analysis for Optimal Velocity Selection. To ensure that all the vehicles in the platoon could pass all the traffic lights without idling at red lights, it must be firstly met that the leader vehicle in a platoon can pass through the intersection during its green phase. The allowable velocity bound for a platoon is shown in Figure 3, with the parameters defined as follows:

(1) $v_{max}^{theory}(i,j)$ and $v_{min}^{theory}(i,j)$ represent the maximum and minimum theory velocity of the leader vehicle of a platoon to pass the ith traffic light without idling during its jth green phase, respectively. Assuming that the vehicles run at constant speed in each segment ignoring the acceleration or deceleration process, then the maximum and minimum theory

velocity for the leader vehicle can be calculated as $v_{max}^{theory}(i,j) = d_i/g_{ij}$, $v_{min}^{theory}(i,j) = d_i/r_{ij}$.

(2) v_{road}^{limit} denotes the maximum velocity limit of the road, which is specified by the government agency on each segment. In this paper, assuming that it is the same for all segments along the road and setting it as 20m/s in following simulation, it is worth noting that its value may be greater or less than v_{max}^{theory}, or even equal to v_{max}^{theory}.

(3) Let $v_{max}^{permit}(i,j)$ present the maximum passing velocity for a platoon to pass the intersection without idling.

For example, if $[v_{min}^{theory}(1,1), v_{max}^{theory}(1,1)] \cap [0, v_{road}^{limit}] \neq \emptyset$ and the leader vehicle wants to pass the first upcoming traffic light during the first green light, the passing velocity v_p should belong to the set intersection$[v_{min}^{theory}(1,1), v_{max}^{theory}(1,1)] \cap [0, v_{road}^{limit}]$, as shown in the shaded part in Figure 2. In this case,

$$v_{\max}^{permit}(i,j) = \begin{cases} \min\left\{v_{\max}^{theory}(i,j), v_{road}^{\lim it}\right\}, & \text{if } v_{\max}^{theory}(i,j) \neq v_{road}^{\lim it} \\ v_{\max}^{theory}(i,j) = v_{road}^{\lim it}, & otherwise. \end{cases} \quad (5)$$

However, if $v_{road}^{limit} < v_{min}^{theory}(1,1)$ which means$[v_{min}^{theory}(1,1), v_{max}^{theory}(1,1)] \cap [0, v_{road}^{limit}] = \emptyset$, the leader vehicle has to decrease current velocity and pass the first upcoming traffic light in its second green phase only if $[v_{min}^{theory}(1,2), v_{max}^{theory}(1,2)] \cap [0, v_{road}^{limit}] \neq \emptyset$, as shown by the blue dotted line in Figure 3; the passing velocity should also follow the restriction of $v_p \in [v_{min}^{theory}(1,2), v_{max}^{theory}(1,2)] \cap [0, v_{road}^{limit}]$.

To sum up, the leader vehicle will find the possibility of passing during jth green phase at ith signalized intersection until the set intersection $[v_{min}^{theory}(i,j), v_{max}^{theory}(i,j)] \cap [0, v_{road}^{limit}]$ is not empty. That is, to ensure that all vehicles can pass all the traffic lights without idling, our optimal velocity solution v_p^i for a platoon should satisfy

$$v_p^i \in \left[\frac{d_i}{r_{ij}}, \frac{d_i}{g_{ij}}\right] \cap \left[0, v_{raod}^{limit}\right] \neq \varnothing, \quad j = 1, 2, \cdots \infty. \quad (6)$$

3.2. Velocity Control and Separation Strategy of Platoon. The detailed process of separation strategy of platoon will be introduced in this section.

According to the concept of vehicle platooning, all vehicles in the same platoon share the same velocity, which means the follower vehicles' trajectory will be parallel to the trajectory of the leader one. If we draw a line parallel to the v_p^i velocity line of the leader vehicle, the intercept on the position axis is the maximum platoon size that can pass the ith intersection during one of its green phases, as shown in Figure 4. It is easy to find that the number of vehicles of a platoon that can pass without idling will increase with the increase of passing velocity.

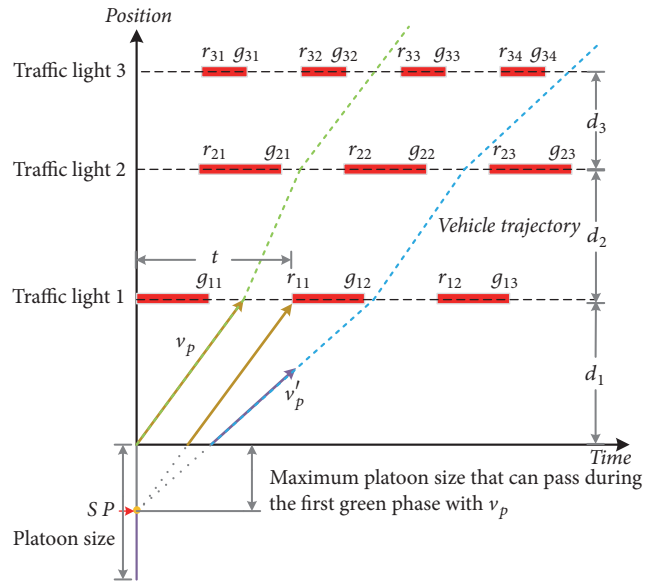

FIGURE 4: Schematic of the separation strategy.

Let $L(v_p)$ denote the maximum platoon size at velocity v_p and $L(platoon)$ represent the real platoon size.

$$L(v_p) = v_p r_{ij} - d_i$$
$$L(platoon) = (n-1)(l+\delta) \quad (7)$$

If $L(v_p)$ is less than $L(platoon)$, some follower vehicles will stop at the red light if they keep the current velocity. To avoid idling at red light for the rest vehicles, they need to decelerate to pass during the next green phase. In other words, the rest vehicles should separate from the original platoon and recombine to a new platoon, that is, our proposed velocity and separation strategy. A new replanning velocity v_p' will be given to this new platoon to ensure that the maximum number of vehicles in this new platoon can pass the traffic light in the next green light.

The maximum number of vehicles that can pass during the first green phase at the first upcoming intersection can be calculated as

$$n_p = \left\lceil \frac{v_p t - d_1}{l+\delta} \right\rceil. \quad (8)$$

As introduced in Section 2.1, each platoon has its own ID, and the vehicles in each platoon also have their own IDs, respectively (e.g., the leader vehicle, 2nd vehicle,. . ., n_pth vehicle, (n_p+1)th vehicle,. . .,mth vehicle). When the platoon needs to do the separation strategy, the leader vehicle will send the separation command to the $(n_p + 1)$th vehicle, who will become the new leader vehicle of a new platoon and obtain a replanning velocity v_p'. Therefore, there exist a separation point (SP) between n_pth vehicle and$(n_p + 1)$th vehicle, as shown in Figure 4.

Vehicles before the separation point (SP) belong to the original platoon, which will pass the first intersection during

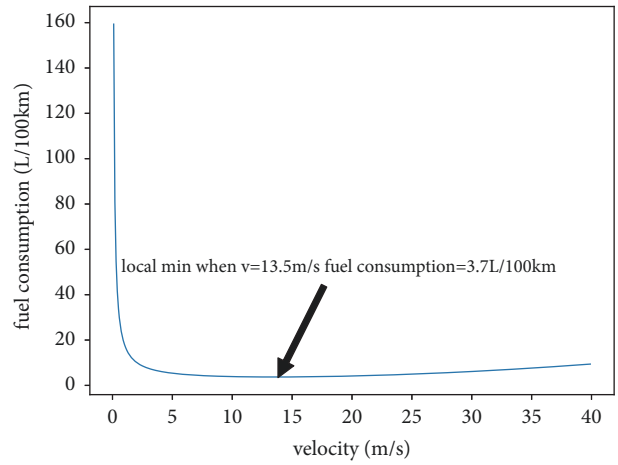

FIGURE 5: The fuel consumption at different velocity.

its first green phase. The new platoon consists of those vehicles behind SP that need to decelerate to v_p' to avoid idling at red light. The velocity space for the replanning velocity v_p' is similar to the passing velocity v_p except $j = 2, 3, \cdots \infty$.

$$v_p' \in \left[\frac{v_p t}{r_{ij}}, \frac{v_p t}{g_{ij}}\right] \cap \left[0, v_{road}^{limit}\right] \neq \varnothing, \quad \mathrm{j} = 2, 3, \cdots \infty \tag{9}$$

Let $v_{optimal}^{fuel}$ denote the optimal velocity in case of lowest fuel consumption. According to the fuel consumption formula (4) with the parameters' value in Table 3, we can see that when the velocity is equal to 13.5m/s, the fuel consumption is minimal, as shown in Figure 5. That is $v_{optimal}^{fuel} = 13.5m/s$.

On the one hand, our first goal in this paper is to improve traffic efficiency by avoiding idling at red light; at each section for a platoon, we can choose the maximum passing velocity v_{max}^{permit} for a platoon, which can ensure that maximum number of vehicles can pass without idling. On the other hand, a goal to minimize fuel consumption as much as possible is also taken into consideration in this paper as mentioned in Section 2. Obviously, the optimal fuel velocity does not necessarily satisfy the need for letting maximum number of vehicles pass at each green phase. In other words, the maximum passing velocity v_{max}^{permit} is not necessarily the most fuel-efficient. Hence, a velocity control strategy is also considered based on the separation strategy. The velocity control and separation strategy to obtain the optimal platoon velocity profiles for all vehicles in the platoon is shown in Figure 6.

Take the first intersection, for example; one optimal solution to the problem defined in Section 2 can be constructed by the following steps:

Step 1. Check if $v_{optimal}^{fuel}$ belongs to the interval$[v_{min}^{theory}(1,1), v_{max}^{permit}(1,1)]$, where $v_{max}^{permit}(1,1)$ satisfies (5); if it belongs to it, turn to Step 2; otherwise, turn to Step 3.

Step 2. Compare the maximum platoon size $L(v_{optimal}^{fuel})$ at velocity $v_{optimal}^{fuel}$ and the actual platoon size L($platoon$), which can be calculated according to (7). If $L(v_{optimal}^{fuel}) \geq L(platoon)$, which means that all vehicles in the original platoon can pass the first intersection during its first green phase with velocity $v_{optimal}^{fuel}$, then choose the passing velocity $v_p = v_{optimal}^{fuel}$. Otherwise, turn to Step 3.

Step 3. Compare the platoon size $L(v_{max}^{permit})$ with velocity v_{max}^{permit} and the actual platoon size $L(platoon)$. If $L(v_{max}^{permit}) \geq L(platoon)$, which means that the platoon can pass the intersection with a velocity below v_{max}^{permit}, taking into account fuel economy, the platoon pass with velocity v_p that minimizes the fuel consumption:

$$v_p = \begin{cases} v_{min}^{all} & if\ J\left(v_{min}^{all}\right) \leq J\left(v_{max}^{permit}\right) \\ v_{max}^{permit} & if\ J\left(v_{min}^{all}\right) > J\left(v_{max}^{permit}\right) \end{cases} \tag{10}$$

where v_{min}^{all} means the minimum velocity that can ensure all vehicles pass without idling when $L(v_{max}^{permit}) \geq L(platoon)$.

$$v_{min}^{all} = \frac{(n-1)(l+\delta) + d_1}{r_{11}} \tag{11}$$

If $L(v_{max}^{permit}) < L(platoon)$, which means that all vehicles cannot pass the intersection during its first green phase, even with the max velocity, then turn to Step 4.

Step 4. The original platoon is separated into two new platoons: platoon 1.1 and platoon 1.2. To ensure that as many vehicles as possible can pass the intersection within a green phase, the new platoon 1.1 will pass the intersection with velocity v_{max}^{permit}. And for the new platoon 1.2, return to Step 1 again to find an optimal passing velocity v_p' to pass the intersection during its next green phase.

For the remaining intersections, the process to find the optimal velocity solution is almost similar to the above steps, except that at Step 1, we check if $v_{optimal}^{fuel}$ belongs to $[v_{min}^{theory}(i,1), v_{max}^{permit}(i,1)]$ for ith intersection.

4. Simulation Case Studies

The route is assumed to have 4 intersections, and the parameters of the traffic light location and timing information are shown in Table 1. The platoon and road information is shown in Table 2. The parameter values of fuel economy model (5) are shown in Table 3. The simulations are run in MATLAB on an Intel® Core™i7 processor with 3.40 GHz processing speed per core, 8 GB of RAM.

4.1. Simulation 1: Conventional Strategy without Separation Strategy. Firstly, we study the case of conventional strategy; the separation strategy is not activated.

In the simulation, we consider a platoon of 20 vehicles. Figure 7 shows the simulation results of the velocity profile of

Table 1: Traffic light location and timing information.

	d_i (m)	t_r^i (s)	t_{cycle}^i (s)	r_{i1} (s)
$i = 1$	500	30	50	10
$i = 2$	500	39	59	9
$i = 3$	500	30	50	45
$i = 4$	500	40	65	22

Table 2: Platoon and road information.

Parameter	Value	Unit
l	5	m
δ	1	m
$n_{vehicle}$	20	veh
v_{road}^{limit}	20	m/s

Table 3: Parameters value of fuel consumption.

Coefficient	Value	Unit
α_0	0.1569	mL/s
α_1	2.450×10^{-2}	mL/m
α_2	-7.415×10^{-4}	mLs/m^2
α_3	5.975×10^{-5}	mLs^2/m^3

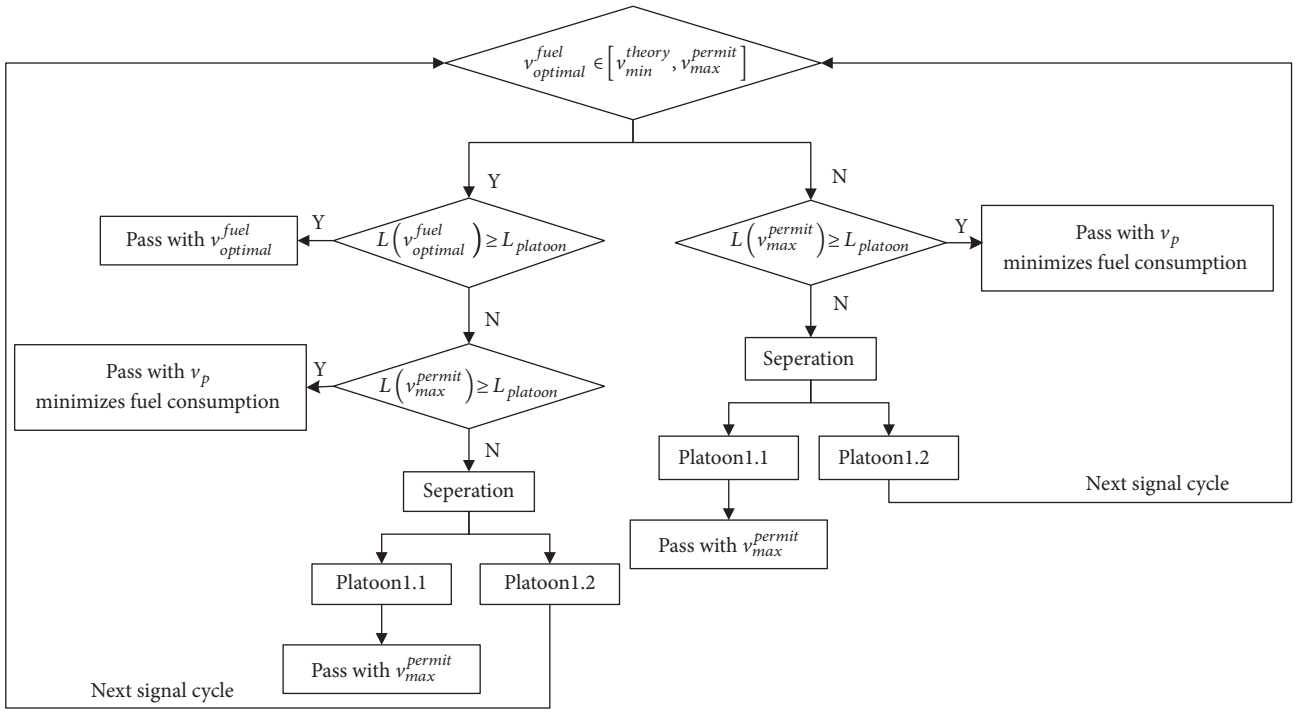

Figure 6: The process of our proposed velocity control and separation strategy.

each vehicle in the platoon under conventional circumstance. It is not difficult to see that most of vehicles in this platoon will be idle at all intersections, except that a small number of vehicles do not have to wait for the red light only at the third intersection. This is because of the lack of velocity control and separation strategy.

4.2. Simulation 2: Separation Strategy with Minimum Fuel Consumption. To solve the deficiency of conventional strategy, we propose a velocity control and separation strategy that takes into account the traffic efficiency and fuel-saving simultaneously as introduced in Section 3.2. The velocity profile of each vehicle in the platoon under this strategy is

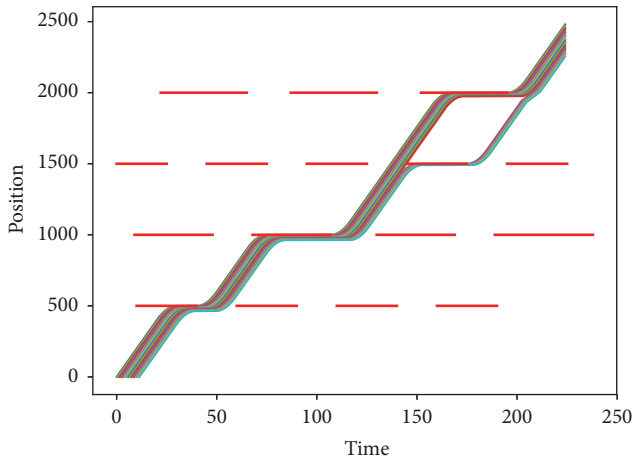

Figure 7: Trajectory of vehicles of platoon without separation strategy.

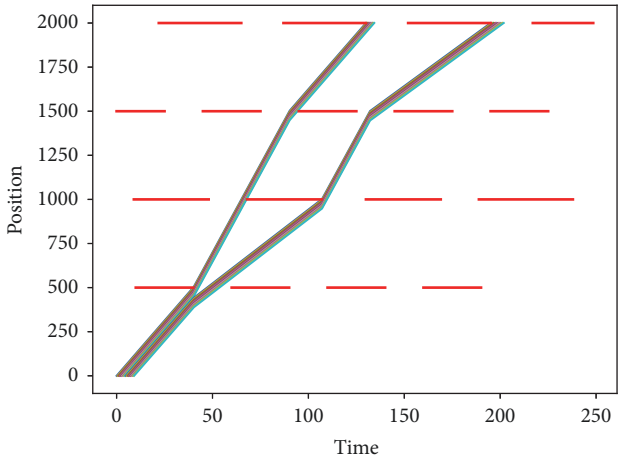

Figure 8: Trajectory of vehicles of platoon with separation strategy (minimum fuel consumption).

shown in Figure 8. One can see that the separation of original platoon occurs at the first intersection, dividing it into two new platoons. The separation point is located at the 11th vehicle, and the velocity profile of 1st vehicle and 11th vehicle is

$$v_p(1) = \{12.5m/s, 20m/s, 18.6m/s, 13.1m/s\}$$
$$v_p(11) = \{12.5m/s, 8.3m/s, 14.5m/s, 9.3m/s\}. \quad (12)$$

4.3. Simulation 3: Separation Strategy without Considering Fuel-Saving. In order to better understand how our proposed velocity control and separation strategy achieves fuel-saving under the premise of guaranteeing that maximum number of vehicles can pass the intersection without idling, we implement another simulation in which all the vehicles choose the maximum velocity to pass intersections without considering fuel-saving. This simulation is almost similar to simulation 2 except that all vehicles pass all the intersections with maximum passing velocity v_{max}^{permit}. Figure 9 shows velocity

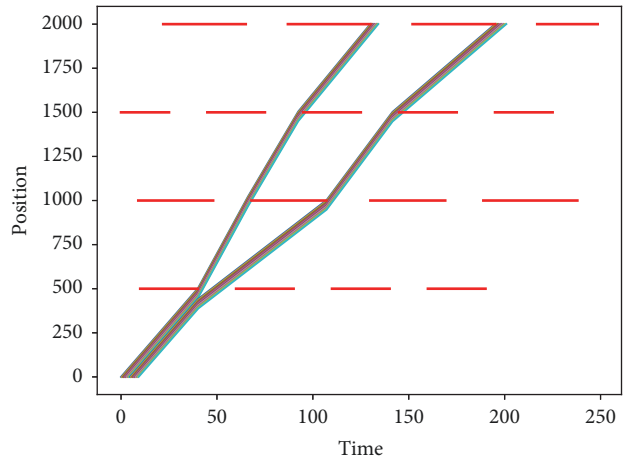

Figure 9: Vehicles' trajectory of platoon with separation strategy (*maximum passing velocity*).

profile of each vehicle in the platoon under this circumstance. The velocity profile of 1st vehicle and 11th vehicle with this strategy is as follows:

$$v_p(1) = \{12.5m/s, 20m/s, 20m/s, 12.5m/s\}$$
$$v_p(11) = \{12.5m/s, 8.3m/s, 20m/s, 7.9m/s\}. \quad (13)$$

Comparing with our proposed separation strategy that considers fuel-saving, we find that the main difference between these two different situations is reflected at the third intersection. Under the premise of ensuring that all vehicles can pass without idling, our proposed separation strategy chooses the velocity that can minimize the fuel consumption, but this strategy chooses the maximum velocity to pass the intersection.

4.4. Evaluation of Proposed Velocity Control and Separation Strategy. Figure 10 shows that the fuel consumption and total travel time decrease with the introduction of our proposed velocity control and separation strategy.

One can see that the fuel consumption of each vehicle decreases dramatically with our proposed separation strategy. For the platoon with 20 vehicles, the total fuel consumption decreases by 18.1% comparing with the conventional strategy. By minimizing the fuel costs, we also implicitly increase some of the societal benefits of our proposed platoon separation strategy. Minimizing fuel consumption is equivalent to minimizing emissions [25]. Also, when we minimize the fuel costs, longer platoons are preferred as the total savings will be higher with more following vehicles in the system.

With our proposed separation strategy, the total travel time decreases by 19.2% compared with the conventional strategy. The first ten cars are particularly noticeable thanks to velocity control and separation strategy. In other words, traffic efficiency has improved. And longer platoons are associated with more efficient road utilization since the vehicles within a platoon drive closer together. The reduced space utilization as a result of platooning might help improve the traffic throughput.

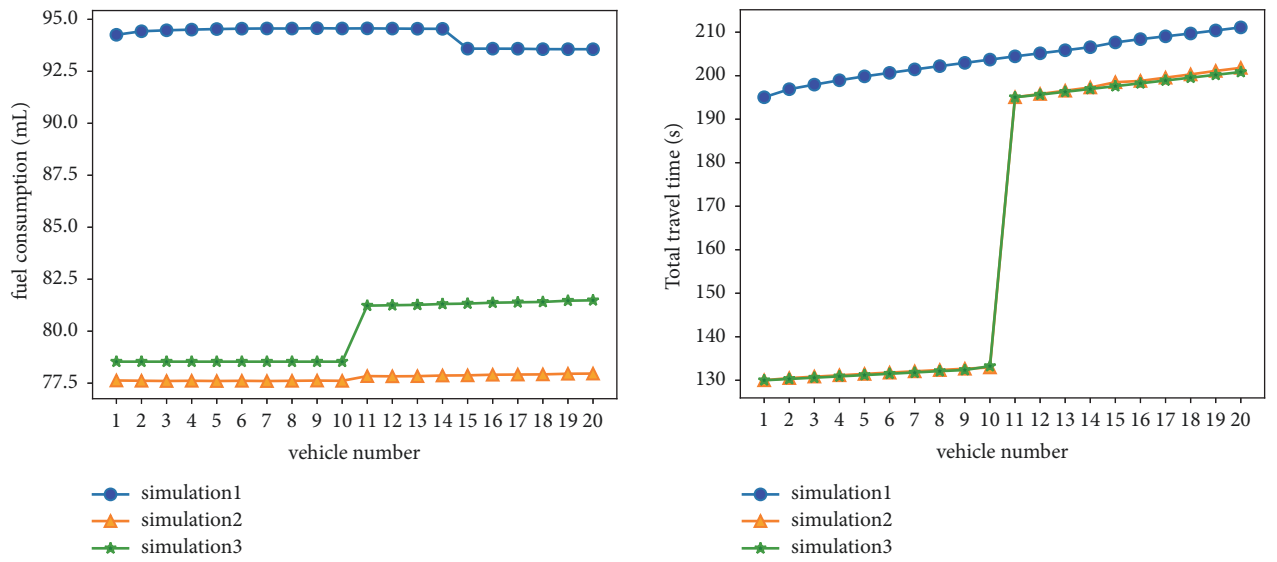

Figure 10: The total fuel consumption and the total travel time of each vehicle.

Intuitively, passing with the maximum velocity means that the travel time is the minimum. It is worth noting that this conclusion is only valid for a single intersection. Interestingly, for multiple intersections, the total travel time is not necessarily the smallest even if the maximum velocity is selected at each intersection, which is determined by the difference of signal phase between two consecutive signalized intersections. If the green phase difference of two adjacent intersections is very gentle, vehicles cannot pass these two intersections continuously during the same green phase due to the maximum velocity limit. In other words, even if the maximum speed is selected at the previous intersection, the platoon can only pass the consecutive intersection until its next green phase by reducing more velocity. This will probably lead to a decrease in the overall average speed, which in turn increases the total travel time. As we can see in Figure 10, the travel time of 10th–20th vehicle in simulation 2 is slightly less than that in simulation 3, although maximum velocity is selected at each intersection in simulation 3. This is because the green phase difference between 3rd and 4th intersection is very gentle. Therefore, passing with the maximum velocity may not necessarily improve traffic efficiency; on the contrary, choosing the optimal fuel consumption may even improve traffic efficiency in some cases.

5. Conclusion

A velocity control and separation strategy aimed at avoiding idling at red light and reducing fuel consumption as much as possible was proposed in this paper. The simulation results suggested that our proposed strategy effectively improves the performance of the platoon. The total travel time and the fuel consumption were reduced by 19.2% and 18.1%, respectively. The ultimate objectives of platooning are to enhance highway safety, improve traffic utility, and reduce fuel consumption. The main novelty and contribution of this work is providing an optimal platoon velocity control method and a separation strategy at signalized intersection that considers both traffic utility improvement and fuel economy. Additionally, it is worth noting that the using scenarios of this strategy involve multiple intersections instead of only one single signalized intersection, and this strategy can be applied to full autonomous or semiautonomous vehicles in the future.

Several extensions to the present study are desired in the future. Some assumptions made in this study could be violated, and we caution against generalizing the results. We would like to mention that the simulation results are based on the assumption that all vehicles run at a constant velocity ignoring the acceleration or deceleration process. Actually, the fuel consumption and the state of the platoon system may change with the acceleration or deceleration process. Additionally, this paper only considers the separation strategy of a single static platoon and ignores the dynamics of platooning process between multiple platoons. The dynamics increase the complexity of the decision-making process.

Therefore, each problem discussed above presents an important and very challenging research topic. In the future work, the impact of acceleration and deceleration process on fuel consumption and travel time needs to be investigated to examine the validation of the simulation results. Nevertheless, this paper provides an explicit strategy to better improve the traffic efficiency and fuel-saving in a vehicle platoon.

Data Availability

The data used to support the findings of this study are available from the corresponding author upon request.

Conflicts of Interest

The authors declare that they have no conflicts of interest.

Acknowledgments

This work was supported by the National Natural Science Foundation of China (Grant no. 61573098).

References

[1] S. Maiti, S. Winter, and L. Kulik, "A conceptualization of vehicle platoons and platoon operations," *Transportation Research Part C: Emerging Technologies*, vol. 80, pp. 1–19, 2017.

[2] A. Ghiasi, O. Hussain, Z. Qian, and X. P. Li, "A mixed traffic capacity analysis and lane management model for connected automated vehicles: A Maekov chain method," *Transportation Research Part B*, vol. 106, pp. 266–292, 2017.

[3] D. Chen, S. Ahn, M. Chitturi, and D. A. Noyce, "Towards vehicle automation: Roadway capacity formulation for traffic mixed with regular and automated vehicles," *Transportation Research Part B: Methodological*, vol. 100, pp. 196–221, 2017.

[4] L. Ye and T. Yamamoto, "Modeling connected and autonomous vehicles in heterogeneous traffic flow," *Physica A: Statistical Mechanics and its Applications*, vol. 490, pp. 269–277, 2018.

[5] A. Olia, S. Razavi, B. Abdulhai, and H. Abdelgawad, "Traffic capacity implications of automated vehicles mixed with regular vehicles," *Journal of Intelligent Transportation Systems: Technology, Planning, and Operations*, pp. 1–19, 2017.

[6] J. Lioris, R. Pedarsani, F. Y. Tascikaraoglu, and P. Varaiya, "Doubling throughput in urban roads by platooning," *IFAC-PapersOnLine*, vol. 49, no. 3, pp. 49–54, 2016.

[7] J. Lioris, R. Pedarsani, F. Y. Tascikaraoglu, and P. Varaiya, "Platoons of connected vehicles can double throughput in urban roads," *Transportation Research Part C: Emerging Technologies*, vol. 77, pp. 292–305, 2017.

[8] Y. Chang and P. Edara, "Evaluation of a reservation-based intersection control algorithm for hurricane evacuation with autonomous vehicles," *International Journal of Disaster Risk Reduction*, 2017.

[9] Organization of Petroleum Exporting Countries, "World Oil Outlook," 2016.

[10] M. P. Lammert, A. Duran, J. Diez, K. Burton, and A. Nicholson, "Effect of Platooning on Fuel Consumption of Class 8 Vehicles Over a Range of Speeds, Following Distances, and Mass," *SAE Commercial Vehicle Engineering Congress (COMVEC)*, vol. 7, no. 2, pp. 626–639, 2014.

[11] A. Al Alam, A. Gattami, and K. H. Johansson, "An experimental study on the fuel reduction potential of heavy duty vehicle platooning," in *Proceedings of the International IEEE Conference on Intelligent Transportation Systems*, pp. 306–311, 2010.

[12] S. Tsugawa, S. Kato, and K. Aoki, "An automated truck platoon for energy saving," in *Proceedings of the IEEE/RSJ International Conference on Intelligent Robots and Systems*, vol. 32, pp. 4109–4114, 2011.

[13] X. Zhang, B. Jia, and R. Jiang, "Impact of safety assistance driving systems on oscillation magnitude, fuel consumption and emission in a car platoon," *Physica A: Statistical Mechanics and its Applications*, vol. 505, pp. 995–1007, 2018.

[14] N. Wan, A. Vahidi, and A. Luckow, "Optimal speed advisory for connected vehicles in arterial roads and the impact on mixed traffic," *Transportation Research Part C: Emerging Technologies*, vol. 69, pp. 548–563, 2016.

[15] C. R. Sekhar, P. Raj, P. Parida, and S. Gangopadhyay, "Estimation of delay and fuel loss during idling of vehicles at signalized intersection in Ahmedabad," *Procedia - Social and Behavioral Sciences*, vol. 104, pp. 1178–1187, 2013.

[16] K. Shi, B. Di, K. Zhang, C. Feng, and L. Svirchev, "Detrended cross-correlation analysis of urban traffic congestion and NO2 concentrations in Chengdu," *Transportation Research Part D: Transport and Environment*, vol. 61, pp. 165–173, 2018.

[17] S. E. Li, Y. Zheng, K. Li et al., "Dynamical Modeling and Distributed Control of Connected and Automated Vehicles: Challenges and Opportunities," *IEEE Intelligent Transportation Systems Magazine*, vol. 9, no. 3, pp. 46–58, 2017.

[18] Y. Zheng, S. E. Li, J. Wang, D. Cao, and K. Li, "Stability and scalability of homogeneous vehicular platoon: Study on the influence of information flow topologies," *IEEE Transactions on Intelligent Transportation Systems*, vol. 17, no. 1, pp. 14–26, 2016.

[19] O. Jabali, T. Van Woensel, and A. G. de Kok, "Analysis of travel times and CO_2 emissions in time-dependent vehicle routing," *Production Engineering Research and Development*, vol. 21, no. 6, pp. 1060–1074, 2012.

[20] T. Bektaş and G. Laporte, "The pollution-routing problem," *Transportation Research Part B: Methodological*, vol. 45, no. 8, pp. 1232–1250, 2011.

[21] Y. Suzuki, "A new truck-routing approach for reducing fuel consumption and pollutants emission," *Transportation Research Part D: Transport and Environment*, vol. 16, no. 1, pp. 73–77, 2011.

[22] Y. Y. Kuo, "Using simulated annealing to minimize fuel consumption fort the time-dependent vehicle routing problem," *Computers & Industrial Engineering*, vol. 59, pp. 157–165, 2010.

[23] M. A. S. Kamal, M. Mukai, J. Murata, and T. Kawabe, "Ecological driving based on preceding vehicle prediction using MPC," *IFAC Proceedings Volumes*, vol. 44, no. 1, pp. 3843–3848, 2011.

[24] Y. Zheng, S. Eben, B. Xu, K. Q. Li, and J. Wang, "Complexity analysis of green light optimal velocity problem: an NP-complete result for binary speed choices," in *Proceedings of the 14th Intelligent Transportation System Asia Pacific Forum*, 2015.

[25] G. Scora and M. Barth, "Comprehensive Modal Emissions Model (CMEM), Version 3.01 User guide," Riverside Centre for Environmental Research and Technology, University of California, 2006.